UC Santa Barbara

UC Santa Barbara Electronic Theses and Dissertations

Title

Rational Design and Synthesis of Membrane-active Conjugated Oligoelectrolytes for Biological Applications

Permalink

https://escholarship.org/uc/item/32m204vc

Author

Limwongyut, Jakkarin

Publication Date

2022

Peer reviewed|Thesis/dissertation

eScholarship.org Powered by the California Digital Library
University of California

UNIVERSITY OF CALIFORNIA

Santa Barbara

Rational Design and Synthesis of Membrane-active Conjugated Oligoelectrolytes for Biological Applications

A dissertation submitted in partial satisfaction of the

requirements for the degree Doctor of Philosophy

in Chemistry

by

Jakkarin Limwongyut

Committee in charge:

Professor Guillermo C. Bazan, Chair

Professor Javier Read de Alaniz

Professor Frederick W. Dahlquist

Professor Kevin W. Plaxco

March 2022

The dissertation of Jakkarin Limwongyut is approved.

_____

Professor Javier Read de Alaniz

_____

Professor Frederick W. Dahlquist

_____

Professor Kevin W. Plaxco

_____

Professor Guillermo C. Bazan, Committee Chair

February 2022

Rational Design and Synthesis of Membrane-active Conjugated Oligoelectrolytes for Biological Applications

Copyright © 2022

by

Jakkarin Limwongyut

dedicated to my family and all of my mentors that inspired me to be a science enthusiast

Acknowledgements

First, I would like to thank my primary thesis advisor, Prof. Guillermo Bazan for all of the guidance and support during my graduate study. He encouraged me to do step out of my comfort zone and explore research in the areas that I am not familiar with. He has also been teaching me to improve my scientific thinking, writing, and presentation skills. He has widened my perspective of conjugated materials and how they can interface with biology. I remembered the first day I joined his research group with an idea of pursuing research in organic photovoltaic materials. After a discussion with him, I decided to challenge myself by working on projects at the interface of materials science, chemistry, and biology. I am very grateful for the opportunity he gave me to work on those projects. I have learned many new skills and my views on organic materials have changed significantly. I also would like to thank Prof. Javier Read de Alaniz for co-advising me and welcoming me as a part of his research group.

I also would like to thank people in the Bazan research group and CPOS for creating such a good environment to work in. I have had very fruitful discussions on research projects with them on research projects as well as other scientific topics in general. Even though I did not have much prior experience in biology, Dr. Hengjing Yan and Dr. Samantha McCuskey have patiently helped me getting started on basic microbiology techniques from preparing food for bacteria to setting up experiments with bacteria. I would like to thank Dr.

Stephanie Fronk for training me on yeast experiments and many discussions on whole-cell biocatalysis, Dr. Bing Wang for many useful conversations on synthesis and biology, Dr. Chenyao Nie for her great contribution and countless discussions on biology part of antimicrobial projects, and Dr. Zichao Zhang for her initiative on antimicrobial projects. In addition, Ziyue Zhu and Luana Llanes have lightened up my life in the lab through many fun conversations and sometimes complaints when our experiments did not go as planned. Lastly, many thanks go to my lab mate, Dr. Alex Moreland. He has immensely helped me on every aspect of chemistry. He was the first person in the synthesis lab I worked with when I joined this group. We have had countless of thought-provoking conversations about organic synthesis and biological experimental design. We also talked a bunch about Mammoth Lakes—his beloved location for fishing—when we were not doing chemistry.

I have had many opportunities to use state-of-the-art shared facilities to do research at UCSB. I would like to thank all of the staffs who run and maintain these facilities across the campus, Dr. Hongjun Zhou, Dr. Dmitriy Uchenik, Dr. Alexander Mikhailovsky, Dr. Jen Smith, Dr. Ben Lopez, Dr. Jerry Hu, Dr. Rachel Behrens, and Dr. Aidan Taylor.

Being in a graduate school can be stressful at (many) times. I am grateful to have friends in my chemistry cohort who have made my graduate school experience much more enjoyable. This would be a very long list of people if I

were to write all of them down. But if any of you are reading this, thank you! I will remember all the good times we had in parties and pint nights.

As an international student, I am far away from my friends and family. I am thankful for a small Thai student community at UCSB: Dr. Piyatida Klumphu, Pinn Siraprapasiri, Dr. Banjaporn Narupai, Dr. Chatarin Wangsanuwat, Dr. Bhornrawin Akkachairin, Inthanon Lapkriengkri, It Fufuengsin, Krittiya Carter, and John Carter. They have made my life abroad so much fun and memorable. We met almost every weekend to cook, hang out, play board games, travel, explore food that Southern California has to offer.

Lastly, I have to thank my family for their support and care in every step of my life. Thank you for always being there for me when I needed help or advice. Thank you for listening to my stories when I was having difficult times. Even though the pandemic has made their plan to visit me during my graduation not feasible for them, I know that they are and will always be with me spiritually. I am forever grateful to have them in my life.

Curriculum Vitae

Jakkarin Limwongyut

EDUCATION

Doctor of Philosophy in Chemistry, University of California, Santa Barbara, February 2022 (expected)

Bachelor of Science in Chemistry (Honors Program, First-class Honors), Suranaree University of Technology, Thailand, July 2016

RESEARCH EXPERIENCE

Graduate Student Researcher, Department of Chemistry and Biochemistry, University of California, Santa Barbara (Bazan Lab, 2016–present)

Graduate Student Mentor, Department of Chemistry and Biochemistry, University of California, Santa Barbara (Mentee: Nathan Incandela, 2019–2021)

Visiting Researcher, School of Molecular Science and Engineering, Vidyasirimedhi Institute of Science and Technology, Thailand (Advised by Professor Vinich Promarak, 2015–2016)

Undergraduate Student Researcher, School of Chemistry, Suranaree University of Technology, Thailand (Advised by Professor Vinich Promarak and Professor Visit Vao-Soongnern, 2014–2015)

Undergraduate Student Researcher, School of Chemistry, Suranaree University of Technology, Thailand (Advised by Professor Albert Schulte, 2014)

PROFESSIONAL EMPLOYMENT

Teaching Assistant, Department of Chemistry and Biochemistry, University of California, Santa Barbara (2016–2017)

PUBLICATIONS

1. *Amide Moieties Modulate Antimicrobial Activities of Conjugated Oligoelectrolytes against Gram-negative Bacteria*, **J. Limwongyut**, A. S. Moreland, C. Nie, J. Read de Alaniz, G. C. Bazan, *ChemistryOpen (in press)*
2. *Predicting antimicrobial activity of conjugated oligoelectrolyte molecules via machine learning*, A. Tiihonen, S. J. Cox-Vazquez, Q. Liang, M.

Ragab, Z. Ren, N. T. P. Hartono, Z. Liu, S. Sun, C. Zhou, N. C. Incandela, **J. Limwongyut**, A. S. Moreland, S. Jayavelu, G. C. Bazan, T. Buonassisi, *J. Am. Chem. Soc.* 2021, 143, 18917–18931.

3. *The impact of bacteria exposure on the plasmonic response of silver nanostructured surfaces*, G. M. Paternò, A. M. Ross, S. M. Pietralunga, S. Normani, N. D. Vedova, **J. Limwongyut**, G. Bondelli, L. Moscardi, G. C. Bazan, F. Scotognella, G. Lanzani, *Chem. Phys. Rev*. 2021, 2, 021401.
4. *Photoswitchable Conjugated Oligoelectrolytes for a Light-Induced Change of Membrane Morphology*, D. Leifert, A. S. Moreland, **J. Limwongyut**, A. A. Mikhailovsky, G. C. Bazan, *Angew. Chem. Intl. Ed.* 2020, 132, 20513–20517.
5. *Molecular design of antimicrobial conjugated oligoelectrolytes with enhanced selectivity toward bacterial cells,* **J. Limwongyut**, C. Nie, A. S. Moreland, G. C. Bazan, *Chem. Sci.* 2020, 11, 8138–8144.
6. *Interactions of a paracyclophane-based conjugated oligoelectrolyte with biological membranes,* **J. Limwongyut**, Y. Liu, G. S. Chilambi, T. Seviour, J. Hinks, Y. Mu, G. C. Bazan, *RSC Adv*. 2018, 8, 39849–39853.
7. *Conjugated Oligoelectrolytes: Materials for Acceleration of Whole Cell Biocatalysis,* B. Wang, S. L. Fronk, Z. D. Rengert, **J. Limwongyut**, G. C. Bazan, *Chem. Mater*. 2018, 30, 5836–5840.

PATENT APPLICATION

1. "Short Conjugated Oligoelectrolytes and Uses Thereof," G. Bazan, Z. Zhang, A. Moreland, M. J. Mahan, D. M. Heithoff, **J. Limwongyut**, C. Nie, Application: PCT/US19/23411, Filing: March 21, 2019.

Abstract

Rational Design and Synthesis of Membrane-active Conjugated Oligoelectrolytes for Biological Applications

by

Jakkarin Limwongyut

Lipid bilayers are omnipresent in biological systems as a barrier protecting intracellular components from the external environment. The semi-permeable behavior of membranes selectively controls flux of chemicals into and out of the cells maintaining chemical balances. This behavior is also a main obstacle for delivering or harvesting chemicals into and from cells. Modifying membrane properties to enhance chemical transport therefore has implications for many cell-based applications.

Conjugated oligoelectrolytes (COEs) are a class of synthetic compounds that contain a π-conjugated backbone with aliphatic linkers bearing ionic functionalities. Given appropriate molecular dimensions and hydrophobic/hydrophilic balance that resemble lipid bilayers, a subset of COEs possess an ability to spontaneously intercalate into membranes and subsequently modify membrane properties. In this work, rational design and structure-property relationships of COEs and their ability to permeabilize and disrupt membranes will be presented.

In the first work, as an effort to improve membrane permeabilization for whole-cell biocatalysis, a COE containing a non-planar conjugated core will be presented and its impact on lipid bilayers will be discussed. *Escherichia coli* and *Saccharomyces cerevisiae* (yeast) will be used as model organisms to show an ability of COEs to accelerate whole-cell biocatalysis rates with reduced toxicity to microorganisms.

In a separate study, a homologous series of distyrylbenzene-based COEs will be presented to elucidate the relationship between their structures and their antimicrobial activities and mammalian cell cytotoxicity. The criteria required to achieve high antibacterial selectivity will be discussed. A subsequent study will investigate the impact of hydrogen bonds—another intermolecular force apart from electrostatic and hydrophobic interactions that can be important in lipid interactions—on antimicrobial activities of the COEs. Activities on periplasmic and cytoplasmic membranes of *Escherichia coli* will be discussed. Additionally, another series of COEs containing amidine moieties will be presented along with preliminary data of their antimicrobial activities against a broad panel of pathogenic bacteria with a focus on *Pseudomonas aeruginosa*—a clinically relevant pathogen associated with difficult-to-treat infections and with a high propensity for developing antibiotic resistance. Finally, additional results towards developing COEs as a novel class of antibiotics and a method to estimate the "hydrophobicity" of COEs will be discussed.

Table of Contents

List of Figures

List of Tables

Chapter 1: Introduction

1.1 Lipid membranes and their functions in living cells

Lipid membranes are ubiquitous in biological systems as they serve as an interface between living cells and their external environments. Despite their abundance, it was not until the 17th century that their presence was hypothesized after the discovery of plant cells by Hooke.[1] During the 20th century was an era that lipid bilayer was finally first recognized as a basis of cell membranes.[2] In 1972, Singer and Nicholson proposed a fluid-mosaic model that is now widely accepted.[3] Their discovery gave rise to many significant discoveries in the structure and functions of cell membranes. Cell membranes generally consist of phospholipid molecules with various lipid headgroups.[4] These phospholipid molecules spontaneously form a two-molecule thick self-assembled structure called a "lipid bilayer" acting as a semi-permeable layer where vital cell machineries are contained within.

In addition to the semi-permeable properties of lipid bilayers, they also harbor a wide range of components that have specialized roles in maintaining crucial processes in living cells e.g., homeostasis, signaling, and ATP production. Lipid headgroup makes possible for membrane-bounded components to function.

Within a cell surrounded by lipid bilayers contains all machineries that are important to sustain its life. These machineries often function cooperatively to

produce molecules that play important roles in the cell. The examples of such roles include, but not limited to, energy production, signaling, reproduction, and sometimes innate defense mechanisms. Human have harnessed their chemical production abilities of unicellular organisms such as bacteria and fungi, especially for food preservation, for thousands of years dating back to the Neolithic period (ca. 10,000 BCE).[5] In present days, microorganisms are still being used by human as a "factory" to produce various functional chemicals.[6–8] Many genetic engineering approaches have been used to redesign their machineries to achieve a higher production output or novel biosynthetic routes.[6,9,10] Apart from genetic modification techniques, materials and chemical approaches can also be employed to enhance desirable functions of microorganisms. These methods usually involve the modulation of cell membrane properties. Especially for whole-cell biocatalysis, the semi-permeable behavior of cell membranes are considered as a road block hampering a high production yield.[11]

As mentioned above, cell membranes offer a protective layer for microorganisms to retain their vital components within their cells. They have been demonstrated to be a target for antimicrobial agents.[12–14] In the nature, living organisms produce antimicrobial peptides (AMPs) as a part of their innate immune system to protect them from pathogenic bacteria. AMPs act through membrane interaction which leads to events that are hypothesized to be fatal for bacteria, for example, pore formation,[15] membrane depolarization[16],

lipid segregation,[17] and damaging intracellular targets.[18] Selectivity of AMPs for bacteria arises from differences in lipid composition of cell membranes between bacteria and eukaryotic cells. To date, many synthetic AMPs and AMP-mimics have been designed. Despite a large library of peptides, many of them still suffer from toxicity, stability, and cost of production.[19–21] Similar membrane-interacting principles have also been used to synthesize small molecule antibiotics. Due to a discovery void in antibiotic space and the rise of antimicrobial resistance (AMR), membrane-active compounds could provide us a promising platform for novel antibiotics that are much needed.

1.2 Introduction to conjugated oligoelectrolytes

Conjugated oligoelectrolytes (COEs) are a class of synthetic compounds that are characterized by a π-conjugated core with ionic pendant functionalities at the molecular termini. Unlike conjugated polyelectrolytes (CPEs), the π-delocalized core only contains several repeating units (Figure 1.1). Provided that there is an appropriate ratio of hydrophilic and hydrophobic components, these COEs can function as membrane intercalating agents due to the similarity the amphiphilic profile of COE molecules to that of lipid bilayers. The COE molecules would align themselves parallel to the normal of lipid bilayer spanning across the membrane as illustrated in Figure 1.1.

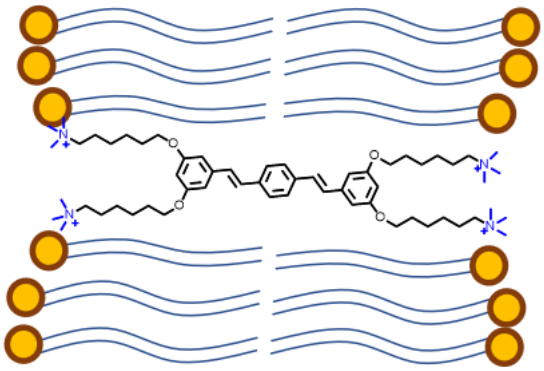

Figure 1.1 Cartoon representation of a membrane-intercalating COE in a lipid bilayer

Our group has successfully demonstrated the uses of COEs in various applications though some of them were not intended specifically for biological systems.[22] An application of COEs that interfaces them with bacteria, although not for their membrane-intercalating properties, was reported in 2010 by Dr. Aidee Duarte.[23] This work utilized Förster resonance energy transfer (FRET) as a tool for an array-based bacteria detection. COEs were developed as FRET donors. They form electrostatic complexes with single-stranded DNAs (ssDNAs) labeled with fluorescein which act as FRET acceptors.

The work that pioneered the uses of COEs as membrane-intercalating agents was also reported in 2010 by Dr. Logan Garner and co-workers.[24] This work demonstrates that **DSBN+** and **DSSN+** can intercalate into lipid vesicles and living yeast cells. Furthermore, they showed that the COEs can facilitate electron transport across membranes and improve the efficiency of yeast microbial fuel cells (MFCs). Many studies were later reported on using these

COEs in bioelectrochemical systems.[25–28] It was originally hypothesized that COEs function as a nanowire that conducts electron across cell membranes. However, it was later shown that the increased electron transfer efficiency arises from the membrane permeabilizing activity of COEs.[29]

Another generation of COEs with a redox active center were synthesized by Dr. Zach Rengert.[30] The design principle of this series of COEs is to mimic the function of hemes in natural membrane proteins found in *S. oneidensis*. Electrons transport across membranes by hopping through ferrocenes–redox active moieties in the conjugated core. The COEs demonstrated marked enhancement in biological electron production, even in non-electrogenic strains (*Mtr* knockouts). Subsequent structure modifications of ferrocene containing COEs were reported.[31] It was found that the increase in current generation were observed only at the potential higher than the redox potential of each COE.

In addition to bioelectronic applications of COEs, Dr. Chelsea Catania started investigating the membrane-permeabilizing properties of COEs as a potentially useful tool for whole-cell biocatalysis.[32] It was found that, upon intercalation into bacterial cells, COEs increased the transport of small molecules across the outer membrane. Furthermore, she found that a periplasmic protein alkaline phosphatase (ALP) was released from the cells. The permeabilizing effect was found to be dependent on the COE concentration. A subsequent study by Dr. Stephanie Fronk and co-workers reported the use of

COEs to permeabilize yeast cells.[33] This work proves that the rate of whole-cell biocatalysis can be improved with little toxicity by the addition of COEs. The extent of acceleration was shown to be highly dependent on the concentration and the structure of COEs. A study of an azobenzene-based COE by Dr. Dirk Leifert also enables a method to permeabilize cells and vesicles upon light irradiation.[34]

Dr. Hengjing Yan screened a set of COEs for their antimicrobial activity and found that the length of the conjugated core significantly impacts the antimicrobial activity.[35] The molecular dynamic (MD) simulation showed that a short COE introduces hydrophobic mismatch and leads to membrane "pinching".[36] In addition, Dr. Bing Wang reported a COE that efficiently generates singlet oxygen upon light irradiation demonstrating a COE for photodynamic antimicrobial therapy.[37] He also reported two narrow-bandgap COEs that are near-infrared absorbing with high photothermal conversion efficiency.[38]

1.3 Overview and objectives

With cell membranes pose a barrier to machineries and other vital components of microorganisms, materials approach to modulate membrane properties using COEs is therefore of great interest. The scope of research in this dissertation is to rationally design and synthesize series of COEs to probe their impacts on membrane properties and their overall effects on biological systems (e.g., bacterial cells and lipid vesicles). Two main applications of COEs

will be featured throughout this dissertation: (1) whole-cell biocatalysis and (2) antimicrobial compound development. The rational design of COEs will feature modular chemical structures that allows many possible structure modulations by changing starting material "building blocks" as depicted in Figure 1.2.

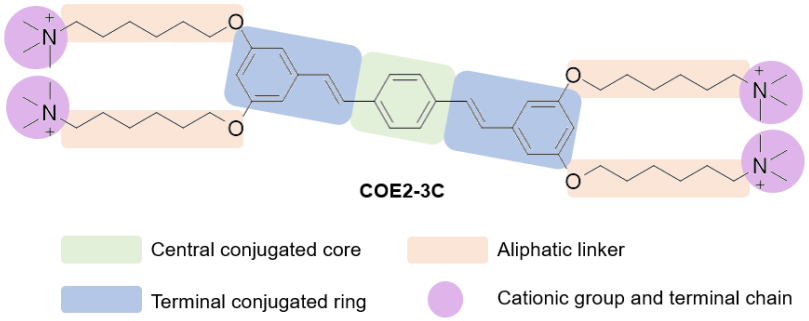

Figure 1.2 Modular structure of COEs. Each colored segment on the structure can be tailored by using different building blocks.

In Chapter 2, the design of a novel COE with a non-planar conjugated core will be described. Based on **COE2-3C** as a parent structure, a phenyl ring in the central conjugated core was replaced by a [2.2]paracyclophane unit which added a dimensionality to the overall conjugated core. Despite its non-planar shape, it is still considered conjugated due to a through-space π-conjugation. Experimental and computational studies of the impacts of this change on cell membranes will be described in detail. These findings show increased in membrane perturbation without increasing antimicrobial activity, thus highlighting the potential of using COEs as cell permeabilizing agents without being toxic to microorganism.

In Chapter 3, based on previous works in our group on antimicrobial activities of COEs, a series of distyrylbenzene-based COEs will be used to

establish structure-activity relationship pertaining to their antimicrobial activities and mammalian cell cytotoxicity. This series of COEs will be based on **COE2-3C** as a parent structure, similar to the work in Chapter 2. Specifically, different length of aliphatic alkoxy linkers and terminal chains were installed to a distyrylbenzene unit. Cationic moieties remained quaternary ammoniums. Detailed investigation of their activities will be presented. The fact that antimicrobial activities and cytotoxicity can be decoupled through careful structure modulation will be highlighted.

Chapter 4 explores another set of COEs that contain amide groups. The addition of amides introduces hydrogen bonding capability to the COEs. COEs in this Chapter will be based on a distyrylbenzene unit with propoxy groups as linkers. Terminal chains containing a primary amide with different alkyl groups were installed on the linker with quaternary ammonium groups serving as cationic moieties. Membrane-active properties of the COEs as well as their antimicrobial activities will be investigated.

In Chapter 5, the findings in Chapter 4 will be utilized in the molecular design of the new series of COEs. The structures of the COEs in this Chapter will be based on the structures from Chapter 4. However, the cationic and terminal groups will be replaced by amidine moieties which provide hydrogen bonding and cationic characteristics within the same unit. Experimental results on their antimicrobial activities and cytotoxicity will be presented.

Chapter 6 contains additional information and experiments that did not get incorporated into the previous chapters. The first part will disclose additional COE structures that were designed for antimicrobial purposes. The second part will be discussing a method to determine relative hydrophobicity of distyrylbenzene-based COEs presented in Chapter 3–5 by a reverse phase HPLC method.

Chapter 2: Increasing dimensionality of a COE to improve membrane permeabilization activity for whole cell biocatalysis[1]

2.1 Introduction

Conjugated oligoelectrolytes (COEs) are defined by a conjugated backbone with ionic pendant groups tethered by hydrocarbon chains.[26,39] COEs typically intercalate within microbial membranes in a well-organized fashion.[40] Several molecular features are known to impact the extent of COE accumulation within cells and their effects on the membrane. For example, the degree to which the COEs intercalate within membranes depends on whether the charged groups are anionic or cationic.[41] Additionally, the number of repeat units affects the distortion of the lipid bilayer and is a strong modulator of antimicrobial efficacy.[35,36] Microbes with COEs have their properties and behavior modified in ways that are desirable for specific applications. Consider, the homologous series of oligophenylenevinylene COEs illustrated by **DSBN+**, **DSSN+** and **COE1-5C** (Figure 2.1). While **DSBN+** has a higher antimicrobial efficacy than **DSSN+**, both increase membrane permeability in *E. coli* K12. **COE1-5C**, in contrast, has been shown to rigidify membranes.[32,36,42]

Oligophenylenevinylene COEs studied thus far largely contain a planar, two-dimensional conjugated fragment. A molecular structural variation that has yet

[1] The contents of this chapter have appeared in J. Limwongyut, Y. Liu, G. S. Chilambi, T. Seviour, J. Hinks, Y. Mu, and G. C. Bazan, *RSC Adv.*, 2018, **8**, 39849–39853.

to be considered concerns introducing dimensionality to the conjugated segment in order to understand possible repercussion of this structural modification on the reorganization of the membrane lipids and the overall perturbation of the bilayer. To accomplish this structural variation, we sought to include a rigid framework within the interior of the conjugated segment with an otherwise similar aspect ratio to phenylene unit. For this purpose, we chose the [2.2]paracyclophane (pCp) moiety. We hypothesized that three-dimensionality from the pCp adduct would increase lipid disorder in the membrane. The structural evolution is illustrated in Figure 2.1.

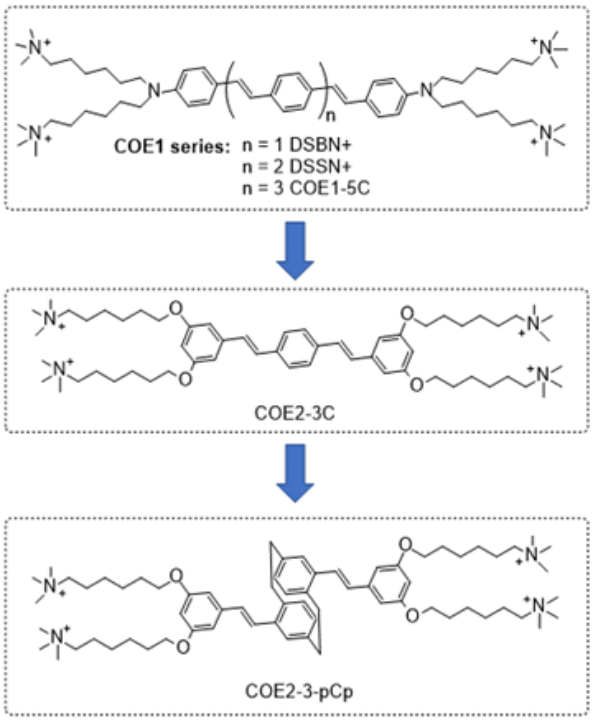

Figure 2.1 Structural evolution from the COE1 series to the paracyclophane-based COE (**COE2-3-pCp**). Iodide counterions are omitted from the structures for clarity.

We compared the properties of **COE2-3-pCp** to those of its linear counterpart **COE2-3C** by first carrying out molecular dynamics simulations to elucidate deformations and disorder within a model lipid bilayer structure. The results of the simulations provide a framework for understanding observed differences in the modification of *E. coli* K12 brought about by membrane modification with additional context provided by biophysical experiments with vesicles and cells. Of interest is the finding that while **COE2-3-pCp** has a lower minimum inhibitory concentration (MIC) relative to **COE2-3C**, it can induce similar levels of membrane permeabilization. Implications of increased permeabilization for whole-cell biocatalysis have been previously investigated using *E. coli* K12 and yeast.[32,43,44]

2.2 Synthesis and photophysical properties of COE2-3-pCp

The synthesis of **COE2-3-pCp** is shown in Figure 2.2. 4,16-Dibromo[2.2]paracyclophane (**1**), a pseudo-para isomer of dibromo[2.2]paracyclophane, was used as the key starting material to maintain the overall linearity of the backbone. Compound **1** was converted into **2** by using *s*-BuLi, followed by addition of *N,N*-dimethylformamide (DMF). Formyl groups were then subjected to reduction and chlorination with sodium borohydride and thionyl chloride, respectively, to yield **4**. The intermediate **5** was synthesized using triethyl phosphite. Precursor **7** was prepared under Horner–Wadsworth–Emmons (HWE) reaction conditions from **5** and **6**. Finally, treatment of **7** with

trimethylamine provides **COE2-3-pCp**. **COE2-3C**, which is the planar analogue of **COE2-3-pCp**, was synthesized according to reported protocols.[26,35]

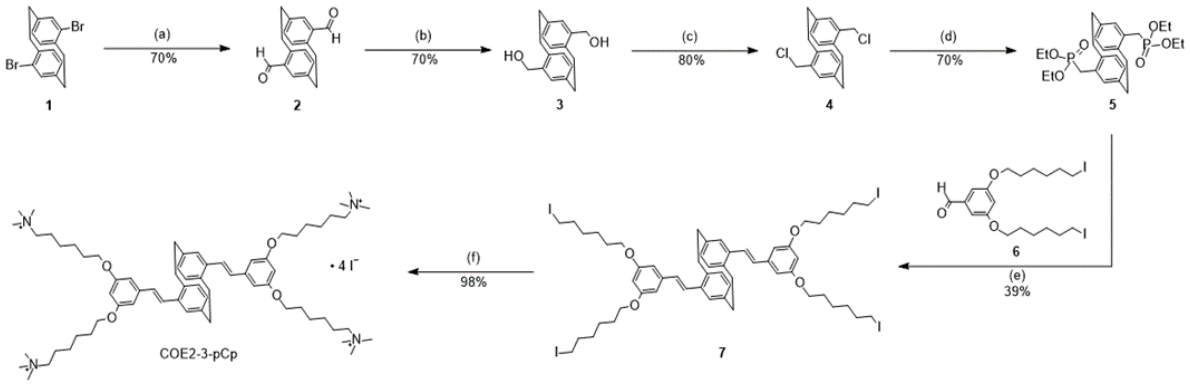

Figure 2.2 Synthesis of paracyclophane-based COE (**COE2-3-pCp**). Reaction conditions: (a) *s*-BuLi (2.3 equiv), DMF (10 equiv), THF, –78 °C to rt, 3 h; (b) $NaBH_4$ (3 equiv), EtOH/THF (1:5), rt, 3 h; (c) $SOCl_2$ (2.4 equiv), MeCN, 50 °C, 5 h; (d) $P(OEt)_3$, 135 °C, 48 h; (e) 6 (1.95 equiv), NaO*t*Bu (2.1 equiv), THF, rt, 6 h; (f) excess NMe_3, THF, MeOH, $CHCl_3$, rt, 48 h.

Absorption and fluorescence spectra of **COE2-3-pCp** are summarized in Figure 2.3 and Table 2.1. The UV-visible absorption spectrum of **COE2-3-pCp** in water shows three absorption peaks in the ultraviolet region, namely, 225 nm, 311 nm and a shoulder peak at 328 nm. The **COE2-3-pCp** fluorescence exhibits an emission maximum at 436 nm. The emission maximum exhibits a hypsochromic shift of 15 nm when treated with a solution of 1,2-dimyristoyl-*sn*-glycero-3-phosphocholine (DMPC) vesicles. In previous studies, it was shown that when COEs intercalate into lipid bilayers, fluorescence emission will shift to shorter wavelength due to the change of environment from a polar (water) to a non-polar (lipid tails) environment. Hence, the observed shift in the emission

of **COE2-3-pCp** in the vesicles suggests that **COE2-3-pCp** similarly intercalates into lipid membranes.[24]

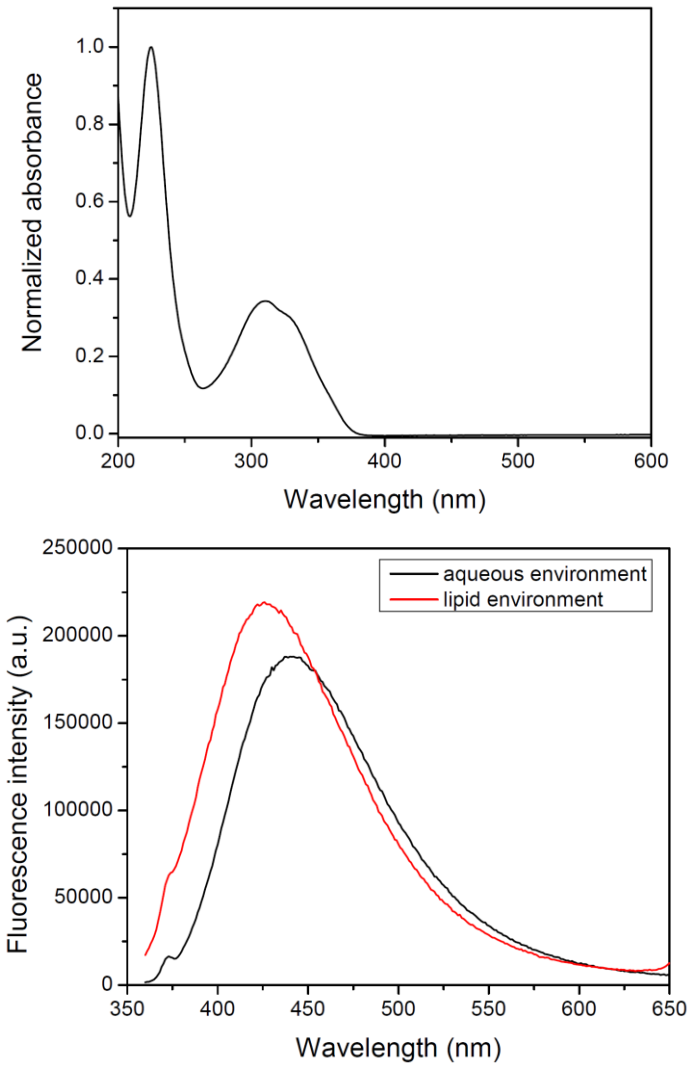

Figure 2.3 UV-Visible absorption spectrum of COE2-3-pCp in water (top); fluorescence spectra of COE2-3-pCp in water (black trend) and when it intercalated into DMPC vesicles (red trend) (bottom).

Table 2.1 Absorption maxima of COE2-3-pCp in water and their molar extinction coefficients (ε).

Absorption maximum (λ_{max} / nm)	Molar extinction coefficient (ε / 10^4 $M^{-1}cm^{-1}$)
225	12.5
311	4.3
328	3.8

2.3 Validation of membrane intercalation of COE2-3-pCp

To validate intercalation into lipid bilayers in microbes, *E. coli* K12 was treated with **COE2-3-pCp** in 50 mM phosphate buffered saline (PBS) at the turbidity of OD_{600} = 1. After staining, cells were centrifuged at 7000 rpm for 7 minutes and the supernatant was collected for UV-visible absorption measurements revealing more than 90% association of **COE2-3-pCp** to *E. coli* K12 cells, even when [**COE2-3-pCp**] = 40 μM (Figure 2.4a). Zeta potentials of cells and liposomes treated with **COE2-3-pCp** in 50 mM PBS were also measured (Figure 2.4b and c). An increase in zeta potential should be observed when COEs intercalate into the bilayers. However, while an increase was observed for liposomes, little change occurred with the cells (Figure 2.4b). The same observations were observed for **COE2-3C** with *E. coli* K12.[45] A plausible reason underlying the relatively constant zeta potential with *E. coli* may be the presence of the lipopolysaccharide (LPS) layer. With the thickness of the LPS being around 2–3 nm in *E. coli* K12, the COE cationic groups may not be able to

reach the surface of the cells after their intercalation into the lipid bilayer due to the molecular length of the COEs.[45–47]

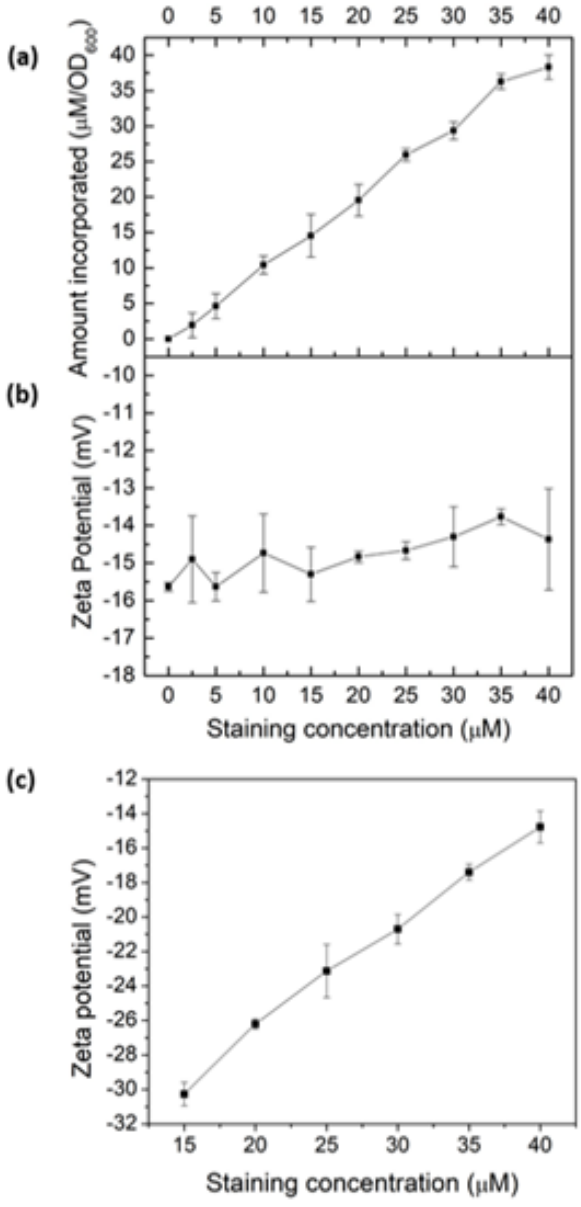

Figure 2.4 (a) **COE2-3-pCp** association to *E. coli* K12 cells; zeta potential of (b) *E. coli* K12, and (c) *E. coli* total lipid extract vesicles at different **COE2-3-pCp** staining concentrations.

To verify **COE2-3-pCp** intercalation, we examined liposomes made of *E. coli* total lipid extract, which lacks the LPS layer. As shown in Figure 2.4c, the zeta potential increased with **COE2-3-pCp** concentration, indicating intercalation into the bilayer. Finally, to visually illustrate COE uptake, fluorescence signals in cell suspensions were imaged using two-photon microscopy. The images clearly show the accumulation of COE on the cells (Figure 2.5).

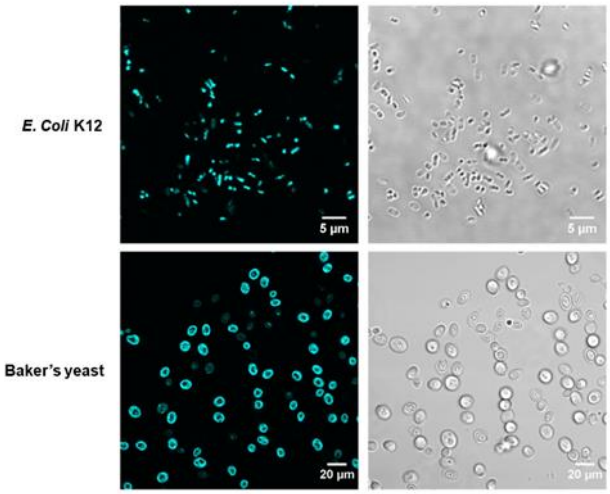

Figure 2.5 Two-photon micrographs of *E. coli* K12 and yeast treated with **COE2-3-pCp** from fluorescence channel (left) and brightfield channel (right). The excitation wavelength was 725 nm.

2.4 Molecular dynamic simulations

Molecular dynamics (MD) simulations were undertaken on Gram-negative model membrane bilayer systems (3∶1 palmitoyloleoylphosphatidylethanolamine/palmitoyloleoylphospatidylglycerol, or POPE/POPG) doped with either **COE2-3-pCp** or **COE2-3C** (COE∶POPE∶POPG = 4∶110∶36). Relative to **COE2-3C**, **COE2-3-pCp** induced a

greater degree of disorder, as illustrated by the more pronounced reduction in deuterium order parameter along the first fatty acid chain (sn1) of POPE predicted for **COE2-3-pCp** (Figure 2.6). The same effect was observed on POPG for both the sn1 and sn2 (*i.e.,* second fatty acid) chain (Figure 2.7).

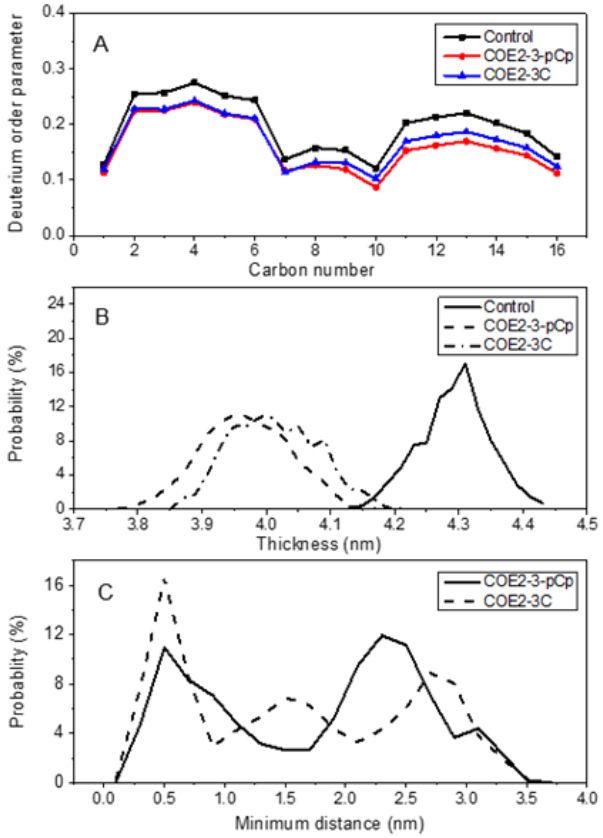

Figure 2.6 (a) Local deuterium order parameter along the sn1 aliphatic chain of POPE for model bilayer system (122∶40, POPE∶POPG) only (*i.e.* control), and with either **COE2-3-pCp** or **COE2-3C** (4∶110∶36, COE∶POPE∶POPG). (b) Probability distribution function for average bilayer thickness for the model bilayer system only (122∶40, POPE∶POPG), and with either **COE2-3-pCp** or **COE2-3C** (4∶110∶36, COE∶POPE∶POPG) based on the center of mass distance between phosphorous atoms in the two leaflets. (c) Probability distribution function of minimum bridging distance between each pair of dopant molecules in model bilayer system simulations with either **COE2-3-pCp** or **COE2-3C** (4∶110∶36, COE∶POPE∶POPG). The data were averaged across the last 50 ns of 3 × 200 ns simulations.

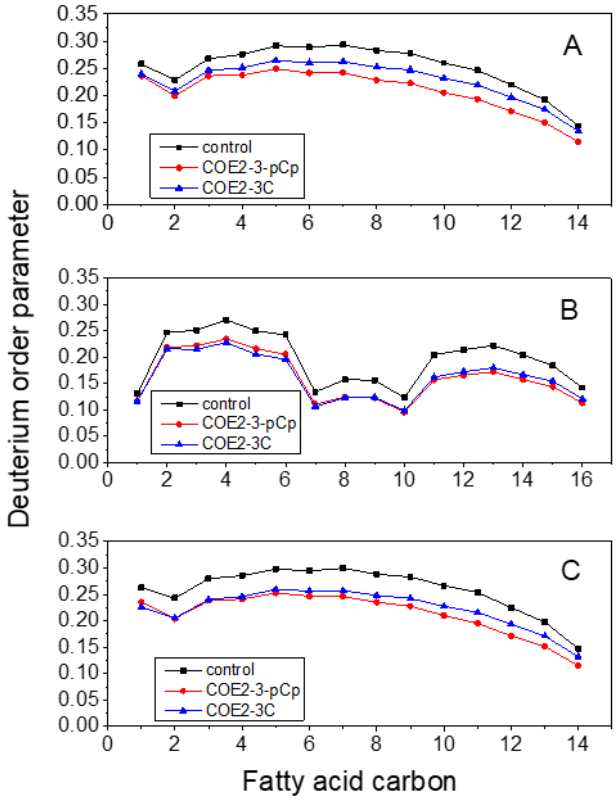

Figure 2.7 (a) Local deuterium order parameter along the sn2 aliphatic chain of POPE for model bilayer system (122:40 POPE:POPG) only (*i.e.* control), and with either **COE2-3-pCp** or **COE2-3C** (4:110:36, COE:POPE:POPG), (b) Local deuterium order parameter along the sn1 aliphatic chain of POPG for model bilayer system (122:40 POPE:POPG) only (*i.e.* control), and with either **COE2-3-pCp** or **COE2-3C** (4:110:36, COE:POPE:POPG), (c) Local deuterium order parameter along the sn2 aliphatic chain of POPG for model bilayer system (122:40 POPE:POPG) only (*i.e.* control), and with either **COE2-3-pCp** or **COE2-3C** (4:110:36, COE:POPE:POPG). The data were averaged across the last 50 ns of 3 × 200 ns simulations.

This increased disorder observed for **COE2-3-pCp** relative to **COE2-3C** resulted in a greater reduction of the average bilayer thickness of the **COE2-3-pCp**-doped lipid bilayer (Figure 2.6b). Earlier studies proposed that the COE length was a key parameter with regards to their antibiotic characteristics. Thus, antimicrobial activity was determined against *E. coli* K12 and yeast using

broth microdilution method.[48] All experiments were performed in triplicate. Specifically, the minimum inhibitory concentrations (MICs) of **COE2-3-pCp** on *E. coli* K12 and yeast are 64 μM and 128 μM, respectively, whereas those of **COE2-3C** are 16 μM and 64 μM, respectively. Modification of the COE by introducing a three-dimensional moiety decreased inhibitory action despite reduction of bilayer thickness. Hinks et al. attributed a reduction in antimicrobial activity of a fluorinated COE to increased range of movement of the COE pendant arm, which reduced the mechanical shock to the lipid bilayer. Another effect of this increased lability was reduced molecular aggregation within the bilayer and it is possible that this also contributed to attenuating **COE2-3-pCp** driven membrane disruption.[36]

According to the probability distribution for intermolecular distance between each COE pair in a four COE simulation (see Section 2.7 for definition) (Figure 2.6c), there was a 36% reduction in the duration that **COE2-3-pCp** molecules exist as an aggregate, relative to **COE2-3C**, as determined from an intermolecular distance of <0.5 nm. While introducing a non-planar aspect to the design of COEs may increase disorder, MD simulations indicate that the effect of this with regards to antimicrobial activity is most reasonably offset by reduced aggregation.

2.5 Whole-cell permeabilization and biocatalysis

COE permeabilization ability was determined by calcein released from *E. coli* total lipid extract vesicles treated with the two COEs. At the COE amount

of 2.5 mol% relative to lipids, **COE2-3-pCp** induced leakage up to 25% in 100 minutes, while **COE2-3C** induced 16% within the same timeframe (Figure 2.8a). This supports the hypothesis that **COE2-3-pCp** has a potential to be a more effective membrane permeabilizer.

The impact of COEs on whole-cell biocatalysis was investigated using *E. coli* K12 hydrolysis of *o*-nitrophenyl ß-D-galactopyranoside (ONPG) by ß-galactosidase.[49,50] Cells treated with COEs show increased catalytic rates. Turnover rates are 2.8 and 2.3-fold faster than untreated cells upon treatment with 25 µM **COE2-3-pCp** and **COE2-3C**, respectively (Figure 2.8b). With the higher MIC of **COE2-3-pCp** compared to **COE2-3C** toward *E. coli* K12, the degree to which association with COEs impacts cell viability can thus be decoupled from the ability to permeabilize the membrane. Such an observation is surprising since these two properties usually follow the same trend.[51]

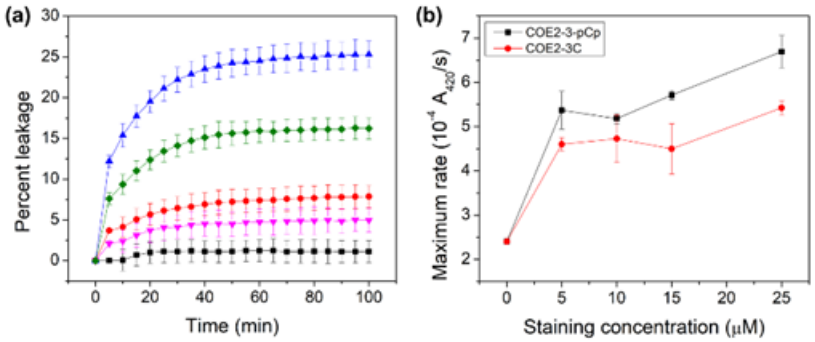

Figure 2.8 (a) Leakage of calcein from *E. coli* total lipid extract vesicles over time (legend: ▲ = 2.5 mol% **COE2-3-pCp**, ● = 1 mol% **COE2-3-pCp**, ♦ = 2.5 mol% **COE2-3C**, ▼ = 1 mol% **COE2-3C**, ■ = control), (b) rate of ONPG hydrolysis at different staining concentrations in *E. coli* K12.

The membrane permeabilization effect was also tested with yeast. Relative extracellular ATP levels were used as an indicator of permeabilization as previously described.[52] The amount of ATP in the supernatant is directly proportional to the observed luminescence signal from the luciferase–luciferin system. Yeast treated with 100 μM of COEs show higher extracellular ATP than control, indicating permeabilization (Figure 2.9a).

The enantioselective hydration of fumarate by fumarase was then chosen for a model system to monitor biocatalysis, as the turnover rate can be accelerated by increasing permeability.[53] Yeast cells were treated with 25 μM COEs per 0.1 g wet cells. Cells with **COE2-3-pCp** show significant catalytic acceleration from untreated cells at comparable degree to those treated with **COE2-3C** (Figure 2.9b). Despite the slightly higher permeabilizing efficacy of **COE2-3-pCp** on *E. coli*, **COE2-3-pCp** is slightly less effective with yeast. Such differences may be related to the differences in membrane composition, but a more precise mechanistic rationale requires further work.

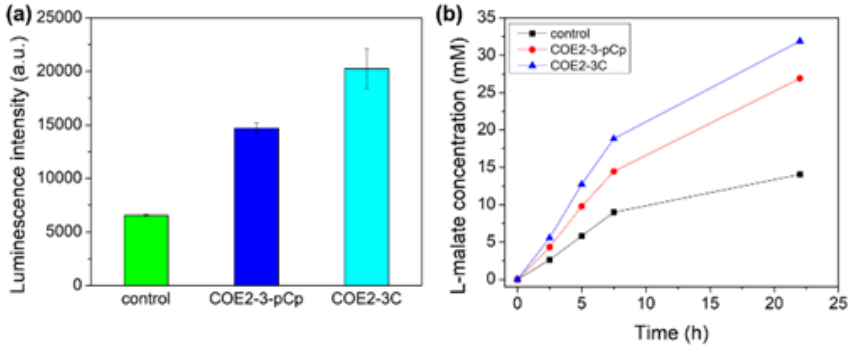

Figure 2.9 (a) Luminescence intensity obtained from extracellular ATP assay with supernatants from yeast cells treated with the COEs, (b) concentration of L-malate produced by yeast over time. Yeast cells were stained with 25 μM of the indicated COEs.

2.6 Conclusions

In summary, the paracyclophane-based **COE2-3-pCp** was designed and synthesized. Despite its similar length and cell association profile to its linear counterpart **COE2-3C**, **COE2-3-pCp** exhibits a higher MIC towards *E. coli* K12 and yeast. Moreover, **COE2-3-pCp** permeabilizes lipid bilayers to a similar extent as **COE2-3C** and thus improves biocatalysis processes in both microorganisms relative to untreated cells. In contrast to the higher MIC of **COE2-3-pCp** compared to **COE2-3C**, MD simulation suggests the pCp unit introduces more lipid disorder with higher extent of membrane thinning. Perhaps more surprisingly, the general molecular topology of **COE2-3-pCp** reduces the tendency to form aggregates in the membrane. To what degree self-association of COEs within the membrane impacts their ability to reduce cell viability remains an open question right now due to the absence of relevant experimental techniques. These insights hint to the strategic design of new COEs to manipulate intermolecular interactions that attenuate growth inhibition, while inducing permeabilization—findings that are relevant within the context of whole-cell biocatalysis.

2.7 Experimental methods

Materials and instruments

All chemicals and solvents were purchased from Sigma-Aldrich, Fisher Scientific, Alfa Aesar, Acros, and 1-Materials and used as received without

further purification unless otherwise stated. Tetrahydrofuran (THF) and *N*,*N*-dimethylformamide (DMF) was purified and dried under solvent purification system. Water was purified using a MilliQ Plus System (Millipore Corporation) to the resistivity of 18 MΩ.cm. Analytical thin layer chromatography was performed using Merck aluminum plate pre-coated with silica gel 60 F254. Flash column chromatography was carried out using silica gel Silicycle SiliaFlash P60 (230-400 mesh). UV-visible absorption spectrum was recorded using Perkin Elmer Lambda 750 spectrometer. Fluorescence spectra were recorded using PTI Quanta Master spectrofluorometer. Nuclear magnetic resonance (NMR) spectra were recorded on a Varian 500 MHz and Varian 600 MHz spectrometers. Cell imaging were performed using an Olympus Fluoview 1000MPE Multiphoton/Laser Scanning Confocal microscope.

Cell culture

A single colony of *E. coli* K12 (ATCC 10798) from an agar plate was cultured in Lysogeny broth (10 g bacto tryptone, 5 g yeast extract, 10 g NaCl in 1 L water) at 37 ºC. Yeast (*S. cerevisiae*) was bought from a local grocery store and rehydrated in yeast selective growth medium (40 g dextrose, 10 g casaminoacids, 3.4 g yeast nitrogen base without $(NH_4)_2SO_4$ and amino acids, 10.6 g $(NH_4)_2SO_4$, 2.7 g Na_2HPO_4, 4.28 g NaH_2PO_4, 100 mg Pen/Strep/Neo, 20 mg Amp, and 20 mg Kan in 1 L water) or 0.1 M neutral phosphate buffer at 30 ºC with 200 rpm shaking.

Zeta potential measurements of *E. coli* K12 cells

E. coli K12 suspension in 50 mM PBS at OD_{600} of 2 was prepared using the same protocol for cell association assay above. 500 μL of the suspension was mixed with 500 μL of COE solution at desired concentrations. The mixtures of COE and cells were then incubated at 30 ºC for 1.5 hours. After incubation, the mixtures were diluted 10-fold. The diluted solutions were used for zeta potential measurements by Zeta Sizer Nano ZS (Malvern Panalytical Inc.)

Zeta potential measurements of *E. coli* total lipid extract vesicles

E. coli total lipid extract (Avanti Polar Lipids) was weighed in a vial, dissolved in chloroform. The lipid solution was dried using rotary evaporator and put under high vacuum overnight. The lipid film was kept at –20 ºC until use. Prepared lipid film was taken out of a freezer and warmed up to room temperature. Then, 50 mM PBS was added to resuspend the lipid. The resulting suspension was extruded through 0.2 μm polycarbonate filter (Whatman) 11 times, followed by 0.1 μm polycarbonate filter (Whatman) 11 times. Freshly prepared vesicles were diluted with the buffer and treated with **COE2-3-pCp** at different final COE concentrations. The final concentration of lipid vesicles was 3 mg mL^{-1}. The vesicles were then incubated at 30 ºC for 1 hour and were sample out for zeta potential measurements using Zeta Sizer Nano ZS (Malvern Panalytical Inc.)

Minimum inhibitory concentration experiments

MIC Experiments were performed based on broth microdilution method on 96-well plates. For *E. coli* K12, cells were inoculated and collected during late log phase. Cell suspension was diluted down in LB to reach 1×10^6 cfu/mL. The resulting suspension was mixed with different concentrations of **COE2-3-pCp** and **COE2-3C** in a 96-well plate (Thermo Fisher). The plate was incubated overnight at 37 °C with 200 rpm shaking. For yeast, cells were rehydrated according to the aforementioned protocol and diluted down in yeast selective growth medium to OD_{600} = 0.04. The resulting suspension was mixed with different concentrations of **COE2-3-pCp** and **COE2-3C** in a 96-well plate (Thermo Fisher). The plate was incubated overnight at 30 °C with 200 rpm shaking for two days. MICs were determined as the lowest concentration of COEs that inhibit visible growth of microorganisms. All experiments were performed in triplicate.

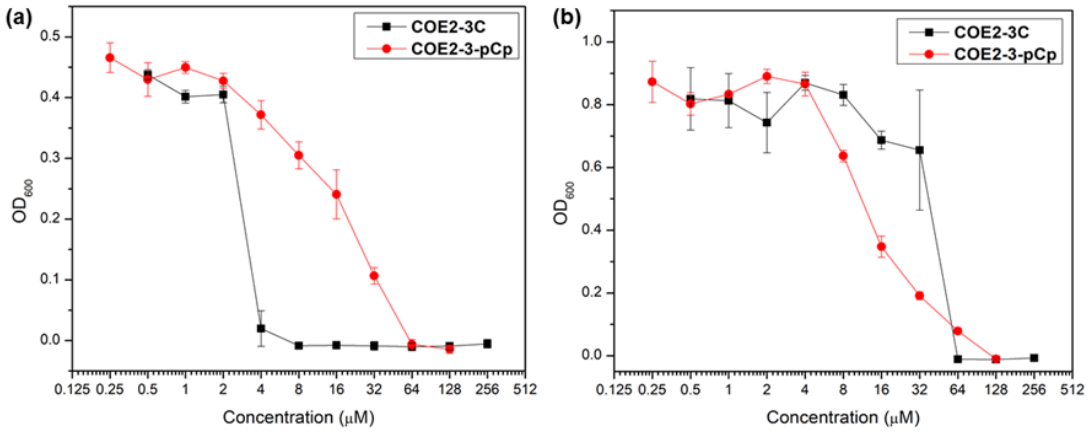

Figure 2.10 Final OD_{600} of (a) *E. coli* K12 and (b) yeast after the incubation with different concentration of **COE2-3C** and **COE2-3-pCp**. MICs are defined as the lowest COE concentration that no growth of microorganisms was observed.

Calcein leakage assay

Lipid film was prepared from *E. coli* total lipid extract (Avanti Polar Lipids) using the same protocol as described in Zeta potential measurements of *E. coli* total lipid extract vesicles. The lipid was resuspended in 20 mM calcein solution in 50 mM PBS. The suspension was extruded through 200-nm and 100-nm filters, respectively. Calcein-loaded liposomes were purified by size exclusion chromatography using Sephadex G50 (bead size 50–150 μm). The liposomes were immediately used after purification. In a 96-well plate (Thermo Fisher), 200 μL of liposome suspension was mixed with 200 μL of **COE2-3-pCp** or **COE2-3C** solution in 50 mM phosphate buffer saline to obtain final COE concentrations of 0, 1, and 2.5 mol% of lipid. The plate was incubated at 30 ºC and the fluorescence signal was recorded every 5 minutes using a Tecan Infinite M200 Plate Reader with the excitation wavelength of 495 nm and the emission wavelength of 520 nm. Liposomes in 3% Triton X-100 was used as a reference for the complete release of calcein.

ONPG turnover assay by *E. coli* K12

A single colony of *E. coli* K12 was inoculated in LB supplemented with 2% lactose to induce *lacZ* expression at 37 ºC overnight with 200 rpm shaking. Cell suspension was then centrifuged at 7000 rpm for 7 minutes to remove the growth medium and washed with M9 minimal salt solution. The cells were resuspended and treated with different concentration of COEs in M9 minimal

salt solution at the final turbidity of 0.6 OD_{600} for 1.5 hours at 30 ºC. Then the cells were centrifuged, washed and resuspended. In a 96-well plate (Thermo Fisher), 100 µL of bacteria suspension, 3.9 mM ONPG solution, and M9 salt solution were mixed together and the absorbance was measured at 420 nm every 5 minutes for 90 minutes at 37 ºC using a Tecan Infinite M200 Plate Reader.

Extracellular ATP assay

The extracellular ATP was quantified as a measure of the membrane damage by **COE2-3-pCp** and **COE2-3C**. Yeast was rehydrated in 0.1 M neutral phosphate buffer at 30 ºC for 1 hour and washed with the buffer. Then, 0.1 g of wet yeast were weighed in clean centrifuge tube and resuspended with 4 mL of the buffer. The yeast was treated with 100 µM of COEs for 120 minutes at 30 ºC. An equal volume of buffer was added in the untreated control. After COE treatment, samples were centrifuged at 4000 × g for 10 min and the supernatant was collected to determine the extracellular ATP concentration. 100 µL of sample was added to 100 µl of BacTiter Glo reagent in a 96-well plate (Corning). After 5 minutes of incubation, the luminescence was measured using a Tecan infinite pro M200 microplate reader. Samples were taken in triplicate and standard deviation was measured. The luminescence was proportional to the amount of extracellular ATP released after membrane damage in the samples.

Fumarate conversion by yeast

In a centrifuge tube with 2 mL of a warm 0.1 M phosphate buffer, 0.3 g of dry yeast cells were suspended, and 12 mL of yeast selective media were added. Cell suspension was incubated at 30 ºC overnight with 200 rpm shaking. After the incubation, the cells were pelleted and washed with the buffer. 0.1 g of wet yeast was used in each reaction tube. The wet yeast cells were treated with 25 μM of COEs in the buffer (4 mL) at 30 ºC for 2 hours. The buffer without any COE was added to the untreated control tube. After that, cells were centrifuged, washed, and resuspended in the buffer containing 50 mM fumaric acid. The tubes were incubated at 30 ºC with 200 rpm shaking. Supernatants were sampled at 2.5, 5, 7.5, and 22 hours of incubation. The aliquots were filtered through 0.22 μm PFTE filter (Thermo Fisher) and diluted 10-fold in an eluent. Amount of L-malate presented in the aliquots was then analyzed by HPLC using a Shimadzu UFLC instrument SIL-20AHT with an organic acid compatible C18 Kinetix column 2.6 μM FS 100A 150 × 4.6 mm. (Pheonomenex). The eluent was 20 mM potassium phosphate pH 2.0 with the flow rate of 1.25 mL/min.

Molecular dynamic simulations

All the Molecular Dynamics (MD) simulations were carried out by Gromacs 4.6.7 package.[54] CHARMM general force field[55] and CHARMM36 lipid force field[56] were used to characterize the COE molecules and the lipid molecules,

respectively. Totally three different systems were simulated in this study (200 ns × 3 repeats), the pure lipid bilayer (referred as control), the lipid bilayer embedded with **COE2-3-pCp** molecules (referred as **COE2-3-pCp**), and the lipid bilayer embedded with **COE2-3C** molecules (referred as **COE2-3C**). The pure lipid bilayer was modeled as a generalized Gram-negative bacterial inner membrane, which contains POPE and POPG with a ratio 122:40. After 200 ns simulation, the last frame was used to build up the COE-embedded bilayers. 6 POPE molecules and 2 POPG molecules were removed from each leaflet of the bilayer to insert 4 COE molecules. The final model (COE:POPE:POPG equals to 4:110:36) is equilibrated for another 50 ns with position restraints of COE molecules before the production run. During the simulation, a leap-frog algorithm was used to integrate Newton's equation of motion, and the time step was set to 2 fs. The Na^+ and Cl^- ions were added to TIP3P water model[57] to neutralize the system and reach a concentration of a 0.15 M physiological salt solution. All the covalent bonds in solutes and solvents were constrained by the LINCS algorithm[58] and the SETTLE algorithm,[59] respectively. The simulations were performed in NPT ensemble with the temperature of 310 K and pressure of 1 bar. The Nose-Hoover algorithm[60] and the semi-isotropic Parrinello-Rahman algorithm[61] were used for the temperature coupling and the pressure coupling. The cut-off for the short-range electrostatics and Lennard-Jones interactions were both set as 1.2 nm and the particle mesh Ewald (PME)[62] algorithm was used to calculate the long-range electrostatic interactions.

The intermolecular distance is defined as the minimum atom-distance in one COE-pair. Two COE molecules are considered contacted if this distance is smaller than 0.5 nm. Four COE molecules lead to six different COE-pairs. The last 50 ns trajectories of the three repeats were used for the statistics. Based on the results, the contacting probability of two COE2-3-pCp molecules is 15.75%, while that of two COE2-3C molecules is 24.57%.

2.8 Synthetic methods

Synthesis of 4,16-diformyl[2.2]paracyclophane (2)

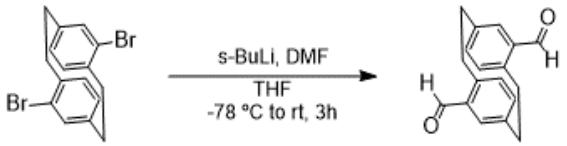

To a dry round bottom flask was charged with 4,16-dibromo[2.2]paracyclophane (**1**) (600 mg, 1.64 mmol) under argon and 36 mL of dry THF was added. The resulting suspension was stirred and cooled down to –78 ºC. Then, *s*-BuLi (1.6 M in cyclohexane) (2.36 mL, 3.77 mmol) was added via syringe. The reaction mixture immediately turned yellow. The solution was stirred at –78 ºC for an hour to ensure complete lithiation. Afterward, 0.6 mL of dry DMF was added. The resulting mixture was heated up to room temperature and kept stirring for 3 hours. Dilute HCl (1 M) was added afterward to quench the reaction. The solution was diluted with dichloromethane, washed with saturated sodium bicarbonate solution followed by brine. Combined organics

were dried over Na_2SO_4. Solvent was removed under reduced pressure. Crude mixture was purified by column chromatography using 2:8 ethyl acetate/hexane as an eluent to obtain white solid (303 mg, 70%).

^{1}H NMR (600 MHz, $CDCl_3$): δ (ppm) = 9.94 (s, 2H), 7.05 (d, 2H, *J* = 2.0 Hz), 6.63 (dd, 2H, *J* = 7.7 Hz, *J* = 2.0 Hz), 6.52 (d, 2H, *J* = 7.7 Hz), 4.15–4.11 (m, 2H), 3.31–3.27 (m, 2H), 3.18–3.13 (m, 2H), 3.04–2.99 (m, 2H); **^{13}C NMR (150 MHz, $CDCl_3$)**: δ (ppm) = 192.04, 143.05, 140.67, 137.11, 136.93, 136.68, 135.38, 34.51, 32.96; **HRMS (ESI)** *m/z* calcd for $C_{18}H_{16}O_2$: 264.1150, found: 264.1160 $[M]^+$.

Synthesis of 4,16-di(hydroxymethyl)[2.2]paracyclophane (3)

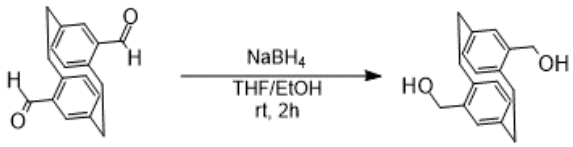

To a dry round bottom flask was charged with 2 (200 mg, 0.757 mmol). 20 mL of THF was later added and the mixture was stirred until all solid dissolved. In a separate flask, $NaBH_4$ (86 mg, 2.27 mmol) was added under inert atmosphere and dissolved in 1 mL of ethanol. The ethanolic solution was immediately transferred to the reaction flask via syringe. The reaction mixture was stirred at room temperature for 2 hours. After reaction completion indicated by TLC, dilute HCl (1 M) was added dropwise to quench any leftover reagent. The resulting mixture was diluted with ethyl acetate, washed with saturated sodium bicarbonate solution and brine. Combined organic phase was dried over Na_2SO_4. Solvent was removed using rotary evaporator. Crude

mixture was recrystallized in ethyl acetate/hexane solvent system to yield compound **3** as white powder (142 mg, 70%).

^{1}H NMR (600 MHz, methanol-d_4): δ (ppm) = 6.63 (dd, 2H, J = 7.7 Hz, J = 1.9 Hz), 6.41 (d, 2H, J = 1.9 Hz), 6.35 (d, 2H, J = 7.7 Hz), 4.69 (d, 2H, J = 13.0 Hz), 4.36 (d, 2H, J = 13.0 Hz), 3.41–3.37 (m, 2H), 3.10–3.01 (m, 4H), 2.88–2.83 (m, 2H); **^{13}C NMR (150 MHz, methanol-d_4):** δ (ppm) = 141.42, 140.75, 138.48, 135.03, 133.84, 129.13, 64.62, 34.60, 33.12; **HRMS (ESI)** *m/z* calcd for $C_{18}H_{20}O_2$: 268.1463, found: 268.1472 $[M]^+$.

Synthesis of 4,16-di(chloromethyl)[2.2]paracyclophane (4)

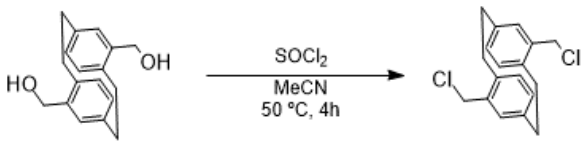

A suspension of 3 (100 mg, 0.373 mmol) in 5 mL of acetonitrile was stirred in a flame-dried round bottom flask under argon. Then, $SOCl_2$ (0.065 mL, 0.894 mmol) was slowly added to the suspension using a syringe. The resulting mixture was stirred under argon at 50 ºC for 4 hours. Excess $SOCl_2$ was quenched via addition of water after the solution cooled down to room temperature. The solution was diluted using dichloromethane, washed with saturated sodium bicarbonate solution and brine. Organic phases were dried over Na_2SO_4. Solvent was removed using rotary evaporator. Crude mixture was recrystallized in dichloromethane/methanol solvent system to yield **4** as white crystalline solid (91 mg, 80%).

^{1}H NMR (600 MHz, $CDCl_3$): δ (ppm) = 6.61 (dd, 2H, *J* = 7.8 Hz, *J* = 1.9 Hz), 6.42 (d, 2H, *J* = 1.9 Hz), 6.38 (d, 2H, *J* = 7.7 Hz), 4.58 (d, 2H, *J* = 11.8 Hz), 4.32 (d, 2H, *J* = 11.8 Hz), 3.46–3.41 (m, 2H), 3.14–3.03 (m, 4H), 2.95–2.90 (m, 2H); **^{13}C NMR (150 MHz, $CDCl_3$):** δ (ppm) = 139.97, 138.17, 136.58, 134.65, 134.44, 130.10, 45.62, 33.94, 32.47; **HRMS (ESI)** *m/z* calcd for $C_{18}H_{18}Cl_2$: 304.0786, found: 304.0791 $[M]^+$.

Synthesis of tetraethyl 4,16-bismethylene[2.2]paracyclophanebisphosphonate (5)

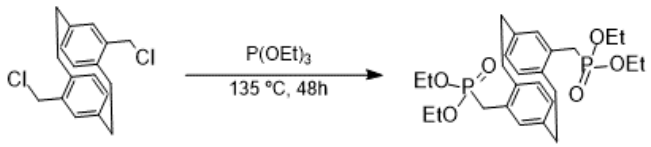

To a dry gas-tight vessel was charged with **4** (142 mg, 0.465 mmol) and 2 mL of $P(OEt)_3$. The vessel was sealed, and the resulting suspension was stirred at 135 °C for 48 hours. After that, the solution was cooled down to room temperature. Precipitates were vacuumed filtered and recrystallized in hot toluene to obtain compound **5** as white crystalline solid (166 mg, 70%).

^{1}H NMR (600 MHz, $CDCl_3$): δ (ppm) = 6.61 (dt, 2H, *J* = 7.9 Hz, *J* = 2.0 Hz), 6.35 (dd, 2H, *J* = 7.9 Hz, *J* = 1.6 Hz), 6.19 (t, 2H, *J* = 1.9 Hz), 3.93–3.82 (m, 8H), 3.48–3.43 (m, 2H), 3.12 (dd, *J* = 14.8 Hz, *J* = 22.0 Hz), 3.08–3.04 (m, 2H), 2.97–2.92 (m, 2H), 2.83 (dd, *J* = 14.8 Hz, *J* = 21.8 Hz), 2.82–2.77 (m, 2H), 1.15 (td, *J* = 7.0 Hz, *J* = 0.8 Hz); **^{13}C NMR (150 MHz, $CDCl_3$):** δ (ppm) = 139.30, 139.28, 138.27, 138.23, 136.76, 136.72, 133.82, 133.80, 131.18, 131.12, 127.42, 127.40, 62.12,

62.08, 62.03, 61.99, 33.24, 33.21, 33.12, 32.32, 16.30, 16.25 (Most peaks appear as doublets which may be caused by C–P couplings); **HRMS (ESI)** *m/z* calcd for $C_{26}H_{38}O_6P_2Na$: 531.2042, found: 531.2046 $[M+Na]^+$.

Synthesis of 7

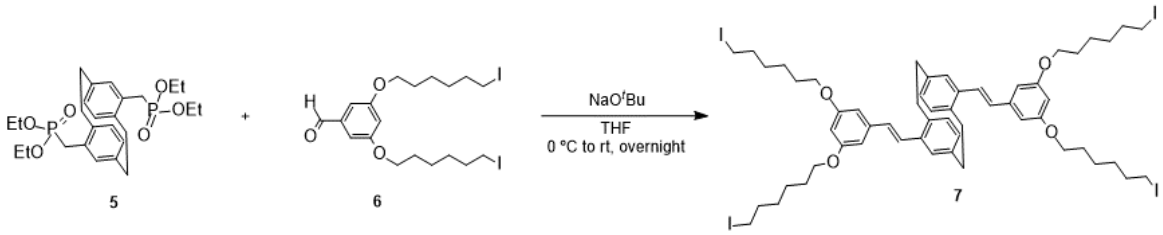

A flame-dried round bottom flask was charged with a Teflon-coated magnetic stir bar, **5** (80 mg, 0.157 mmol), 3,5-bis(6-iodohexyloxy)benzaldehyde (**6**) (171 mg, 0.307 mmol). Anhydrous THF was later added to the flask to dissolve compounds. The resulting solution was cooled down to 0 ºC in an ice bath. Sodium tert-butoxide (32 mg, 0.330 mmol) was taken out of the glovebox in a round-bottom flask and was connected to Schlenk manifold. THF was added to the base and the resulting solution was immediately transferred to the reaction flask via syringe. After complete addition of the base, the reaction was heated up to room temperature and stirred overnight. The mixture was then diluted with dichloromethane, washed with water and brine, dried over Na_2SO_4, and concentrated *in vacuo*. Crude reaction mixture was purified by column chromatography using 1:1 dichloromethane/hexane as an eluent to yield **7** as white powder (81 mg, 39%)

^{1}H NMR (600 MHz, $CDCl_3$): δ (ppm) = 7.16 (d, 2H, *J* = 16.2 Hz), 6.78 (d, 2H, *J* = 16.2 Hz), 6.71 (d, 4H, *J* = 2.4 Hz), 6.66–6.64 (m, 4H), 6.42–6.40 (m, 4H), 4.02 (t, 8H, *J* = 6.6 Hz), 3.56 (t, 2H, *J* = 13.2 Hz), 3.22 (t, 8H, *J* = 7.2 Hz), 3.08 (t, 2H, *J* = 13.2 Hz), 3.02–2.97 (m, 2H), 2.94–2.89 (m, 2H), 1.91-1.82 (m, 16H), 1.57–1.50 (m, 16H); **^{13}C NMR (150 MHz, $CDCl_3$):** δ (ppm) = 160.62, 140.02, 139.60, 138.40, 137.37, 133.70, 130.36, 129.71, 129.56, 127.60, 105.41, 100.62, 68.02, 34.65, 33.56, 33.52, 30.42, 29.28, 25.29, 7.16; **MS (FD)** *m/z* calcd for: 1316.16, found: 1316.2.

Synthesis of COE2-3-pCp

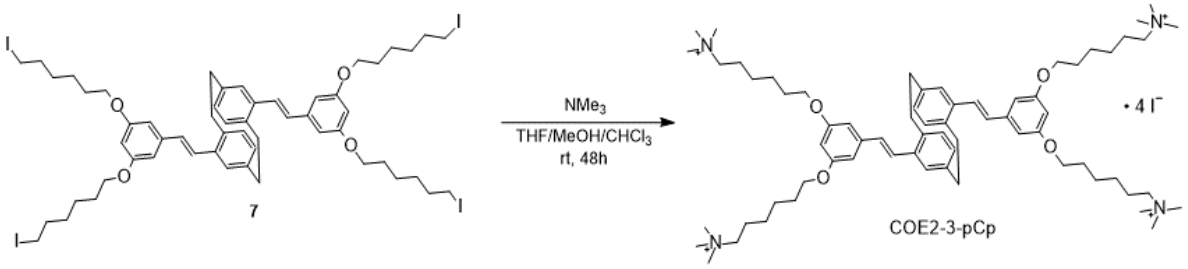

To a round-bottom flask charged with a magnetic stir bar was added **7** (68 mg, 0.052 mmol) under argon. 5 mL of dry THF was added to dissolve all of the solid. Then, a 3.2 M methanolic solution of trimethylamine (0.16 mL, 0.520 mmol) was added via a syringe. The resulting solution was stirred at room temperature for 48 hours. Small portions of chloroform were later added to the flask periodically to dissolve any precipitates formed during the course of the reaction. Organic solvents were removed under reduced pressure and deionized water was added to the flask to dissolve the desired compound. The aqueous

solution was filtered through 0.2 μm filter and freeze dried to yield **COE2-3-pCp** as white fluffy solid (79 mg, 98%).

^{1}H NMR (500 MHz, DMSO-d$_6$): δ (ppm) = 7.26 (d, 2H, *J* = 16.1 Hz), 6.90 (d, 2H, *J* = 16.1 Hz), 6.84 (s, 4H), 6.74 (s, 2H), 6.52 (d, 2H, *J* = 7.7 Hz), 6.44 (d, 2H, *J* = 7.7 Hz), 6.42 (s, 2H), 4.03 (t, 8H, *J* = 6.4 Hz), 3.63–3.61 (m, 2H), 3.06 (s, 36H), 2.92–2.88 (m, 6H), 1.80–1.70 (m, 16H), 1.55–1.49 (m, 8H), 1.40–1.34 (m, 8H); **^{13}C NMR (125 MHz, DMSO-*d*$_6$):** δ (ppm) = 160.05, 139.63. 139.11, 138.17, 137.06, 133.41, 129.92, 129.23, 129.09, 127.15, 105.12, 100.36, 67.39, 65.27, 52.44, 52.21, 52.18, 34.00, 32.69, 28.51, 25.51, 25.12, 22.04; **HRMS (ESI)** *m/z* calcd for $[C_{68}H_{108}N_4O_4I_2]^{2+}$: 649.3230, found: 649.3230 $[M\text{-}2I]^{2+}$.

Chapter 3: Molecular designs of antimicrobial COEs with enhanced selectivity towards bacterial cells[1]

3.1 Introduction

Antimicrobial resistance is expected to cause up to 10 million deaths per year by 2050, along with a massive economic burden.[63,64] Indeed, learned opinions have placed the problem at par with possible damage by climate change.[65–67] Despite the foreseeable crisis, there have been few new antibiotics introduced to the market, in part because of the long drug development cycle, rapid acquisition of drug resistance, and poor investment return.[68,69] Studies of new antimicrobial compounds at a basic research level are thus warranted.[70,71]

Different approaches are being considered for designing new antibiotics that target different machineries in bacterial cells. Examples include cell wall synthesis,[72,73] DNA and RNA synthesis,[74,75] protein biosynthesis,[76] folic acid metabolism,[77] and the cell membrane.[78,79] Compounds that target cell membranes typically kill bacterial cells by selectively disrupting bacterial membranes over mammalian cell membranes due to difference in lipid compositions between the two cell types.[80] Potential advantages of this mechanism include that bacteria are known to be less likely to develop resistance to membrane-disrupting compounds[81,82] and its potential to eradicate persistent infections in which bacteria are in dormant states.[83]

[1] The contents of this chapter have appeared in J. Limwongyut, C. Nie, A. S. Moreland, and G. C. Bazan, *Chem. Sci.*, 2020, **11**, 8138–8144.

Conjugated oligoelectrolytes (COEs) are a class of synthetic water-soluble conjugated molecules containing a conjugated core and pendant ionic groups. COEs have been reported to spontaneously interact with lipid bilayers and modify the properties of bilayers.[24,40] The extent of membrane perturbation can be fine-tuned via molecular design approaches.[33,35] A general guiding principle is that the mismatch between the bilayer thickness and length of the COE leads to membrane disruption.[36,84]

In particular, the distyrylbenzene derivative **COE2-3C-C6** (previously referred to as **COE2-3C**, see Figure 3.1) was reported to have the lowest minimum inhibitory concentration (MIC) against *E. coli* K12 among a homologous series of structures that differed in the number of phenylenevinylene units.[35] We also recently reported a subsequent study that illustrated the relationship between antimicrobial activity and the hydrophobicity of stilbene-based COEs with an apparent correlation between increased hydrophobicity and increased antimicrobial potency.[85] Up to now, the cytotoxicity of COEs against mammalian cells has yet to be explored despite its importance in determining suitable chemical structures for drug development.[86]

With prior information in hand, we describe herein a series of COEs based on the distyrylbenzene core that is generated by modulating two molecular features: linker length (parameter *n*) and terminal alkyl chains length (parameter *m*), see Figure 3.1. We examined antimicrobial efficacy and

mammalian cell cytotoxicity. Bacterial selectivity was determined and the optimal compound in the series was identified thereafter.

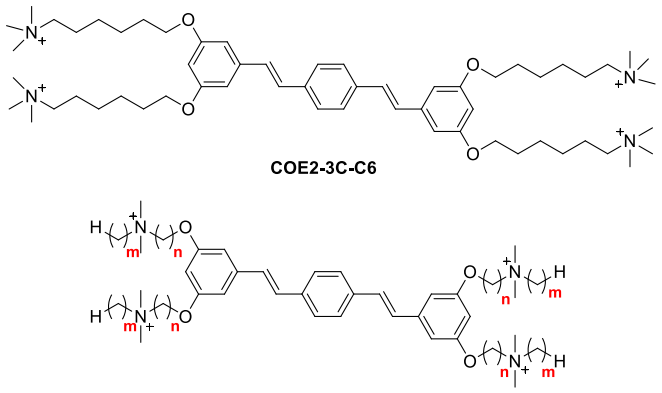

Figure 3.1 Chemical structure of **COE2-3C-C6** (top) and general structure of COEs in this study (bottom).

3.2 Synthesis of distyrylbenzene COEs

The general synthetic approach to generate the new series of COEs is shown in Figure 3.2. Aldehyde precursors were first synthesized by alkylation of methyl 3,5-dihydroxybenzoate with α,ω-dibromoalkanes. Isolated aryl ether products **1a**–**1c** were subsequently reduced by using diisobutylaluminium hydride (DIBAL) and then oxidized with MnO_2 to obtain the aldehyde derivatives **2a**–**2c**. Next, the aldehydes were reacted with compound **3** via Horner–Wadsworth–Emmons (HWE) reaction to obtain distyrylbenzene intermediates **4a**–**4c**. Finkelstein halide exchange reactions were then used for bromide/iodide exchange, thereby yielding neutral intermediates **5a**–**5c**. Finally, **5a**–**5c** underwent quaternization reactions with various tertiary amines to

obtain target molecules. **COE2-3C-C3propyl** (n = 3, m = 3) and **COE2-3C-C4propyl** (n = 4, m = 3) were synthesized via a slightly different pathway (Figure 3.3). Abbreviations of the COEs are listed in Table 3.1.

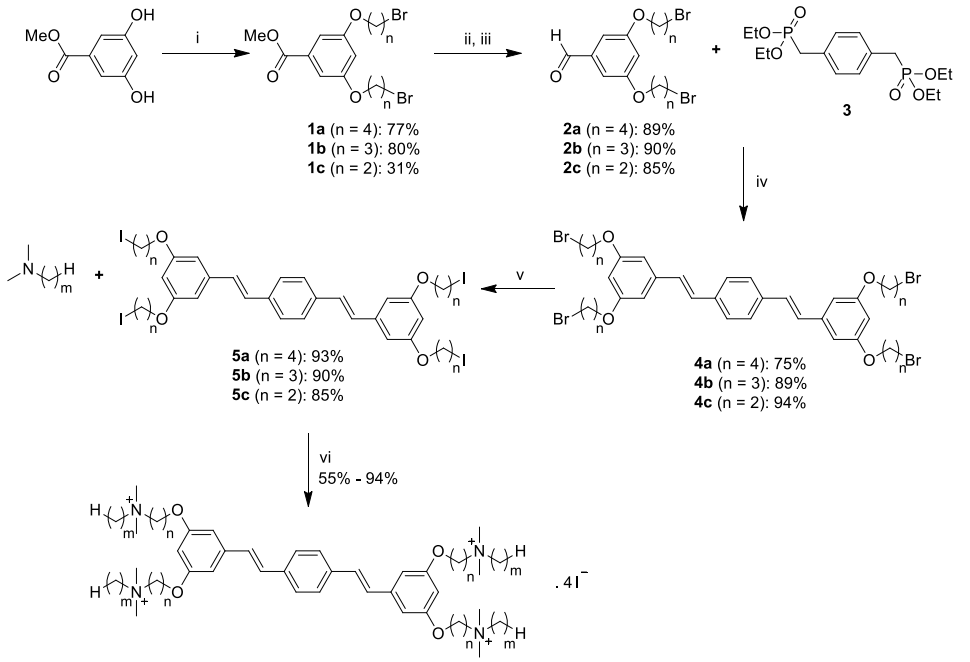

Figure 3.2 Preparation of COEs reported in this study: (i) α,ω-dibromoalkanes, K_2CO_3, acetone, reflux, 2 d; (ii) DIBAL, THF, −78 °C to rt, overnight; (iii) MnO_2, DCM, rt, overnight; (iv) NaO*t*Bu, THF, −78 °C to rt, overnight; (v) NaI, acetone, reflux, 2 d; (vi) DMF, 45 °C, 2 d.

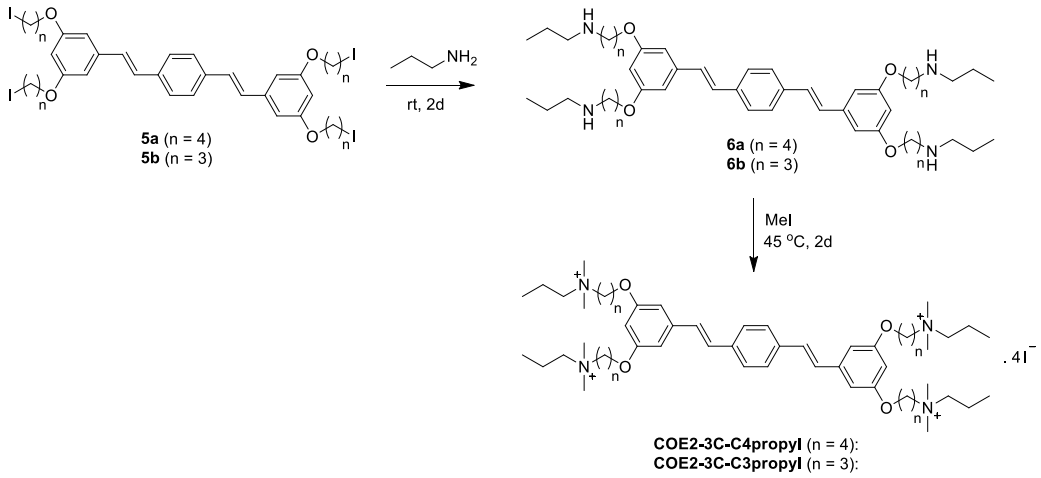

Figure 3.3 Preparation of **COE2-3C-C3propyl** and **COE2-3C-C4propyl** from the intermediates **5a** and **5b**.

Table 3.1 Names of the synthesized COEs in this study.

m	n = 2	n = 3	n = 4
1	**COE2-3C-C2**	**COE2-3C-C3**	**COE2-3C-C4**
2	**COE2-3C-C2ethyl**	**COE2-3C-C3ethyl**	**COE2-3C-C4ethyl**
3	—	**COE2-3C-C3propyl**	**COE2-3C-C4propyl**
4	**COE2-3C-C2butyl**	**COE2-3C-C3butyl**	**COE2-3C-C4butyl**
5	—	—	**COE2-3C-C4pentyl**
6	**COE2-3C-C2hexyl**	**COE2-3C-C3hexyl**	**COE2-3C-C4hexyl**

3.3 Antimicrobial efficacy

The antimicrobial efficacies of COEs were screened by determining minimum inhibitory concentrations (MICs) against Gram-negative bacteria *E. coli* K12 (Figure 3.4a). When the terminal alkyl chains, *i.e., N* substituents, are short ($m \leq 2$), one observes that the MIC gradually increased (less potent antibiotics) in response to decreasing linker length (parameter *n*). For example, at $m = 1$, the MIC values increase from 16 μg mL^{-1} for **COE2-3C-C6** ($n = 6$, $m = 1$) to 128 μg mL^{-1} for **COE2-3C-C2** ($n = 2$, $m = 1$). Similarly, for $m = 2$, MIC increases from 16 μg mL^{-1} for **COE2-3C-C4ethyl** ($n = 4$, $m = 2$) to 64 μg mL^{-1} for **COE2-3C-C2ethyl** ($n = 2$, $m = 2$). Upon elongation of the terminal alkyl chains, the MIC is largely insensitive relative to linker length. As seen in Figure 3.4a, COEs with *N*-substituents of butyl or longer ($m \geq 4$) have similar antimicrobial efficacies, with MICs around 4 μg mL^{-1}. This similarity of the MICs suggests that effects from the terminal alkyl chains dominate over the influence by the

linkers. Therefore, for this limited set of compounds, COEs with $m \geq 4$ are desirable for maintaining good antimicrobial efficacy regardless of linkers. In addition to antimicrobial activities against *E. coli* K12, MICs for a subset of COEs against another Gram-negative bacteria (*K. pneumoniae*) and two Gram-positive bacteria (*E. faecium*, and *S. aureus*) were determined (see Section 3.10, Table 3.3) at Emery Pharma (Alameda, CA). In short, similar trends in MICs were observed in those bacterial strains and all these COEs showed relatively low MICs toward tested Gram-positive bacteria.

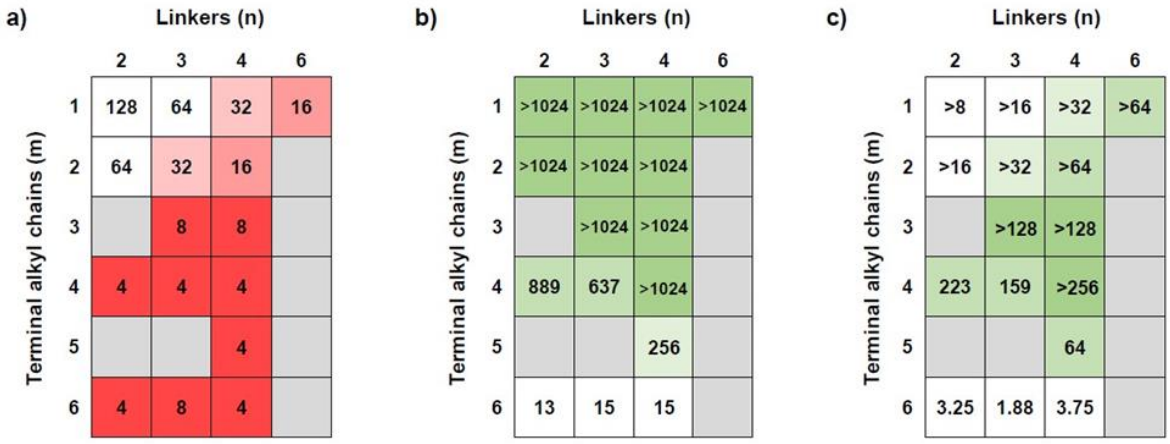

Figure 3.4 (a) MICs of COEs against *E. coli* K12; (b) IC_{50} of COEs against HepG2 cell line; (c) heatmap of IC_{50}/MIC values of each COE. The greener box indicates the higher selectivity toward bacterial cells. All MIC and IC_{50} values are reported in μg mL^{-1}.

3.4 Mammalian cell cytotoxicity

Antimicrobial compounds need to have low MICs against bacteria but also low cytotoxicity toward mammalian cells. In order to determine cytotoxicity,

half maximal inhibitory concentration (IC_{50}) values were determined in vitro against human hepatocellular carcinoma cell line (HepG2) by using the MTT assay. As shown in Figure 3.4b, COEs with $m \leq 3$ show low cytotoxicity, as their IC_{50} values are higher than 1024 μg mL^{-1}, the highest concentration tested. Cytotoxicity generally increases in response to an increase in *m*. For instance, at $n = 4$, IC_{50} decreases from >1024 μg mL^{-1} ($m = 1–4$) to 256 μg mL^{-1} and 15 μg mL^{-1} for pentyl ($m = 5$) and hexyl ($m = 6$) groups, respectively. When the terminal groups are butyl ($m = 4$), there is a slight reduction in IC_{50} values for COEs containing linkers with 3 carbon atoms or less ($n \leq 3$; 889 μg mL^{-1} and 637 μg mL^{-1} for $n = 1$ and 2, respectively). According to the trends of IC_{50}, minimizing cytotoxicity can be realized by having terminal alkyl chains that are butyl groups or shorter ($m \leq 4$). Additionally, at $m = 4$, the four-carbon linker ($n = 4$) is slightly favored due to a small increase in cytotoxicity of COEs with shorter linkers ($n = 2$ and 3).

3.5 Bacterial selectivity analysis

An optimal structure of COEs requires balance between antimicrobial properties and mammalian cell cytotoxicity. With the data in Figure 3.4a and b, a ratio between IC_{50} and MIC was used to evaluate the bacterial selectivity of COEs. Higher IC_{50}/MIC values are more desirable. Figure 3.4c illustrates a heatmap of IC_{50}/MIC values, showing the trend of bacterial selectivity. The heatmap shows that COEs with methyl or ethyl terminal alkyl chains ($m = 1$

and 2) exhibit low selectivity indices due to their low antimicrobial activities (MIC ≥ 16 μg mL^{-1}) despite their low cytotoxicity. On the other hand, COEs containing longer terminal alkyl chains (m = 5 and 6) do not show promising selectivity indices due to cytotoxicity. COEs with hexyl groups (m = 6) have extremely low IC_{50}/MIC values at 3.25, 1.88, and 3.75 for n = 2, 3 and, 4 respectively. **COE2-3C-C4butyl** (n = 4, m = 4) is shown to have highest selectivity index with IC_{50}/MIC greater than 256. Thus, it was identified as the optimal structure for this specific set of compounds.

3.6 Hemolytic activity

Hemolytic activity is an essential measure that determines suitability for in vivo clinical chemistry tests. Thus, the HC_{50} values (defined as a concentration at which 50% of red blood cells were lysed) of COEs were determined towards fresh CD-1 mouse red blood cells, see Table 3.2. In these experiments, red blood cells were collected from whole blood, washed with phosphate buffered saline (PBS) and incubated with different concentrations of **COE2-3C-C4** analogs (n = 4) at 37 °C for 1 hour. After incubation, the red blood cells were removed and the amount of hemoglobin in the supernatant was determined from absorption at 450 nm. Of particular interest from Table 3.2 is that significant hemolysis is observed only with m = 6, with HC_{50} = 53 μg mL^{-1}. At the maximum concentration tested (1024 μg mL^{-1}), there is no significant hemolysis (<5%) of red blood cells treated with COEs with $m \leq 4$. An abrupt change in hemolytic

activity of **COE2-3C-C4pentyl** (m = 5) and **COE2-3C-C4hexyl** (m = 6) suggests that there is a threshold of the length of alkyl chain termini that triggers significant hemolysis. A similar behavior was reported in membrane-active antimicrobial agents with different alkyl side chains.[87,88] The observed hemolytic activity of **COE2-3C-C4** series generally agrees with its trend of cytotoxicity (IC_{50}, Figure 3.4b, n = 4, m = 1–6).

Table 3.2 HC_{50} and percent hemolysis of CD-1 mouse red blood cells treated with COE2-3C-C4 series at 1024 μg mL^{-1} in PBS

Compound	HC_{50} (μg mL^{-1})	Hemolysis at 1024 μg mL^{-1} (%)
COE2-3C-C4	>1024	3.0 ± 0.1
COE2-3C-C4ethyl	>1024	2.3 ± 0.3
COE2-3C-C4propyl	>1024	1.6 ± 0.2
COE2-3C-C4butyl	>1024	4.9 ± 0.6
COE2-3C-C4pentyl	>1024	20.4 ± 2.7
COE2-3C-C4hexyl	53	75.8 ± 1.0

3.7 Cell association studies

Cell association experiments were performed using bacterial and mammalian cells in order to see to what extent COE associating affinity could be correlated to antimicrobial and cytotoxicity profiles. *E. coli* K12 (OD = 1) and HepG2 cells (2×10^6 cells per mL) were treated at 37 °C for 2 hours in Hank's balanced salt solution (HBSS) without calcium and magnesium ions. Cells were

centrifuged and the amount of net unassociated COE in the buffer was determined from the absorbance at 380 nm. The results of these studies are summarized in Figure 3.5 and the numbers of COE molecules associated to each *E. coli* K12 and HepG2 cell were calculated (see Section 3.10, Table 3.4). From Figure 3.5a, one observes that for $n = 4$ there is an increase in association with *E. coli* K12 as m increases from 1 to 6. **COE2-3C-C4hexyl** ($n = 4$, $m = 6$) also shows the highest association to HepG2 cells. However, from $m = 1$ to 5, the associations to HepG2 cells are similar within experimental errors (approximately 20% associated). Figure 3.5b provides the cell association profile for $m = 1$ and $n = 2$–6. Highest association to *E. coli* K12 and HepG2 cells is observed for **COE2-3C-C6** (*i.e.,* $n = 6$, $m = 1$). In this series, association to both cell types decrease for $n \leq 4$. Specifically, association to *E. coli* K12 decreases in a "step function" fashion from 83 ± 1% when $n = 6$ to less than 10% when $n \leq 4$. A decrease in association was also observed for HepG2 cells from 58 ± 3% to 14 ± 11% when n decreases from $n = 6$ to $n = 4$, but is followed by a trend that is difficult to discern given the experimental uncertainties.

By and large, *E. coli* K12 association tracks well with the hydrophobic content in the end groups (Figure 3.5a, parameter m). Considering the linker length (Figure 3.5b), the most hydrophobic compound ($n = 6$, $m = 1$) in the series also shows the highest cell association. A similar behavior has been observed in certain antimicrobial peptides (AMPs).[89] However, the trend of cell association is less clear when $n < 6$ (*i.e.,* 4, 3, and 2). One possible line of thought is that

apart from hydrophobicity, the distance between charges also impacts the equilibrium for intercalation within lipid bilayers because of structural mismatch.

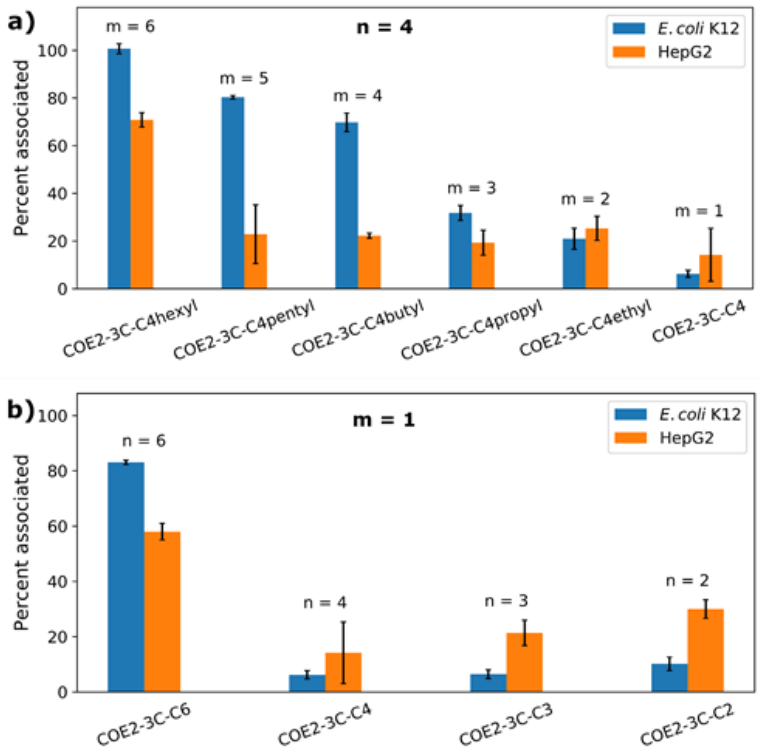

Figure 3.5 Cell association of (a) COEs with different terminal alkyl groups (**COE2-3C-C4** series, n = 4 and m = 1–6) and (b) COEs with different linker length and methyl terminal groups (n = 2, 3, 4, and 6 and m = 1) at the concentration of 20 μM in HBSS with *E. coli* K12 and HepG2 cells.

It is worth noting that there is a similar cell association for **COE2-3C-C4hexyl** (n = 4, m = 6; 101 ± 2% and 14 ± 1% to *E. coli* K12 and HepG2 cells, respectively) and **COE2-3C-C6** (n = 6, m = 1; 83 ± 1% and 12 ± 1% to *E. coli* K12 and HepG2 cells, respectively). However, their MIC and IC_{50} values are different. Specifically, **COE2-3C-C4hexyl** has significantly higher antimicrobial

activity and cytotoxicity (MIC = 4 μg mL^{-1} and IC_{50} = 15 μg mL^{-1}) than **COE2-3C-C6** (MIC = 16 μg mL^{-1} and IC_{50} > 1024 μg mL^{-1}; Figure 3.4a and b). Another interesting observation arises from a similar percent association to cells for **COE2-3C-C4pentyl** (*n* = 4, *m* = 5; 80 ± 1% and 23 ± 12% to *E. coli* K12 and HepG2 cells, respectively) and **COE2-3C-C4butyl** (*n* = 4, *m* = 4; 70 ± 4% and 22 ± 1% to *E. coli* K12 and HepG2 cells, respectively) (Figure 3.5a). Despite their similar associations, they have different IC_{50}/MIC values (64 for **COE2-3C-C4pentyl** and >256 for **COE2-3C-C4butyl**). These two phenomena imply contribution by a specific, molecular-structure-dependent mechanism that impacts cytotoxicity and antimicrobial efficacy.

3.8 Bactericidal activity of COE2-3C-C4butyl against *E. coli*

As a final note, the bactericidal activity of **COE2-3C-C4butyl** was investigated by an *in vitro* time-kill kinetic assay based on its optimal IC_{50}/MIC ratio. It bears noting that according to a time-dependent cell association assay, **COE2-3C-C4butyl** reaches its maximal association to *E. coli* K12 within 30 minutes after treatment (see Section 3.10, Figure 3.11). *E. coli* K12 was challenged with **COE2-3C-C4butyl** at 4× MIC (16 μg mL^{-1}) and 10× MIC (40 μg mL^{-1}). As shown in Figure 3.6, with an exposure at 40 μg mL^{-1} (10× MIC) for 2 hours, a 3 log_{10}-fold decrease in colony forming units (cfu) was observed. Meanwhile, a 3 log_{10}-fold decrease in colony forming units was also achieved within 4 hours with exposure at 16 μg mL^{-1} (4× MIC). As bactericidal activity is

defined as greater than 3 $\log_{10}$-fold decrease in colony forming units, which is equivalent to 99.9% killing of the inoculum, these results indicate an excellent bactericidal activity.

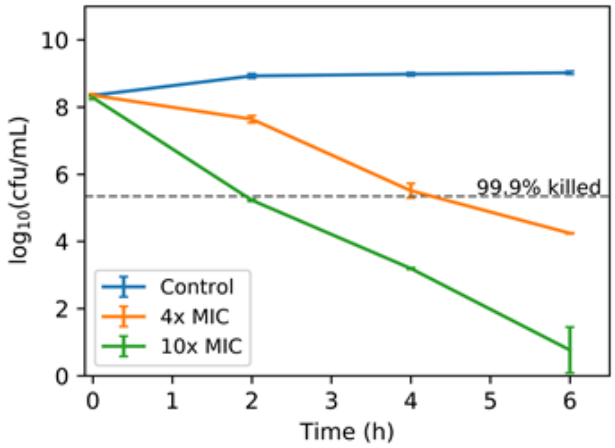

Figure 3.6 Time-kill curves of *E. coli* K12 treated with **COE2-3C-C4butyl** at concentrations of 4× MIC (16 μg mL^{-1}) and 10× MIC (40 μg mL−1).

3.9 Conclusions

In conclusion, we synthesized a series of distyrylbenzene-based COEs with different linker and terminal alkyl chain lengths to explore relationships between molecular features and antimicrobial efficacies and mammalian cell cytotoxicity. We found that hydrophobicity exerts influence over the degree of interactions between COEs and the cells. However, their biological activities were also found to be subtle structure dependent, as seen in cases where COEs exhibit different antimicrobial efficacy or cytotoxicity but a similar degree of cell association. Changes in terminal alkyl chains of COEs have more significant

impacts on MIC and cytotoxicity compared to changes in linker lengths. Although the mechanism underlying this observation is not clear, the data suggest the presence of poorly understood specific interactions that warrant further investigation. The optimal structure within the series of COEs studied here was found to be **COE2-3C-C4butyl** based on its highest IC_{50}/MIC value and minimal hemolytic activity. It is worth noting that this conclusion is specific for tested cell types. Importantly, **COE2-3C-C4butyl** also shows bactericidal activity against *E. coli* K12. These findings provide indications on how to strategically design antimicrobial COEs with low mammalian cell cytotoxicity based on the distyrylbenzene framework.

3.10 Experimental methods

Materials and instruments

Solvent and reagents were purchased from common suppliers unless specified otherwise (*e.g.,* Sigma-Aldrich, Acros Organics, Fisher Scientific, and TCI) and used as received. Dry and inhibitor-free THF and DMF were received from a solvent purification system using packed alumina columns under argon.

Flash chromatography was carried out either on Silicycle SiliaFlash P60 silica gel with pressurized air up to 0.5 bar or on Biotage SNAP C18 columns. For thin layer chromatography (TLC), EMD Millipore Analytical Chromatography TLC Silica gel 60 F254 with aluminum back were used with UV light (254/366 nm) for detection.

^{1}H-NMR (500 MHz and 600 MHz) and ^{13}C-NMR (125 MHz and 151 MHz) were measured on an actively shielded Varian Unity Inova 500 MHz spectrometer or Varian VNMRS 600 MHz. The multiplicity of all signals was described by s (singlet), d (doublet), t (triplet), q (quartet), p (pentet), and m (multiplet). Chemical shifts (δ in ppm) were referenced to the solvent residual peak of $CDCl_3$ (^{1}H-NMR: δ = 7.26; ^{13}C-NMR: δ = 77.0) or DMSO-d_6 (^{1}H NMR: δ = 2.50; ^{13}C-NMR: δ = 39.52). Mass spectra were collected on Waters Micromass LCT-Premier mass spectrometer or Bruker Microflex LDF MALDI-TOF mass spectrometer.

Minimum inhibitory concentration experiments

MICs were determined using broth microdilution method.[48] Prior to MIC experiment, bacterial strains were plated out for single colonies on agar plates from frozen glycerol stocks stored at −80 °C. *E. coli* K12 (ATCC 47076) from a single colony on agar plate was inoculated in LB medium (10 g L^{-1} bactotryptone, 5 g L^{-1} yeast extract, and 10 g L^{-1} NaCl) and cultured at 37 °C with 200 rpm shaking for 5 hours before use. Based on optical density at 600 nm, bacteria suspensions were diluted to the concentration around 1×10^6 cells per mL. Compound solutions were added to sterile 96-well plates and further diluted with 2-fold dilution successively. Later, by adding the bacteria suspensions with the same volume, the final concentrations of compound ranged from 0.5 to 128 μg mL^{-1} and the final concentration of bacteria suspension was

5×10^5 cells per mL. The assay plates were incubated at 37 °C with 200 rpm shaking overnight. A group with no compound treatment was set as a negative control and a group with no bacteria was set as background. OD_{600} of the assay plates were measured on a plate reader (Tecan Spark 10M Multimode). The MICs were read as the lowest treatment concentration where less than 10% relative growth (treatment group relative to control) was found. A commercially available antibiotic, colistin, was used as a positive control and the MIC toward *E. coli* K12 was measured to be 1 μg mL^{-1}, which is in accordance with what is reported in the literature.[90] Experiments were performed with biological replicates.

MICs of selected COEs were determined by Emery Pharma (Alameda, CA) per Clinical and Laboratory Standards Institute (CLSI) guidelines.[91,92] Bacterial strains tested include two Gram-positive bacteria: *Enterococcus faecium* VRE (EF; 1674620), methicillin-resistant *Staphylococcus aureus* (SA; ATCC 33591); and one Gram-negative bacteria: *Klebsiella pneumoniae* MDR (KP; ATCC BAA-2473). COEs were dissolved in DMSO and serially diluted in a 96-well plate while maintaining a final DMSO concentration at 1% v/v in every well. For each bacterial strain, bacteria were inoculated in Cation-Adjusted Mueller Hinton broth (CAMHB) from a single colony picked from a Trypticase Soy Agar (TSA) plate. The inocula were diluted and pipetted into the 96-well plate to achieve 5×10^5 cfu mL^{-1}. The highest concentration of COEs tested was 64 μg mL^{-1}. Plates were incubated for 18–20 hours at 37 ºC. The experiments were

performed in triplicate for each compound. Gentamicin was used as a positive control in the studies. The results are summarized in Table 3.3.

Table 3.3 MICs of selected COEs against *E. faecium* (EA), *S. aureus* (SA), and *K. pneumoniae* (KP).

n	m	Compound	MIC (μg mL^{-1})		
			EF	SA	KP
2	4	**COE2-3C-C2butyl**	1	1	4
3	4	**COE2-3C-C3butyl**	0.25	0.5	4
	6	**COE2-3C-C3hexyl**	0.25	2	2
4	1	**COE2-3C-C4**	8	2	32
	2	**COE2-3C-C4ethyl**	4	1	16
	3	**COE2-3C-C4propyl**	1	1	8
	4	**COE2-3C-C4butyl**	0.5	0.5	8
	6	**COE2-3C-C4hexyl**	0.25	0.5	4
		Gentamicin	>64	1	2

Mammalian cell viability assay

Cellular cytotoxicity was assessed using an MTT viability assay. HepG2 (ATCC HB-8065) cells were seeded at 1 × 10^4 cells per well in 96-well plates overnight at 37 °C in Dulbecco's Modified Eagle's medium (DMEM, Gibco, GlutaMAX™) supplemented with 10% fetal bovine serum (FBS, Gibco, USDA-approved regions) before use. Compounds were serially diluted with 2-fold dilution in PBS and further diluted in culture media to afford a concentration ranging from 2 to 128 μg mL^{-1} and containing 10% PBS (v/v) each. For tests

with higher concentration of compounds, compound stock solutions were prepared in DMSO and diluted in culture media to obtain a concentration ranging from 128 to 1024 μg mL^{-1} and maintain the final DMSO concentration to be less than 1%. The previous culture media were replaced with 100 μL of treatment solutions per well, the assay plates were incubated at 37 °C with 5% CO_2. After 24 hours of incubation, cells were washed with PBS before adding 100 μL of fresh culture media and 10 μL of a 5 mg mL^{-1} solution of 3-(4,5-dimethylthiazol-2-yl)-2,5-diphenyltetrazolium bromide (MTT, Thermofisher Scientific) to each well. After incubation for 2–4 hours, 100 μL of DMSO as solubilizing solution was added to each well, and absorbance at 570 nm were measured on a plate reader (Tecan Spark 10M Multimode). Percent viability was determined by dividing background-corrected absorbance measurements by background-corrected measurements for untreated cells. The percentage of cell viability was plotted against the concentration of COE (Figure 3.7 and Figure 3.8) and IC_{50} values were determined by curve-fitting (Figure 3.9).

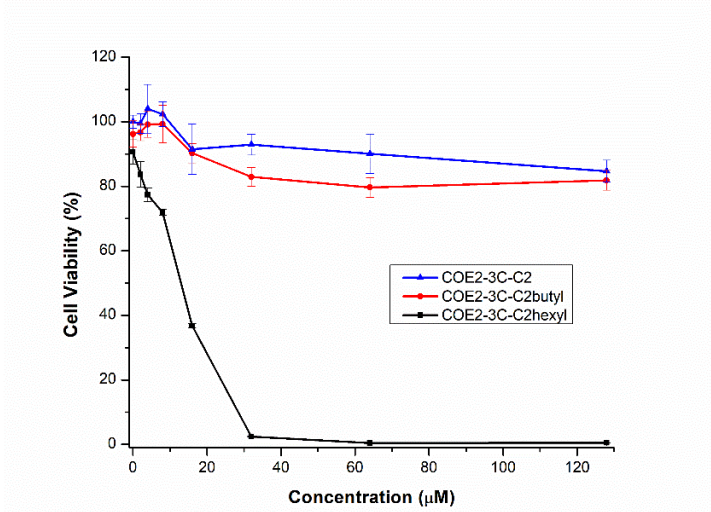

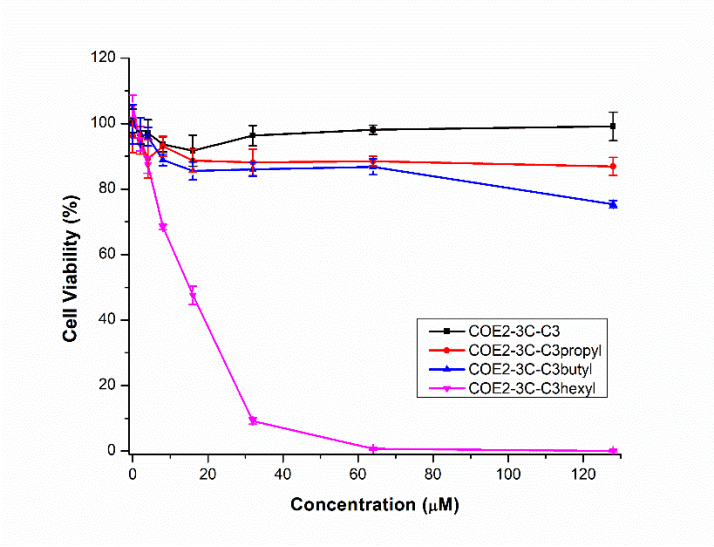

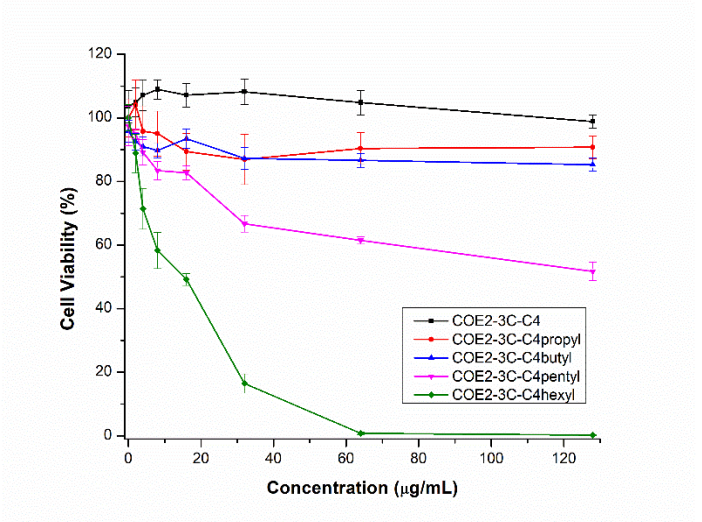

Figure 3.7 Percent viability of HepG2 after treatments with different concentrations of COEs.

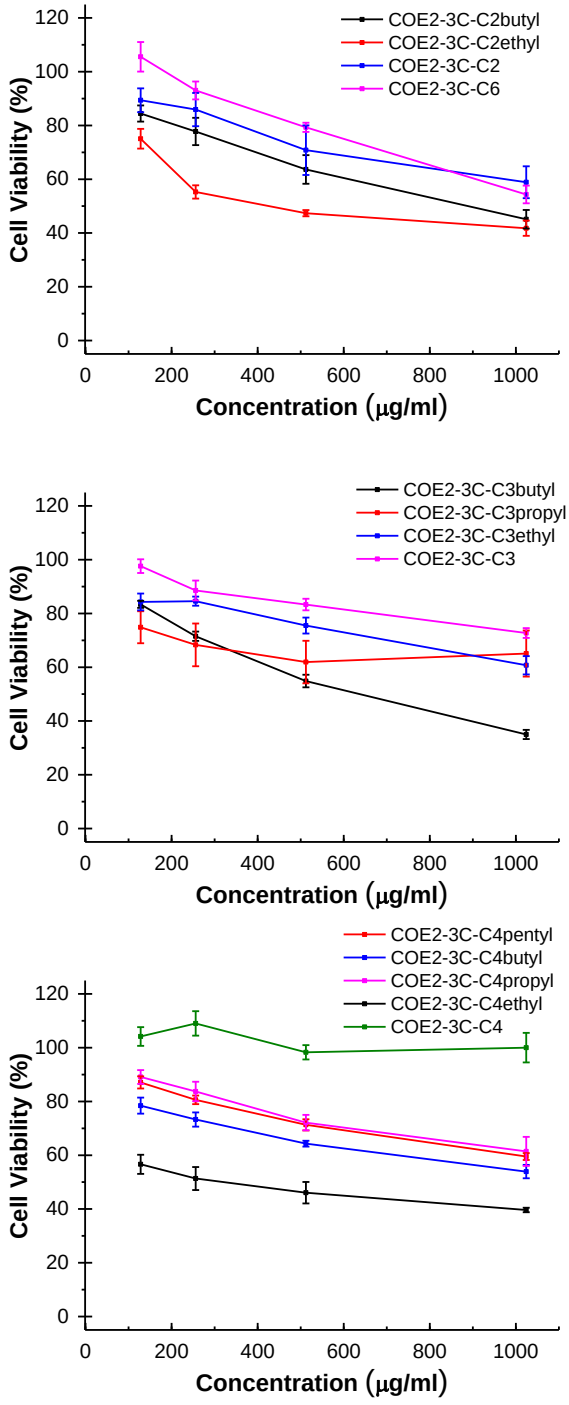

Figure 3.8 Percent viability of HepG2 after treatments with different concentrations of COEs.

Determination of IC_{50} by curve fitting method

The method for IC_{50} curve-fitting was adapted from the method published by Lambert and Pearson for determining MIC values.[93] The data, plotted as cell viability (from 0 to 1) versus the logarithm of COE concentrations, was fit to a Gompertz model. The resulting fit equation was used to determine the IC_{50} by solving for the COE concentration that resulted in $y = 0.5$ (*i.e.,* where cell viability was equal to 50% of control). An example of the fitted data (black), model fit (blue line), and calculated IC_{50} (red) is provided below.

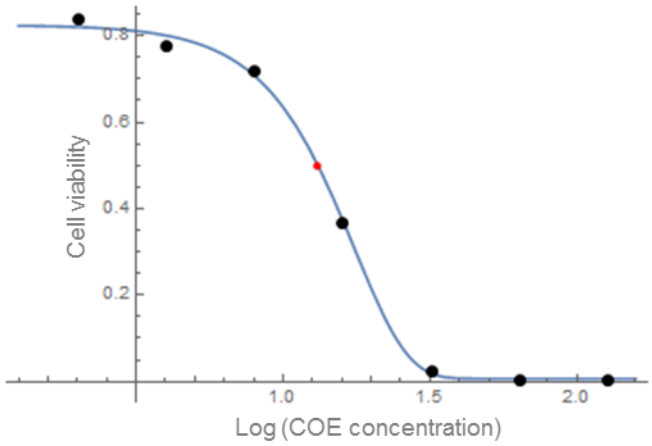

Figure 3.9 Curve fitting method for IC_{50} determination

Hemolytic activity

Fresh CD-1 mouse red blood cells (IC05-3054, Innovative Research, Inc.) were washed with PBS for three times with centrifuge at 500 × g for 5 minutes. The pellet was resuspended to yield a 5% (v/v) suspension in PBS. 160 µL of compound solutions were added to a conical bottom 96-well plate as triplicates and dilute with 2-fold dilution sequentially. A 40 µL portion of 5% red blood cell

solution was added to each well of the 96-well plate. The final concentration of compounds ranged from 16 to 1024 μg mL^{-1} and the final concentration of the red blood cells was 1%. Red blood cells with PBS alone were used as a negative control and with 1% Triton X-100 (Sigma-Aldrich) treatment as a positive control. After incubation for 1 hour at 37 °C, cells were centrifuged at 800 × g. A 100 μL portion of the resulting supernatant was transferred to a flat-bottomed 96-well plate and analyzed on a microplate reader via absorbance measurements at 450 nm. Percent hemolysis was determined by dividing background-corrected absorbance by background-corrected absorbance with 1% Triton X-100 treatment. The percentage of hemolysis was plotted against the concentration of COE (Figure 3.10).

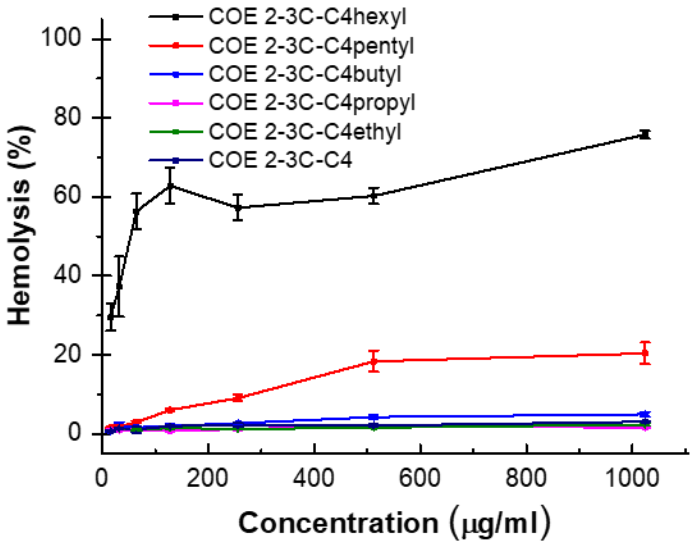

Figure 3.10 Percent hemolysis of CD-1 mouse red blood cells incubated with **COE2-3C-C4** series for 1 h at 37 ºC in PBS.

Cell association experiments

Cell association experiments were performed in both Gram-negative bacteria (*E. coli* K12, ATCC 47076) and mammalian cells (HepG2, ATCC HB-8065). In these experiments, the stock solution of COEs were prepared directly with Hank's Balanced Salt Solution with no calcium and magnesium (HBSS, Gibco). Specific protocols for each cell type are described as follows:

Cell association in *E. coli* K12. Prior the experiments, a single colony of *E. coli* K12 from an agar plate was aerobically inoculated in LB medium at 37 °C for 5 hours with 200 rpm shaking. Cells were spun down at 6500 × g for 5 minutes and washed twice with HBSS and cell density was adjusted to be twice of 1 OD_{600}. In a 96-well PCR plate, 100 µL of the cell suspension was mixed with 100 µL of a COE solution in HBSS in each well. The final concentration of COEs was 20 µM. The plate was sealed prior incubation. After the incubation at 37 °C for 2 hours, the cells were spun down at 3000 × g for 30 minutes and 100 µL of supernatant from each well was transferred to another 96-well plate. Amount of the COEs left in the supernatant was determined by measuring absorbance of the supernatant at 380 nm using Tecan Infinite M200 Plate Reader.

Cell association in HepG2 cells. Prior the experiments, HepG2 cells were cultured in DMEM supplemented with 10% FBS. Cells were then harvested from culture and washed three times with HBSS. Then cell density was adjusted to be around 4×10^6 mL^{-1}. In a 96-well PCR plate, 100 µL of the cell suspension was mixed with 100 µL of a COE solution in HBSS in each well. The

final concentration of COEs was 20 μM. The plate was sealed prior incubation. After the incubation at 37 °C for 2 hours, the cells were centrifuged at 400 × g for 10 minutes and 100 μL of supernatant from each well was transferred to a flat bottom 96-well plate. Amount of the COEs left in the supernatant was determined by measuring absorbance of the supernatant at 360 nm using Tecan Spark 10M Multimode Plate Reader.

After the experiments, the number of COE molecules associated in each cell was determined by the following equation:

$$\text{Molecules associated} = \%\ \text{associated} \times (1.2 \times 10^{13}) / \text{number of cells}$$

The numbers of *E. coli* K12 and HepG2 cells used in each study were 7.4×10^7 cells and 8.0×10^5 cells, respectively. The number of molecules was calculated from the final concentration and volume of COE solutions in these experiments (200 μL of 20 μM solution). The results are shown in Table 3.4.

Table 3.4 The number of COE molecules associated to each *E. coli* K12 and HepG2 cell at 37 ºC for 2 hours in HBSS. The concentration of COEs used was 20 μM.

n	m	Compound	10^5 molecules associated	
			E. coli K12	Hep G2
2	1	**COE2-3C-C2**	0.16 ± 0.04	45.0 ± 5.0
3	1	**COE2-3C-C3**	0.10 ± 0.03	32.1 ± 6.9
4	1	**COE2-3C-C4**	0.10 ± 0.02	21.3 ± 16.7
	2	**COE2-3C-C4ethyl**	0.34 ± 0.07	38.0 ± 7.7
	3	**COE2-3C-C4propyl**	0.51 ± 0.05	29.0 ± 7.8
	4	**COE2-3C-C4butyl**	1.12 ± 0.06	33.3 ± 1.7
	5	**COE2-3C-C4pentyl**	1.28 ± 0.01	34.2 ± 18.5
	6	**COE2-3C-C4hexyl**	1.61 ± 0.04	106.2 ± 4.5
6	1	**COE2-3C-C6**	1.33 ± 0.01	87.0 ± 4.5

Time-dependent cell association experiments with *E. coli*

A single colony of *E. coli* K12 from an LB agar plate was inoculated in LB medium and cells were harvested during a mid-log phase. The cells were centrifuged at 7000 rpm for 5 minutes to remove LB, washed with HBSS, and resuspended in HBSS to achieve the cell concentration twice of the concentration in 1 OD_{600}. The cell suspension was mixed with a solution of **COE2-3C-C4butyl** in HBSS to achieve the COE final concentrations of 10 μM, 20 μM, and 27 μM in microcentrifuge tubes. The tubes were incubated in an incubator at 37 ºC. Treated bacterial suspension was sampled out after 5, 15, 30, 60, 90, and 120 minutes of incubation. Supernatants from the sampled suspension was obtained by pelleting cells at 7000 rpm for 4.5 minutes. The

amount of COE left in the supernatant was determined by the absorption at 380 nm using Tecan Infinite M200 Plate Reader.

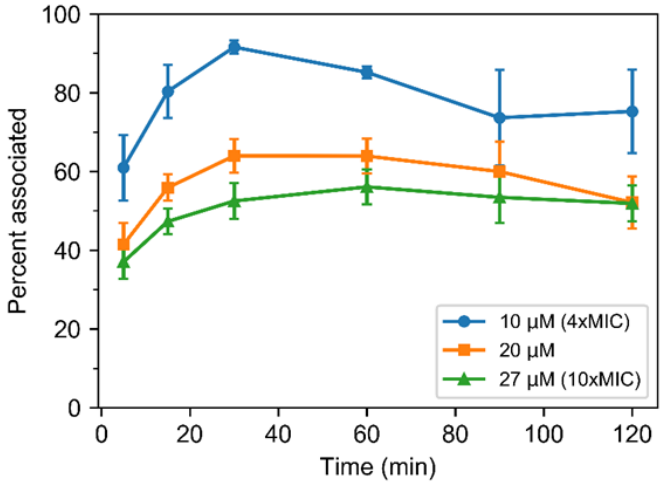

Figure 3.11 Percent association of **COE2-3C-C4butyl** to 1 OD_{600} of *E. coli* K12 in HBSS with the initial concentrations of COEs of 10 µM, 20 µM, and 27 µM.

Time kill kinetics

E. coli K12 (ATCC 47076) from a single colony on agar plate was inoculated in LB medium and cultured at 37 °C and 200 rpm shaking for around 4 hours before use. The bacteria suspension was diluted in LB to afford an OD_{600} value to be around 0.15. The diluted bacteria suspension was then challenged with **COE2-3C-C4butyl** at 10× MIC (40 µg mL^{-1}) and 4× MIC (16 µg mL^{-1}) respectively in culture tubes at 37 °C and 280 rpm shaking. Bacteria suspension without treatment was used as a control. At intervals, 100 µL aliquots from each sample were diluted with 10-fold serial dilution in PBS and were further plated on LB agar plates with 100 µL inoculation. After overnight incubation at

37 °C, colonies were counted and cfu per mL was calculated. Experiments were performed in triplicate.

3.11 Synthetic methods

COE2-3C-C6 in this study was synthesized according to the previously reported procedure.[26]

General procedure for alkylation of 3,5-dihydroxybenzoate

In a round bottomed flask with a magnetic stir bar, methyl 3,5-dihydroxybenzoate (1.0 eq) and K_2CO_3 (2.5 eq) were suspended in acetone followed by an addition of α,ω-dibromoalkane (10 eq). The reaction flask was equipped with a condenser and heated to reflux under inert atmosphere. After stirring for 2 days, the reaction mixture was allowed to cool down. The mixture was diluted with dichloromethane and washed with water. Combined organic phases were washed with brine, dried over Na_2SO_4, and filtered. Solvents in the resulting solution were removed under reduced pressure. Crude product was then purified by silica gel column chromatography (1:1 DCM/hexane) to yield the desired compound.

Methyl 3,5-bis(4-bromobutoxy)benzoate (1a)

1,4-Dibromobutane was used. The product was obtained as white solid (77%). **^{1}H-NMR (500 MHz, $CDCl_3$)**: δ (ppm) 7.16 (d, J = 2.5 Hz, 2H), 6.62 (t, J =

2.5 Hz, 1H), 4.01 (t, J = 6 Hz, 4H), 3.90 (s, 3H), 3.47 (t, J = 6.5 Hz, 4H), 2.10 – 2.04 (m, 4H), 1.98 – 1.92 (m, 4H); **^{13}C-NMR (126 MHz, $CDCl_3$):** δ (ppm) 167.19, 160.29, 132.41, 108.16, 106.98, 67.59, 52.65, 33.73, 29.82, 28.19; **HRMS (ESI):** ($[M+Na]^+$) calcd: 460.9763, found: 460.9754.

Methyl 3,5-bis(3-bromopropoxy)benzoate (1b)

1,3-Dibromopropane was used. The product was obtained as white solid (80%). **^{1}H-NMR (500 MHz, $CDCl_3$):** δ (ppm) 7.19 (d, J = 2.5 Hz, 2H), 6.65 (t, J = 2.5 Hz, 1H), 4.12 (t, J = 5.5 Hz, 4H), 3.91 (s, 3H), 3.59 (t, J = 6 Hz, 4H), 2.53-2.29 (m, 4H); **^{13}C-NMR (126 MHz, $CDCl_3$):** δ (ppm) 166.85, 159.86, 132.24, 108.12, 106.80, 65.77, 52.42, 32.36, 29.94; **HRMS (ESI):** (M^+) calcd: 407.9572, found: 407.9575.

Methyl 3,5-bis(2-bromoethoxy)benzoate (1c)

1,2-Dibromoethane was used. The product was obtained as white solid (31%). **^{1}H-NMR (500 MHz, $CDCl_3$):** δ (ppm) 7.21 (d, J = 2.5 Hz, 2H), 6.69 (t, J = 2.5 Hz, 1H), 4.31 (t, J = 6 Hz, 4H), 3.91 (s, 3H), 3.63 (t, J = 6 Hz, 4H); **^{13}C-NMR (126 MHz, $CDCl_3$):** δ (ppm) 166.51, 159.33, 132.45, 108.61, 107.37, 68.27, 52.50, 28.97; **HRMS (ESI):** (M^+) calcd: 381.9239, found: 381.9240.

General procedure for the synthesis of 3,5-bis(bromoalkoxy)benzaldehydes (2a-2c)

A flame-dried round bottomed flask was charged with a stir bar, methyl 3,5-bis(bromoalkoxy)benzoate (1 eq), and THF. The solution was cooled down to –78 °C in an acetone-dye ice bath. DIBAL (2.5 eq) was added dropwise to the solution via a syringe. The resulting solution was warmed up to room temperature and stirred overnight. The reaction was worked up using Fieser work-up procedure.[94] The crude product was directly transferred to another round bottom flask equipped with a stir bar without further purification. Activated MnO_2 (15 eq) and DCM were added to the flask. The suspension was stirred overnight at room temperature and then filtered through Celite. The solvent was dried under reduced pressure to obtain the desired product.

3,5-bis(4-bromobutoxy)benzaldehyde (2a)

Methyl 3,5-bis(4-bromobutoxy)benzoate (**1a**) was used. The product was obtained as white solid (89% over two steps). **^{1}H-NMR (500 MHz, $CDCl_3$):** δ (ppm) 9.89 (s, 1H), 6.99 (d, J = 2 Hz, 2H), 6.68 (t, J = 2 Hz, 1H), 4.03 (t, J = 6 Hz, 4H), 3.48 (t, J = 6.5 Hz, 4H), 2.10–2.04 (m, 4H), 1.99-1.94 (m, 4H); **^{13}C-NMR (126 MHz, $CDCl_3$):** δ (ppm) 192.01, 160.65, 138.55, 108.12, 107.85, 67.46, 33.39, 29.53, 27.90; **HRMS (ESI):** ($[M+Na+MeOH]^+$) calcd: 462.9919, found: 462.9913.

3,5-bis(3-bromopropoxy)benzaldehyde (2b)

Methyl 3,5-bis(3-bromopropoxy)benzoate (**1b**) was used. The product was obtained as white solid (90% over two steps). **^{1}H-NMR (500 MHz, $CDCl_3$):** δ (ppm) 9.91 (s, 1H), 7.03 (d, J = 2 Hz, 2H), 6.72 (t, J = 2.5 Hz, 1H), 4.15 (t, J = 6 Hz, 4H), 3.59 (t, J = 6.5 Hz, 4H), 2.36-2.32 (m, 4H); **^{13}C-NMR (126 MHz, $CDCl_3$):** δ (ppm) 191.91, 160.49, 138.60, 108.20, 108.05, 65.89, 32.28, 29.84; **HRMS (ESI):** ($[M+Na+MeOH]^+$) calcd: 434.9606, found: 434.9615.

3,5-bis(2-bromoethoxy)benzaldehyde (2c)

Methyl 3,5-bis(2-bromoethoxy)benzoate was used (**1c**). The product was obtained as white solid (85% over two steps). **^{1}H-NMR (500 MHz, $CDCl_3$):** δ (ppm) 9.91 (s, 1H), 7.04 (d, J = 2 Hz, 2H), 6.75 (t, J = 2 Hz, 1H), 4.33 (t, J = 6 Hz, 4H), 3.65 (t, J = 6.5 Hz, 4H); **^{13}C-NMR (126 MHz, $CDCl_3$):** δ (ppm) 191.60, 159.97, 138.72, 108.59, 108.48, 68.33, 28.85; **HRMS (ESI):** ($[M]^+$) calcd: 351.9133, found: 351.9124.

General procedure for HWE reactions of 3,5-bis(bromoalkoxy)benzalhydes (2a-2c).

A flame dried round bottomed flask equipped with a stir bar was charged with 3,5-bis(bromoalkoxy)benzaldehyde (1.95 eq), compound **3** (1 eq), and THF under inert atmosphere. The solution was stirred and cooled down to 0 °C in an ice bath. A solution of sodium *tert*-butoxide (2.2 eq) in dry THF was slowly

added to the reaction flask with a syringe. The resulting solution was allowed to warm up to room temperature and was stirred overnight. The reaction mixture was diluted and extracted with DCM, washed with water and brine, dried over Na_2SO_4. Organic solvents were removed under vacuum. The crude product was purified using silica gel column chromatography (2:3 DCM/hexane) to obtain the desire product.

Compound 4a

The product was obtained as pale yellow solid (75%). **^{1}H-NMR (500 MHz, $CDCl_3$):** δ (ppm) 7.50 (s, 4H), 7.06 (d, *J* = 16.5 Hz, 2H), 7.01 (d, *J* = 16 Hz, 2H), 6.66 (d, *J* = 2.5 Hz, 4H), 6.37 (t, *J* = 2.5 Hz, 2H), 4.02 (t, *J* = 6 Hz, 8H), 3.50 (t, *J* = 6.5 Hz, 8H), 2.12–2.06 (m, 8H), 1.99–1.94 (m, 8H); **^{13}C-NMR (126 MHz, $CDCl_3$):** δ (ppm) 160.40, 139.51, 136.76, 128.93, 128.70, 127.07, 105.38, 101.11, 67.09, 33.59, 29.63, 28.04; **MS (MALDI-TOF):** calcd: 886.0; found: 886.2.

Compound 4b

The product was obtained as white solid (89%). **^{1}H-NMR (500 MHz, $CDCl_3$):** δ (ppm) 7.50 (s, 4H), 7.07 (d, *J* = 16 Hz, 2H), 7.02 (d, *J* = 16.5 Hz, 2H), 6.69 (d, *J* = 2 Hz, 4H), 6.41 (t, *J* = 2 Hz, 2H), 4.13 (t, *J* = 6 Hz, 8H), 3.61 (t, *J* = 6 Hz, 8H), 2.37–2.32 (m, 8H); **^{13}C-NMR (126 MHz, $CDCl_3$):** δ (ppm) 160.23, 139.61, 136.76, 129.06, 128.62, 127.10, 105.59, 101.25, 65.59, 32.51, 30.14; **MS (MALDI-TOF):** calcd: 829.946; found: 830.052.

Compound 4c

Due to very low solubility of the product, the product was purified from crude reaction by vacuum filtration and washed three times with methanol. The product was obtained as white solid (94%). **^{1}H-NMR (500 MHz, DMSO-d_6):** δ (ppm) 7.61 (s, 1H), 7.31 (d, J = 16.5 Hz, 2H), 7.20 (d, J = 16.5 Hz, 2H), 6.85 (d, J = 2.5 Hz, 4H), 6.48 (t, J = 2 Hz, 2H), 4.36 (t, J = 5 Hz, 8H), 3.81 (t, J = 6 Hz, 8H); **MS (MALDI-TOF):** calcd: 773.884; found: 773.969.

General Procedure for Finkelstein Reactions of 4a–4c

In a gas-tight vessel equipped with a magnetic stir bar, **4a**, **4b**, or **4c** (1 eq), NaI (20 eq), and acetone were added under inert atmosphere. The vessel was sealed and heated up to 70 °C (90 °C for 4c) with stirring for 2 days. The reaction mixture was diluted with DCM and filtered through a silica plug. Organic solvents were removed under reduced pressure to yield a target molecule.

Compound 5a

Crude product was purified by recrystallization in DCM/MeOH to obtain the compound as pale yellow solid (93%). **^{1}H-NMR (500 MHz, $CDCl_3$):** δ (ppm) 7.50 (s, 4H), 7.06 (d, J = 16.5 Hz, 2H), 7.01 (d, J = 16 Hz, 2H), 6.66 (d, J = 2.5 Hz, 4H), 6.36 (t, J = 2 Hz, 2H), 4.01 (t, J = 6 Hz, 8H), 3.27 (t, J = 7 Hz, 8H), 2.08–2.02 (m, 8H), 1.95–1.89 (m, 8H); **^{13}C-NMR (126 MHz, $CDCl_3$):** δ (ppm) 160.40,

139.51, 136.76, 128.94, 128.70, 127.07, 105.38, 101.11, 66.89, 30.33, 30.29, 6.55; **MS (MALDI-TOF):** calcd: 1074.0, found: 1074.3.

Compound 5b

Crude product was purified by recrystallization in DCM/MeOH to obtain the compound as yellow solid (90 %). **^{1}H-NMR (500 MHz, $CDCl_3$):** δ (ppm) 7.50 (s, 4H), 7.08 (d, J = 16 Hz, 2H), 7.02 (d, J = 16 Hz, 2H), 6.69 (d, J = 2.5 Hz, 4H), 6.40 (t, J = 2 Hz, 2H), 4.07 (t, J = 6 Hz, 8H), 3.38 (t, J = 7 Hz, 8H), 2.32–2.27 (m, 8H); **^{13}C-NMR (126 MHz, $CDCl_3$):** δ (ppm) 160.22, 139.60, 136.76, 129.07, 128.62, 127.10, 105.60, 101.27, 67.54, 33.12, 2.63; **MS (MALDI-TOF):** calcd: 1017.895, found: 1017.980.

Compound 5c

The product was obtained by vacuum filtration from crude reaction as pale yellow solid (85 %) and was used for quaternization reactions without any further purification.

N,N-dimethylpentylamine

To a flame-dried round bottom flask equipped with a magnetic stir bar, dimethylamine (11.1 mL, 2 M in THF) was added under inert atmosphere. The solution was cooled down to –78 °C using dry ice-acetone bath. 1-Iodopentane (0.3 mL, 2.22 mmol) was added to the flask using a syringe. The reaction flask

was allowed to warm up to room temperature and kept stirring overnight. The reaction mixture was washed with saturated K_3PO_4 solution, extracted with diethyl ether. Combined organic layers were dried over Na_2SO_4. Solvents were removed under reduced pressure to obtain the product as slightly yellow liquid. The product was used without further purification. **^{1}H-NMR: δ (ppm) (500 MHz, $CDCl_3$):** 2.21 (t, *J* = 6 Hz, 2H), 2.21 (s, 6H), 1.48–1.42 (m, 2H), 1.36–1.24 (m, 4H), 0.88 (t, *J* = 7 Hz, 3H); **^{13}C-NMR: δ (ppm) (126 MHz, $CDCl_3$):** 60.11, 45.69, 29.87, 27.64, 22.80, 14.20.

General procedure for quaternization reactions

In a 1 Dr vial equipped with a magnetic stir bar, 20 mg of **5a**, **5b**, or **5c** was added under inert atmosphere. DMF (1 mL) and an amine (10 eq) were then added to the reaction vial. The reaction vial was sealed and kept stirring at 45 °C for 2 days. After cooling down to room temperature, the reaction mixture was precipitated and washed with diethyl ether twice. The precipitate was subjected to reverse phase column chromatography (3:7 MeOH:water) to obtain a pure target molecule. For the ease of handling of the product, the product was dissolved in water and lyophilized.

COE2-3C-C4hexyl

The product was obtained as white solid (60 %). **^{1}H-NMR: δ (ppm) (500 MHz, CD_3OD):** 7.58 (s, 4H), 7.21 (d, *J* = 17 Hz, 2H), 7.14 (d, *J* = 17 Hz, 2H), 6.80 (s,

4H), 6.52 (s, 2H), 4.13 (t, J = 6 Hz, 8H), 3.45–3.48 (m, 8H), 3.35–3.37 (m, 8H), 3.14 (s, 23H), 1.99–2.04 (m, 8H), 1.90–1.94 (m, 8H), 1.76–1.80 (m, 8H), 1.34–1.41 (m, 24H), 0.91 (t, J = 7 Hz, 12H); **^{13}C-NMR: δ (ppm) (126 MHz, CD_3OD):** 161.64, 141.01, 138.15, 129.91, 129.61, 128.03, 106.57, 102.15, 68.18, 65.42, 64.83, 51.48, 32.41, 27.10, 23.60, 23.53, 20.66, 14.31; **HRMS (ESI):** ($[M-2I]^{2+}$) calcd: 668.3778; found: 668.3784.

COE2-3C-C4pentyl

The product was obtained as white solid (65 %). **^{1}H-NMR: δ (ppm) (600 MHz, DMSO-d_6):** 7.61 (s, 4H), 7.28 (d, J = 17 Hz, 2H), 7.20 (d, J = 16 Hz, 2H), 6.82 (s, 4H), 6.45 (s, 2H), 4.06 (t, J = 6 Hz, 8H), 3.35–3.37 (m, 8H), 3.26–3.27 (m, 8H), 3.04 (s, 23H), 1.82–1.84 (m, 8H), 1.76–1.77 (m, 8H), 1.66–1.69 (m, 8H), 1.32–1.35 (m, 8H), 1.23–1.28 (m, 8H), 0.88 (t, J = 6 Hz, 12H); **^{13}C-NMR: δ (ppm) (151 MHz, DMSO-d_6):** 159.80, 139.11, 136.35, 128.54, 128.35, 126.88, 105.18, 100.91, 66.73, 63.00, 62.48, 50.05, 27.90, 25.57, 21.62, 21.40, 18.81, 13.73; **HRMS (ESI):** ($[M-2I]^{2+}$) calcd: 640.3465, found: 640.3456.

COE2-3C-C4butyl

The product was obtained as white solid (75 %). **^{1}H-NMR: δ (ppm) (500 MHz, CD_3OD):** 7.58 (s, 4H), 7.20 (d, J = 17 Hz, 2H), 7.13 (d, J = 17 Hz, 2H), 6.79 (t, J = 2 Hz, 4H), 6.51 (s, 2H), 4.12 (t, J = 6 Hz, 8H), 3.44–3.47 (m, 8H), 3.34–3.38 (m, 8H), 1.98–2.04 (m, 8H), 1.88–1.92 (m, 10H), 1.73–1.79 (m, 8H), 1.38–1.44 (m,

10H), 0.99 (t, J = 8 Hz, 12H); **^{13}C-NMR: δ (ppm) (151 MHz, DMSO-d_6):** 159.81, 139.13, 136.36, 127.01, 126.80, 105.31, 105.30, 105.06, 101.06, 66.76, 62.84, 62.50, 50.03, 25.58, 23.71, 19.20, 18.82, 13.53; **HRMS (ESI):** ($[M-2I]^{2+}$) calcd: 612.3152, found: 612.3157.

COE2-3C-C4ethyl

The product was obtained as white solid (94 %). **^{1}H-NMR: δ (ppm) (500 MHz, DMSO-d_6):** 7.61 (s, 4H), 7.29 (d, J = 16 Hz, 2H), 7.20 (d, J = 16 Hz, 2H), 6.82 (s, 4H), 6.46 (s, 2H), 4.06 (t, J = 6 Hz, 8H), 3.34–3.39 (m, 15H), 3.02 (s, 23H), 1.81–1.87 (m, 8H), 1.74–1.79 (m, 8H), 1.24 (t, J = 7 Hz, 12H); **^{13}C-NMR: δ (ppm) (126 MHz, DMSO-d_6):** 159.81, 139.13, 136.36, 128.56, 128.36, 126.91, 105.19, 100.96, 66.83, 62.00, 58.61, 49.50, 25.62, 18.80, 7.86; **HRMS (ESI):** ($[M-2I]^{2+}$) calcd: 556.2526; found: 556.2526.

COE2-3C-C4

The product was obtained as white solid (94 %). **^{1}H-NMR: δ (ppm) (600 MHz, DMSO-d_6):** 7.60 (s, 4H), 7.25 (dd, J = 36.5, 15.9 Hz, 4H), 6.81 (s, 4H), 6.44 (s, 2H), 4.05 (t, J = 6.2 Hz, 8H), 3.43–3.37 (m, 8H), 3.10–3.04 (m, 36H), 1.90–1.79 (m, 8H), 1.74 (p, J = 6.8 Hz, 8H); **^{13}C-NMR: δ (ppm) (151 MHz, DMSO-d_6):** 160.27, 139.60, 136.82, 129.03, 128.82, 127.36, 109.99, 105.67, 101.43, 67.32, 65.45, 52.74, 52.72, 52.69, 40.43, 40.30, 40.16, 40.02, 39.88, 39.81, 39.74, 39.60, 26.10, 19.70; **HRMS (ESI):** ($[M-2I]^{2+}$) calcd: 528.2213, found: 528.2205.

COE2-3C-C3hexyl

The product was obtained as white solid (62 %). **^{1}H-NMR: δ (ppm) (600 MHz, DMSO-d_6):** 7.63 (s, 4H), 7.27 (dd, J = 28.2, 16.5 Hz, 4H), 6.85 (d, J = 2.1 Hz, 4H), 6.47 (t, J = 2.1 Hz, 2H), 4.11 (t, J = 5.9 Hz, 8H), 3.51–3.45 (m, 8H), 3.09 (s, 24H), 2.22–2.13 (m, 8H), 1.73–1.64 (m, 8H), 1.32–1.27 (m, 24H), 0.88 (t, J = 6.7 Hz, 8H); **^{13}C-NMR: δ (ppm) (151 MHz, DMSO-d_6):** 159.98, 139.76, 136.82, 129.21, 128.73, 127.41, 105.98, 101.61, 65.29, 63.50, 60.86, 50.72, 40.42, 40.28, 40.15, 40.01, 39.87, 39.73, 39.59, 31.12, 25.86, 22.70, 22.34, 22.14, 14.29; **HRMS (ESI):** ($[M-2I]^{2+}$) calcd: 640.3465, found: 640.3469.

COE2-3C-C3butyl

The product was obtained as white solid (72 %). **^{1}H-NMR: δ (ppm) (600 MHz, DMSO-d_6):** 7.63 (s, 4H), 7.27 (dd, J = 26.7, 16.3 Hz, 4H), 6.85 (d, J = 2.3 Hz, 4H), 6.47 (d, J = 1.7 Hz, 4H), 4.11 (t, J = 6.0 Hz, 8H), 3.53–3.44 (m, 8H), 3.09 (s, 24H), 2.24–2.11 (m, 8H), 1.72–1.64 (m, 8H), 1.33 (h, J = 7.4 Hz, 8H), 0.95 (t, J = 7.4 Hz, 12H); **^{13}C-NMR: δ (ppm) (151 MHz, DMSO-d_6):** 159.98, 139.75, 136.83, 129.22, 128.73, 127.43, 105.98, 101.61, 65.31, 63.34, 60.91, 50.72, 40.42, 40.28, 40.14, 40.00, 39.86, 39.72, 39.59, 24.19, 22.71, 19.63, 14.05, 13.98; **HRMS (ESI):** ($[M-2I]^{2+}$) calcd: 584.2839, found: 584.2831.

COE2-3C-C3ethyl

The product was obtained as white solid (80 %). **^{1}H-NMR: δ (ppm) (600 MHz, DMSO-d_6):** 7.63 (s, 4H), 7.28 (dd, J = 30.0, 16.4 Hz, 4H), 6.85 (s, 2H), 6.47 (t, J = 2.2 Hz, 1H), 4.12 (t, J = 6.0 Hz, 8H), 3.52–3.44 (m, 8H), 3.42 (q, J = 7.2 Hz, 8H), 3.07 (s, 24H), 2.21–2.13 (m, 8H), 1.28 (t, J = 7.2 Hz, 13H); **^{13}C-NMR: δ (ppm) (151 MHz, DMSO-d_6):** 160.01, 139.75, 136.83, 129.22, 128.73, 127.43, 105.98, 101.58, 65.33, 60.38, 59.11, 50.16, 40.43, 40.29, 40.15, 40.01, 39.87, 39.73, 39.59, 22.68, 8.36; **HRMS (ESI):** ($[M-2I]^{2+}$) calcd: 528.2213, found: 528.2213.

COE2-3C-C3

The product was obtained as white solid (76 %). **^{1}H-NMR: δ (ppm) (600 MHz, DMSO-d_6):** 7.63 (s, 4H), 7.27 (dd, J = 30.9, 15.9 Hz, 4H), 6.85 (s, 4H), 6.48 (s, 2H), 4.11 (t, J = 6.0 Hz, 8H), 3.56–3.50 (m, 8H), 3.14 (s, 36H), 2.20 (dq, J = 11.9, 6.0 Hz, 8H); **^{13}C-NMR (151 MHz, DMSO-d_6):** 160.02, 139.75, 136.82, 129.23, 128.72, 127.43, 105.98, 101.56, 65.37, 63.47, 63.45, 63.43, 52.87, 52.84, 52.82, 40.41, 40.27, 40.13, 39.99, 39.85, 39.71, 39.57, 23.09; **HRMS (ESI):** ($[M-2I]^{2+}$) calcd: 500.1900, found: 500.1905.

COE2-3C-C2hexyl

The product was obtained as white solid (55 %). **^{1}H-NMR: δ (ppm) (500 MHz, DMSO-d_6):** 7.64 (s, 4H), 7.34 (d, J = 17 Hz, 2H), 7.24 (d, J = 17 Hz, 2H), 6.94 (s, 4H), 6.55 (s, 2H), 4.51 (t, J = 5 Hz, 8H), 3.78 (t, J = 5 Hz, 8H), 3.39–3.42 (m, 8H),

3.16 (s, 22H), 1.72–1.75 (m, 8H), 1.29–1.36 (m, 23H), 0.87 (t, J = 7 Hz, 12H); **^{13}C-NMR: δ (ppm) (126 MHz, DMSO-d_6):** 158.72, 139.43, 136.35, 129.02, 128.08, 126.97, 105.92, 101.40, 64.09, 61.88, 61.69, 50.89, 30.70, 25.44, 21.88, 21.82, 13.83; **HRMS (ESI):** ($[M-2I]^{2+}$) calcd: 612.3152, found: 612.3157.

COE2-3C-C2butyl

The product was obtained as white solid (71 %). **^{1}H-NMR: δ (ppm) (500 MHz, DMSO-d_6):** 7.65 (s, 4H), 7.36 (d, J = 16 Hz, 2H), 7.25 (d, J = 16 Hz, 2H), 6.95 (s, 4H), 6.56 (s, 2H), 4.51 (t, J = 5 Hz, 8H), 3.79 (t, J = 5 Hz, 8H), 3.41–3.44 (m, 8H), 3.17 (s, 23H), 1.71–1.74 (m, 8H), 1.32–1.36 (m, 8H), 0.94 (t, J = 8 Hz, 12H); **^{13}C-NMR: δ (ppm) (126 MHz, DMSO-d_6):** 159.22, 139.96, 136.86, 129.55, 128.59, 127.49, 106.41, 101.95, 64.22, 62.39, 62.23, 51.41, 24.34, 19.72, 14.03; **HRMS (ESI):** ($[M-2I]^{2+}$) calcd: 556.2526, found: 556.2534.

COE2-3C-C2ethyl

The product was obtained as white solid (75 %). **^{1}H-NMR: δ (ppm) (500 MHz, DMSO-d_6)**: 7.64 (s, 4H), 7.36 (d, J = 16.5 Hz, 2H), 7.24 (d, J = 16 Hz, 2H), 6.95 (d, J = 2 Hz, 4H), 6.60 (s, 2H), 4.51 (t, J = 5 Hz, 8H), 3.79 (t, J = 5 Hz, 8H), 3.53-3.50 (m, 8H), 3.15 (s, 24H), 1.30 (t, J = 7 Hz, 12H); **^{13}C-NMR: δ (ppm) (126 MHz, DMSO-d_6):** 158.72, 139.37, 136.34, 129.01, 128.04, 126.95, 105.98, 101.41, 61.70, 61.38, 59.70, 50.29, 8.01; **HRMS (ESI):** ($[M-2I]^{2+}$) calcd: 500.1900, found: 500.1896.

COE2-3C-C2

The product was obtained as white solid (81 %). **^{1}H-NMR: δ (ppm) (600 MHz, DMSO-d_6):** 7.64 (s, 4H), 7.36 (d, J = 16 Hz, 2H), 7.25 (d, J = 16 Hz, 2H), 6.96 (d, J = 2 Hz, 4H), 6.60 (t, J = 2 Hz, 2H), 4.52 (t, J = 5 Hz, 8H), 3.82 (t, J = 5 Hz, 8H), 3.23 (s, 36H); **^{13}C-NMR: δ (ppm) (151 MHz, DMSO-d_6):** 158.71, 139.41, 136.36, 129.01, 128.07, 126.96, 106.04, 101.53, 64.87, 64.04, 53.23; **HRMS (ESI):** ([M-2I]$^{2+}$) calcd: 472.1587, found: 472.1596.

General procedure for COE2-3C-C*n*propyl (*n* = 3 or 4)

In a 1 Dr vial equipped with a magnetic stir bar, **5a** or **5b** was added followed by the addition of propylamine and THF (2:3). The reaction vial was then sealed and kept stirring under inert atmosphere at room temperature. After the solution was stirred for 2 days, the solvent was removed under reduced pressure and the crude reaction was azeotroped with methanol twice. The crude reaction was used without further purification. To the vial, K_2CO_3 (10 eq), iodomethane (20 eq), and DMF was added under inert atmosphere. The resulting suspension was stirred at 45 °C for 2 days. The crude product was precipitated and washed with diethyl ether, purified by reverse phase column chromatography to obtain a pure product. The product was dissolved in water and lyophilized for the ease of handling.

COE2-3C-C4propyl

The product was obtained as white solid (73 %). **^{1}H-NMR: δ (ppm) (500 MHz, DMSO-d_6):** 7.62 (s, 4H), 7.30 (d, J = 17 Hz, 2H), 7.21 (d, J = 17 Hz, 2H), 6.83 (s, 4H), 6.45 (t, J = 3 Hz, 2H), 4.06 (t, J = 7 Hz, 8H), 3.36–3.39 (m, 8H), 3.24–3.27 (m, 8H), 1.82–1.88 (m, 8H), 1.76–1.70 (m, 8H), 1.66–1.75 (m, 8H), 0.89 (t, J = 7 Hz, 12H); **^{13}C-NMR: δ (ppm) (126 MHz, DMSO-d_6):** 167.02, 145.12, 142.17, 133.91, 133.67, 132.16, 109.16, 104.67, 68.47, 65.94, 64.09, 50.71, 24.75, 17.59, 13.98, 8.77; **HRMS (ESI):** ($[M-2I]^{2+}$) calcd: 584.2839, found: 584.2826.

COE2-3C-C3propyl

The product was obtained as white solid (77 %). **^{1}H-NMR: δ (ppm) (500 MHz, DMSO-d_6):** 7.63 (s, 4H), 7.30 (d, J = 17 Hz, 2H), 7.22 (d, J = 17 Hz, 2H), 6.85 (d, J = 2 Hz, 4H), 6.47 (t, J = 2 Hz, 2H), 4.10 (t, J = 6 Hz, 8H), 3.48–3.51 (m, 8H), 3.29–3.31 (m, 8H), 3.09 (s, 22H), 2.15–2.21 (m, 8H), 1.68–1.75 (m, 8H), 0.91 (t, J = 7 Hz, 12H); **^{13}C-NMR: δ (ppm) (126 MHz, DMSO-d_6):** 159.50, 139.25, 136.33, 128.72, 128.22, 126.93, 105.50, 101.12, 64.85, 64.41, 60.55, 50.21, 22.22, 15.41, 10.46; **HRMS (ESI):** ($[M-2I]^{2+}$) calcd: 556.2526, found: 556.2536.

Chapter 4: Amide moieties modulate antimicrobial activities of COEs against Gram-negative bacteria[1]

4.1 Introduction

Failure to combat drug-resistant bacteria is anticipated to result in a sharp increase in lethal infections[63,95] and in the risk of acquiring difficult to treat infections from hospitals.[96] Moreover, a significant increase in antibiotic use against secondary infections during the COVID-19 pandemic is likely to aggravate the prevalence of antibiotic-resistant bacteria.[97–99] Despite the alarming crisis, few new antibiotic classes have been introduced due to factors, such as a long development processes and poor investment incentives.[68,100] Developing novel classes of antimicrobial compounds is, therefore, greatly warranted.

Amphiphilic cationic molecules have emerged as novel antimicrobial agents.[101–103] This class of compounds acts against bacteria by disrupting their membranes and compromising cell integrity and is of relevance due to low resistance acquisition rate and an ability to eradicate metabolically dormant bacteria.[83,104–107] Selectivity towards bacteria is due to differences in lipid compositions between bacteria and mammalian cells.[105]

Considering lipid compositions of bacteria, a fraction of lipid head groups

[1] The contents of this Chapter have been accepted for publication (J. Limwongyut, A. S. Moreland, C. Nie, J. Read de Alaniz, G. C. Bazan, *ChemistryOpen,* 2022).

contains phosphatidylglycerol (PG), which is not commonly present in mammalian cells.[108] PG head groups can act as a hydrogen bond donor. Thus, introducing groups that have a potential hydrogen bonding ability with PG, in addition to electrostatic interactions from cationic groups, may enhance the selectivity of amphiphilic compounds. Indeed, molecular dynamic simulations of an amphiphilic polymer reveal that amide groups form hydrogen bonds with PG head groups and increase specificity towards bacterial membranes.[109]

Conjugated oligoelectrolytes (COEs) are being studied in the context of antibiotic development.[39,85,110] They are a class of amphiphilic compounds bearing a π-conjugated core and cationic pendant groups. In previous work, we showed that cationic COEs with a distyrylbenzene (DSB) framework can be tailored to achieve antimicrobial activities with low cytotoxicity.[111] DSB-COEs reported in the literature only have quaternary ammonium moieties on their side chains. Herein, we report a new series of DSB COEs that include non-peptidic amides on the side chains (Figure 4.1, top). Hydrophobicity was modulated by varying the length of R groups on the side chains. Antimicrobial activities and cytotoxicity profiles of these COEs were explored and compared to two representative COEs that only have quaternary ammonium groups (Figure 4.1, bottom). We also show that the COEs in this study are membrane-active and can disrupt the cytoplasmic membrane (CM) of *E. coli*, a representative Gram-negative bacterium.

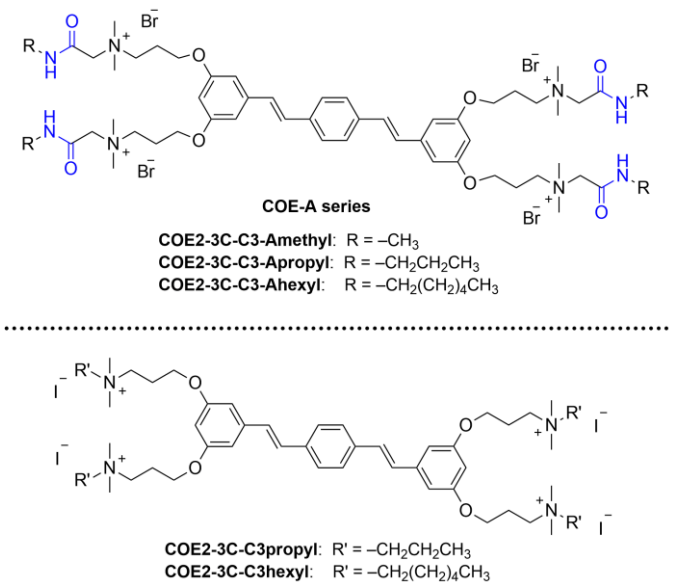

Figure 4.1 Amide-containing COEs (top) and quaternary ammonium COEs used for comparisons in this study (bottom).

4.2 Synthesis of amide containing COEs

The preparation of amide-containing COEs reported herein relies on **COE2-3I-C3**[111] as a common starting material, see Figure 4.2. In brief, **COE2-3I-C3** was reacted with $HNMe_2$ in THF to yield intermediate **1** in quantitative yield. Bromomethyl-functionalized amides **2b**–**2c** were synthesized from the reaction between bromoacetyl bromide and primary amines in the presence of K_2CO_3. Compound **2a** is commercially available. Finally, intermediate **1** was subjected to quaternization reactions with compounds **2a**–**2c** in DMF at 55°C. Target molecules were obtained in a good yield by precipitating reaction mixtures in diethyl ether, followed by purifications using reverse-phase column chromatography. With one common intermediate **1** and straightforward purification, the synthesis is relatively simple and of low cost. Compounds

COE2-3C-C3propyl and **COE2-3C-C3hexyl** were synthesized according to a previously reported procedures.[111]

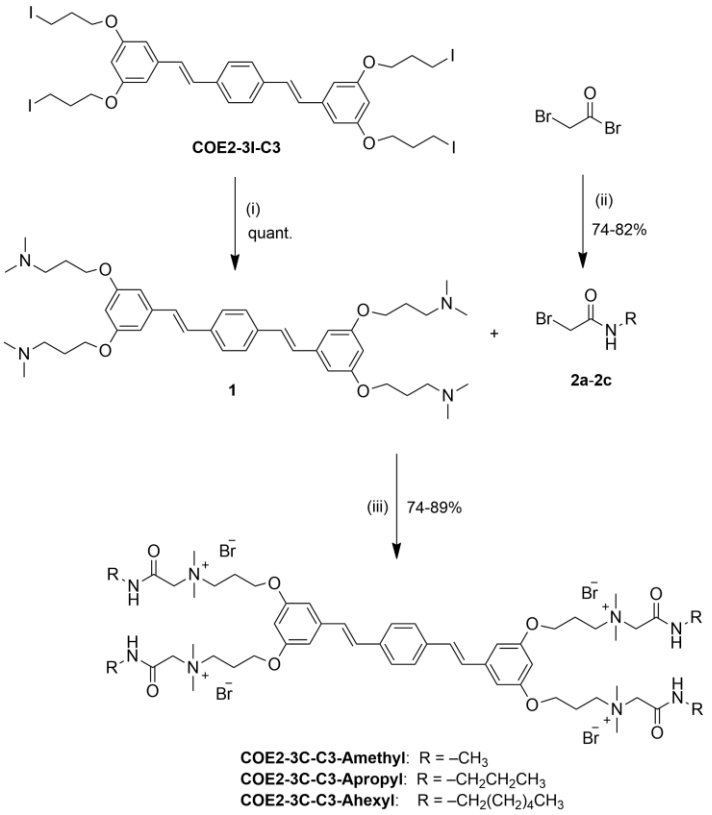

Figure 4.2 Synthesis pathway of amide-containing COEs from **COE2-3I-C3**. Reaction conditions: (i) excess $NH(CH_3)_2$, THF, rt, 48 h; (ii) R–NH_2 (0.91 equiv.), K_2CO_3 (1.1 equiv.), DCM, –5°C to rt, 3 h; (iii) DMF, 55°C, 48 h.

4.3 Antimicrobial activities

Antimicrobial activities were evaluated against *E. coli* K12 (ATCC 47076) by determining their minimum inhibitory concentrations (MICs) in an LB medium (Table 4.1). The decrease in MIC from **COE2-3C-C3-Amethyl** (16 μg mL^{-1}) to **COE2-3C-C3-Apropyl** (2 μg mL^{-1}) would be reasonably attributed to an increase

in hydrophobicity with longer alkyl chains. However, the MIC of **COE2-3C-C3-Ahexyl** is 8 μg mL^{-1}. We note that **COE2-3C-C3-Ahexyl** solutions turn turbid in LB at concentrations >128 μg mL^{-1}, despite its high water solubility (>10 mg mL^{-1}). Since LB broth contains undefined proteins, this could indicate that **COE2-3C-C3-Ahexyl** binds to proteins in the medium resulting in a lower effective concentration and concomitant decreased antimicrobial efficacy. Such phenomenon has been observed in other antimicrobial agents.[112] **COE2-3C-C3propyl** and **COE2-3C-C3hexyl** both have an MIC of 8 μg mL^{-1}. To demonstrate that COEs have antimicrobial activities against other Gram-negative bacteria, MICs of COEs against *K. pneumoniae* and *S. enterica* Typhimurium were also determined (Table 4.3). The relative activities against these two bacteria show a similar trend to the activities against *E. coli* K12.

We measured MIC values in the presence of 40 g L^{-1} human serum albumin (HSA) in LB.[113,114] Table 4.1 shows that antimicrobial activities of COEs with hexyl chains (**COE2-3C-C3-Ahexyl** and **COE2-3C-C3hexyl**) suffer with the presence of HSA with a four-fold increase in MIC (32 μg mL^{-1}). **COE2-3C-C3-Amethyl** has slightly increased in MIC (2-fold increase) while the activities of **COE2-3C-C3-Apropyl** and **COE2-3C-C3propyl** were not affected. **COE2-3C-C3-Apropyl** therefore has the lowest MIC against *E. coli* and its antimicrobial activity was not affected by the presence of HSA.

Table 4.1 Summary of MICs, IC_{50}'s, HC_{50}'s and selectivity indices of COEs in this study.

Compound	MIC[a] (μg mL^{-1})	MIC with HSA[b] (μg mL^{-1})	IC_{50}[c] (μg mL^{-1})	HC_{50} (μg mL^{-1})	Selectivity index (HC_{50}/MIC)
COE2-3C-C3-Amethyl	16	32	>1,024	>1,024	>64
COE2-3C-C3-Apropyl	2	2	740	>1,024	>512
COE2-3C-C3-Ahexyl	8	32	10	40	5
COE2-3C-C3propyl	8	8	>1,024	>1,024	>128
COE2-3C-C3hexyl	8	32	15	197	15

[a] MIC against *E. coli* K12 in LB, [b] The concentration of HSA was 40 g L^{-1}, [c] IC_{50} against the HepG2 cell line.

4.4 Cytotoxicity and hemolytic activities

In vitro cytotoxicities against the human hepatocellular carcinoma cell line (HepG2) were measured and are reported in terms of half maximal inhibitory concentration (IC_{50}) values. According to Table 4.1 and Figure 4.3, IC_{50} values show a correlation to the length of the alkyl groups on the side chains. There is no detectable cytotoxicity from **COE2-3C-C3-Amethyl**, even up to of 1,024 μg mL^{-1}. **COE2-3C-C3-Apropyl** retains relatively low cytotoxicity with IC_{50} = 740 μg mL^{-1}. However, **COE2-3C-C3-Ahexyl** is cytotoxic (IC_{50} = 10 μg mL^{-1}). This trend is also observed for **COE2-3C-C3propyl** and **COE2-3C-C3hexyl**, which have IC_{50} values of >1,024 μg mL^{-1} and 15 μg mL^{-1}, respectively. These data

suggest that considerations of hydrophobicity are particularly useful to minimize undesirable cytotoxicity profiles.[111]

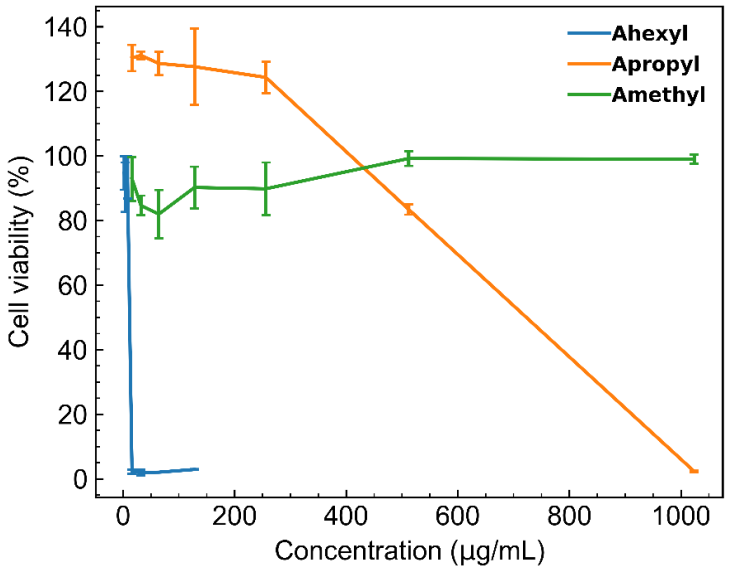

Figure 4.3 Cell viability of HepG2 cells after treatments of COEs measured by Cell Counting Kit-8 (CCK-8)

The half maximal hemolytic concentration (HC_{50}) value for each compound was determined towards human red blood cells, as described previously.[111] One can observe from Table 4.1 that among amide-containing COEs, only **COE2-3C-C3-Ahexyl** shows high hemolytic activity (HC_{50} = 40 µg mL^{-1}), whereas no hemolytic activity was detected, even up to 1,024 µg mL^{-1}, for **COE2-3C-C3-Amethyl** and **COE2-3-C3-Apropyl** (Figure 4.4). A similar observation was observed with **COE2-3C-C3propyl** (HC_{50} >1,024 µg mL^{-1}) and **COE2-3C-C3hexyl** (HC_{50} = 197 µg mL^{-1}). Like cytotoxicity against HepG2 cells, hemolytic activities corelate well to general considerations of hydrophobicity. Taking activity and

safety considerations into account, **COE2-3C-C3-Apropyl** was identified to be the optimal compound with a selectivity index (HC_{50}/MIC) greater than 512.

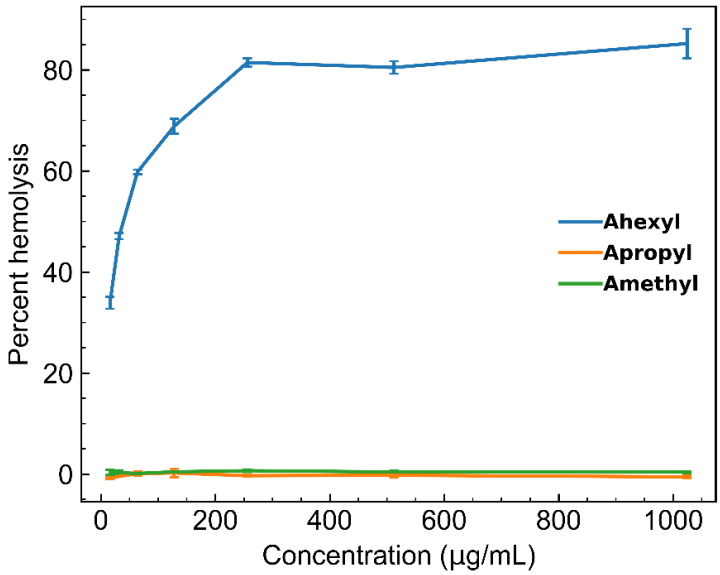

Figure 4.4 Percent hemolysis of human red blood cells after treatments with COEs.

4.5 Effects of COEs on membrane model vesicles

Insights into how structural variations impact membrane stability were sought by measuring calcein leakage from model lipid vesicles. Vesicles mimicking bacterial membranes comprised 1-palmitoyl-2-oleoyl-*sn*-glycero-3-phosphoethanolamine (POPE) and 1-palmitoyl-2-oleoyl-*sn*-glycero-3-phosphoglycerol (POPG) in a ratio of 3:1.[115] As shown in Figure 4.5a, **COE2-3C-C3-Ahexyl** induced the highest level of leakage at 57%. **COE2-3C-C3-Apropyl** and **COE2-3C-C3hexyl** induced a similar level of permeabilization, with leakages of 29% and 34%, respectively. **COE2-3C-C3-Amethyl** (11%) and **COE2-**

3C-C3propyl (13%) were the least disruptive. In general, amide containing COEs are more effective as illustrated by that **COE2-3C-C3-Apropyl** induced calcein leakage 2.2 times higher than **COE2-3C-C3propyl** and **COE2-3C-C3-Ahexyl** induced 1.7 times more leakage compared to **COE2-3C-C3hexyl**. According to the relative hydrophobicity of COEs, as determined by RP-HPLC retention time measurements, amide containing COEs have similar hydrophobicity compared to non-amide COEs with the same terminal alkyl groups (Table 4.2).

Table 4.2 RP-HPLC retention times of COEs in this study.

Compound	Retention time (min)
COE2-3C-C3-Amethyl	13.4
COE2-3C-C3-Apropyl	20.8
COE2-3C-C3-Ahexyl	11.1
COE2-3C-C3propyl	14.8
COE2-3C-C3hexyl	21.2

This suggests that significant increases in leakage-inducing activities of amide containing COEs are not due to the increased hydrophobicity of the molecules. That the general trend in permeability in Figure 4.5a does not correlate to the MIC trend on Table 4.1 hints to possible non-specific interactions of COEs with components in the LB media (*vide supra*) or interactions between COEs and other cell wall components.

Unlike bacteria, mammalian cell lipids largely consist of the zwitterionic head group phosphatidylcholine (PC).[108] Mammalian cell lipid mimic vesicles were thus prepared from egg yolk L-α-phosphatidylcholine (EYPC). Calcein release measurements (Figure 4.5b) show a different trend from that observed for the POPE/POPG system. Specifically, **COE2-3C-C3hexyl** treatment resulted in complete release of calcein. **COE2-3C-C3-Ahexyl** also caused a high level of leakage (73%), followed by **COE2-3C-C3-Apropyl** (12%). No increase in calcein signal was observed in vesicles treated with **COE2-3C-C3propyl**. This trend fits well with *in vitro* cytotoxicity profiles in Table 4.1. To our surprise, we observed a decrease in calcein emission with **COE2-3C-C3-Amethyl**. According to dynamic light scattering measurements, there was no observable change in vesicle size compared to control (Figure 4.6). We found that **COE2-3C-C3-Amethyl** can partially quench calcein emission (Figure 4.7) and hypothesize that this COE may associate with EYPC vesicles by an unknown mechanism and to interact with calcein.

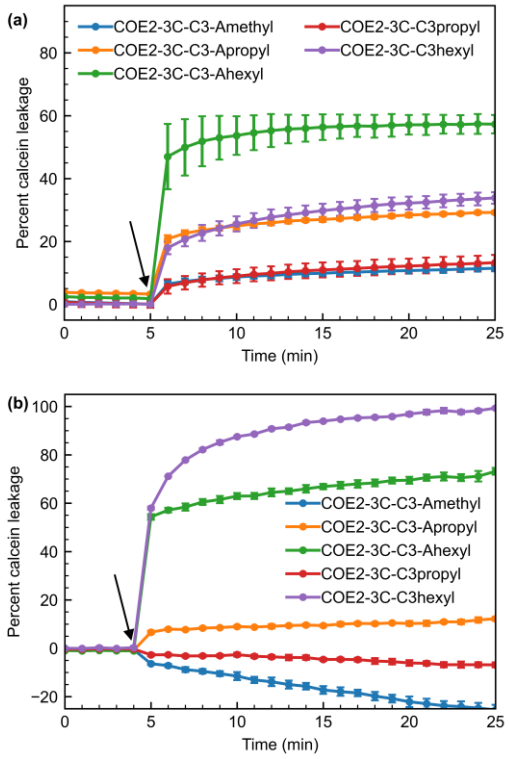

Figure 4.5 Calcein leakage from (a) bacterial lipid model vesicles (3:1 POPE/POPG) and (b) mammalian lipid model vesicles (EYPC). The arrows indicate the instances when COEs were added.

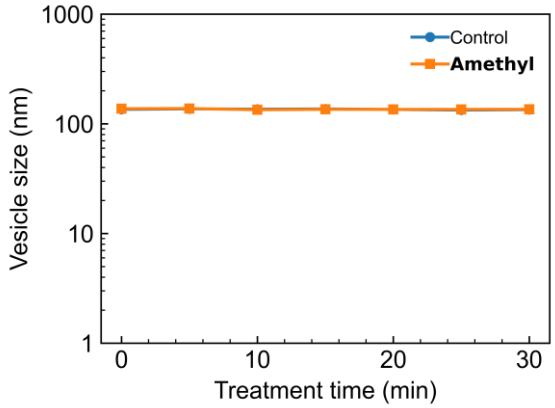

Figure 4.6 EYPC vesicle size after COE treatments measured by a dynamic light scattering technique. COE concentration was 2 mol% relative to lipids.

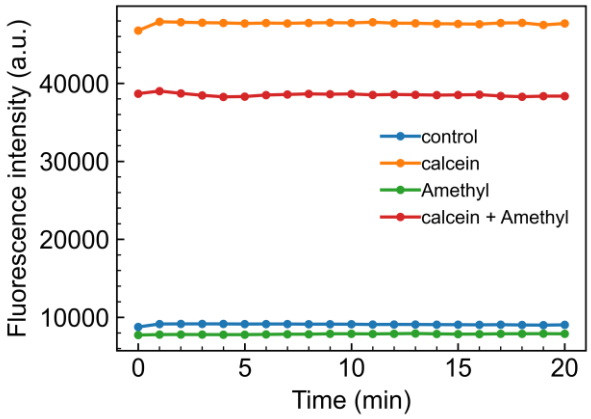

Figure 4.7 COE2-3C-C3-Amethyl is shown to partially quench fluorescence signal of 10 μM calcein in 50 mM PBS. The excitation wavelength was 495 nm and the emission wavelength was 520 nm.

4.6 Effects of COEs on *E. coli* membranes

The outer membrane (OM) is an important barrier before compounds enter or exit Gram-negative bacteria. From Figure 4.8, the OM of *E. coli* was permeabilized, as indicated by an increase in Nile Red fluorescence compared to controls. The degree of permeabilization is dependent on the length of terminal alkyl groups. We also observed that **COE2-3C-C3-Apropyl** permeabilized the OM slightly more than its non-amide analog, **COE2-3C-C3propyl**. Similarly, **COE2-3C-C3-Ahexyl** was more effective than **COE2-3C-C3hexyl**. The data follow the trend observed in calcein leakage assays. In the buffer for this assay (5 mM HEPES with 20 mM glucose), almost all COEs "associated" to *E. coli* immediately after treatments as shown by time-dependent cell association experiments (Figure 4.9). Cell association behavior of COEs is in accordance with an immediate increase in Nile Red fluorescence after treatments. This

suggests that COEs permeabilize the OM of *E. coli* effectively upon association. The lack of a correlation between the OM permeability and MICs suggests that this is not an important process in bacterial killing mechanism of COEs.

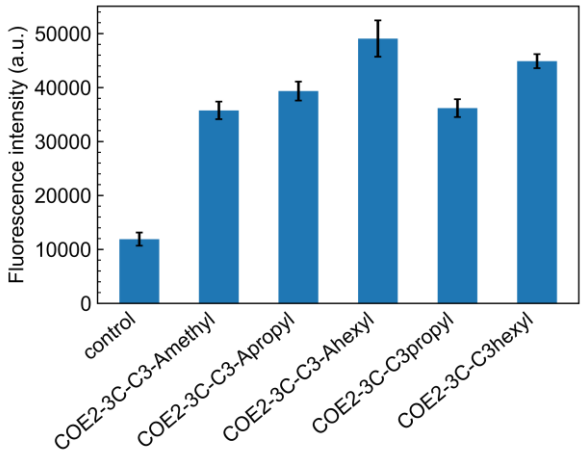

Figure 4.8 Fluorescence signal from Nile Red uptake assay with *E. coli* K12 after COE treatment at 8 μg mL^{-1}. An increase in fluorescence intensity indicates OM permeabilization.

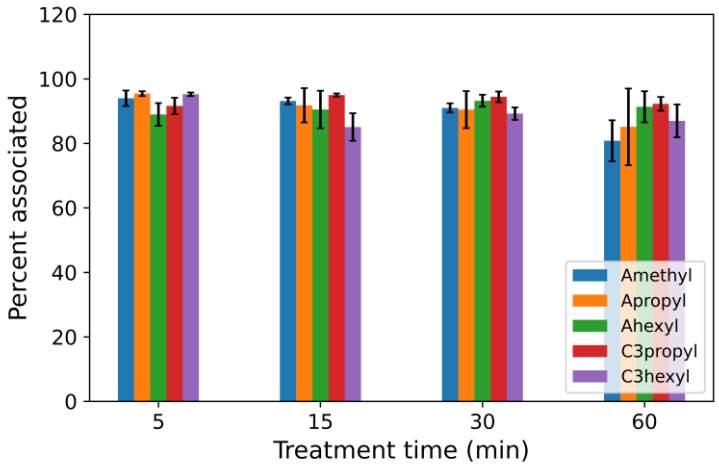

Figure 4.9 Percent of COEs associated to *E. coli* K12 cells after incubation at different time points in 5 mM HEPES with 20 mM glucose.

By confining components essential to viability inside the cytoplasm, the cytoplasmic membrane (CM) provides yet another layer of protection in Gram-negative bacteria. CM depolarization assays in the presence of different COEs

were thus performed using 3,3´-dipropylthiacarbocyanine iodide ($DiSC_3(5)$). $DiSC_3(5)$ accumulates in CM of bacterial cells and forms self-quenched aggregates. Upon membrane potential disruption, $DiSC_3(5)$ is released to the medium where its fluorescence intensity increases. The results of these studies are provided in Figure 4.10. One observes that **COE2-3C-C3-Ahexyl** and **COE2-3C-C3hexyl** exhibit the strongest effect. **COE2-3C-C3propyl** and **COE2-3C-C3hexyl** depolarized the CM to a higher extent than their amide-containing counterparts (**COE2-3C-C3-Apropyl** and **COE2-3C-C3-Ahexyl**). Noticeably, the extent of membrane depolarization induced by non-amide COEs is higher than that induced by amide containing COEs with the same alkyl group. It is possible that amide moieties may attenuate depolarizing activities of COEs by an unknown process. However, the absence of correspondence between the rank order of impact in Figure 4.10 and the MIC values in Table 4.1 suggests that CM depolarization, as determined by the $DiSC_3(5)$ assay, does not contribute significantly to the COE bactericidal mechanism of action.

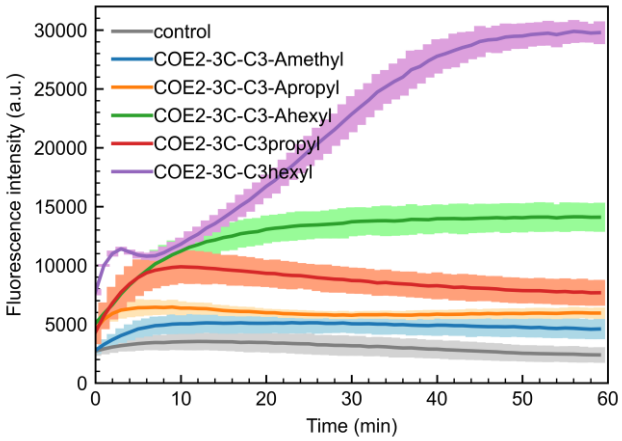

Figure 4.10 Changes in fluorescence signal of $DiSC_3(5)$ in CM depolarization assays with *E. coli* after COE treatment at 8 μg mL^{-1}.

Another measure of CM damage is an increase in permeability. Propidium iodide (PI) permeates compromised membranes and binds to DNA in the cytoplasm. An increase in fluorescence from PI in *E. coli* cells thus reflects CM damage. As shown in Figure 4.11a, **COE2-3C-C3-Apropyl** and **COE2-3C-C3hexyl** caused the highest degree of permeabilization. **COE2-3C-C3-Ahexyl** permeabilized CM less than **COE2-3C-C3-Apropyl** and **COE2-3C-C3hexyl**, followed by **COE2-3C-C3-Amethyl**. According to the calcein leakage and OM permeability assays, one would expect that **COE2-3C-C3-Ahexyl** should have higher permeabilizing activity than other amide COEs. The unexpectedly lower degree of PI uptake observed could be attributed to high non-specific interactions of the COE to proteins or other cellular components. Interestingly, the effect by **COE2-3C-C3propyl** appears to take a longer time than the other COEs. From Figure 4.11a, one surmises that the amide moieties help COEs to more effectively permeabilize the CM. According to the trend of CM permeabilization, this is the most diagnostic assay, yet not perfect, for the MICs of COEs in this study.

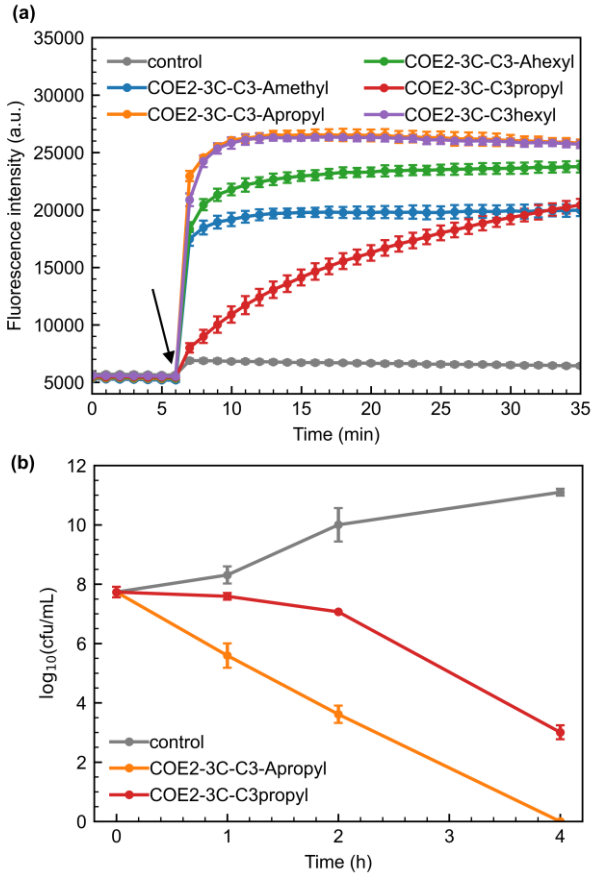

Figure 4.11 (a) Fluorescence signal of propidium iodide (PI) in CM permeabilization assay. The arrow indicates the time when COEs were added; (b) time-kill kinetics studies of **COE2-3C-C3-Apropyl** and **COE2-3C-C3propyl** against *E. coli* at 16 μg mL^{-1}.

4.7 Time-kill kinetics studies

Time-kill kinetics of **COE2-3C-C3-Apropyl**, the optimal compound in this series, were measured and compared with those of its non-amide analog, **COE2-3C-C3propyl**. *E. coli* in LB was challenged with these two COEs at 16 μg mL^{-1}. As shown in Figure 4.11b, **COE2-3C-C3-Apropyl** eradicated 99.9% of bacteria within 1.5 hours. Eradication of bacteria to <10 cfu mL^{-1} was also observed 4 hours after treatment. **COE2-3C-C3propyl** requires approximately twice of the

time in order to achieve the same bactericidal effect. It is also worth noting that **COE2-3C-C3propyl** also permeabilizes the CM of *E. coli* but at a slower rate.

4.8 Conclusions

To summarize, we disclose a series of DSB-based COEs with amide moieties on side chains and compared their antimicrobial activities against *E coli* K12 with structural counterparts bearing only quaternary ammonium groups. Among this series, **COE2-3C-C3-Apropyl** was found to be the optimal compound on the basis of the lowest MIC and largest HC_{50}/MIC ratio. A series of tests that center on probing membrane perturbations were also carried out to gain insight into the mechanism of action. By and large these experiments, namely calcein release from model vesicles, uptake of Nile Red and PI dyes, and CM depolarization are consistent with the COEs disrupting the integrity and function of the membrane. We found best correspondence between antimicrobial activity (MIC) and the PI uptake, which would imply that permeabilization of the CM is important, although it is too early to make firmer claims. We also found that amide containing COEs rapidly permeabilize the CM of *E. coli* and **COE2-3C-C3-Apropyl** possesses a higher killing rate than its non-amide counterpart. More to the point, the general absence of trends observed for biophysical tests with MIC hints that COEs may have interactions other than lipid bilayer intercalation that warrant future investigations. From a molecular design perspective, this work suggests an important role for hydrogen bonds, a

category of intermolecular interactions distinct from electrostatic and hydrophobic interactions, for tuning activity of COEs against bacterial cells and increasing selectivity relative to mammalian cells.

4.9 Experimental methods

Materials and Instruments

All solvents and chemicals were obtained from common suppliers (*e.g.*, MilliporeSigma, Acros Organics, TCI, Fisher Scientific, and Combi-Blocks) and were used without further purification unless otherwise stated. Dry and inhibitor free THF and DMF were received from a solvent purification system using packed alumina columns under argon.

Flash chromatography was carried out either on Silicycle SiliaFlash P60 silica gel with pressurized air up to 0.5 bar or on Biotage SNAP C18 columns. EMD Millipore Analytical Chromatography TLC Silica gel 60 F254 with aluminum back were used to perform thin layer chromatography (TLC) with UV light (254/366 nm) or iodine stain for detection.

High performance liquid chromatography (HPLC) measurements were performed using a Shimadzu UFLC model SIL-20AHT. Data were collected using LCSolutions software. The column used for analyses was a Phenomenex Kinetex 2.6 μm PS C18 100 Å column (150 × 4.6 mm). Eluents were of HPLC grade.

^{1}H NMR (500 MHz) and ^{13}C NMR (125 MHz) were measured on an actively shielded Varian Unity Inova 500 MHz spectrometer. The multiplicity of all signals was described by s (singlet), d (doublet), t (triplet), q (quartet), p (pentet), and m (multiplet). Chemical shifts (δ in ppm) were referenced to solvent residual peak of $CDCl_3$ (^{1}H NMR: δ = 7.26 ppm, ^{13}C NMR: δ = 77.1 ppm) or DMSO-d_6 (^{1}H NMR: δ = 2.50 ppm, ^{13}C NMR: δ = 39.52 ppm). Mass spectra were collected on Waters Micromass LCT-Premier mass spectrometer.

Minimum inhibitory concentration experiments

Minimum inhibitory concentrations (MICs) of COEs were determined using broth microdilution method. *E. coli* K12 (ATCC 47076) from a –80°C glycerol frozen stock was plated on an LB agar plate. A single colony of *E. coli* K12 from an agar plate was inoculated in LB medium (10 g L^{-1} bactotryptone, 5 g L^{-1} yeast extract, and 10 g L^{-1} NaCl) at 37°C with 200 rpm orbital shaking for 4 hours before use. Bacteria culture was diluted to the cell density around 1×10^6 cfu mL^{-1}. For MIC experiments with the presence of human serum albumin (HSA), the LB medium was supplemented with 40 g L^{-1} HSA and was sterile filtered through a 0.22 μm filter before use. Compounds were added to a sterile 96-well plate and were further diluted with 2-fold dilutions. The same volume of the bacteria suspension was then added to each well in the plate to achieve the final cell density of 5×10^5 cfu mL^{-1}. The final concentrations of COEs were 0.5 to 64 μg mL^{-1}. The 96-well plate was incubated at 37°C with 200 rpm shaking

overnight. A group with no compound treatment was set as a negative control and a group with only growth medium was set as a blank. The optical density at 600 nm (OD_{600}) was measured from the plate with a plate reader (Tecan Spark M10). The minimum concentrations with bacterial growth less than 10% relative to the control group were determined as the MICs. A commercially available antibiotic, polymyxin B, was used as a positive control for this assay. The MIC of polymyxin B was found to be 1 μg mL^{-1} which is in a good agreement to the value reported in the literature.[116] Experiments were performed with biological replicates.

For MIC experiments against other Gram-negative bacteria (i.e., *K. pneumoniae* ATCC 700603 and *S. enterica* Typhimurium ATCC 14028), a single colony from an agar plate of each type of bacteria was inoculated in cation-adjusted Mueller-Hinton Broth (CA-MHB) at 37 °C with 200 rpm shaking for 5 hours. The resulting bacterial suspensions were subjected to the same protocol as described above in CA-MHB without HSA supplements. The results are shown below in Table 4.3.

Table 4.3 MICs of COEs in this study against *K. pneumoniae* and *S. enterica* Typhimurium.

Compound	MIC against *K. pneumoniae* (μg mL^{-1})	MIC against *S. enterica* Typhimurium (μg mL^{-1})
COE2-3C-C3-Amethyl	16	8
COE2-3C-C3-Apropyl	8	4
COE2-3C-C3-Ahexyl	32	32
COE2-3C-C3propyl	8	8
COE2-3C-C3hexyl	8	8

Cytotoxicity assay

Cellular cytotoxicity was assessed using Cell Counting Kit-8 (CCK-8, Dojindo Molecular Technologies, Inc.). HepG2 (ATCC HB-8065) cells were seeded at 1×10^4 cells per well in 96-well plates overnight at 37 °C in Dulbecco's Modified Eagle's medium (DMEM, Gibco, GlutaMAX™) supplemented with 10% fetal bovine serum (FBS, Gibco, USDA-approved regions) before use. Compounds were serially diluted with 2-fold dilution in PBS and further diluted in culture media to afford a concentration ranging from 16 to 1,024 μg mL^{-1} for each COE except **COE2-3C-C3Ahexyl** which was diluted to afford a concentration ranging from 2 to 128 μg mL^{-1}. Each treatment solution contains 10% PBS (v/v). The previous culture media were replaced with 100 μL of treatment solutions per well, the assay plates were incubated at 37 °C with 5% CO2. After 24 hours of incubation, cells were washed with PBS before adding 100 μL of fresh culture media and 10 μL of CCK-8 to each well. After incubation

for 1–2 hours, the absorbance of each well at 450 nm were measured on a microplate reader (Tecan Infinite 200). Percent viability was determined by dividing background-corrected absorbance measurements by background-corrected measurements for untreated cells.

Hemolysis assay

Human red blood cells (SciMed, Singapore) were washed with PBS for three times with centrifuge at 500×g for 5 minutes. The pellet was resuspended to yield a 5% (v/v) suspension in PBS. 160 μL of compound solutions were added to a conical bottom 96-well plate as triplicates and dilute with 2-fold dilution sequentially. A 40 μL portion of 5% red blood cell solution was added to each well of the 96-well plate. The final concentration of compounds ranged from 16 to 1,024 μg mL^{-1} and the final concentration of the red blood cells was 1%. Red blood cells with PBS alone were used as a negative control and with 1% Triton X-100 (Sigma-Aldrich) treatment as a positive control. After incubation for 1 hour at 37 °C, cells were centrifuged at 800×g. A 100 μL portion of the resulting supernatant was transferred to a flat-bottomed 96-well plate and analyzed on a microplate reader via absorbance measurements at 450 nm. Percent hemolysis was determined by dividing background-corrected absorbance by background-corrected absorbance with 1% Triton X-100 treatment.

Lipid film preparation

Prior the experiment, lipids were dissolved in chloroform (4:1 POPE/POPG for a Gram-negative bacteria model and EYPC for a mammalian lipid model). Chloroform was evaporated from lipid solutions under reduced pressure and the resulting films were further dried under vacuum overnight at room temperature. Dried lipid films were stored under argon at –20°C.

Calcein leakage assays

Lipid films prepared according to the stated protocol was resuspended 20 mM calcein in 50 mM PBS. The lipid suspension was incubated at 37°C with 200 rpm shaking for 30 minutes. The resulting suspension was extruded through a 0.2 μm polycarbonate filter (Whatman) 11 times, followed by extrusions through a 0.1 μm polycarbonate filter (Whatman) for 11 times. Free calcein was removed from the vesicles by size exclusion chromatography (SEC) using Sephadex G50 (bead size 50–150 μm). The purified vesicles were diluted to achieve the concentration of 2 mM based on an average molecular weight of lipids and were used in the assay immediately after purification. In a black clear-bottom 96-well plate, 100 μL of vesicle suspension was mixed with 100 μL of COE solutions in 50 mM PBS to obtain the final concentration of COE of 2 mol% of lipid. Fluorescence signal was recorded for 25 minutes using Tecan Spark 10M at the excitation wavelength of 495 nm and the emission wavelength

of 520 nm. 3% Triton X-100 was used as a positive control. Percent leakage of calcein in each well was calculated using the equation:

$$\text{Percent leakage (\%)} = (I - I_o)/(I_T - I_o) \times 100$$

where I = fluorescence intensity at a certain time point after compound treatment, I_o = fluorescence intensity of a negative control, and I_T = fluorescence intensity of a positive control (Triton X-100).

HPLC analyses and HPLC traces of COEs

To evaluate relative hydrophobicity of COEs in this study, COEs were analyzed by a reverse phase HPLC method to determine their retention time on a column. The retention time of COEs could be used to rank their hydrophobicity.[117,118] Eluent gradient used was 5% to 40% acetonitrile in water with 0.1% acetic acid as an additive.

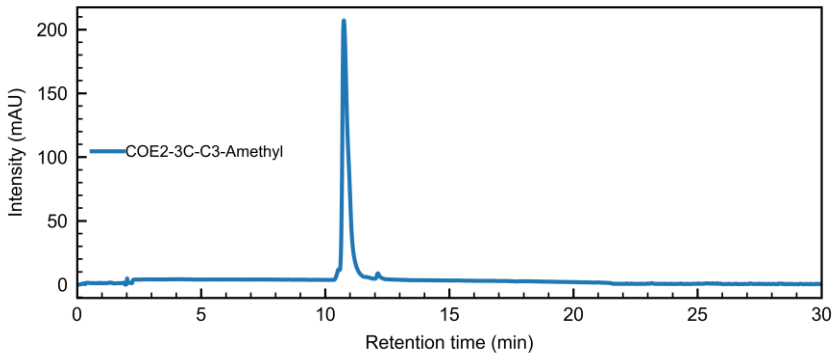

Figure 4.12 HPLC chromatogram of COEs in this study

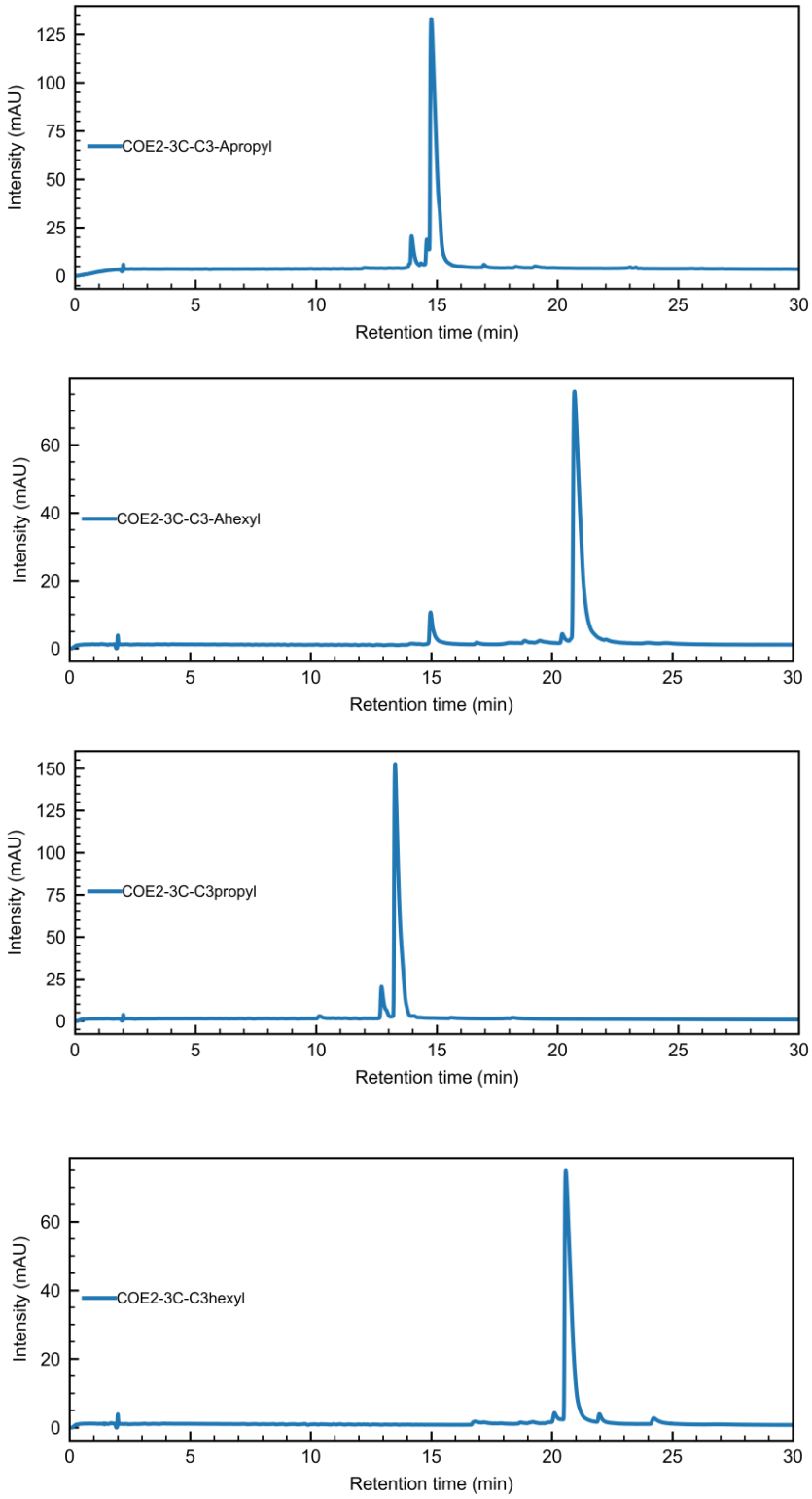

Figure 4.12 HPLC chromatogram of COEs in this study (continued)

Dynamic light scattering experiments of EYPC vesicles

Egg yolk L-α-phosphatidylcholine film was hydrated with 50 mM PBS and was incubated at 37°C for 30 minutes. The resulting suspension was extruded through a 0.2 μm polycarbonate filter (Whatman) for 11 times and through 0.1 μm polycarbonate filter (Whatman) for 11 times. Extruded vesicles were diluted with 50 mM PBS to achieve a concentration of 2 mM. In a cuvette, 500 μL of lipid vesicles was mixed with 500 μL of **COE2-3C-C3-Amethyl** or **COE2-3C-C3-Apropyl** (or buffer for a control experiment). The final concentration of COE was 2 mol% of lipids. Vesicle sizes were measured by Zeta Sizer Nano ZS (Malvern Panalytical Inc.) every 5 minutes for 30 minutes. No change in vesicle size was observed after COE treatments.

Cell association experiments

A single colony of *E. coli* K12 from an LB agar plate was inoculated in LB medium and cells were harvested during a mid-log phase. The cells were centrifuged at 7,000 rpm for 4 minutes to remove LB, washed, and resuspended in 5 mM HEPES buffer with 20 mM glucose (pH 7.3) to achieve the cell density twice of that at 1 OD_{600}. The cell suspension was mixed with a solution of COEs to achieve the COE final concentrations of 32 μg mL^{-1} in microcentrifuge tubes. Treated bacterial suspension was sampled out after 5, 15, 30, 60, 90, and 120 minutes of incubation. Supernatants from the sampled suspensions were obtained by pelleting cells at 7,000 rpm for 4 minutes. The amount of COE left

in the supernatant was determined by the absorption at 380 nm using Tecan Spark 10M Plate Reader.

Outer membrane permeabilization assay

A log phase liquid culture of *E. coli* K12 was centrifuged at 7,000 rpm for 4 minutes. Cells were washed twice to get rid of a growth medium and resuspended in 5 mM HEPES buffer (pH 7.3) with 20 mM glucose at OD_{600} of 0.5. In a clear-bottomed black 96-well plate, 100 μL of bacterial suspension was pipetted into each well and was allowed to thermally equilibrate inside a plate reader (Tecan Spark 10M) at 30°C. After a thermal equilibration, 2 μL of Nile Red solution (50 μM in 1:4 EtOH/water) and 100 μL of each compound were added to achieve a final concentration of 8 μg mL^{-1} for all compounds. Fluorescence signals of Nile Red were measured for 30 minutes with the excitation wavelength of 525 nm and the emission wavelength of 630 nm.

Cytoplasmic membrane depolarization assay

E. coli K12 was harvested from an LB liquid culture during log phase by centrifugation at 7,000 rpm for 4 minutes, washed twice. Cell pellet was resuspended in 5 mM HEPES buffer (pH 7.3) containing 20 mM glucose and 5 mM EDTA to achieve the cell density of OD_{600} = 0.05. Then, cells were treated with 0.4 μM $DiSC_3(5)$ from a 1 mM stock solution in DMSO. The cell suspension was incubated in the dark for 30 minutes to allow dye uptake by bacteria. In a

black clear-bottom 96-well plate, 75 μL of the cell suspension was pipetted into each well. Fluorescence signal was monitored until the stable baseline was achieved. After that, 25 μL of each compound was added to each well. The final concentration of the compounds was 8 μg mL^{-1}. The fluorescence intensity of $DiSC_3(5)$ was monitored for an hour after compound treatments. The excitation and emission wavelengths for this assay were 622 nm and 670 nm, respectively.

Cytoplasmic membrane permeabilization assay

Propidium iodide (PI) was used as a dye to evaluate inner membrane permeability. In brief, a log phase culture of *E. coli* K12 was harvested by centrifugation at 7000 rpm for 4 minutes, washed, and resuspended in 5 mM HEPES buffer (pH 7.3) with 20 mM glucose to achieve cell density at OD_{600} of 0.1. The cell suspension was treated with 10 μM PI immediately before the assay. In a clear-bottomed black 96-well plate, 75 μL of the cell suspension was pipetted into each well. Fluorescence intensity of PI was measured for several minutes to ensure a stable baseline. Then, 25 μL of each compound was added to each well and the fluorescence signal was monitored for another 30 minutes. The excitation and emission wavelengths were 535 nm and 617 nm, respectively.

Time-kill kinetics

A single colony of *E. coli* K12 from an agar plate was cultured in LB for 4 hours at 37°C with 200 rpm shaking before use. The bacteria suspension was diluted in LB to afford the OD_{600} to be around 0.1. In sterile culture tubes, the diluted bacteria suspension was challenged with **COE2-3C-C3Apropyl** or **COE2-3C-C3propyl** at a concentration of 16 μg mL^{-1} at 37°C with 280 rpm shaking. A bacteria suspension without treatment was used as a control. At intervals, 20 μL aliquots from each sample were serially diluted with 10-fold serial dilution. The appropriate dilutions were further plated on LB agar plates with 50 μL or 100 μL aliquots. After overnight incubation at 37°C, bacteria colonies on agar plates were counted and cfu per mL were calculated. Experiments were performed in triplicate.

4.10 Synthetic methods

Synthesis of intermediate 1

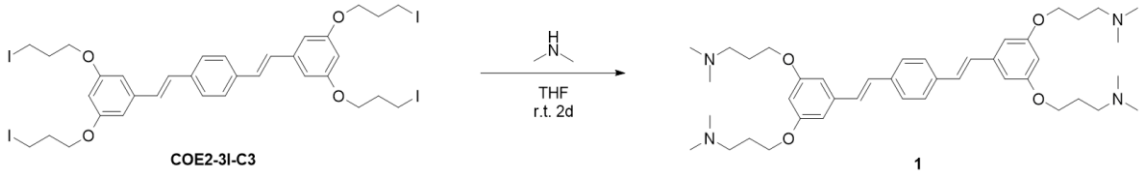

To a round-bottom flask equipped with a magnetic stir bar was charged with **COE2-3I-C3** (146 mg). The starting material was dissolved in 12 mL of THF under inert atmosphere. Dimethylamine (2 M in THF) (40 eqiv) was then added to the reaction flask via a syringe. After stirring the reaction mixture at room temperature for 2 days, the reaction mixture was diluted in DCM and poured

into a K_3PO_4 solution. Crude reaction was extracted with DCM, dried over Na_2SO_4. Solvents were removed under reduced pressure to obtain the intermediate **1** as pale-yellow solid with a quantitative yield. **^{1}H NMR (500 MHz, $CDCl_3$):** δ (ppm) 7.49 (s, 4H), 7.06 (d, J = 16.5 Hz, 2H), 7.01 (d, J = 16 Hz, 2H), 6.67 (d, J = 2.5 Hz, 4H), 6.40 (t, J = 2 Hz, 2H), 4.03 (t, J = 6.5 Hz, 8H), 2.45 (t, J = 7 Hz, 8H), 2.27 (s, 24H), 1.94 (p, J = 7 Hz, 8H); **^{13}C NMR (125 MHz, $CDCl_3$):** δ (ppm) 160.53, 139.37, 136.78, 128.80, 128.77, 127.03, 105.35, 101.15, 66.49, 56.61, 45.71, 27.75; **HRMS (ESI):** ($[M]^{2+}$) calcd: 344.2464, found: 344.2459.

General procedure for synthesis of intermediate 2b and 2c

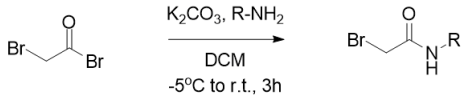

In a flame-dried round-bottom flask with a magnetic stir bar, bromoacetyl bromide (1 g, 1.1 equiv) and K_2CO_3 (1.1 equiv.) was added to 10 mL of dry DCM under inert atmosphere. The resulting suspension was cooled down to –5°C. Then, primary amine (1 equiv) was added to the reaction via a syringe. After warming up to room temperature, the reaction mixture was stirred for 3 hours before it was quenched by water. The reaction mixture was extracted with DCM, washed with water and brine, dried over Na_2SO_4. Solvents were removed from the organic layer under reduced pressure to obtain intermediate **2b** or **2c**.

2b: the product was obtained as white solid (74%). **^{1}H NMR (500 MHz, $CDCl_3$):** δ (ppm) 6.52 (s, 1H), 3.88 (s, 2H), 3.23 (q, J = 6.5 Hz, 2H), 1.53 (m, 2H), 0.92 (t, J = 7.5 Hz, 3H); **^{13}C NMR (125 MHz, $CDCl_3$):** δ (ppm) 165.37, 42.01, 29.52, 22.69, 11.39; **HRMS (ESI):** ($[M+Na]^+$) calcd: 201.9843, found: 201.9852.

2c: the product was obtained as white solid (82%). **^{1}H NMR (500 MHz, $CDCl_3$):** δ (ppm) 6.47 (s, 1H), 3.88 (s, 2H), 3.26 (q, J = 6.5 Hz, 2H), 1.27 (m, 6H), 0.88 (t, J = 6.5 Hz, 3H); **^{13}C NMR (125 MHz, $CDCl_3$):** δ (ppm) 165.28, 40.41, 31.54, 29.57, 29.38, 26.61, 22.66, 14.13; **HRMS (ESI):** ($[M+Na]^+$) calcd: 244.0313, found: 244.0322.

General procedure for synthesis of target molecules

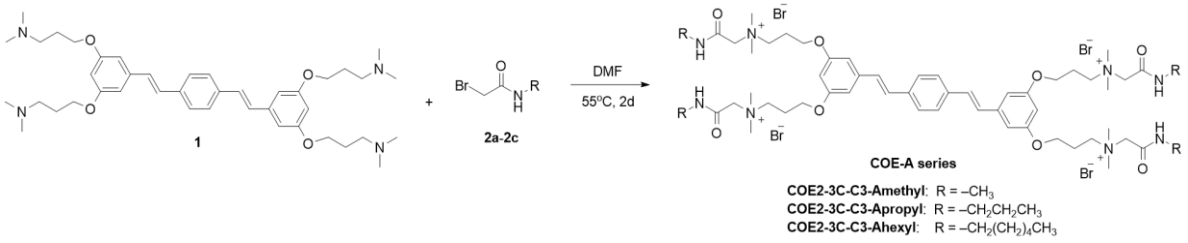

In a 1 Dram vial equipped with a magnetic stir bar, 30 mg of **1** and **2a**, **2b**, or **2c** (10 eqiv) were added under inert atmosphere. 1 mL of DMF was then added to dissolve starting materials. The reaction vessel was sealed and heated with stirring at 55°C for 2 days. After cooling down to room temperature, the reaction mixture was precipitated and washed twice in diethyl ether. The crude reaction mixture was subjected to reverse phase column chromatography (3:7 MeOH/water) to obtain a target molecule. The purified molecule was lyophilized

and store under inert atmosphere for the ease of handling due to its hygroscopic properties.

COE2-3C-C3-Amethyl: the product was obtained as white solid (89%). **^{1}H NMR (500 MHz, DMSO-d_6):** δ (ppm) 8.61 (q, J = 4 Hz, 4H), 7.62 (s, 4H), 7.30 (d, J = 16.5 Hz, 2H), 7.21 (d, J = 16.5 Hz, 2H), 6.84 (d, J = 2 Hz, 4H), 6.46 (s, 2H), 4.19 (s, 8H), 4.10 (t, J = 6 Hz, 8H), 3.71 (m, 8H), 3.27 (s, 24H), 2.66 (d, J = 4.5 Hz, 12H), 2.19 (m, 8H); **^{13}C NMR (125 MHz, DMSO-d_6):** δ (ppm) 163.50, 159.50, 139.27, 136.36, 128.77, 128.25, 126.94, 105.33, 101.09, 64.81, 62.06, 62.00, 51.26, 25.47, 22.43; **HRMS (ESI):** ($[M+2Br]^{2+}$) calcd: 566.2468, found: 566.2480.

COE2-3C-C3-Apropyl: the product was obtained as white solid (88%). **^{1}H NMR (500 MHz, DMSO-d_6):** δ (ppm) 8.63 (t, J = 5.5 Hz, 4H), 7.62 (s, 4H), 7.29 (d, J = 16.5 Hz, 2H), 7.21 (d, J = 16 Hz, 2H), 6.83 (d, J = 2 Hz, 4H), 6.44 (t, J = 2 Hz, 2H), 4.17 (s, 8H), 4.09 (t, J = 6 Hz, 8H), 3.70 (m, 8H), 3.26 (s, 24H), 3.07 (q, J = 6.5 Hz, 8H), 2.19 (m, 8H), 1.42 (m, 8H), 0.85 (t, J = 7.5 Hz, 12H); **^{13}C NMR (125 MHz, DMSO-d_6):** δ (ppm) 162.97, 159.52, 139.28, 136.37, 128.77, 128.28, 126.96, 105.51, 101.04, 64.81, 62.04, 51.32, 40.41, 22.45, 21.94, 11.39; **HRMS (ESI):** ($[M+2Br]^{2+}$) calcd: 622.3094, found: 622.3106.

COE2-3C-C3-Ahexyl: the product was obtained as white solid (74%). **^{1}H NMR (500 MHz, DMSO-d_6):** δ (ppm) 8.63 (t, J = 6 Hz, 4H), 7.62 (s, 4H), 7.29 (d, J =

16.5 Hz, 2H), 7.20 (d, J = 16 Hz, 2H), 6.83 (d, J = 2 Hz, 4H), 6.44 (t, J = 2 Hz, 2H), 4.17 (s, 8H), 4.09 (t, J = 6 Hz, 8H), 3.69 (m, 8H), 3.26 (s, 24H), 3.10 (q, J = 6.5 Hz, 8H), 2.19 (m, 8H), 1.40 (m, 8H), 1.21 (m, 24H), 0.82 (t, J = 7 Hz, 12H); **^{13}C NMR (125 MHz, DMSO-d_6):** δ (ppm) 162.91, 159.33, 139.27, 136.37, 128.76, 128.26, 126.94, 105.50, 101.01, 64.81, 62.04, 61.96, 51.36, 38.64, 30.88, 28.57, 26.03, 22.46, 22.03, 13.90; **HRMS (ESI):** ($[M+2Br]^{2+}$) calcd: 706.4033, found: 706.4039.

Chapter 5: Amidine-based conjugated oligoelectrolytes

5.1 Introduction

As mentioned in Chapter 3 and 4, the number of antibiotic resistant bacteria is growing at an alarming rate. Antibiotics that were approved in the market are based on classes of antibiotics discovered in 1980s or earlier.[119] Therefore, exploring chemical spaces to generate a variety of antimicrobial compounds is greatly warranted to combat such emerging crisis.

Amphiphilic compounds have gained attention from researchers as a new strategy for antimicrobial compound development. Inspired by host defense peptides (HDPs) which contains variety degrees of hydrophobic and hydrophilic segments, many small molecules and polymers mimicking amphiphilic nature of HDPs have been designed and reported, including COEs designed in our group.[85,111,120,121] Notably, a significant number of these compounds contains quaternary ammonium cations serving as permanently-charged hydrophilic segments. Even though these compounds show minimum or undetectable *in vitro* cytotoxicity, concerns regarding *in vivo* toxicity of quaternary ammonium compounds have been raised.[122–124] One of the concerns is related to acute toxicity due to off-target ion channel blockades. The human ether-à-go-go-related gene (hERG) channel is of particular importance. Inhibition of the hERG channel could lead to torsades de pointes (TdP) and cardiac arrest.[125,126]

Due to such QACs concerns, we sought to explore alternative chemical moieties to replace quaternary ammoniums. Amidines are an attractive option for this purpose. Charge delocalization over three atoms in an amidine moiety gives rise to a larger and more polarizable cationic unit compared to a quaternary ammonium moiety which could potentially reduce off-target interactions with ion channels. Amidine groups contain two different characteristics from quaternary ammonium groups and amide groups: positively charged and hydrogen bond forming. Their high basicity (pK_a = 12) allows them to exist as protonated species under a physiological condition, thus retaining an ability of COEs to interact with bacterial membranes. In addition, they also have an ability to act as hydrogen bond acceptors due to hydrogen atoms on two different nitrogen sites, therefore they could potentially possess rapid cytoplasmic membrane permeabilizing and bactericidal activities as observed in the amide-containing COEs reported in Chapter 4.

In this work, COEs with different amidines were designed with three different locations of functionalization including imino nitrogen, amino nitrogen, and end group. Chemical structures of COEs in this series are depicted in Figure 5.1. Different substitutions on each type of nitrogen atoms were synthesized to study the impact of substituent positions on biological activities of COEs. Amidine side chains were varied to modulate hydrophobicity of the molecules.

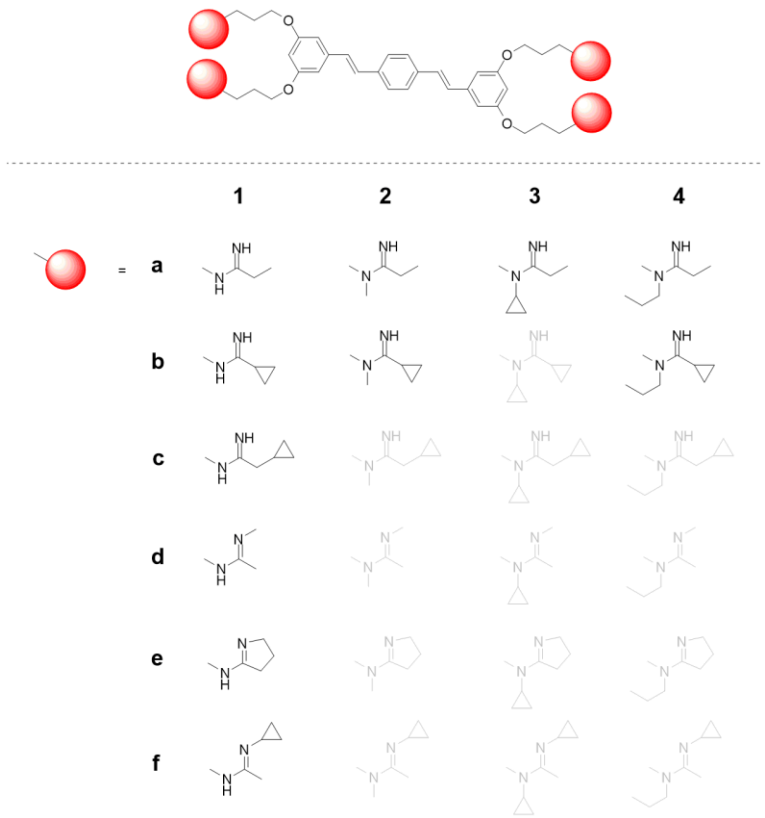

Figure 5.1 List of synthesized compounds in amidine-based COE series.

5.2 Synthesis of amidine-based COEs

Amidine moieties in this series of COEs were furnished onto side chains of conjugated core as late-stage modifications by Pinner reactions between various amines installed on the side chains of the COE and imidate salts (Pinner salts). Distyrylbenzene conjugated cores of amidine-based COEs were synthesized from two different pathways as illustrated in Figure 5.2.

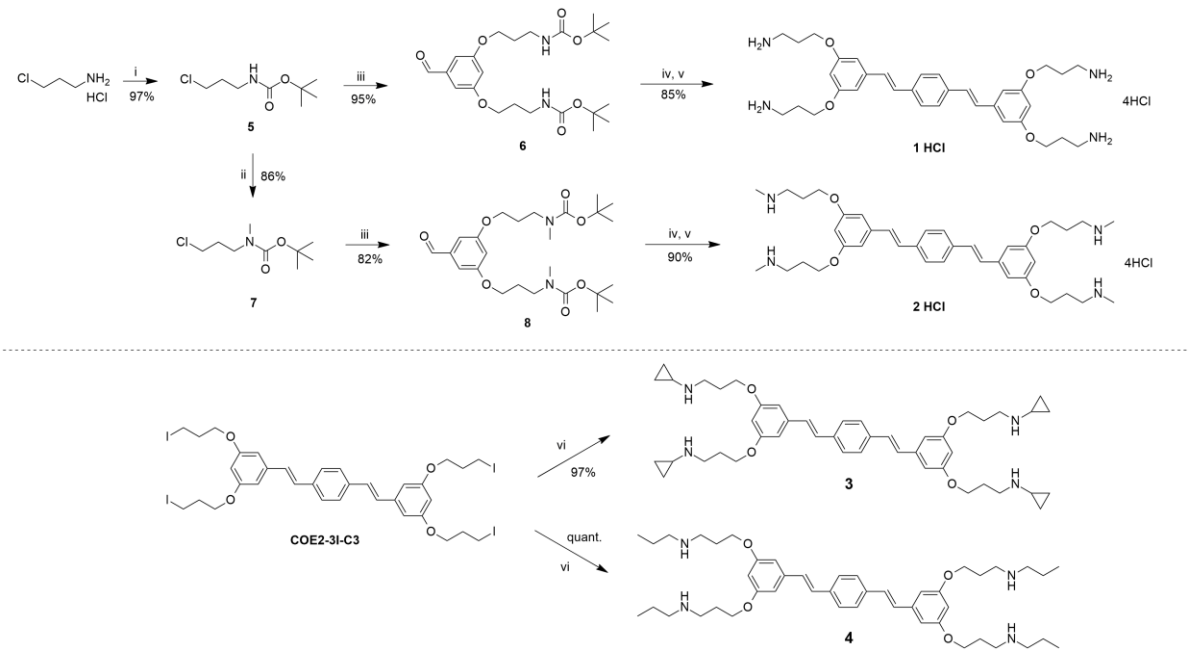

Figure 5.2. Synthetic scheme of conjugated cores **1**–**4**. Intermediate **1** and **2** were synthesized as HCl salts. Reaction conditions: (i) Boc_2O, TEA, DCM, 0°C to rt, o.n.; (ii) CH_3I, NaH, rt, o.n.; (iii) 3,5-dihydroxybenzaldehyde, K_2CO_3, DMF, 100°C, 5 h; (iv) tetraethyl (1,4-phenylenebis(methylene))bis(phosphonate), NaO*t*Bu, THF, 0°C to rt, o.n.; (v) HCl (g), $CHCl_3$, MeOH, rt, 5 h; (vi) R-NH_2, THF, rt, o.n.

For intermediate **1** and **2**, 3-chloro-*n*-propylamine HCl was reacted with Boc_2O to yield Boc-protected 3-chloro-*n*-propylamine (**5**). Some of intermediate **5** was methylated at the NHBoc position with methyl iodide to yield intermediate **7**. Then, both intermediates **5** and **7** were reacted with 3,5-dihydroxybenzaldehyde under a Williamson ether synthesis condition to form intermediates **6** and **8** in excellent yields. Finally, to form distyrylbenzene units, compounds **6** and **8** were subjected to a Horner-Wadsworth-Emmons (HWE) reaction condition with tetraethyl (1,4-phenylenebis(methylene)) bis(phosphonate), followed by a Boc deprotection condition with HCl yielding compounds **1 HCl** and **2 HCl** in excellent yields. Intermediates **3** and **4** were

synthesized directly from **COE2-3I-C3** with either cyclopropylamine or *n*-propylamine. Another set of fragments that is a reagent for Pinner amidine synthesis is imidate salts. Figure 5.3 shows the synthetic scheme for imidate salts **a**–**f**.

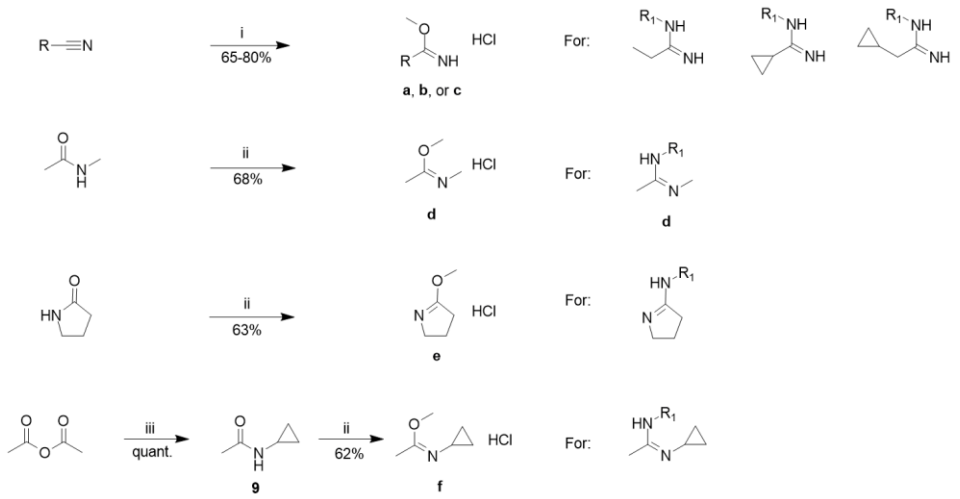

Figure 5.3 Synthetic scheme of imidate salts **a**–**f**. Reaction conditions: (i) HCl (g), MeOH, rt, 5 h; (ii) MeOTf, Et_2O, 0°C to rt, o.n., then K_2CO_3, then HCl; (iii) cyclopropylamine, Et_3N, DCM, 0°C to rt, o.n.

Two different approaches to form imidate salts were employed. For derivatives with unsubstituted imino nitrogens, standard Pinner reaction conditions were used to synthesize their imidate salts. In short, alkyl nitriles were dissolved in dry MeOH that was pre-saturated with HCl to obtain their imidate salt derivatives **a**–**c** in moderate to good yields. Imidate salts with substituted imino nitrogens were synthesized from secondary amides. *N*-methylacetamide and pyrrolidin-2-one are commercially available. *N*-cyclopropylacetamide (**9**) was synthesized from a reaction between acetic anhydride and cyclopropylamine in a quantitative yield. These amides were

methylated at the carbonyl oxygen atom by methyl triflate. Triflate anions were removed by a treatment of K_2CO_3 followed by a filtration into etherated HCl to form imidate HCl salts **d**–**f** in moderate yields.

With amine and imidate salt intermediates prepared, amidine moieties were formed under the Pinner reaction conditions. Attempts to form amidines directly from HCl salts failed with no detectable amount of products observed. Solubility of the COE cores **1**–**4** as HCl salts proved to be a problem during the reaction. Therefore, we decided to neutralize all HCl salts of the starting materials beforehand. Intermediates **1 HCl** and **2 HCl** were neutralized with either basic water extraction or Amberlyst A21 resin. Prior to setting up Pinner reactions, imidate salts **a**–**f** were neutralized with 1 M K_2CO_3. The free base forms were then extracted with chloroform and were added directly to reactions. Acetic acid was later added to the reaction vessels to provide acetate counterions. Figure 5.4 shows the general scheme of the Pinner reaction condition.

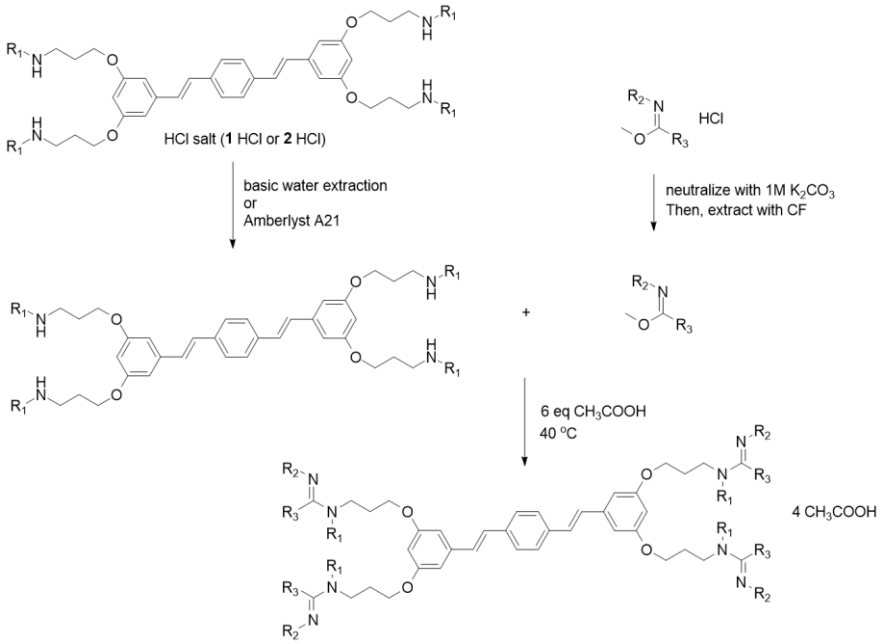

Figure 5.4 General synthetic scheme of amidine-based COEs

5.3 Antimicrobial activity of amidine-based COEs

Synthesized COEs were tested for their antimicrobial activities by determining their minimum inhibitory concentrations (MICs) against four different strains of Gram-negative bacteria, including *E. coli* K12, *E. coli* ATCC 25922, *K. pneumoniae* ATCC 700603, *P. aeruginosa* ATCC 27853, *S. enterica* Typhimurium ATCC 14028, and one strain of Gram-positive bacteria (*S. aureus* ATCC 29123) in LB medium. The results are shown in Table 5.1.

Table 5.1 Summary of MICs of amidine-based COEs against different strain of bacteria in LB medium. MICs are reported in μg mL^{-1}.

Compound	EC-K12[a]	EC[b]	ST[c]	KPN[d]	PA[e]	SA[f]
1a	2	1	2	8	8	1
1b	2	1	1	4	2	< 0.5
1c	2	2	2	4	8	1
1d	4	2	2	16	32	1
1e	2	2	2	16	16	1
1f	2	2	2	8	32	1
2a	2	1	2	16	8	1
2b	2	1	1	8	8	1
3a	2	2	2	8	16	1
4a	2	2	2	8	16	1
4b	2	2	2	8	32	1

[a] *E. coli* K12, [b] *E. coli* ATCC 25922, [c] *S. enterica* Typhimurium ATCC 14028, [d] *K. pneumoniae* ATCC 700603, [e] *P. aeruginosa* ATCC 27853, [f] *S. aureus* ATCC 29123.

To conform with the standard protocol for antimicrobial susceptibility testing by the Clinical and Laboratory Standards Institute (CLSI),[91] two representative compounds with best antimicrobial activity from the initial screening were chosen to determine their MIC values in cation-adjusted Mueller Hinton Broth (CA-MHB). Table 5.2 shows that there is no significant change in antimicrobial activities of compound **1a** and **1b** against *E. coli* ATCC 25922 in CA-MHB confirming their potent antimicrobial efficacies.

Table 5.2 MICs of compound 1a and 1b against *E. coli* ATCC 25922 in LB and CA-MHB.

Compound	MIC in LB ($\mu g\ mL^{-1}$)	MIC in CA-MHB ($\mu g\ mL^{-1}$)
1a	1	1
1b	1	1

In addition to the bacterial strains tested in Table 5.1, due to the low MIC against *P. aeruginosa* of compound **1b**, the compound **1b** was further tested for its MICs against a broader panel of *P. aeruginosa* by the Walter Reed Army Institute of Research (WRAIR). A total of 100 strains of *P. aeruginosa* were tested with levofloxacin as an antibiotic control. The results are summarized as a histogram in Figure 5.5. **1b** shows a good MIC distribution against *P. aeruginosa* strains with the 90th percentile MIC (MIC_{90}) of 16 $\mu g\ mL^{-1}$, whereas the MIC_{90} of levofloxacin is 64 $\mu g\ mL^{-1}$. This implies that **1b** can inhibit the growth of 90% of *P. aeruginosa* strains at a lower concentration than levofloxacin.

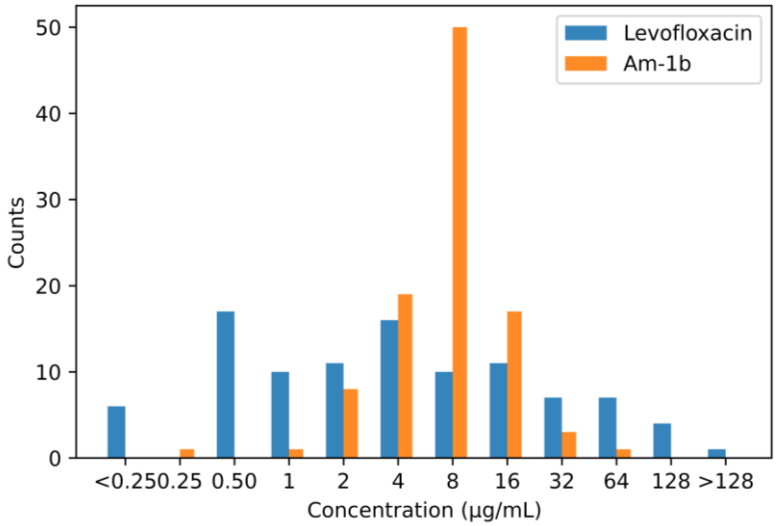

Figure 5.5 Histogram of MIC distribution of compound **1b** and levofloxacin against a broad panel of *P. aeruginosa*.

5.4 Cytotoxicity of amidine COEs

To preliminarily screen whether each amidine COEs has suitable cytotoxicity towards mammalian cells and to elucidate the correlation of COE structure and cytotoxicity, the MTT assay was performed with HepG2 cells. Figure 5.6 shows the IC_{50} of each COE against HepG2 cells.

	1	2	3	4
a	1,024	>1,024	128	32
b	1,024	1,024		16
c	256			
d	>1,024			
e	1,024			
f	>1,024			

Figure 5.6 IC_{50} values of amidine COEs against HepG2 cells evaluated by the MTT assay. The values are in the unit of μg mL^{-1}.

According to the data shown in Figure 5.6, the most active compound (**1b**) has little cytotoxicity against HepG2 cells. Notably, cytotoxicity is highly sensitive to hydrophobicity of a substituent on an amino nitrogen of an amidine unit. Compounds with propyl substituents on amino nitrogens (**3a**, **4a**, and **4b**) show high cytotoxic effects. **3a** has slightly lower cytotoxicity (IC_{50} = 128 μg mL^{-1}) compared to **4a** and **4b** (IC_{50} = 32 and 16 μg mL^{-1}, respectively) due to a lower hydrophobicity of cyclopropyl substituents compared to *n*-propyl substituents. Hydrophobicity of terminal alkyl groups also affects cytotoxicity of COEs. As terminal alkyl groups get larger (more hydrophobic), one observes a decrease in IC_{50}. For example, **1c** has significantly lower IC_{50} (256 μg mL^{-1}) compared to **1a** and **1b** (1,024 μg mL^{-1}). This could be explained by the high hydrophobicity of a methylcyclopropyl group in **1c** compared to ethyl and cyclopropyl groups in **1a** and **1b**, respectively. Similar trend can also be observed for **4a** and **4b** which have an IC_{50} of 32 and 16 μg mL^{-1}, respectively. While toxicity profile is highly sensitive to substituents on amino nitrogens, it was interestingly not found to be highly dependent on substituents on imino nitrogens. There is no IC_{50} reduction in **1f** compared to **1d** (>1,024 μg mL^{-1}) which has methyl and cyclopropyl substituents at imino nitrogens, respectively. In addition, a COE with cyclopropyl groups on amino nitrogens (**1c**) exhibits significantly higher cytotoxicity compared to a COE with cyclopropyl groups on imino nitrogens (**1f**).

5.5 Conclusions

In summary, we report a novel series of COEs with amidine groups with various substituents and terminal alkyl groups. Amidine groups simultaneously act as cationic and hydrogen bond forming moiety thus replacing quaternary ammonium and amide groups in COEs structures in Chapter 4. Overall, we found an amidine unit to be a "privileged" scaffold for antimicrobial applications as it markedly improves broad spectrum activity of COEs compared to quaternary ammonium groups. **1b** has the most potent broad spectrum antimicrobial activity with undetectable *in vitro* cytotoxicity. However, its potency against *P. aeruginosa* biofilms has not yet been explored. *In vitro* cytotoxicity of the COEs shows strong correlation to hydrophobicity of substituents on terminal alkyl groups and on amino nitrogens of amidine units, whereas there is little change in the cytotoxicity across various substituents on imino nitrogens. This work paves a path for COE designs that do not contain quaternary ammonium cations yet maintain excellent antimicrobial efficacy which could be further improved to address *in vivo* toxicity liabilities.

5.6 Experimental methods

Materials and instruments

Solvent and reagents were purchased from common suppliers unless specified otherwise (e.g., Sigma-Aldrich, Acros Organics, Fisher Scientific, and

TCI) and used as received. Dry and inhibitor-free THF and DMF were received from a solvent purification system using packed alumina columns under argon.

Flash chromatography was carried out either on Silicycle SiliaFlash P60 silica gel with pressurized air up to 0.5 bar or on Biotage Sfär Duo C18 columns. For thin layer chromatography (TLC), EMD Millipore Analytical Chromatography TLC Silica gel 60 F254 with aluminum back were used with UV light (254/366 nm) for detection. Purities of target compounds were analyzed by high performance liquid chromatography (HPLC) (Shimadzu) with a PS-C18 column (Phenomenex) using 5% to 40% acetonitrile in water as an eluent system with 0.1% acetic acid as an additive.

^{1}H-NMR (500 MHz and 600 MHz) and ^{13}C-NMR (125 MHz and 151 MHz) spectra were obtained from an actively shielded Varian Unity Inova 500 MHz spectrometer or Varian VNMRS 600 MHz. The multiplicity of all signals was described by s (singlet), d (doublet), t (triplet), and m (multiplet). Chemical shifts (δ in ppm) were referenced to the solvent residual peak of $CDCl_3$ (^{1}H-NMR: δ = 7.26; ^{13}C-NMR: δ = 77.0), CD_3CN (^{1}H-NMR: δ = 1.94; ^{13}C-NMR: δ = 1.32 and 118.36), or DMSO-d_6 (^{1}H NMR: δ = 2.50; ^{13}C-NMR: δ = 39.52). Mass spectra were collected on Waters Micromass LCT-Premier mass spectrometer.

Minimum inhibitory concentration experiments

The experiments were performed by a broth-microdilution method. First, each bacterial stain from a frozen stock were incubated on an LB agar plate

overnight at 37 °C. A single colony from an agar plate was inoculated in either LB or CA-MHB for 3-5 hours at 37 °C with 200 rpm orbital shaking. Bacterial cultures were harvested at mid-log phase and were diluted in LB or CA-MHB to achieve the cell density of 1×10^6 cfu mL^{-1}. COEs and antibiotic solutions were serially diluted in 96-well plates. Each well contains 50 μL of COE or antibiotic solutions. Then, 50 μL of the diluted bacterial suspensions were added to each well. The 96-well plates were incubated at 37 °C with 200 rpm orbital shaking overnight. The concentrations that inhibit the growth of bacteria by visible eyes are recorded as MICs.

5.7 Synthetic methods

Synthesis of *N*-Boc-3-chloropropylamine (5)

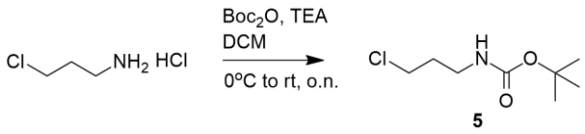

5

In a round-bottomed flask equipped with a magnetic stir bar and a dropping funnel, 3-chloropropylamine HCl (5 g, 1 equiv) and TEA (11 mL, 2.1 equiv) was suspended in 30 mL of DCM. The suspension was cooled down to 0 °C by an ice bath. A solution of Boc_2O (9.2 g, 1.1 equiv) in 25 mL DCM was added to the dropping funnel and was added to the reaction flask dropwise. Then, the reaction mixture was allowed to warm up to room temperature and stirred overnight. The crude reaction was diluted in DCM and washed with water and brine. Combined organic layers were dried over Na_2SO_4 and evaporated under

reduced pressure. The product was purified by a silica gel column chromatography (20% EA/hexanes) to obtain compound **5** as a clear oil (97%).

^{1}H NMR (500 MHz, $CDCl_3$): δ (ppm) 4.64 (s, 1H), 3.59 (t, J = 6 Hz, 2H), 3.26–3.30 (m, 2H), 1.95–1.98 (m, 2H), 1.44 (s, 9H); **^{13}C NMR (125 MHz, $CDCl_3$):** δ (ppm) 156.09, 42.51, 38.05, 32.71, 28.52, 27.55.

Synthesis of compound 6

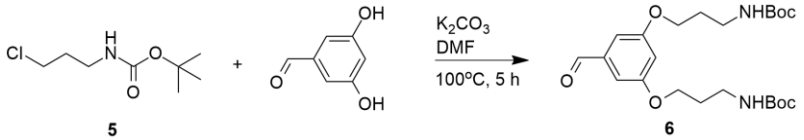

5 6

In a flame-dried round bottom flask equipped with a stir bar, 3,5-dihydroxybenzaldehyde (650 mg, 1 equiv), compound **5** (2 g, 2.3 equiv), and K_2CO_3 (1.5 g, 2.5 equiv) were added under inert atmosphere followed by an addition of 20 mL dry DMF. The resulting suspension was stirred under inert atmosphere at 100 °C for 5 hours. After cooling down to room temperature, the reaction mixture was diluted in DCM, washed with 1 M LiCl, water, and brine. The combined organics were dried over Na_2SO_4 and solvents were evaporated using a rotary evaporator. The crude reaction was purified by a silica gel column chromatography (40% EA/hexanes) to obtain compound **6** as a clear viscous liquid (95%).

^{1}H NMR (500 MHz, $CDCl_3$): δ (ppm) 9.89 (s, 1H), 6.99 (d, J = 2.5 Hz, 2H), 6.69 (t, J = 2.5 Hz, 1H), 4.71 (s, 2H), 4.05 (t, J = 6 Hz, 4H), 3.31–3.35 (m, 4H),

1.97–2.02 (m, 4H), 1.44 (s, 18H); **^{13}C NMR (125 MHz, $CDCl_3$):** δ (ppm) 191.74, 160.32, 155.86, 138.27, 107.91, 107.69, 79.23, 65.97, 37.70, 31.48, 29.37, 28.29.

Synthesis of compound 7

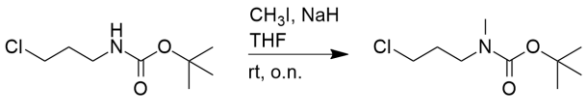

5 **7**

In a dry round bottom flask was added **5** and dry THF. NaH (60% in mineral oil, 1.1 equiv) was slowly added to the reaction flask at room temperature and the mixture was stirred for 1 hour. Then, methyl iodide (1.2 equiv) was added via a syringe. The resulting mixture was stirred overnight at room temperature. The mixture was concentrated under reduced pressure and diluted in ethyl acetate. The crude mixture was washed with water and brine, dried over Na_2SO_4. Solvents were removed by using a rotary evaporator. The pure product was afforded by silica gel column chromatography (8% EA/hexanes) as a clear liquid (80%).

^{1}H NMR (500 MHz, $CDCl_3$): δ (ppm) 3.54 (t, J = 6 Hz, 2H), 3.35 (t, J = 7 Hz, 2H), 2.87 (s, 3H), 1.45 (s, 9H); **^{13}C NMR (125 MHz, $CDCl_3$):** δ (ppm) 155.91, 105.15, 46.48, 42.45, 34.67, 31.19, 28.57.

Synthesis of compound 8

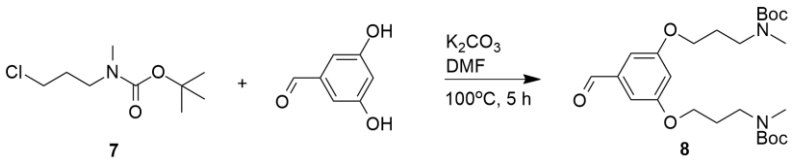

Compound **8** was synthesized according to the procedure for compound **6**. **^{1}H NMR (500 MHz, $CDCl_3$):** δ (ppm) 9.88 (s, 1H), 6.98 (d, *J* = 3 Hz, 2H), 6.68 (t, *J* = 3 Hz, 1H), 4.01 (t, *J* = 7.5 Hz, 4H), 3.41 (t, *J* = 8.5 Hz, 2H), 2.87 (s, 6H), 1.98 – 2.04 (m, 4H), 1.43 (s, 18H); **^{13}C NMR (125 MHz, $CDCl_3$):** δ (ppm) 192.01, 160.65, 155.95, 138.50, 108.04, 79.62, 65.89, 46.00, 34.76, 28.57, 27.79.

General procedure for the Horner-Wadsworth-Emmons reactions

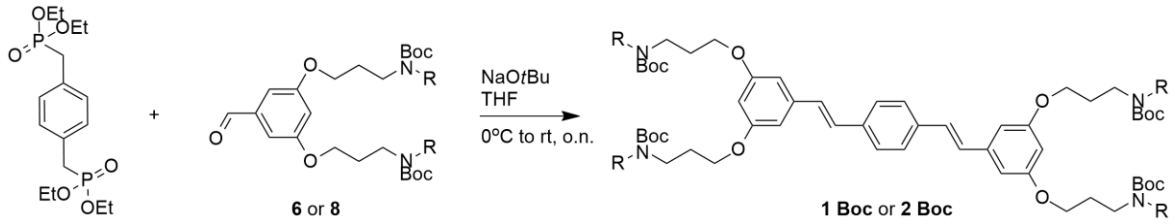

A flame-dried round-bottomed flask equipped with a magnetic stir bar was added tetraethyl (1,4-phenylenebis(methylene))bis(phosphonate) (1 eqiv) and benzaldehyde intermediate **6** or **8** (1.95 eqiv) in dry THF under inert atmosphere. After cooling the solution down in an ice bath, a solution of NaO*t*Bu in dry THF (2.1 eqiv) was slowly added to the reaction mixture via a syringe. The reaction was warmed up to room temperature and was stirred overnight. Then, the reaction mixture was diluted in DCM, washed with water and brine. Combined organic layers were dried over Na_2SO_4. Volatile solvents

were removed using a rotary evaporator. The crude reaction was recrystallized in DCM/hexanes to obtain a pure product.

Compound 1 Boc

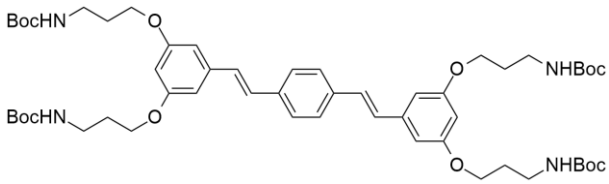

^{1}H NMR (500 MHz, $CDCl_3$): δ (ppm) 7.49 (s, 4H), 7.06 (d, J = 16 Hz, 2H), 7.01 (d, J = 16.5 Hz, 2H), 6.67 (d, J = 2 Hz, 4H), 6.38 (t, J = 2 Hz, 2H), 4.76 (s, 3H), 4.05 (t, J = 5.5 Hz, 8H), 3.32–3.36 (m, 8H), 1.97–2.01 (m, 8H), 1.45 (s, 36H); **^{13}C NMR (125 MHz, $CDCl_3$):** δ (ppm) 160.30, 156.16, 139.52, 136.74, 128.97, 128.64, 127.07, 105.47, 101.16, 79.40, 66.00, 38.13, 29.69, 28.57.

Compound 2 Boc

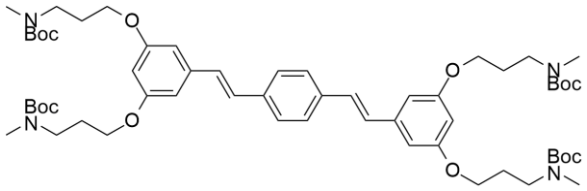

^{1}H NMR (500 MHz, $CDCl_3$): δ (ppm) 7.49 (s, 4H), 7.05 (d, J = 16 Hz, 2H), 7.00 (d, J = 16.5 Hz, 2H), 6.65 (d, J = 2.5 Hz, 4H), 6.37 (t, J = 2.5 Hz, 2H), 4.00 (t, J = 6 Hz, 8H), 3.42 (t, J = 7 Hz, 8H), 2.89 (s, 12H), 2.00–2.03 (m, 8H), 1.45 (s, 36H); **^{13}C NMR (125 MHz, $CDCl_3$):** δ (ppm) 160.38, 155.98, 139.43, 136.75, 128.82, 128.73, 127.04, 105.29, 101.08, 79.54, 65.29, 46.08, 28.60, 28.11.

General procedure for Boc deprotection reactions

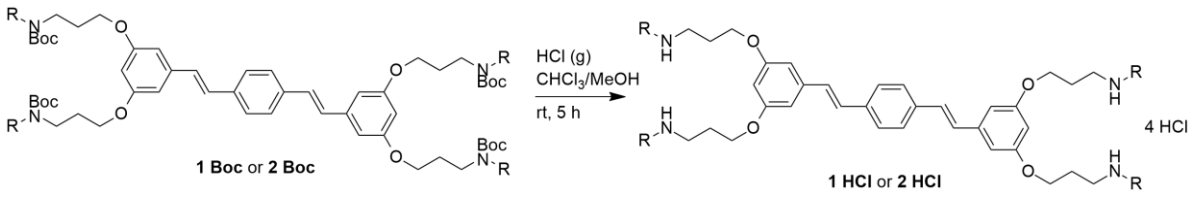

A dry reaction vessel containing compound **1 Boc** or **2 Boc** was added dry chloroform to dissolve the starting material. After that, HCl (g) was periodically bubbled into the solution at room temperature while stirring. During the course of the reaction, small amounts of MeOH was added over time to help dissolve precipitates. After 5 hours, the reaction was dried under reduced pressure to yield the corresponding amine HCl salt.

Compound 1 HCl

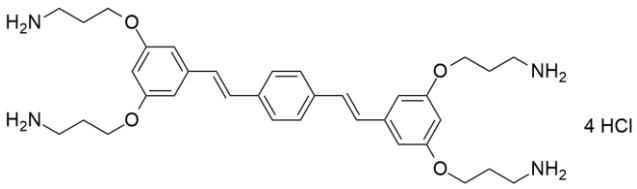

^{1}H NMR (500 MHz, CD_3OD): δ (ppm) 7.56 (s, 4H), 7.18 (d, *J* = 16.5 Hz, 2H), 7.12 (d, *J* = 16.5 Hz, 2H), 6.81 (d, *J* = 2 Hz, 4H), 6.51 (t, *J* = 2 Hz, 2H), 4.17 (t, *J* = 5.5 Hz, 8H), 3.18 (t, *J* = 7.5 Hz, 8H), 2.15–2.20 (m, 8H); **^{13}C NMR (125 MHz, CD_3OD):** δ (ppm) 161.34, 141.06, 138.11, 129.99, 129.49, 128.01, 106.59, 102.22, 66.43, 38.65, 28.37.

Compound 2 HCl

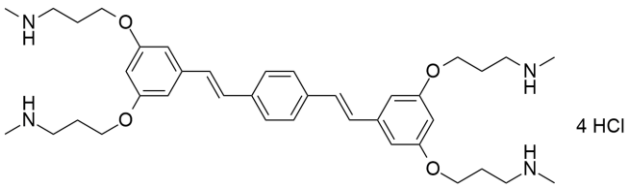

^{1}H NMR (500 MHz, CD_3OD): δ (ppm) 7.56 (s, 4H), 7.18 (d, *J* = 16.5 Hz, 2H), 7.12 (d, *J* = 16.5 Hz, 2H), 6.82 (d, *J* = 2 Hz, 4H), 6.52 (t, *J* = 2 Hz, 2H), 4.17 (t, *J* = 6 Hz, 8H), 3.25 (t, *J* = 7 Hz, 8H), 2.76 (s, 12H), 2.18–2.23 (m, 8H); **^{13}C NMR (125 MHz, CD_3OD):** δ (ppm) 161.32, 141.12, 138.15, 130.06, 129.49, 128.02, 106.65, 102.26, 66.40, 48.38, 33.93, 27.21.

General procedure for the preparation of amine intermediates from an alkyl iodide

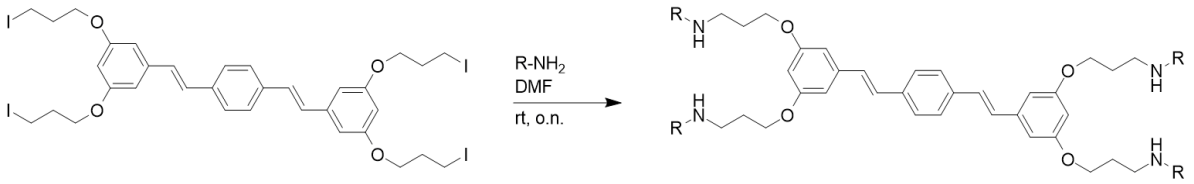

To a dry 1-Dram vial was added **COE2-3I-C3** and dry DMF under inert atmosphere. Thereafter, appropriate primary amine (40 equiv) was added while stirring vigorously. The reaction mixture was stirred overnight at room temperature. The mixture was then poured into 3 M HCl solution in diethyl ether. Precipitate was collected via centrifugation and washed with two additional portions of diethyl ether. The precipitate was dissolved in water and partitioned between DCM and 2 M NaOH. The organic layers were collected, and the aqueous layer was extracted with 5 additional portions of DCM. The

organic layers were combined and dried over Na_2SO_4. Evaporation of volatile solvents yielded a green viscous oil.

Compound 3

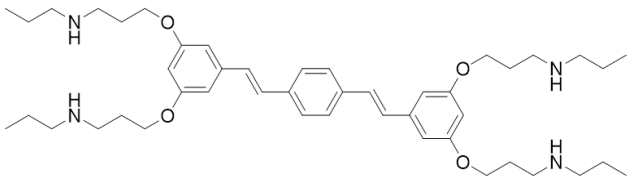

Yield: 97%; **^{1}H NMR (500 MHz, $CDCl_3$):** δ (ppm) 7.48 (s, 4H), 7.05 (d, *J* = 16.5 Hz, 2H), 7.00 (d, *J* = 16.5 Hz, 2H), 6.66 (d, *J* = 2.5 Hz, 4H), 6.40 (t, *J* = 2.5 Hz, 2H), 4.07 (t, *J* = 6 Hz, 8H), 2.81 (t, *J* = 7 Hz, 8H), 2.61 (t, *J* = 7.5 Hz, 8H), 1.96–2.01 (m, 8H), 1.49–1.56 (m, 8H), 0.93 (t, *J* = 7.5 Hz, 12H); **^{13}C NMR (125 MHz, $CDCl_3$):** δ (ppm) 160.48, 139.37, 136.74, 128.77, 128.75, 127.00, 105.33, 101.15, 66.65, 52.10, 47.06, 29.98, 23.36, 11.92.

Compound 4

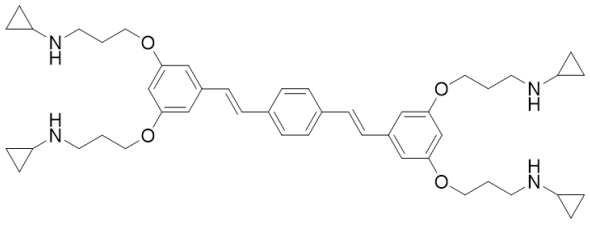

Yield: 98%; **^{1}H NMR (500 MHz, $CDCl_3$):** δ (ppm) 7.49 (s, 4H), 7.06 (d, *J* = 16.5 Hz, 2H), 7.01 (d, *J* = 16 Hz, 2H), 6.67 (d, *J* = 2.5 Hz, 4H), 6.40 (t, *J* = 2 Hz, 2H), 4.06 (t, *J* = 6.5 Hz, 8H), 2.90 (t, *J* = 6.5 Hz, 8H), 2.13–2.18 (m, 4H), 1.96–2.01 (m, 8H), 0.43–0.47 (m, 8H), 0.34–0.36 (m, 8H); **^{13}C NMR (125 MHz, $CDCl_3$):** δ (ppm)

160.51, 139.38, 136.75, 128.79, 128.77, 127.02, 105.35, 101.18, 66.63, 46.75, 30.57, 29.86, 6.45.

Synthesis of compound 9[127]

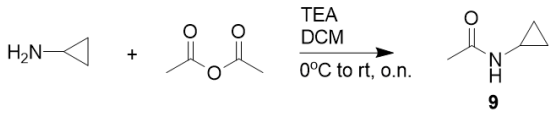

9

To a flame dried round bottom flask was added cyclopropylamine, triethylamine (1.1 equiv), and DCM. The solution was cooled down to 0°C with an ice bath and acetic anhydride (1.1 equiv) was slowly added. After the addition, the reaction mixture was stirred at room temperature overnight. Volatile organic compounds were removed *in vacuo*. The residue was then diluted in diethyl ether and K_2CO_3 was added to the solution. After stirring for 2 hours, K_2CO_3 was filtered off and the residue was dried *in vacuo*. Crude residue was then purified using silica gel column chromatography to obtain a product as a mixture of two conformers in a ratio of 5:1 in quantitative yield.

^{1}H NMR (500 MHz, $CDCl_3$): δ (ppm) 5.90 (s, 1H), 5.72 (s, 0.2H), 2.64–2.69 (m, 1H), 2.55–2.58 (m, 0.2H), 1.92 (s, 3H), 2.13 (s, 0.6H), 0.71–0.75 (m, 2H), 0.78–0.82 (m, 0.4H), 0.46–0.49 (m, 2H), 0.56–0.59 (m, 0.4H); **^{13}C NMR (125 MHz, $CDCl_3$):** δ (ppm) 171.71, 24.50, 23.22, 22.77, 21.14, 8.31, 6.59.

General procedure for the syntheses of imidate salts

Procedure A

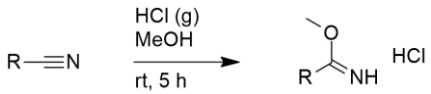

In a dry microwave reaction tube with a magnetic stir bar was added 2 mL of dry MeOH under inert atmosphere. MeOH was bubbled with HCl (g) for 30 minutes at room temperature. After saturating MeOH with HCl, nitrile (1 g) was added to the reaction vessel. The reaction vessel was then sealed and stirred at room temperature for 5 hours. Removal of volatile compounds from the reaction under high vacuum yielded the corresponding imidate salt.

Procedure B

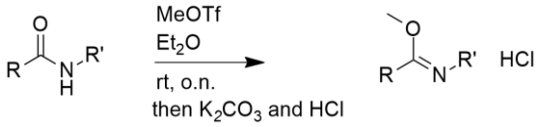

Amide is added to a flame-dried round bottomed flask equipped with a stir bar and is dissolved in dry diethyl ether. Methyl triflate was then slowly added to the solution via a syringe. The resulting mixture was allowed to stir at room temperature overnight. Dry K_2CO_3 powder was then added, and the suspension was stirred for 30 minutes. The reaction mixture was filtered and added to etherated HCl (2 M). The mixture was then centrifuged, and supernatant was discarded. The resulting oil was dried under high vacuum to obtain the corresponding imidate salt as a clear oil.

Compound a

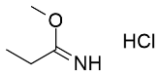

Yield: 65%; **^{1}H NMR (500 MHz, CD_3CN):** δ (ppm) 4.16 (s, 3H), 2.70 (q, J = 7.5 Hz, 2H), 1.23 (t, J = 7.5 Hz, 3H); **^{13}C NMR (125 MHz, CD_3CN):** δ (ppm) 182.55, 61.09, 27.25, 9.83.

Compound b

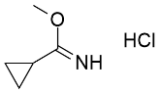

Yield: 80%; **^{1}H NMR (500 MHz, CD_3CN):** δ (ppm) 12.26 (s, 1H), 10.62 (s, 1H), 4.08 (s, 3H), 2.28–2.33 (m, 1H), 1.19–1.28 (m, 4H); **^{13}C NMR (125 MHz, CD_3CN):** δ (ppm) 181.96, 60.63, 13.29, 11.12.

Compound c

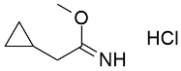

Yield: 70%; **^{1}H NMR (500 MHz, CD_3CN):** δ (ppm) 12.20 (s, 1H), 11.22 (s, 1H), 4.19 (s, 3H), 2.58 (d, J = 7 Hz, 2H), 1.07–1.13 (m, 1H), 0.50–0.60 (m, 2H), 0.33–0.36 (m, 2H); **^{13}C NMR (125 MHz, CD_3CN):** δ (ppm) 181.53, 61.20, 37.76, 7.93, 4.95.

Compound d

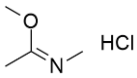

Yield: 68% (a mixture of two different conformers at 3:1 ratio); **^{1}H NMR (500 MHz, CD_3CN):** δ (ppm) 4.17 (s, 3H), 4.14 (s, 1H), 3.12 (d, J = 4.5 Hz, 3H), 2.92 (d, J = 4.5 Hz, 1H), 2.37 (s, 1H), 2.30 (s, 3H); **^{13}C NMR (125 MHz, CD_3CN):** δ (ppm) 61.15, 60.60, 32.21, 18.28, 17.27.

Compound e

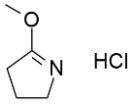

Yield: 63%; **^{1}H NMR (500 MHz, CD_3CN):** δ (ppm) 4.45 (s, 3H), 4.00 (t, J = 7.5 Hz, 2H), 3.08 (t, J = 8 Hz, 2H), 2.41–2.47 (m, 2H); **^{13}C NMR (125 MHz, CD_3CN):** δ (ppm) 63.63, 49.07, 31.64, 20.01.

Compound f

Yield: 62% (a mixture of two different conformers at 3:1 ratio); **^{1}H NMR (500 MHz, CD_3CN):** δ (ppm) 4.18 (s, 3H), 4.15 (s, 1H), 3.01–3.07 (m, 0.33H), 2.92–2.97 (m, 1H), 2.53 (s, 1H), 2.46 (s, 3H), 1.11–1.15 (m, 2H), 0.95–0.99 (m, 2.6H), 0.85–0.89 (m, 0.7H); **^{13}C NMR (125 MHz, CD_3CN):** δ (ppm) 61.75, 60.61, 28.43, 18.73, 17.19, 6.86, 5.82.

General procedure for the syntheses of amidine COEs

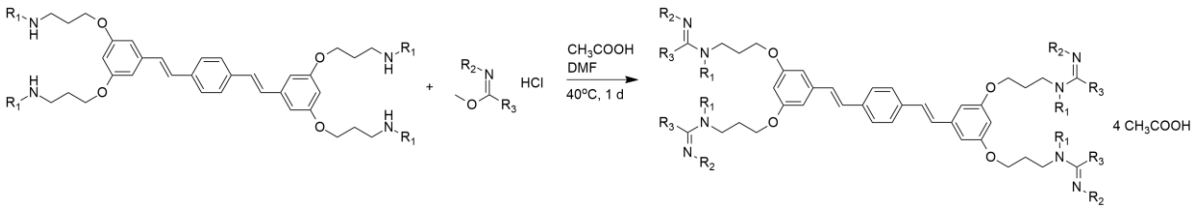

Note: If the amine intermediate is a HCl salt, neutralize the amine HCl by basic water extractions or treatments with Amberlyst A21 resin to obtain a free base form and evaporate solvents to complete dryness before use.

In a flame-dried 1-Dram vial, amine intermediate (18 mg) was dissolved in 0.4 mL of dry DMF under inert atmosphere. Meanwhile, in another 1-Dram vial, imidate HCl salt was neutralized with 2 M K_2CO_3 and extracted with chloroform. After the extraction, 0.2 mL of chloroform (containing 10 equiv of imidate) was transferred to the reaction vial. Acetic acid (4 equiv) was slowly added to the reaction mixture. The reaction was stirred at 40 °C for 1 day. Thereafter, the crude reaction was poured into Et_2O containing extra equivalent of acetic acid to precipitate the product. The crude product was centrifuged and washed with Et_2O, and dried. Then, the crude product was dissolved in a minimal water and was purified by a reverse-phase silica gel column chromatography using a flash chromatography system (Gradient: 0% to 40% acetonitrile/water with 0.1% acetic acid as an additive). Purified fractions were combined and lyophilized to obtain pure product as white solid.

Compound 1a

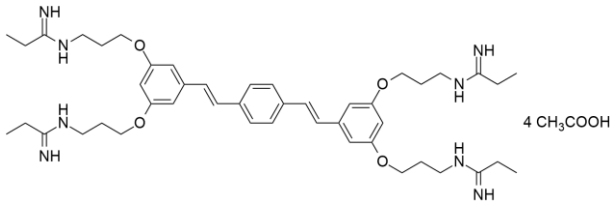

Yield: 91%; **^{1}H NMR (500 MHz, DMSO-d_6):** δ (ppm) 7.60 (s, 4H), 7.26 (d, J = 16.5 Hz, 2H), 7.17 (d, J = 16 Hz, 2H), 6.79 (s, 4H), 6.44 (d, J = 2.5 Hz, 2H), 4.08 (t, J = 6.5 Hz, 8H), 3.36 (t, J = 7 Hz, 8H), 2.38–2.43 (m, 8H), 1.96–2.00 (m, 8H), 1.67 (s, 12H), 1.14 (t, J = 8 Hz, 12H); **^{13}C NMR (125 MHz, DMSO-d_6):** δ (ppm) 174.55, 168.00, 159.80, 139.11, 136.38, 128.55, 128.38, 126.91, 105.32, 100.93, 65.04, 38.65, 27.30, 25.99, 24.91, 11.83; **HRMS (ESI):** ($[M+2H]^{2+}$) calcd: 398.2682, found: 398.2671.

Compound 1b

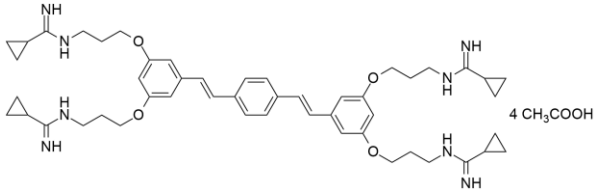

Yield: 92%; **^{1}H NMR (500 MHz, DMSO-d_6):** δ (ppm) 7.60 (s, 4H), 7.27 (d, J = 16.5 Hz, 2H), 7.18 (d, J = 16.5 Hz, 2H), 6.80 (s, 4H), 6.44 (s, 2H), 4.08 (t, J = 6.5 Hz, 8H), 3.39 (t, J = 7 Hz, 8H), 1.96–2.02 (m, 8H), 1.93–1.94 (m, 4H), 1.69 (s, 12H), 1.04–1.11 (m, 8H), 0.97–1.03 (m, 8H); **^{13}C NMR (125 MHz, DMSO-d_6):** δ (ppm) 174.52, 168.14, 159.80, 159.75, 139.12, 136.39, 128.58, 128.38, 126.92,

105.28, 100.92, 65.09, 27.33, 24.58, 12.75, 8.35; **HRMS (ESI):** ([M+2H]$^{2+}$) calcd: 422.2682, found: 422.2668.

Compound 1c

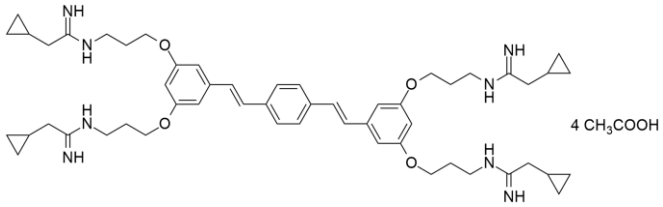

Yield: 86%; **^{1}H NMR (500 MHz, DMSO-d_6):** δ (ppm) 7.60 (s, 4H), 7.27 (d, J = 16.5 Hz, 2H), 7.18 (d, J = 16.5 Hz, 2H), 6.80 (s, 4H), 6.44 (s, 2H), 4.10 (t, J = 6 Hz, 8H), 3.42 (t, J = 7 Hz, 8H), 2.33 (d, J = 7.5 Hz, 8H), 1.98–2.04 (m, 8H), 1.71 (s, 9H), 1.06–1.10 (m, 4H), 0.43–0.47 (m, 8H), 0.27–0.31 (m, 8H); **^{13}C NMR (125 MHz, DMSO-d_6):** δ (ppm) 174.27, 166.79, 159.77, 139.13, 136.38, 128.60, 128.34, 126.92, 105.34, 101.01, 64.90, 38.70, 36.29, 27.19, 24.32, 8.96, 4.08; **HRMS (ESI):** ([M+2H]$^{2+}$) calcd: 450.2995, found: 450.2993.

Compound 1d

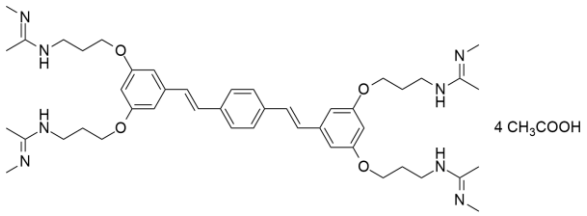

Yield: 82% (NMR shows a mixture of two different conformers at imino nitrogen); **^{1}H NMR (500 MHz, DMSO-d_6):** δ (ppm) 7.60 (s, 4H), 7.27 (d, J = 16.5 Hz, 2H), 7.18 (d, J = 16 Hz, 2H), 6.79 (s, 4H), 6.43 (s, 2H), 4.07 (t, J = 6.5 Hz,

8H), 3.36–3.44 (m, 8H), 2.79–2.86 (m, 12H), 2.15 (s, 12H), 1.99 (t, J = 6 Hz, 8H), 1.70 (s, 12H).; **^{13}C NMR (125 MHz, DMSO-d_6):** δ (ppm) 175.00, 163.62, 163.06, 160.27, 139.60, 136.85, 129.04, 128.85, 127.37, 105.67, 101.31, 65.44, 30.66, 29.58, 28.85, 27.76, 25.27, 16.88, 16.50; **HRMS (ESI):** ($[M+2H]^{2+}$) calcd: 398.2682, found: 398.2675.

Compound 1e

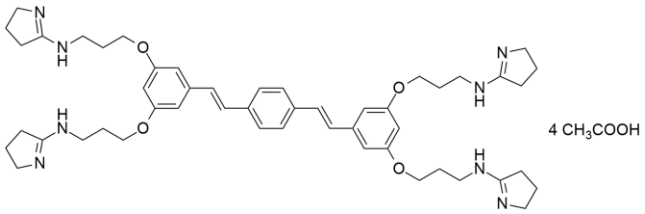

Yield: quant.; **^{1}H NMR (500 MHz, DMSO-d_6):** δ (ppm) 7.62 (s, 4H), 7.30 (d, J = 16 Hz, 2H), 7.20 (d, J = 17 Hz, 2H), 6.82 (s, 4H), 6.46 (s, 2H), 4.09–4.10 (m, 8H), 3.50–3.54 (m, 8H), 3.39–3.42 (m, 8H), 2.73–2.75 (m, 8H), 1.97–2.01 (m, 16H), 1.74 (s, 6H).; **^{13}C NMR (125 MHz, DMSO-d_6):** δ (ppm) 175.60, 168.25, 160.26, 139.60, 136.86, 129.08, 128.82, 127.39, 105.72, 101.46, 65.41, 48.82, 31.19, 28.26, 24.47, 21.23; **HRMS (ESI):** ($[M+2H]^{2+}$) calcd: 422.2682, found: 422.2673.

Compound 1f

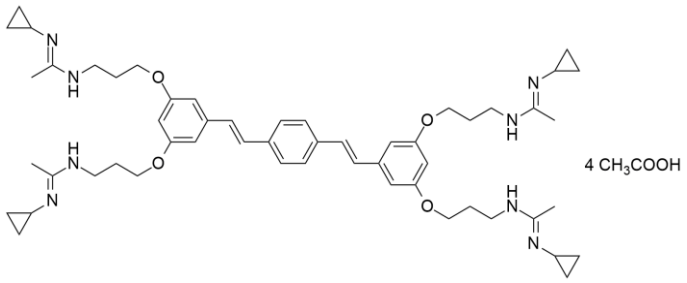

Yield: quant. (NMR shows a mixture of two different conformers at imino nitrogen); **^{1}H NMR (500 MHz, DMSO-d_6):** δ (ppm) 7.60 (s, 4H), 7.26 (d, J = 16.5 Hz, 2H), 7.18 (d, J = 16 Hz, 2H), 6.79 (s, 4H), 6.43 (s, 2H), 4.06 (t, J = 6 Hz, 8H), 3.23–3.51 (m, 8H), 2.62 (m, 4H), 2.19 (s, 12H), 1.96 (m, 8H), 1.70 (s, 12H), 0.71 (m, 8H), 0.57 (m, 8H); **^{13}C NMR (125 MHz, DMSO-d_6):** δ (ppm) 174.84, 159.81, 139.13, 136.39, 128.56, 128.40, 126.91, 105.18, 100.87, 65.01, 28.21, 24.23, 6.49; **HRMS (ESI):** ($[M+2H]^{2+}$) calcd: 450.2995, found: 450.2996.

Compound 2a

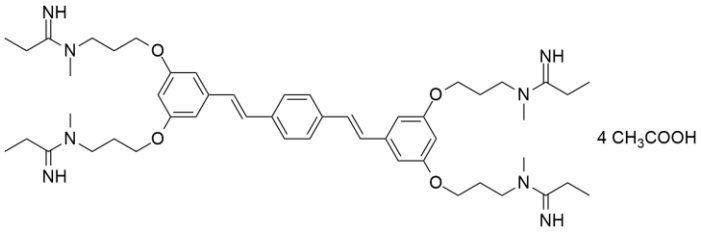

Yield: quant.; **^{1}H NMR (500 MHz, DMSO-d_6):** δ (ppm) 7.56 (s, 4H), 7.22 (d, J = 16 Hz, 2H), 7.14 (d, J = 16 Hz, 2H), 6.76 (s, 4H), 6.38 (d, J = 2.5 Hz, 2H), 4.02 (t, J = 5.5 Hz, 8H), 3.58 (t, J = 7 Hz, 8H), 3.04 (s, 12H), 2.45–2.50 (m, 8H), 1.97–2.01 (m, 8H), 1.64 (s, 12H), 1.08 (t, J = 6 Hz, 12H); **^{13}C NMR (125 MHz, DMSO-d_6):** δ (ppm) 173.68, 168.29, 159.66, 139.21, 136.39, 128.64, 128.38, 126.93,

105.20, 100.85, 64.84, 48.05, 36.92, 26.32, 24.56, 24.41, 11.10; **HRMS (ESI):** ($[M+2H]^{2+}$) calcd: 426.2995, found: 426.2994.

Compound 2b

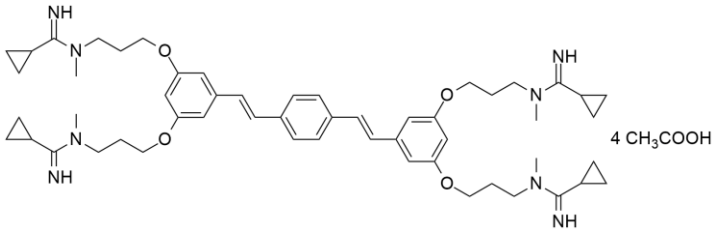

Yield: quant.; **^{1}H NMR (500 MHz, DMSO-d_6):** δ (ppm) 7.61 (s, 4H), 7.28 (d, J = 16.5 Hz, 2H), 7.19 (d, J = 16 Hz, 2H), 6.80 (d, J = 2 Hz, 4H), 6.44 (t, J = 2 Hz, 2H), 4.08 (t, J = 6 Hz, 8H), 3.75 (t, J = 7.5 Hz, 8H), 3.13 (s, 12H), 2.02–2.08 (m, 8H), 1.90–1.96 (m, 4H), 1.70 (s, 9H), 0.96–0.98 (m, 8H), 0.91–0.95 (m, 8H); **^{13}C NMR (125 MHz, DMSO-d_6):** δ (ppm) 173.44, 167.11, 159.73, 139.19, 136.40, 128.64, 128.39, 126.94, 105.20, 100.87, 64.96, 48.35, 37.36, 26.52, 24.28, 12.54, 7.02, 6.95; **HRMS (ESI):** ($[M+2H]^{2+}$) calcd: 450.2995, found: 450.2994.

Compound 3a

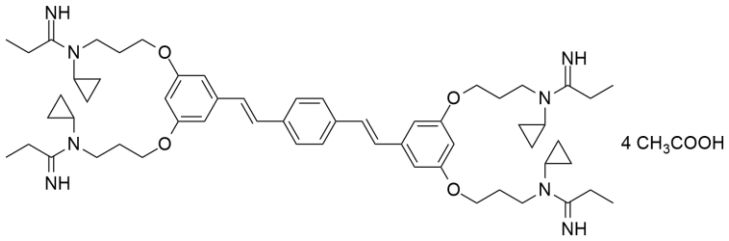

Yield: quant.; **^{1}H NMR (500 MHz, DMSO-d_6):** δ (ppm) 7.61 (s, 4H), 7.27 (d, J = 16.5 Hz, 2H), 7.20 (d, J = 16.5 Hz, 2H), 6.80 (d, J = 2 Hz, 4H), 6.44 (s, 2H),

4.07 (t, J = 6 Hz, 8H), 3.60 (t, J = 7 Hz, 8H), 2.76–2.79 (m, 4H), 2.57–2.62 (m, 8H), 2.02–2.06 (m, 8H), 1.71 (s, 12H), 1.11 (t, J = 7.5 Hz, 12H), 0.93–0.97 (m, 8H), 0.78–0.82 (m, 8H); **^{13}C NMR (125 MHz, DMSO-d_6):** δ (ppm) 173.52, 170.54, 159.73, 139.17, 136.39, 128.60, 128.42, 126.93, 105.18, 100.87, 65.18, 45.65, 30.32, 26.78, 24.84, 24.15, 11.05, 8.38; **HRMS (ESI):** ($[M+2H]^{2+}$) calcd: 478.3308, found: 478.3300.

Compound 4a

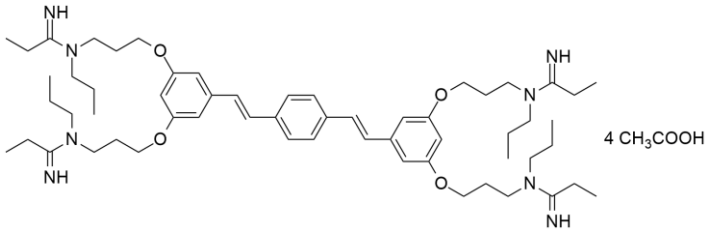

Yield: quant.; **^{1}H NMR (500 MHz, DMSO-d_6):** δ (ppm) 7.61 (s, 4H), 7.27 (d, J = 16.5 Hz, 2H), 7.19 (d, J = 16.5 Hz, 2H), 6.80 (d, J = 2H, 4H), 6.44 (t, J = 2.5 Hz, 2H), 4.07 (t, J = 6 Hz, 8H), 3.57 (t, J = 7.5 Hz, 8H), 3.35 (t, J = 8 Hz, 8H), 2.50 2.54 (m, 8H), 2.00–2.05 (m, 8H), 1.68 (s, 12H), 1.55–1.60 (m, 8H), 1.13 (t, J = 7.5 Hz, 12H), 0.88 (t, J = 7.5 Hz, 12H); **^{13}C NMR (125 MHz, DMSO-d_6):** δ (ppm) 173.64, 167.89, 159.68, 139.22, 136.39, 128.64, 128.38, 126.94, 105.28, 100.86, 64.88, 50.00, 45.67, 26.71, 24.62, 24.47, 20.19, 11.85, 11.61, 11.58, 10.72; **HRMS (ESI):** ($[M+2H]^{2+}$) calcd: 482.3621, found: 482.3619.

Compound 4b

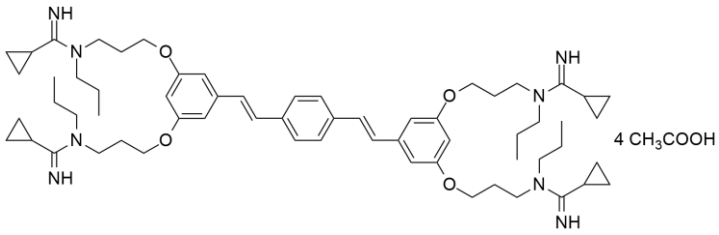

Yield: quant.; **^{1}H NMR (500 MHz, DMSO-d_6):** δ (ppm) 7.61 (s, 4H), 7.28 (d, J = 16.5 Hz, 2H), 7.20 (d, J = 16.5 Hz, 2H), 6.81 (d, J = 2.5 Hz, 4H), 6.44 (t, J = 2.5 Hz, 2H), 4.09 (t, J = 6 Hz, 8H), 3.70 (t, J = 7.5 Hz, 8H), 3.48 (t, J = 8 Hz, 8H), 2.03–2.08 (m, 8H), 1.94–1.99 (m, 4H), 1.72 (s, 9H), 1.57–1.65 (m, 8H), 1.02–1.05 (m, 8H), 0.95–1.00 (m, 8H), 0.89 (t, J = 7.5 Hz, 12H); **^{13}C NMR (125 MHz, DMSO-d_6):** δ (ppm) 173.34, 166.74, 159.71, 139.21, 136.39, 128.63, 128.38, 126.93, 105.27, 100.91, 64.96, 50.77, 46.39, 26.67, 23.84, 20.13, 12.41, 10,82, 7.50.

Chapter 6: Additional experiments

6.1 Additional structures of COEs for antimicrobial applications

In addition to the structures discussed in the previous chapters, especially Chapter 3–5, some other variations of COEs with different conjugated core, side chains and quaternary ammonium units were synthesized to further explore chemical spaces of COEs for antimicrobial applications. Dr. Hengjing Yan and co-workers discovered that antimicrobial activities of COEs are higher when the conjugated core is shortened. On an important note, however, reducing the conjugated core to stilbene **COE2-2C** did not provide results that conform to the trend (Figure 6.1).[35] Because one of the major driving forces of amphiphiles to interact with membranes is hydrophobic interaction, one surmises that stilbene unit with trimethyl ammonium groups may not have adequate hydrophobicity needed for membrane insertion.[103,128]

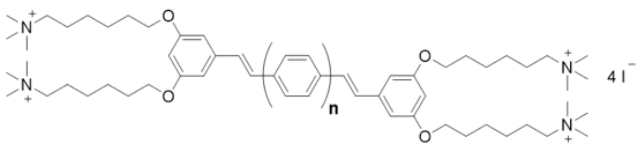

n	Compound	MIC (*E. coli* K12) (μM)
3	**COE2-5C**	512
2	**COE2-4C**	256
1	**COE2-3C**	64
0	**COE2-2C**	128

Figure 6.1 Trend of MICs of the COEs at different core length. At n = 0, the MIC does not further decrease, but rather increases to 128 μM. Note that **COE2-3C** was named as **COE2-3C-C6** in Chapter 3.

Structural modification of **COE2-2C** was preliminarily performed by Dr. Zichao Zhang and Dr. Alex Moreland. By replacing a methyl group on each quaternary ammonium cation with a variety of hydrocarbon units, a compound with hexyl groups **COE2-2hexyl** shows a significant reduction in MIC compared to **COE2-2C** (169 μg mL^{-1} for **COE2-2C** and 4 μg mL^{-1} for **COE2-2hexyl** against *E. coli* K12). The structure of **COE2-2hexyl** is shown in Figure 6.2.

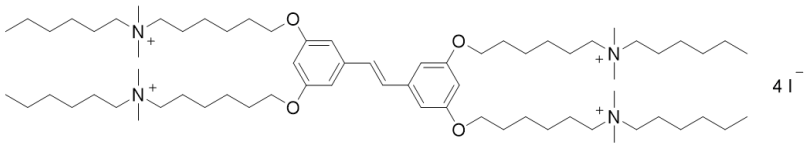

Figure 6.2 Chemical structure of **COE2-2hexyl**.

After a surprising discovery of **COE2-2hexyl**, many of its derivatives were synthesized with some help from Dr. Alex Moreland aiming at different size and shape of terminal alkyl groups. In addition, similar modifications were also made to a distyrylbenzene core. In brief, terminal alkyl groups were varied between 4 to 7 carbons. Some structures contain either branched or cyclic terminal groups. Moreover, COEs with terminal groups capped with extra functional groups namely, NH_2, glycerol, and SO_3^- were also synthesized in our group. A comprehensive diagram of chemical structures of COEs synthesized is shown in Figure 6.3. Note that some of them were a part of the study in Chapter 3.

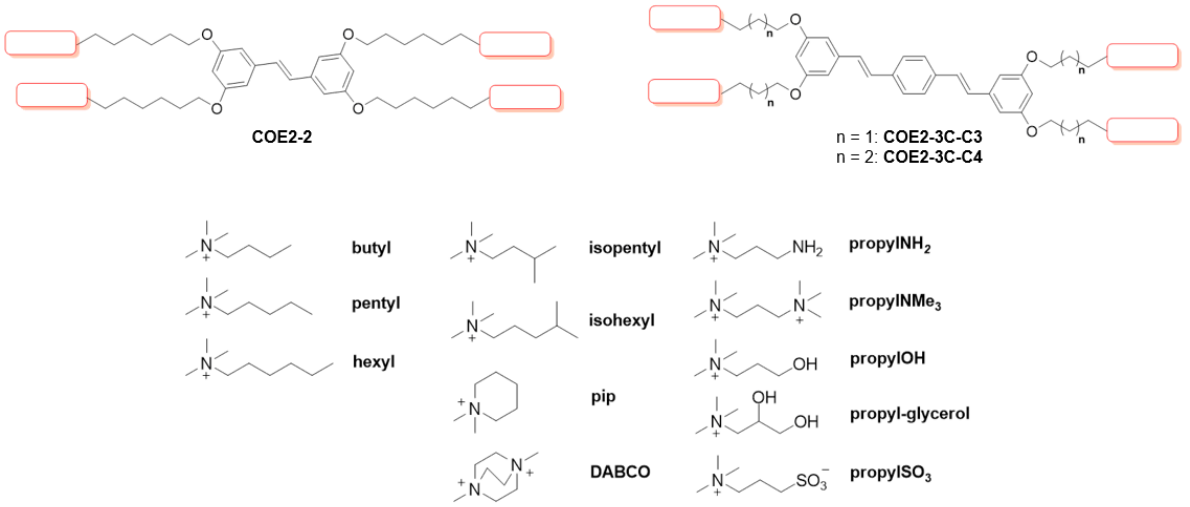

Figure 6.3 Chemical structures of possible cores and end groups of additional synthesized COEs

With help from Dr. Chenyao Nie, their antimicrobial activities against *E. coli* K12 and cytotoxicity against HepG2 cells were screened to analyze the structure-activity relationship. The MICs and IC_{50}'s of the COEs are shown in Table 6.1.

Table 6.1 Summary of MICs and IC_{50}'s of COEs in this study.

Compound	MIC[a] ($\mu g\ mL^{-1}$)	IC_{50}[b] ($\mu g\ mL^{-1}$)
COE2-2hexyl	4	7.3
COE2-2pentyl	4	41.3
COE2-2butyl	4	>128
COE2-2isohexyl	4	n.d.
COE2-2isopentyl	4	n.d.
COE2-2pip	128	n.d.
COE2-3C-C4hexyl	4	15.3
COE2-3C-C4pentyl	4	320.5

Compound	MIC[a] (μg mL^{-1})	IC_{50}[b] (μg mL^{-1})
COE2-3C-C4butyl	4	>1,024
COE2-3C-C4isohexyl	4	n.d.
COE2-3C-C4isopentyl	4	n.d.
COE2-3C-C4pip	4	473.6
COE2-3C-C3DABCO	>128	>128
COE2-3C-C3propylNH$_2$	32	>128
COE2-3C-C3propylNMe$_3$	>128	n.d.
COE2-3C-C3propylOH	>128	n.d.
COE2-3C-C3propyl-glycerol	>128	>1,024
COE2-3C-C3propylSO$_3$	>128	n.d.

[a] MICs against *E. coli* K12 in LB, [b] IC_{50}'s against HepG2 cells, n.d. = not determined

According to Table 6.1, consider the COEs with terminal alkyl chains that have no functional groups, the length of terminal alkyl groups greater than four carbons do not have any impact on antimicrobial activities. Moreover, the shape of the terminal alkyl chains also does not seem to impact the MICs. The MICs of all unbranched, branched, and cyclic terminal alkyl chains were 4 μg mL^{-1} regardless of a conjugated core, except **COE2-2pip** which has the MIC of 128 μg mL^{-1}. A significant increase in the MIC of **COE2-2pip** was unexpected. This may indicate unique properties of **COE2-2pip**. However, further investigation is warranted to fully understand this outlier.

Incorporation of additional functional groups to the terminal alkyl chains proved to be detrimental to antimicrobial activities. Consider **COE2-3C-**

C3DABCO and **COE2-3C-C3propylNMe3**, both structures contain an extra quaternary ammonium cation. It was hypothesized that this could give rise to higher bacterial selectivity since it could improve electrostatic interactions with negatively charged lipid head groups on bacterial membranes. However, both compounds completely lose their antimicrobial efficacy. This could be attributed to high hydrophilicity of the COEs making them lack driving forces for membrane insertion, as observed in **COE2-2C**. The introduction of hydroxy groups (**COE2-3C-C3propylOH** and **COE2-3C-C3propyl-glycerol**) also did not yield satisfactory results. Similarly, an addition of a sulfonate group to make a zwitterionic COE (**COE2-3C-C3propylSO3**) completely abolished its antimicrobial activity.

On the cytotoxicity aspect, there seems to be a difference between COEs with stilbene and distyrylbenzene cores. For the COEs with the same terminal alkyl chains, distyrylbenzene-based COEs show lower cytotoxicity (higher IC_{50}) towards HepG2 cells compared to stilbene-based COEs. For example, the IC_{50}'s of **COE2-2hexyl** and **COE2-3C-C3hexyl** are 7.3 and 15.3 μg mL^{-1}, respectively. Similar trend can be observed for COEs with pentyl chains (the IC_{50}'s of **COE2-2pentyl** and **COE2-3C-C3-pentyl** are 41.3 and 320.5 μg mL^{-1}, respectively). This data justified the use of a distyrylbenzene as a conjugated core for the design of antimicrobial COEs throughout Chapter 3–5. Lastly, it is worth noting that introduction of another functional group to COEs did not significantly increase cytotoxicity.

6.1.1 Synthetic procedures

In this section, synthetic procedures of the COEs that I led an effort to synthesize will be described. According to Figure 6.3, those COEs contain two different types of conjugated cores: (1) stilbene and (2) distyrylbenzene. Herein, only synthesis of the stilbene core will be described. One should refer to Chapter 3 for the syntheses of **COE2-3I-C3** and **COE2-3I-C4**, referred to in Chapter 3 as compound **5b** and **5c**, respectively. The synthetic scheme of the intermediate **COE2-2I** is shown in Figure 6.4. Briefly, compound **1** was subjected to a Wittig reaction condition with PPh_3CH_3Br and NaHMDS to achieve styrene derivative **2**. Bromides on 2 were converted into iodide under a Finkelstein reaction and the intermediate was directly subjected to olefin metathesis with Grubb's catalyst 2nd generation to yield **COE2-2I**.

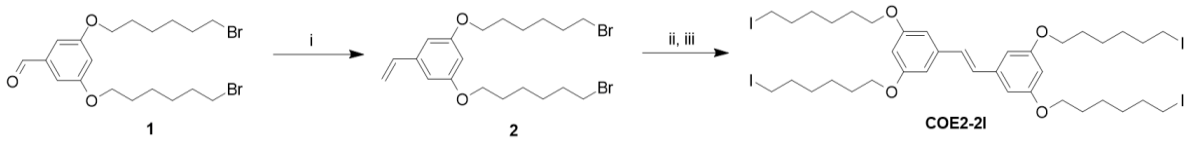

Figure 6.4 Synthetic scheme of **COE2-2I.** Conditions: (i) PPh_3CH_3Br (1.2 equiv), NaHMDS (1.1 equiv), THF, 0°C to rt, 3 h; (ii) NaI (excess), acetone, reflux, o.n.; (iii) Grubb's 2nd generation (0.01 mol%), DCM, reflux, 2 d.

The intermediates **COE2-2I**, **COE2-3I-C3**, and **COE2-3I-C4** were quarternized by various amines in DMF to yield target COEs with moderate to excellent yields.

Synthesis of compound 2

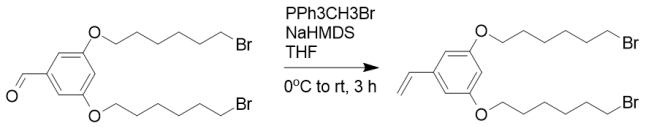

1 2

To a flame-dried round bottom flask equipped with a magnetic stir bar was charged with PPh_3CH_3Br (1.2 equiv) and dry THF at 0°C under inert atmosphere. NaHMDS (2 M in THF, 1.1 equiv) was slowly added to the reaction flask via a syringe. The reaction mixture was then stirred at 0°C for 15 minutes. After that, a solution of **1** in dry THF was cannulated into the reaction. The reaction mixture was warmed to room temperature and stirred for 3 hours. Upon completion of the reaction, the reaction mixture was diluted in ethyl acetate, washed with water and brine, dried over Na_2SO_4. Organic solvents were removed under reduced pressure. The crude mixture was purified by silica gel column chromatography (5% ethyl acetate/hexanes then 15% DCM/hexanes) to obtain compound **2** as white solid (78%). **^{1}H NMR (500 MHz, $CDCl_3$):** δ (ppm) 6.62 (dd, J = 10.5 Hz, J = 17.5 Hz, 1H), 6.54 (d, J = 2.5 Hz, 2H), 6.37 (t, J = 2 Hz, 1H), 5.70 (d, J = 17.5 Hz, 1H), 5.22 (d, J = 10.5 Hz, 1H), 3.95 (t, J = 6 Hz, 4H), 3.43 (t, J = 7 Hz, 4H), 1.87–1.93 (m, 4H), 1.77–1.82 (m, 4H), 1.49–1.52 (m, 8H); **^{13}C NMR (125 MHz, $CDCl_3$):** δ (ppm) 160.35, 139.47, 136.92, 114.11, 104.83, 100.96, 77.25, 77.00, 76.74, 67.93, 33.97, 32.77, 29.21, 29.16, 28.68, 28.08, 25.95.

Synthesis of COE2-2I

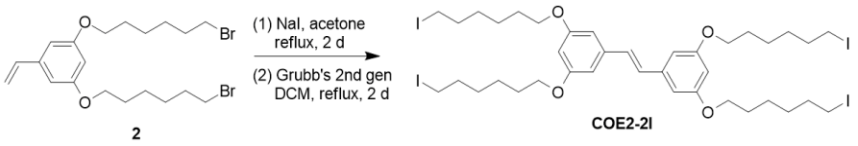

In a gas-tight vessel, compound **2** was and excess NaI were dissolved in acetone. The vessel was sealed and heated at reflux temperature for 2 days. After that, the crude reaction was diluted in DCM as passed through a silica gel plug. Solvents were dried under vacuum and the crude reaction was used in an olefin metathesis reaction without further purification.

To a flame-dried round bottom flask equipped with a stir bar and a condenser was charged with the crude reaction and dry DCM under inert atmosphere. Grubb's catalyst 2nd generation (0.01 mol%) was then added to the reaction flask. The reaction mixture was heated to reflux temperature for 2 days. After cooling down to room temperature, the reaction mixture was diluted in DCM, washed with water and brine, dried over Na_2SO_4. Organic solvents were evaporated *in vacuo*. The crude reaction was purified with silica gel column chromatography (30% DCM/hexanes) to obtain **COE2-2I** as white solid (80% over 2 steps). Characterization data match the previously reported spectra in the literature.[35]

General procedure for syntheses of COEs

In a 1-Dram vial equipped with a stir bar, COE precursor (**COE2-2I** or **COE2-3I-C4**) was dissolved in dry DMF under inert atmosphere. An amine (10 equiv) was then added to the reaction mixture. The reaction was stirred at room

temperature for 2 days. After that, the crude reaction was precipitated by pouring the reaction mixture into diethyl ether. The crude mixture was purified by reverse phase silica gel flash column chromatography (30% MeOH/water) and lyophilized to obtain a target COE as white or off-white solid.

COE2-2hexyl

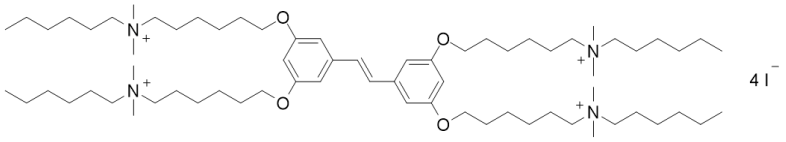

Yield: 80%; **^{1}H NMR (500 MHz, DMSO-d_6):** δ (ppm) 7.19 (s, 2H), 6.75 (d, J = 2 Hz, 4H), 6.39 (t, J = 2.5 Hz, 2H), 3.99 (t, J = 6.5 Hz, 8H), 3.22–3.27 (m, 16H), 3.00 (s, 24H), 1.72–1.77 (m, 8H), 1.61–1.70 (m, 16H), 1.45–1.51 (m, 8H), 1.34–1.38 (m, 8H), 1.26–1.34 (m, 24H), 0.87 (t, J = 6.5 Hz, 12H); **^{13}C NMR (125 MHz, CD_3OD):** δ (ppm) 161.87, 140.70, 130.25, 106.36, 102.46, 69.07, 65.52, 65.40, 51.40, 48.49, 32.39, 32.37, 30.05, 27.05, 27.03, 26.67, 23.59, 23.57, 23.53, 23.51, 14.33.

COE2-2pentyl

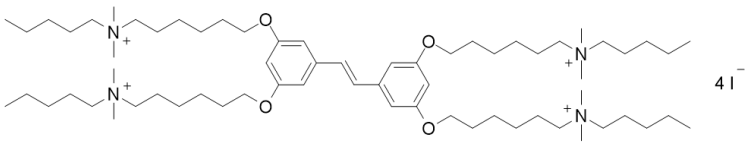

Yield: 75%; **^{1}H NMR (500 MHz, CD_3OD):** δ (ppm) 7.12 (s, 2H), 6.75 (d, J = 2 Hz, 4H), 6.39 (t, J = 2 Hz, 2H), 4.03 (t, J = 7 Hz, 8H), 3.33–3.37 (m, 8H), 3.09 (s, 23H), 1.74–1.87 (m, 25H), 1.59–1.66 (m, 9H), 1.33–1.52 (m, 26H), 0.95 (t, J = 7

Hz, 12H); **^{13}C NMR (125 MHz, DMSO-d_6):** δ (ppm) 160.46, 139.44, 129.33, 105.45, 101.25, 67.86, 63.46, 63.40, 50.43, 28.93, 28.36, 25.99, 25.53, 22.16, 22.09, 21.89, 14.21; **HRMS (ESI):** ([M-2I]$^{2+}$) calcd: 645.3856, found: 645.3850.

COE2-2butyl

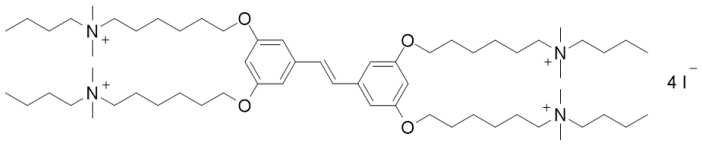

Yield: 80%; **^{1}H NMR (500 MHz, CD_3OD):** δ (ppm) 7.16 (s, 2H), 6.78 (s, 4H), 6.41 (t, J = 3 Hz, 2H), 4.04 (t, J = 6 Hz, 8H), 3.35-3.38 (m, 8H), 3.10 (s, 24H), 1.72–1.87 (m, 25H), 1.60–1.66 (m, 8H), 1.41–1.52 (m, 17H), 1.02 (t, J = 8 Hz, 12H); **^{13}C NMR (125 MHz, DMSO-d_6):** δ (ppm) 159.99, 138.94, 128.87, 104.96, 100.72, 67.37, 62.92, 62.81, 49.97, 28.50, 25.55, 25.08, 23.70, 21.68, 19.19, 13.49; **HRMS (ESI):** ([M-2I]$^{2+}$) calcd: 617.3543, found: 617.3544.

COE2-2isohexyl

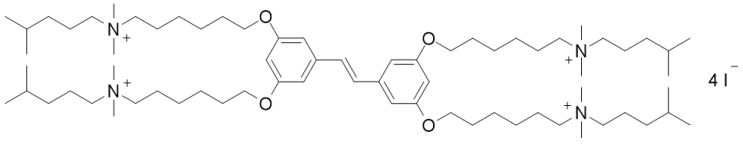

Yield: 64%; **^{1}H NMR (500 MHz, CD_3OD):** δ (ppm) 7.15 (s, 2H), 6.78 (d, J = 2 Hz, 4H), 6.41 (t, J = 2 Hz, 2H), 4.05 (t, J = 6 Hz, 8H), 3.37–3.40 (m, 8H), 3.12 (s, 24H), 1.75–1.88 (m, 26H), 1.61–1.70 (m, 13H), 1.48–1.54 (m, 9H), 0.96 (d, J = 7 Hz, 23H);); **^{13}C NMR (125 MHz, CD_3OD):** δ (ppm) 161.88, 140.72, 130.22,

106.31, 102.31, 68.94, 65.70, 65.43, 51.30, 36.32, 30.07, 28.87, 27.06, 26.70, 23.57, 22.81, 21.63; **HRMS (ESI):** ($[M-2I]^{2+}$) calcd: 673.4169, found: 673.4156.

COE2-2isopentyl

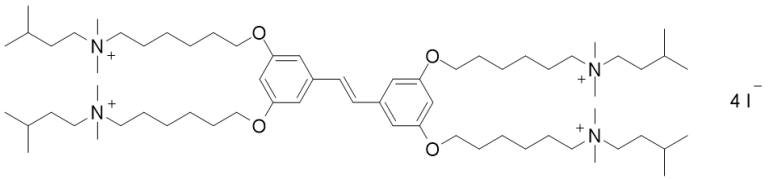

Yield: 78%; **^{1}H NMR (500 MHz, DMSO-d_6):** δ (ppm) 7.19 (s, 2H), 6.76 (d, J = 3 Hz, 4H), 6.39 (s, 2H), 3.98 (t, J = 7 Hz, 8H), 3.25–3.29 (m, 17H), 3.01 (s, 24H), 1.73–1.76 (m, 8H), 1.67–1.70 (m, 9H), 1.53–1.60 (m, 13H), 1.46–1.51 (m, 9H), 1.33–1.38 (m, 9H), 0.92 (d, J = 6 Hz, 24H); **^{13}C NMR (125 MHz, DMSO-d_6):** δ (ppm) 159.99, 138.94, 128.86, 104.96, 100.72, 67.37, 62.76, 61.87, 49.95, 30.03, 28.49, 25.69, 25.54, 25.08, 22.18, 21.67; **HRMS (ESI):** ($[M-2I]^{2+}$) calcd: 645.3856, found: 645.3860.

COE2-2pip

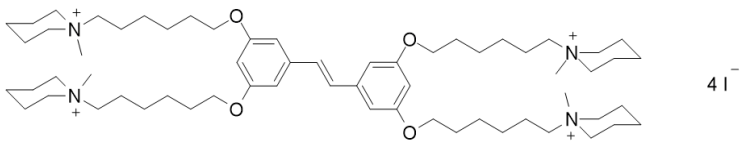

Yield: 80%; **^{1}H NMR (500 MHz, CD_3OD):** δ (ppm) 7.06 (s, 2H), 6.68 (s, 4H), 6.32 (s, 2H), 3.96 (t, J = 7 Hz, 8H), 3.23 (s, 12H), 3.00 (s, 12H), 1.71–1.83 (m, 31H), 1.59–1.67 (m, 9H), 1.51–1.58 (m, 8H), 1.39–1.45 (m, 8H); **^{13}C NMR (125 MHz, DMSO-d_6):** δ (ppm) 160.02, 139.98, 128.89, 105.00, 100.78, 67.40, 62.32,

59.99, 48.59, 48.46, 47.10, 47.08, 28.50, 25.63, 25.11, 20.95, 20.69, 19.30; **HRMS (ESI):** ($[M-2I]^{2+}$) calcd: 613.3230, found: 613.3238.

COE2-3C-C4isohexyl

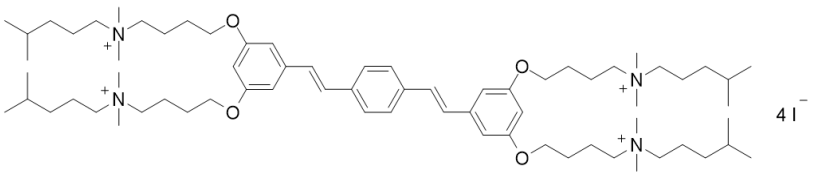

Yield: 55%; **^{1}H NMR (500 MHz, DMSO-d_6):** δ (ppm) 7.61 (s, 4H), 7.28 (d, J = 16 Hz, 2H), 7.19 (d, J = 16 Hz, 2H), 6.81 (s, 4H), 6.44 (s, 2H), 4.05 (t, J = 6 Hz, 8H), 3.35–3.39 (m, 8H), 3.24–3.27 (m, 8H), 3.04 (m, 22H), 1.81–1.87 (m, 8H), 1.73–1.79 (m, 8H), 1.63–1.70 (m, 8H), 1.53–1.61 (m, 5H), 1.13–1.17 (m, 8H), 0.88 (d, J = 7 Hz, 23H); **^{13}C NMR (125 MHz, DMSO-d_6):** δ (ppm) 159.81, 139.12, 136.36, 128.55, 128.54, 126.90, 105.18, 100.92, 66.76, 63.21, 62.54, 50.03, 34.76, 27.07, 25.99, 22.30, 19.73, 18.85; **HRMS (ESI):** ([M-2I]2+) calcd: 668.3778, found: 668.3784.

COE2-3C-C4isopentyl

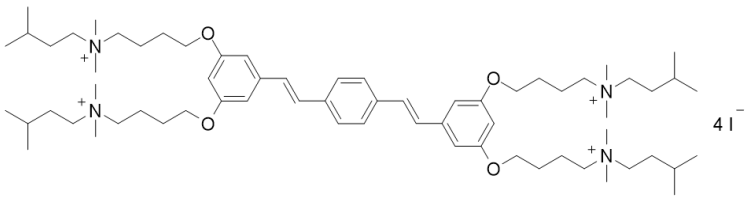

Yield: 75%; **^{1}H NMR (500 MHz, DMSO-d_6):** δ (ppm) 7.61 (s, 4H), 7.27 (d, J = 17 Hz, 2H), 7.19 (d, J = 16 Hz, 2H), 6.81 (d, J = 2 Hz, 4H), 6.45 (t, J = 2 Hz, 2H), 4.05 (t, J = 6 Hz, 8H), 3.33–3.37 (m, 8H), 3.03 (s, 23H), 1.81–1.85 (m, 8H), 1.75–

1.79 (m, 12H), 0.92 (d, J = 6 Hz, 23H); **HRMS (ESI):** ([M-2I]$^{2+}$) calcd: 640.3465, found: 640.3465.

COE2-3C-C4pip

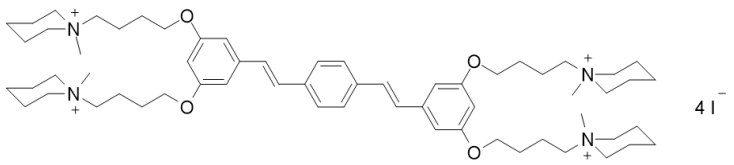

Yield: 81%; **^{1}H NMR (500 MHz, DMSO-d_6):** δ (ppm) 7.62 (s, 4H), 7.29 (d, J = 17 Hz, 2H), 7.20 (d, J = 16 Hz, 2H), 6.82 (d, J = 2 Hz, 4H), 6.46 (t, J = 2 Hz, 2H), 4.06 (t, J = 6 Hz, 8H), 3.41–3.44 (m, 8H), 3.33–3.36 (m, 16H), 3.03 (s, 12H), 1.77–1.91 (m, 33H), 1.50–1.60 (m, 8H); **^{13}C NMR (125 MHz, DMSO-d_6):** δ (ppm) 159.83, 139.13, 136.36, 128.56, 128.37, 126.91, 105.20, 100.96, 66.88, 61.92, 60.03, 47.17, 25.72, 20.68, 19.27, 18.12; **HRMS (ESI):** ([M-2I]$^{2+}$) calcd: 608.2839, found: 608.2842.

6.2 Estimation of "hydrophobicity" of COEs by HPLC

Several studies in Chapter 3–5 have demonstrated a correlation between hydrophobicity of terminal alkyl chains and cytotoxicity and hemolytic activity. To get a better understanding of the relationship between hydrophobicity of COEs and their biological activities, there is a need for a convenient method to estimate the hydrophobicity of COEs.

Traditionally, in medicinal chemistry, hydrophobicity or lipophilicity are quantified by descriptors log$P$ and log$D$, where P and D are partition coefficient

and distribution coefficient, respectively. Distribution coefficient is dependent on pH for ionizable compounds. These two descriptors can be experimentally determined by measuring the concentrations of a compound that partitioned into water and 1-octanol by a shake flask method.[129,130] Major drawbacks of this method are that it is a time consuming process, often requires a relatively large amount of compounds, and suffers from data reproducibility.[131] Due to relatively small scale reactions (often smaller than 30 mg scale) when synthesizing a number of COEs, a method that provides an estimated hydrophobicity while consuming little amount of compounds is preferrable.

A reverse phase high performance liquid chromatography (RP-HPLC) method is advantageous because it consumes very little amount of compound. It has been reported that the retention time of a compound in a RP-HPLC column can be correlated to its hydrophobicity.[132,133] Therefore, I designed a RP-HPLC method to determine the retention time of each COE. The preliminary results were promising as there is a strong correlation between the retention time of COEs and the length of their terminal alkyl chains with $R^2 = 0.9999$ and 0.9985 for **COE2-3C-C3** series and amide COE series, respectively (Figure 6.5).

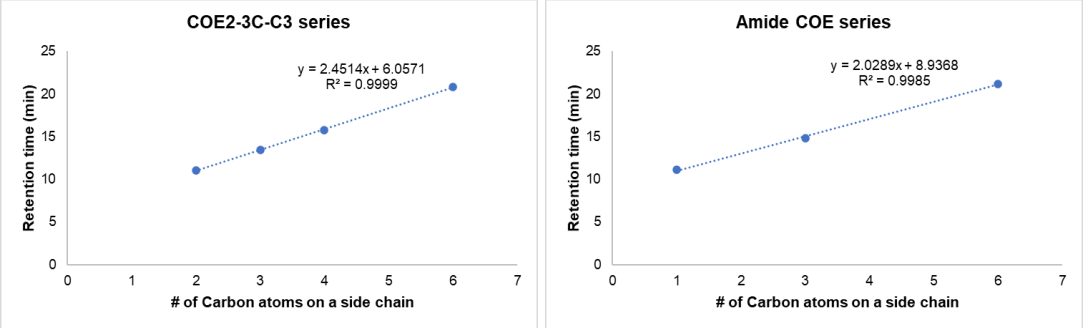

Figure 6.5 Linear correlation between the number of carbon atoms on each side chain of COEs in **COE2-3C-C3** series (left) and amide COE series (right) and retention time in a RP-HPLC column.

Following the results in Figure 6.5, additional distyrylbenzene-based COEs were tested to determine their retention times to explore whether there is a correlation to cytotoxicity or antimicrobial activity. Figure 6.6 shows correlations between retention times of the COEs to $\log_2$(IC_{50}'s against HepG2 cells) and MICs against *E. coli* K12. There is indeed a strong trend between retention time and cytotoxicity suggesting that a major factor that governs cytotoxicity of COEs is the overall hydrophobicity. Thus, this method proves to be useful to preliminary predict cytotoxicity of distyrylbenzene-based COEs. Further work is warranted to demonstrate whether this method is applicable to COEs that have different conjugated cores.

Interestingly, the plot between retention times and MICs of the COEs shows a "parabolic"-like curve. The trend indicates that there is a narrow range of hydrophobicity (retention time of 18 to 23 minutes) that makes COEs active against *E. coli* K12. After taking the trend of cytotoxicity into consideration, the desirable retention time range for distyrylbenzene-based COEs would be

approximately 18 to 20 minutes. According to the data in Figure 6.6, COEs with this range of retention time are active against *E. coli* K12 and have little *in vitro* cytotoxicity towards HepG2 cells. This method of hydrophobicity estimation could be very valuable for the development of antimicrobial COEs in the future as one can easily and quickly predict the biological properties of the COEs without setting up lengthy in vitro experiments, especially when there is a need to screen a large library of COEs.

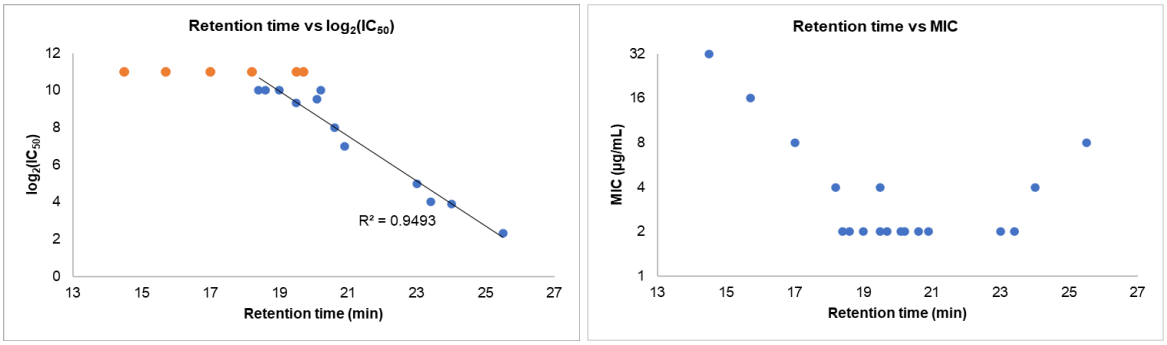

Figure 6.6 Plots showing correlation between retention times of COEs and $\log_2(IC_{50})$ (left) and MIC against *E. coli* K12 (right).

Summary and outlook

Through rational molecular design, several potential applications of COEs on bacterial or yeast cells by means of membrane properties modification have been realized. Modular structure of COEs allows us to easily generate a diverse library of compounds. It was shown on Chapter 2 that the incorporation of a rigid non-planar unit to the conjugated core of a COE reduces its antimicrobial activity which is likely due to changes in aggregation behavior of the COE in membranes. The COE was able to maintain membrane permeabilizing activity and accelerate whole-cell biocatalysis processes. Chapter 3 shows that, by fine-tuning COE structures, antimicrobial activities and cytotoxicity can be modulated to achieve a compound with high bacterial selectivity. This opens up a possibility of using a COE framework to develop a novel class of antimicrobial agents. Chapter 4 shows that additional modifications of COEs with hydrogen bonding moieties further improve their activities against Gram-negative bacteria through a higher membrane disruption ability and a rapid cytoplasmic membrane disruption. In Chapter 5, an effort to address the *in vivo* toxicity has been made by doing away with quaternary ammoniums. The COEs still show potent antimicrobial activities. However, *in vivo* toxicity of the COEs has not yet been fully tested.

Although the membrane permeabilizing and disrupting abilities of COEs have been leveraged, much still need to be studied to get a good understanding of the precise mechanisms of such abilities. Naturally, one would hypothesize

that high membrane permeabilization will lead to high antimicrobial activity. However, results from Chapter 2 along with additional data from our group show that these two parameters can be decoupled by a careful design of COEs. Such observations suggest that mechanisms of membrane permeabilization and bactericidal activities may be different or independent from each other.

We have shown that COEs can be tailored to perturb bacterial membranes selectively and effectively. In Gram-negative bacteria, cytoplasmic membrane integrity was observed to be important for their viability. Despite these observations, there may be more unexplored processes that contribute to bactericidal action at play. Elucidation of the underlying mechanisms of membrane permeabilization and bactericidal action could be of great benefits for leveraging untapped potentials of COEs and the rational design of COEs for microorganism-based applications.

Bibliography

(1) Ribatti, D. An Historical Note on the Cell Theory. *Experimental Cell Research* **2018**, *364* (1), 1–4. https://doi.org/10.1016/j.yexcr.2018.01.038.

(2) Gorter, E.; Grendel, F. ON BIMOLECULAR LAYERS OF LIPOIDS ON THE CHROMOCYTES OF THE BLOOD. *Journal of Experimental Medicine* **1925**, *41* (4), 439–443. https://doi.org/10.1084/jem.41.4.439.

(3) Singer, S. J.; Nicolson, G. L. The Fluid Mosaic Model of the Structure of Cell Membranes. *Science* **1972**, *175* (4023), 720–731. https://doi.org/10.1126/science.175.4023.720.

(4) Alberts, B.; Johnson, A.; Lewis, J.; Raff, M.; Roberts, K.; Walter, P. *Molecular Biology of the Cell*, 4th ed.; Garland Science: New York, 2002.

(5) Bourdichon, F.; Casaregola, S.; Farrokh, C.; Frisvad, J. C.; Gerds, M. L.; Hammes, W. P.; Harnett, J.; Huys, G.; Laulund, S.; Ouwehand, A.; Powell, I. B.; Prajapati, J. B.; Seto, Y.; Ter Schure, E.; Van Boven, A.; Vankerckhoven, V.; Zgoda, A.; Tuijtelaars, S.; Hansen, E. B. Food Fermentations: Microorganisms with Technological Beneficial Use. *International Journal of Food Microbiology* **2012**, *154* (3), 87–97. https://doi.org/10.1016/j.ijfoodmicro.2011.12.030.

(6) Park, H.; Park, G.; Jeon, W.; Ahn, J.-O.; Yang, Y.-H.; Choi, K.-Y. Whole-Cell Biocatalysis Using Cytochrome P450 Monooxygenases for Biotransformation of Sustainable Bioresources (Fatty Acids, Fatty Alkanes, and Aromatic Amino Acids). *Biotechnology Advances* **2020**, *40*, 107504. https://doi.org/10.1016/j.biotechadv.2020.107504.

(7) Baker Dockrey, S. A.; Doyon, T. J.; Perkins, J. C.; Narayan, A. R. H. Whole-Cell Biocatalysis Platform for Gram-Scale Oxidative Dearomatization of Phenols. *Chemical Biology & Drug Design* **2019**, *93* (6), 1207–1213. https://doi.org/10.1111/cbdd.13443.

(8) Cheng, H. N.; Gross, R. A. Biocatalysis in Polymer Science: An Overview. In *Biocatalysis in Polymer Science*; ACS Symposium Series; American Chemical Society, 2002; Vol. 840, pp 1–32. https://doi.org/10.1021/bk-2003-0840.ch001.

(9) Ni, Y.; Chen, R. R. Accelerating Whole-Cell Biocatalysis by Reducing Outer Membrane Permeability Barrier. *Biotechnology and Bioengineering* **2004**, *87* (6), 804–811. https://doi.org/10.1002/bit.20202.

(10) Kell, D. B.; Swainston, N.; Pir, P.; Oliver, S. G. Membrane Transporter Engineering in Industrial Biotechnology and Whole Cell Biocatalysis. *Trends in Biotechnology* **2015**, *33* (4), 237–246. https://doi.org/10.1016/j.tibtech.2015.02.001.

(11) Chen, R. R. Permeability Issues in Whole-Cell Bioprocesses and Cellular Membrane Engineering. *Appl Microbiol Biotechnol* **2007**, *74* (4), 730–738. https://doi.org/10.1007/s00253-006-0811-x.

(12) Kondejewski, L. H.; Farmer, S. W.; Wishart, D. S.; Hancock, R. E. w.; Hodges, R. S. Gramicidin S Is Active against Both Gram-Positive and Gram-Negative Bacteria. *International Journal of Peptide and Protein Research* **1996**, *47* (6), 460–466. https://doi.org/10.1111/j.1399-3011.1996.tb01096.x.
(13) Huang, E.; Yousef, A. E. The Lipopeptide Antibiotic Paenibacterin Binds to the Bacterial Outer Membrane and Exerts Bactericidal Activity through Cytoplasmic Membrane Damage. *Appl. Environ. Microbiol.* **2014**, *80* (9), 2700–2704. https://doi.org/10.1128/AEM.03775-13.
(14) Dixon, R. A.; Chopra, I. Polymyxin B and Polymyxin B Nonapeptide Alter Cytoplasmic Membrane Permeability in Escherichia Coli. *Journal of Antimicrobial Chemotherapy* **1986**, *18* (5), 557–563. https://doi.org/10.1093/jac/18.5.557.
(15) Jean-François, F.; Elezgaray, J.; Berson, P.; Vacher, P.; Dufourc, E. J. Pore Formation Induced by an Antimicrobial Peptide: Electrostatic Effects. *Biophysical Journal* **2008**, *95* (12), 5748–5756. https://doi.org/10.1529/biophysj.108.136655.
(16) Westerhoff, H. V.; Juretić, D.; Hendler, R. W.; Zasloff, M. Magainins and the Disruption of Membrane-Linked Free-Energy Transduction. *PNAS* **1989**, *86* (17), 6597–6601. https://doi.org/10.1073/pnas.86.17.6597.
(17) Wadhwani, P.; Epand, R. F.; Heidenreich, N.; Bürck, J.; Ulrich, A. S.; Epand, R. M. Membrane-Active Peptides and the Clustering of Anionic Lipids. *Biophysical Journal* **2012**, *103* (2), 265–274. https://doi.org/10.1016/j.bpj.2012.06.004.
(18) Kragol, G.; Lovas, S.; Varadi, G.; Condie, B. A.; Hoffmann, R.; Otvos, L. The Antibacterial Peptide Pyrrhocoricin Inhibits the ATPase Actions of DnaK and Prevents Chaperone-Assisted Protein Folding. *Biochemistry* **2001**, *40* (10), 3016–3026. https://doi.org/10.1021/bi002656a.
(19) Kang, S.-J.; Park, S. J.; Mishig-Ochir, T.; Lee, B.-J. Antimicrobial Peptides: Therapeutic Potentials. *Expert Review of Anti-infective Therapy* **2014**, *12* (12), 1477–1486. https://doi.org/10.1586/14787210.2014.976613.
(20) Goldman, M. J.; Anderson, G. M.; Stolzenberg, E. D.; Kari, U. P.; Zasloff, M.; Wilson, J. M. Human β-Defensin-1 Is a Salt-Sensitive Antibiotic in Lung That Is Inactivated in Cystic Fibrosis. *Cell* **1997**, *88* (4), 553–560. https://doi.org/10.1016/S0092-8674(00)81895-4.
(21) Greco, I.; Molchanova, N.; Holmedal, E.; Jenssen, H.; Hummel, B. D.; Watts, J. L.; Håkansson, J.; Hansen, P. R.; Svenson, J. Correlation between Hemolytic Activity, Cytotoxicity and Systemic in Vivo Toxicity of Synthetic Antimicrobial Peptides. *Sci Rep* **2020**, *10* (1), 13206. https://doi.org/10.1038/s41598-020-69995-9.
(22) Woo, H. Y.; Liu, B.; Kohler, B.; Korystov, D.; Mikhailovsky, A.; Bazan, G. C. Solvent Effects on the Two-Photon Absorption of Distyrylbenzene Chromophores Emerging Technologies Such as Memory Storage , Photody-. **2005**, No. 10, 14721–14729.

(23) Duarte, A.; Chworos, A.; Flagan, S. F.; Hanrahan, G.; Bazan, G. C. Identification of Bacteria by Conjugated Oligoelectrolyte/Single-Stranded DNA Electrostatic Complexes. *J. Am. Chem. Soc.* **2010**, *132* (36), 12562–12564. https://doi.org/10.1021/ja105747b.
(24) Garner, L. E.; Park, J.; Dyar, S. M.; Chworos, A.; Sumner, J. J.; Bazan, G. C. Modification of the Optoelectronic Properties of Membranes via Insertion of Amphiphilic Phenylenevinylene Oligoelectrolytes. *Journal of the American Chemical Society* **2010**, *132* (29), 10042–10052.
(25) Garner, L. E.; Thomas, A. W.; Sumner, J. J.; Harvey, S. P.; Bazan, G. C. Conjugated Oligoelectrolytes Increase Current Response and Organic Contaminant Removal in Wastewater Microbial Fuel Cells. *Energy Environ. Sci.* **2012**, *5* (11), 9449–9452. https://doi.org/10.1039/C2EE22839D.
(26) Hou, H.; Chen, X.; Thomas, A. W.; Catania, C.; Kirchhofer, N. D.; Garner, L. E.; Han, A.; Bazan, G. C. Conjugated Oligoelectrolytes Increase Power Generation in E. Coli Microbial Fuel Cells. *Advanced Materials* **2013**, *25* (11), 1593–1597. https://doi.org/10.1002/adma.201204271.
(27) Wang, V. B.; Du, J.; Chen, X.; Thomas, A. W.; Kirchhofer, N. D.; Garner, L. E.; Maw, M. T.; Poh, W. H.; Hinks, J.; Wuertz, S.; Kjelleberg, S.; Zhang, Q.; Loo, J. S. C.; Bazan, G. C. Improving Charge Collection in Escherichia Coli–Carbon Electrode Devices with Conjugated Oligoelectrolytes. *Phys. Chem. Chem. Phys.* **2013**, *15* (16), 5867–5872. https://doi.org/10.1039/C3CP50437A.
(28) Du, J.; Catania, C.; Bazan, G. C. Modification of Abiotic–Biotic Interfaces with Small Molecules and Nanomaterials for Improved Bioelectronics. *Chem. Mater.* **2014**, *26* (1), 686–697. https://doi.org/10.1021/cm401912j.
(29) Sivakumar, K.; Wang, V. B.; Chen, X.; Bazan, G. C.; Kjelleberg, S.; Loo, S. C. J.; Cao, B. Membrane Permeabilization Underlies the Enhancement of Extracellular Bioactivity in Shewanella Oneidensis by a Membrane-Spanning Conjugated Oligoelectrolyte. *Appl Microbiol Biotechnol* **2014**, *98* (21), 9021–9031. https://doi.org/10.1007/s00253-014-5973-3.
(30) Kirchhofer, N. D.; Rengert, Z. D.; Dahlquist, F. W.; Nguyen, T.-Q.; Bazan, G. C. A Ferrocene-Based Conjugated Oligoelectrolyte Catalyzes Bacterial Electrode Respiration. *Chem* **2017**, *2* (2), 240–257. https://doi.org/10.1016/j.chempr.2017.01.001.
(31) McCuskey, S. R.; Rengert, Z. D.; Zhang, M.; Helgeson, M. E.; Nguyen, T.-Q.; Bazan, G. C. Tuning the Potential of Electron Extraction from Microbes with Ferrocene-Containing Conjugated Oligoelectrolytes. *Advanced Biosystems* **2019**, *3* (2), 1800303. https://doi.org/10.1002/adbi.201800303.
(32) Catania, C.; Ajo-Franklin, C. M.; Bazan, G. C. Membrane Permeabilization by Conjugated Oligoelectrolytes Accelerates Whole-Cell Catalysis. *RSC Adv.* **2016**, *6* (102), 100300–100306. https://doi.org/10.1039/C6RA23083K.
(33) Wang, B.; Fronk, S. L.; Rengert, Z. D.; Limwongyut, J.; Bazan, G. C. Conjugated Oligoelectrolytes: Materials for Acceleration of Whole Cell

Biocatalysis. *Chem. Mater.* **2018**, *30* (17), 5836–5840. https://doi.org/10.1021/acs.chemmater.8b02848.
(34) Leifert, D.; Moreland, A. S.; Limwongyut, J.; Mikhailovsky, A. A.; Bazan, G. C. Photoswitchable Conjugated Oligoelectrolytes for a Light-Induced Change of Membrane Morphology. *Angewandte Chemie International Edition* **2020**, *59* (46), 20333–20337. https://doi.org/10.1002/anie.202004448.
(35) Yan, H.; Rengert, Z. D.; Thomas, A. W.; Rehermann, C.; Hinks, J.; Bazan, G. C. Influence of Molecular Structure on the Antimicrobial Function of Phenylenevinylene Conjugated Oligoelectrolytes. *Chemical Science* **2016**, *7* (9), 5714–5722. https://doi.org/10.1039/C6SC00630B.
(36) Hinks, J.; Wang, Y.; Poh, W. H.; Donose, B. C.; Thomas, A. W.; Wuertz, S.; Loo, S. C. J.; Bazan, G. C.; Kjelleberg, S.; Mu, Y.; Seviour, T. Modeling Cell Membrane Perturbation by Molecules Designed for Transmembrane Electron Transfer. *Langmuir* **2014**, *30* (9), 2429–2440. https://doi.org/10.1021/la403409t.
(37) Wang, B.; Wang, M.; Mikhailovsky, A.; Wang, S.; Bazan, G. C. A Membrane-Intercalating Conjugated Oligoelectrolyte with High-Efficiency Photodynamic Antimicrobial Activity. *Angewandte Chemie International Edition* **2017**, *56* (18), 5031–5034. https://doi.org/10.1002/anie.201701146.
(38) Wang, B.; Feng, G.; Seifrid, M.; Wang, M.; Liu, B.; Bazan, G. C. Antibacterial Narrow-Band-Gap Conjugated Oligoelectrolytes with High Photothermal Conversion Efficiency. *Angewandte Chemie International Edition* **2017**, *56* (50), 16063–16066. https://doi.org/10.1002/anie.201709887.
(39) Wang, Y.; Tang, Y.; Zhou, Z.; Ji, E.; Lopez, G. P.; Chi, E. Y.; Schanze, K. S.; Whitten, D. G. Membrane Perturbation Activity of Cationic Phenylene Ethynylene Oligomers and Polymers: Selectivity against Model Bacterial and Mammalian Membranes. *Langmuir* **2010**, *26* (15), 12509–12514. https://doi.org/10.1021/la102269y.
(40) Yan, H.; Catania, C.; Bazan, G. C. Membrane-Intercalating Conjugated Oligoelectrolytes: Impact on Bioelectrochemical Systems. *Advanced Materials* **2015**, *27* (19), 2958–2973. https://doi.org/10.1002/adma.201500487.
(41) Thomas, A. W.; Catania, C.; Garner, L. E.; Bazan, G. C. Pendant Ionic Groups of Conjugated Oligoelectrolytes Govern Their Ability to Intercalate into Microbial Membranes. *Chemical Communications* **2015**, *51*, 9294–9297. https://doi.org/10.1039/C5CC01724F.
(42) Hinks, J.; Wang, Y.; Matysik, A.; Kraut, R.; Kjelleberg, S.; Mu, Y.; Bazan, G. C.; Wuertz, S.; Seviour, T. Increased Microbial Butanol Tolerance by Exogenous Membrane Insertion Molecules. *ChemSusChem* **2015**, *8* (21), 3718–3726. https://doi.org/10.1002/cssc.201500194.
(43) Epand, R. F.; Pollard, J. E.; Wright, J. O.; Savage, P. B.; Epand, R. M. Depolarization, Bacterial Membrane Composition, and the Antimicrobial Action of Ceragenins. *Antimicrobial Agents and Chemotherapy* **2010**, *54* (9), 3708–3713. https://doi.org/10.1128/AAC.00380-10.

(44) Presečki, A. V.; Zelić, B.; Vasić-Rački, D. Comparison of the L-Malic Acid Production by Isolated Fumarase and Fumarase in Permeabilized Baker's Yeast Cells. *Enzyme and Microbial Technology* **2007**, *41* (5), 605–612. https://doi.org/10.1016/j.enzmictec.2007.05.007.
(45) Catania, C.; Thomas, A. W.; Bazan, G. C. Tuning Cell Surface Charge in E. Coli with Conjugated Oligoelectrolytes. *Chemical Science* **2016**, *7* (3), 2023–2029. https://doi.org/10.1039/C5SC03046C.
(46) Kastowsky, M.; Gutberlet, T.; Bradaczek, H. Molecular Modelling of the 3-Dimensional Structure and Conformational Flexibility of Bacterial Lipopolysaccharide. *J Bacteriol* **1992**, *174* (14), 4798–4806.
(47) Lu, Q.; Wang, J.; Faghihnejad, A.; Zeng, H.; Liu, Y. Understanding the Molecular Interactions of Lipopolysaccharides during E. Coli Initial Adhesion with a Surface Forces Apparatus. *Soft Matter* **2011**, *7* (19), 9366. https://doi.org/10.1039/c1sm05554b.
(48) Wiegand, I.; Hilpert, K.; Hancock, R. E. W. Agar and Broth Dilution Methods to Determine the Minimal Inhibitory Concentration (MIC) of Antimicrobial Substances. *Nature Protocols* **2008**, *3* (2), 163–175. https://doi.org/10.1038/nprot.2007.521.
(49) Huber, R. E.; Kurz, G.; Wallenfels, K. A Quantitation of the Factors Which Affect the Hydrolase and Transgalactosylase Activities of ß-Galactosidase (E. Coli) on Lactose. *Biochemistry* **1976**, *15* (9), 1994–2001. https://doi.org/10.1021/bi00654a029.
(50) Mostafa, H. E.; Heller, K. J.; Geis, A. Cloning of Escherichia Coli LacZ and LacY Genes and Their Expression in Gluconobacter Oxydans and Acetobacter Liquefaciens. *Applied and Environmental Microbiology* **2002**, *68* (5), 2619–2623. https://doi.org/10.1128/AEM.68.5.2619-2623.2002.
(51) de Carvalho, C. C. C. R. Whole Cell Biocatalysts: Essential Workers from Nature to the Industry. *Microbial Biotechnology* **2017**, *10* (2), 250–263. https://doi.org/10.1111/1751-7915.12363.
(52) Zaknoon, F.; Sarig, H.; Rotem, S.; Livne, L.; Ivankin, A.; Gidalevitz, D.; Mor, A. Antibacterial Properties and Mode of Action of a Short Acyl-Lysyl Oligomer. *Antimicrobial Agents and Chemotherapy* **2009**, *53* (8), 3422–3429. https://doi.org/10.1128/AAC.00010-09.
(53) Presečki, A. V.; Vasić-Rački, D. Production of L-Malic Acid by Permeabilized Cells of Commercial Saccharomyces Sp. Strains. *Biotechnology Letters* **2005**, *27* (23–24), 1835–1839. https://doi.org/10.1007/s10529-005-3890-3.
(54) Berendsen, H. J. C.; van der Spoel, D.; van Drunen, R. GROMACS: A Message-Passing Parallel Molecular Dynamics Implementation. *Computer Physics Communications* **1995**, *91* (1–3), 43–56. https://doi.org/10.1016/0010-4655(95)00042-E.
(55) Vanommeslaeghe, K.; Hatcher, E.; Acharya, C.; Kundu, S.; Zhong, S.; Shim, J.; Darian, E.; Guvench, O.; Lopes, P.; Vorobyov, I.; Mackerell, A. D. CHARMM General Force Field: A Force Field for Drug-like Molecules

Compatible with the CHARMM All-Atom Additive Biological Force Fields. *Journal of Computational Chemistry* **2010**, *30* (10), 671–690. https://doi.org/10.1002/jcc.21367.
(56) Klauda, J. B.; Venable, R. M.; Freites, J. A.; O'Connor, J. W.; Tobias, D. J.; Mondragon-Ramirez, C.; Vorobyov, I.; MacKerell, A. D.; Pastor, R. W. Update of the CHARMM All-Atom Additive Force Field for Lipids: Validation on Six Lipid Types. *Journal of Physical Chemistry B* **2010**, *114* (23), 7830–7843. https://doi.org/10.1021/jp101759q.
(57) Jorgensen, W. L.; Chandrasekhar, J.; Madura, J. D.; Impey, R. W.; Klein, M. L. Comparison of Simple Potential Functions for Simulating Liquid Water. *The Journal of Chemical Physics* **1983**, *79* (2), 926–935. https://doi.org/10.1063/1.445869.
(58) Hess, B.; Bekker, H.; Berendsen, H. J. C.; Fraaije, J. G. E. M. LINCS: A Linear Constraint Solver for Molecular Simulations. *Journal of Computational Chemistry* **1997**, *18* (12), 1463–1472. https://doi.org/10.1002/(SICI)1096-987X(199709)18:12<1463::AID-JCC4>3.0.CO;2-H.
(59) Miyamoto, S.; Kollman, P. A. SETTLE: An Analytical Version of the SHAKE and RATTLE Algorithm for Rigid Water Models. *Journal of Computational Chemistry* **1992**, *13* (8), 952–962. https://doi.org/10.1002/jcc.540130805.
(60) Hoover, W. G. Canonical Dynamics: Equilibrium Phase-Space Distributions. *Physical Review A* **1985**, *31* (3), 1695–1697. https://doi.org/10.1103/PhysRevA.31.1695.
(61) Parrinello, M.; Rahman, A.; Parrinello M, R. a. Crystal Structure and Pair Potentials: A Molecular-Dynamics Study. *Physical Review Letters* **1980**, *45* (14), 1196–1199. https://doi.org/10.1103/PhysRevLett.45.1196.
(62) Essmann, U.; Perera, L.; Berkowitz, M. L.; Darden, T.; Lee, H.; Pedersen, L. G. A Smooth Particle Mesh Ewald Method. *The Journal of Chemical Physics* **1995**, *103* (19), 8577–8593. https://doi.org/10.1063/1.470117.
(63) Tackling-Drug-Resistant-Infections-Globally_-Final-Report-and-Recommendations.Pdf.
(64) Stone, M. R. L.; Butler, M. S.; Phetsang, W.; Cooper, M. A.; Blaskovich, M. A. T. Fluorescent Antibiotics: New Research Tools to Fight Antibiotic Resistance. *Trends in Biotechnology* **2018**, *36* (5), 523–536. https://doi.org/10.1016/j.tibtech.2018.01.004.
(65) Davies, S. C.; Fowler, T.; Watson, J.; Livermore, D. M.; Walker, D. Annual Report of the Chief Medical Officer: Infection and the Rise of Antimicrobial Resistance. *The Lancet* **2013**, *381* (9878), 1606–1609. https://doi.org/10.1016/S0140-6736(13)60604-2.
(66) Gelband, H.; Laxminarayan, R. Tackling Antimicrobial Resistance at Global and Local Scales. *Trends in Microbiology* **2015**, *23* (9), 524–526. https://doi.org/10.1016/j.tim.2015.06.005.

(67) Torjesen, I. Antimicrobial Resistance Presents an "Apocalyptic" Threat Similar to That of Climate Change, CMO Warns. *BMJ* **2013**, *346*, f1597. https://doi.org/10.1136/bmj.f1597.
(68) Nielsen, T. B.; Brass, E. P.; Gilbert, D. N.; Bartlett, J. G.; Spellberg, B. Sustainable Discovery and Development of Antibiotics — Is a Nonprofit Approach the Future? *New England Journal of Medicine* **2019**, *381* (6), 503–505. https://doi.org/10.1056/NEJMp1905589.
(69) Fitchett, J. R. Antibiotics, Copayments, and Antimicrobial Resistance: Investment Matters. *The Lancet Infectious Diseases* **2015**, *15* (10), 1125–1127. https://doi.org/10.1016/S1473-3099(15)00057-2.
(70) Perros, M. A Sustainable Model for Antibiotics. *Science* **2015**, *347* (6226), 1062–1064. https://doi.org/10.1126/science.aaa3048.
(71) Schäberle, T. F.; Hack, I. M. Overcoming the Current Deadlock in Antibiotic Research. *Trends in Microbiology* **2014**, *22* (4), 165–167. https://doi.org/10.1016/j.tim.2013.12.007.
(72) Cho, H.; Uehara, T.; Bernhardt, T. G. Beta-Lactam Antibiotics Induce a Lethal Malfunctioning of the Bacterial Cell Wall Synthesis Machinery. *Cell* **2014**, *159* (6), 1300–1311. https://doi.org/10.1016/j.cell.2014.11.017.
(73) Kimura, K.; Bugg, T. D. H. Recent Advances in Antimicrobial Nucleoside Antibiotics Targeting Cell Wall Biosynthesis. *Nat. Prod. Rep.* **2003**, *20* (2), 252–273. https://doi.org/10.1039/B202149H.
(74) Panchal, R. G.; Ulrich, R. L.; Lane, D.; Butler, M. M.; Houseweart, C.; Opperman, T.; Williams, J. D.; Peet, N. P.; Moir, D. T.; Nguyen, T.; Gussio, R.; Bowlin, T.; Bavari, S. Novel Broad-Spectrum Bis-(Imidazolinylindole) Derivatives with Potent Antibacterial Activities against Antibiotic-Resistant Strains. *Antimicrobial Agents and Chemotherapy* **2009**, *53* (10), 4283–4291. https://doi.org/10.1128/AAC.01709-08.
(75) Ishiguro, K.; Sakiyama, S.; Takahashi, K.; Arai, T. Mode of Action of Saframycin A, a Novel Heterocyclic Quinone Antibiotic. Inhibition of RNA Synthesis in Vivo and in Vitro. *Biochemistry* **1978**, *17* (13), 2545–2550. https://doi.org/10.1021/bi00606a014.
(76) Mukhtar, T. A.; Wright, G. D. Streptogramins, Oxazolidinones, and Other Inhibitors of Bacterial Protein Synthesis. *Chem. Rev.* **2005**, *105* (2), 529–542. https://doi.org/10.1021/cr030110z.
(77) Bourne, C. R. Utility of the Biosynthetic Folate Pathway for Targets in Antimicrobial Discovery. *Antibiotics* **2014**, *3* (1), 1–28. https://doi.org/10.3390/antibiotics3010001.
(78) Wang, Y.; Jett, S. D.; Crum, J.; Schanze, K. S.; Chi, E. Y.; Whitten, D. G. Understanding the Dark and Light-Enhanced Bactericidal Action of Cationic Conjugated Polyelectrolytes and Oligomers. *Langmuir* **2013**, *29* (2), 781–792. https://doi.org/10.1021/la3044889.
(79) Liu, D.; Choi, S.; Chen, B.; Doerksen, R. J.; Clements, D. J.; Winkler, J. D.; Klein, M. L.; DeGrado, W. F. Nontoxic Membrane-Active Antimicrobial

Arylamide Oligomers. *Angewandte Chemie International Edition* **2004**, *43* (9), 1158–1162. https://doi.org/10.1002/anie.200352791.
(80) Choi, S.; Isaacs, A.; Clements, D.; Liu, D.; Kim, H.; Scott, R. W.; Winkler, J. D.; DeGrado, W. F. De Novo Design and in Vivo Activity of Conformationally Restrained Antimicrobial Arylamide Foldamers. *PNAS* **2009**, *106* (17), 6968–6973. https://doi.org/10.1073/pnas.0811818106.
(81) Ghosh, C.; Haldar, J. Membrane-Active Small Molecules: Designs Inspired by Antimicrobial Peptides. *ChemMedChem* **2015**, *10* (10), 1606–1624. https://doi.org/10.1002/cmdc.201500299.
(82) Nederberg, F.; Zhang, Y.; Tan, J. P. K.; Xu, K.; Wang, H.; Yang, C.; Gao, S.; Guo, X. D.; Fukushima, K.; Li, L.; Hedrick, J. L.; Yang, Y.-Y. Biodegradable Nanostructures with Selective Lysis of Microbial Membranes. *Nature Chemistry* **2011**, *3* (5), 409–414. https://doi.org/10.1038/nchem.1012.
(83) Hurdle, J. G.; O'Neill, A. J.; Chopra, I.; Lee, R. E. Targeting Bacterial Membrane Function: An Underexploited Mechanism for Treating Persistent Infections. *Nature Reviews Microbiology* **2011**, *9* (1), 62–75. https://doi.org/10.1038/nrmicro2474.
(84) Strandberg, E.; Esteban-Martín, S.; Ulrich, A. S.; Salgado, J. Hydrophobic Mismatch of Mobile Transmembrane Helices: Merging Theory and Experiments. *Biochimica et Biophysica Acta (BBA) - Biomembranes* **2012**, *1818* (5), 1242–1249. https://doi.org/10.1016/j.bbamem.2012.01.023.
(85) Zhou, C.; Chia, G. W. N.; Ho, J. C. S.; Seviour, T.; Sailov, T.; Liedberg, B.; Kjelleberg, S.; Hinks, J.; Bazan, G. C. Informed Molecular Design of Conjugated Oligoelectrolytes To Increase Cell Affinity and Antimicrobial Activity. *Angewandte Chemie International Edition* **2018**, *57* (27), 8069–8072. https://doi.org/10.1002/anie.201803103.
(86) Niles, A. L.; Moravec, R. A.; Riss, T. L. Update on in Vitro Cytotoxicity Assays for Drug Development. *Expert Opinion on Drug Discovery* **2008**, *3* (6), 655–669. https://doi.org/10.1517/17460441.3.6.655.
(87) Yamamura, H.; Miyagawa, A.; Sugiyama, H.; Murata, K.; Mabuti, T.; Mitsuhashi, R.; Hagiwara, T.; Nonaka, M.; Tanimoto, K.; Tomita, H. Rule of Hydrophobicity/Hydrophilicity Balance in Membrane-Disrupting Antimicrobial Activity of Polyalkylamino Cyclodextrins Synthesized via Click Chemistry. *ChemistrySelect* **2016**, *1* (3), 469–472. https://doi.org/10.1002/slct.201500017.
(88) Hoque, J.; Konai, M. M.; Sequeira, S. S.; Samaddar, S.; Haldar, J. Antibacterial and Antibiofilm Activity of Cationic Small Molecules with Spatial Positioning of Hydrophobicity: An in Vitro and in Vivo Evaluation. *J. Med. Chem.* **2016**, *59* (23), 10750–10762. https://doi.org/10.1021/acs.jmedchem.6b01435.
(89) Wieprecht, T.; Dathe, M.; Krause, E.; Beyermann, M.; Maloy, W. L.; MacDonald, D. L.; Bienert, M. Modulation of Membrane Activity of Amphipathic, Antibacterial Peptides by Slight Modifications of the

Hydrophobic Moment. *FEBS Letters* **1997**, *417* (1), 135–140. https://doi.org/10.1016/S0014-5793(97)01266-0.
(90) Sundaramoorthy, N. S.; Suresh, P.; Selva Ganesan, S.; GaneshPrasad, A.; Nagarajan, S. Restoring Colistin Sensitivity in Colistin-Resistant E. Coli : Combinatorial Use of MarR Inhibitor with Efflux Pump Inhibitor. *Sci Rep* **2019**, *9* (1), 19845. https://doi.org/10.1038/s41598-019-56325-x.
(91) CLSI. *Methods for Dilution Antimicrobial Susceptibility Tests for Bacteria That Grow Aerobically. CLSI Standard M07.*, 11th ed.; 2018.
(92) CLSI. *Performance Standards for Antimicrobial Susceptibility Testing. CLSI Supplement M100.*, 28th ed.; 2018.
(93) Lambert, R. J. W.; Pearson, J. Susceptibility Testing: Accurate and Reproducible Minimum Inhibitory Concentration (MIC) and Non-Inhibitory Concentration (NIC) Values. *Journal of Applied Microbiology* **2000**, *88* (5), 784–790. https://doi.org/10.1046/j.1365-2672.2000.01017.x.
(94) Fieser, L. F.; Fieser, M. Reagents for Organic Synthesis, Vol. 1; Wiley: New York, 1967; pp 581–595.
(95) Martens, E.; Demain, A. L. The Antibiotic Resistance Crisis, with a Focus on the United States. *The Journal of Antibiotics* **2017**, *70* (5), 520–526. https://doi.org/10.1038/ja.2017.30.
(96) Federal Task Force on Combating Antibiotic-Resistant Bacteria*, National Action Plan for Combating Antibiotic-Resistant Bacteria 2020-2025*, **2020**.
(97) Vijay, S.; Bansal, N.; Rao, B. K.; Veeraraghavan, B.; Rodrigues, C.; Wattal, C.; Goyal, J. P.; Tadepalli, K.; Mathur, P.; Venkateswaran, R.; Venkatasubramanian, R.; Khadanga, S.; Bhattacharya, S.; Mukherjee, S.; Baveja, S.; Sistla, S.; Panda, S.; Walia, K. Secondary Infections in Hospitalized COVID-19 Patients: Indian Experience. *IDR* **2021**, *14*, 1893–1903. https://doi.org/10.2147/IDR.S299774.
(98) Afshinnekoo, E.; Bhattacharya, C.; Burguete-García, A.; Castro-Nallar, E.; Deng, Y.; Desnues, C.; Dias-Neto, E.; Elhaik, E.; Iraola, G.; Jang, S.; Łabaj, P. P.; Mason, C. E.; Nagarajan, N.; Poulsen, M.; Prithiviraj, B.; Siam, R.; Shi, T.; Suzuki, H.; Werner, J.; Zambrano, M. M.; Bhattacharyya, M. COVID-19 Drug Practices Risk Antimicrobial Resistance Evolution. *The Lancet Microbe* **2021**, *2* (4), e135–e136. https://doi.org/10.1016/S2666-5247(21)00039-2.
(99) Rodríguez-Baño, J.; Rossolini, G. M.; Schultsz, C.; Tacconelli, E.; Murthy, S.; Ohmagari, N.; Holmes, A.; Bachmann, T.; Goossens, H.; Canton, R.; Roberts, A. P.; Henriques-Normark, B.; Clancy, C. J.; Huttner, B.; Fagerstedt, P.; Lahiri, S.; Kaushic, C.; Hoffman, S. J.; Warren, M.; Zoubiane, G.; Essack, S.; Laxminarayan, R.; Plant, L. Antimicrobial Resistance Research in a Post-Pandemic World: Insights on Antimicrobial Resistance Research in the COVID-19 Pandemic. *Journal of Global Antimicrobial Resistance* **2021**, *25*, 5–7. https://doi.org/10.1016/j.jgar.2021.02.013.

(100) Brown, D. G.; Wobst, H. J. A Decade of FDA-Approved Drugs (2010–2019): Trends and Future Directions. *J. Med. Chem.* **2021**, *64* (5), 2312–2338. https://doi.org/10.1021/acs.jmedchem.0c01516.
(101) Bai, S.; Wang, J.; Yang, K.; Zhou, C.; Xu, Y.; Song, J.; Gu, Y.; Chen, Z.; Wang, M.; Shoen, C.; Andrade, B.; Cynamon, M.; Zhou, K.; Wang, H.; Cai, Q.; Oldfield, E.; Zimmerman, S. C.; Bai, Y.; Feng, X. A Polymeric Approach toward Resistance-Resistant Antimicrobial Agent with Dual-Selective Mechanisms of Action. *Science Advances* **2021**, *7* (5), eabc9917. https://doi.org/10.1126/sciadv.abc9917.
(102) Zhang, N.; Ma, S. Recent Development of Membrane-Active Molecules as Antibacterial Agents. *European Journal of Medicinal Chemistry* **2019**, *184*, 111743. https://doi.org/10.1016/j.ejmech.2019.111743.
(103) Findlay, B.; Zhanel, G. G.; Schweizer, F. Cationic Amphiphiles, a New Generation of Antimicrobials Inspired by the Natural Antimicrobial Peptide Scaffold. *Antimicrobial Agents and Chemotherapy* **2010**, *54* (10), 4049–4058. https://doi.org/10.1128/AAC.00530-10.
(104) Zhou, M.; Zheng, M.; Cai, J. Small Molecules with Membrane-Active Antibacterial Activity. *ACS Appl. Mater. Interfaces* **2020**, *12* (19), 21292–21299. https://doi.org/10.1021/acsami.9b20161.
(105) Zasloff, M. Antimicrobial Peptides of Multicellular Organisms. *Nature* **2002**, *415* (6870), 389–395. https://doi.org/10.1038/415389a.
(106) Eun, Y.-J.; Foss, M. H.; Kiekebusch, D.; Pauw, D. A.; Westler, W. M.; Thanbichler, M.; Weibel, D. B. DCAP: A Broad-Spectrum Antibiotic That Targets the Cytoplasmic Membrane of Bacteria. *J. Am. Chem. Soc.* **2012**, *134* (28), 11322–11325. https://doi.org/10.1021/ja302542j.
(107) Yang, T.; Moreira, W.; Nyantakyi, S. A.; Chen, H.; Aziz, D. binte; Go, M.-L.; Dick, T. Amphiphilic Indole Derivatives as Antimycobacterial Agents: Structure–Activity Relationships and Membrane Targeting Properties. *J. Med. Chem.* **2017**, *60* (7), 2745–2763. https://doi.org/10.1021/acs.jmedchem.6b01530.
(108) Nelson, G. J. Lipid Composition of Erythrocytes in Various Mammalian Species. *Biochimica et Biophysica Acta (BBA) - Lipids and Lipid Metabolism* **1967**, *144* (2), 221–232. https://doi.org/10.1016/0005-2760(67)90152-X.
(109) Uppu, D. S. S. M.; Konai, M. M.; Baul, U.; Singh, P.; Siersma, T. K.; Samaddar, S.; Vemparala, S.; Hamoen, L. W.; Narayana, C.; Haldar, J. Isosteric Substitution in Cationic-Amphiphilic Polymers Reveals an Important Role for Hydrogen Bonding in Bacterial Membrane Interactions. *Chem. Sci.* **2016**, *7* (7), 4613–4623. https://doi.org/10.1039/C6SC00615A.
(110) Zamani, E.; Chatterjee, S.; Changa, T.; Immethun, C.; Sarella, A.; Saha, R.; Dishari, S. K. Mechanistic Understanding of the Interactions of Cationic Conjugated Oligo- and Polyelectrolytes with Wild-Type and Ampicillin-Resistant Escherichia Coli. *Sci Rep* **2019**, *9* (1), 1–12. https://doi.org/10.1038/s41598-019-56946-2.

(111) Limwongyut, J.; Nie, C.; Moreland, A. S.; Bazan, G. C. Molecular Design of Antimicrobial Conjugated Oligoelectrolytes with Enhanced Selectivity toward Bacterial Cells. *Chem. Sci.* **2020**, *11* (31), 8138–8144. https://doi.org/10.1039/D0SC03679J.
(112) Marr, A. K.; Gooderham, W. J.; Hancock, R. E. Antibacterial Peptides for Therapeutic Use: Obstacles and Realistic Outlook. *Current Opinion in Pharmacology* **2006**, *6* (5), 468–472. https://doi.org/10.1016/j.coph.2006.04.006.
(113) Gopal, D. M.; Kalogeropoulos, A. P.; Georgiopoulou, V. V.; Tang, W. W. H.; Methvin, A.; Smith, A. L.; Bauer, D. C.; Newman, A. B.; Kim, L.; Harris, T. B.; Kritchevsky, S. B.; Butler, J. Serum Albumin Concentration and Heart Failure Risk: The Health, Aging, and Body Composition Study. *American Heart Journal* **2010**, *160* (2), 279–285. https://doi.org/10.1016/j.ahj.2010.05.022.
(114) Health, Aging and Body Composition Study. Lower Serum Albumin Concentration and Change in Muscle Mass: The Health, Aging and Body Composition Study. *The American Journal of Clinical Nutrition* **2005**, *82* (3), 531–537. https://doi.org/10.1093/ajcn/82.3.531.
(115) Dowhan, W. MOLECULAR BASIS FOR MEMBRANE PHOSPHOLIPID DIVERSITY: Why Are There So Many Lipids? *Annu. Rev. Biochem.* **1997**, *66* (1), 199–232. https://doi.org/10.1146/annurev.biochem.66.1.199.
(116) Chung, J.; Bhat, A.; Kim, C.-J.; Yong, D.; Ryu, C.-M. Combination Therapy with Polymyxin B and Netropsin against Clinical Isolates of Multidrug-Resistant Acinetobacter Baumannii. *Scientific Reports* **2016**, *6* (1), 28168. https://doi.org/10.1038/srep28168.
(117) Krokhin, O. V.; Craig, R.; Spicer, V.; Ens, W.; Standing, K. G.; Beavis, R. C.; Wilkins, J. A. An Improved Model for Prediction of Retention Times of Tryptic Peptides in Ion Pair Reversed-Phase HPLC: Its Application to Protein Peptide Mapping by Off-Line HPLC-MALDI MS *. *Molecular & Cellular Proteomics* **2004**, *3* (9), 908–919. https://doi.org/10.1074/mcp.M400031-MCP200.
(118) Kim, S.; Kim, S. S.; Lee, B. J. Correlation between the Activities of α-Helical Antimicrobial Peptides and Hydrophobicities Represented as RP HPLC Retention Times. *Peptides* **2005**, *26* (11), 2050–2056. https://doi.org/10.1016/j.peptides.2005.04.007.
(119) Silver, L. L. Challenges of Antibacterial Discovery. *Clinical Microbiology Reviews* **2011**. https://doi.org/10.1128/CMR.00030-10.
(120) Tew, G. N.; Clements, D.; Tang, H.; Arnt, L.; Scott, R. W. Antimicrobial Activity of an Abiotic Host Defense Peptide Mimic. *Biochimica et Biophysica Acta (BBA) - Biomembranes* **2006**, *1758* (9), 1387–1392. https://doi.org/10.1016/j.bbamem.2006.03.001.
(121) Chen, S.; Shao, X.; Xiao, X.; Dai, Y.; Wang, Y.; Xie, J.; Jiang, W.; Sun, Y.; Cong, Z.; Qiao, Z.; Zhang, H.; Liu, L.; Zhang, Q.; Zhang, W.; Zheng, L.; Yu, B.; Chen, M.; Cui, W.; Fei, J.; Liu, R. Host Defense Peptide Mimicking

Peptide Polymer Exerting Fast, Broad Spectrum, and Potent Activities toward Clinically Isolated Multidrug-Resistant Bacteria. *ACS Infect. Dis.* **2020**, *6* (3), 479–488. https://doi.org/10.1021/acsinfecdis.9b00410.

(122) Anthoni, U.; Bohlin, L.; Larsen, C.; Nielsen, P.; Nielsen, N. H.; Christophersen, C. Tetramine: Occurrence in Marine Organisms and Pharmacology. *Toxicon* **1989**, *27* (7), 707–716. https://doi.org/10.1016/0041-0101(89)90037-8.

(123) Lv, H.; Zhang, S.; Wang, B.; Cui, S.; Yan, J. Toxicity of Cationic Lipids and Cationic Polymers in Gene Delivery. *Journal of Controlled Release* **2006**, *114* (1), 100–109. https://doi.org/10.1016/j.jconrel.2006.04.014.

(124) Choi, K.-H.; Song, C.; Shin, D.; Park, S. HERG Channel Blockade by Externally Applied Quaternary Ammonium Derivatives. *Biochimica et Biophysica Acta (BBA) - Biomembranes* **2011**, *1808* (6), 1560–1566. https://doi.org/10.1016/j.bbamem.2011.02.008.

(125) Sanguinetti, M. C.; Tristani-Firouzi, M. HERG Potassium Channels and Cardiac Arrhythmia. *Nature* **2006**, *440* (7083), 463–469. https://doi.org/10.1038/nature04710.

(126) Recanatini, M.; Poluzzi, E.; Masetti, M.; Cavalli, A.; De Ponti, F. QT Prolongation through HERG K+ Channel Blockade: Current Knowledge and Strategies for the Early Prediction during Drug Development. *Medicinal Research Reviews* **2005**, *25* (2), 133–166. https://doi.org/10.1002/med.20019.

(127) Miyamura, S.; Araki, M.; Suzuki, T.; Yamaguchi, J.; Itami, K. Stereodivergent Synthesis of Arylcyclopropylamines by Sequential C□H Borylation and Suzuki–Miyaura Coupling. *Angewandte Chemie International Edition* **2015**, *54* (3), 846–851. https://doi.org/10.1002/anie.201409186.

(128) Zhang, Y.; Algburi, A.; Wang, N.; Kholodovych, V.; Oh, D. O.; Chikindas, M.; Uhrich, K. E. Self-Assembled Cationic Amphiphiles as Antimicrobial Peptides Mimics: Role of Hydrophobicity, Linkage Type, and Assembly State. *Nanomedicine: Nanotechnology, Biology and Medicine* **2017**, *13* (2), 343–352. https://doi.org/10.1016/j.nano.2016.07.018.

(129) Andrés, A.; Rosés, M.; Ràfols, C.; Bosch, E.; Espinosa, S.; Segarra, V.; Huerta, J. M. Setup and Validation of Shake-Flask Procedures for the Determination of Partition Coefficients (LogD) from Low Drug Amounts. *European Journal of Pharmaceutical Sciences* **2015**, *76*, 181–191. https://doi.org/10.1016/j.ejps.2015.05.008.

(130) Leo, A.; Hansch, C.; Elkins, D. Partition Coefficients and Their Uses. *Chem. Rev.* **1971**, *71* (6), 525–616. https://doi.org/10.1021/cr60274a001.

(131) Harnisch, M.; Möckel, H. J.; Schulze, G. Relationship between Log Pow, Shake-Flask Values and Capacity Factors Derived from Reversed-Phase High-Performance Liquid Chromatography for n-Alkylbenzenes and Some Oecd Reference Substances. *Journal of Chromatography A* **1983**, *282*, 315–332. https://doi.org/10.1016/S0021-9673(00)91610-8.

(132) Valkó, K.; Bevan, C.; Reynolds, D. Chromatographic Hydrophobicity Index by Fast-Gradient RP-HPLC: A High-Throughput Alternative to Log P/Log D. *Anal. Chem.* **1997**, *69* (11), 2022–2029. https://doi.org/10.1021/ac961242d.
(133) Bartalis, J.; Halaweish, F. T. Relationship between Cucurbitacins Reversed-Phase High-Performance Liquid Chromatography Hydrophobicity Index and Basal Cytotoxicity on HepG2 Cells. *Journal of Chromatography B* **2005**, *818* (2), 159–166. https://doi.org/10.1016/j.jchromb.2004.12.020.

Appendix: NMR spectra

Chapter 2

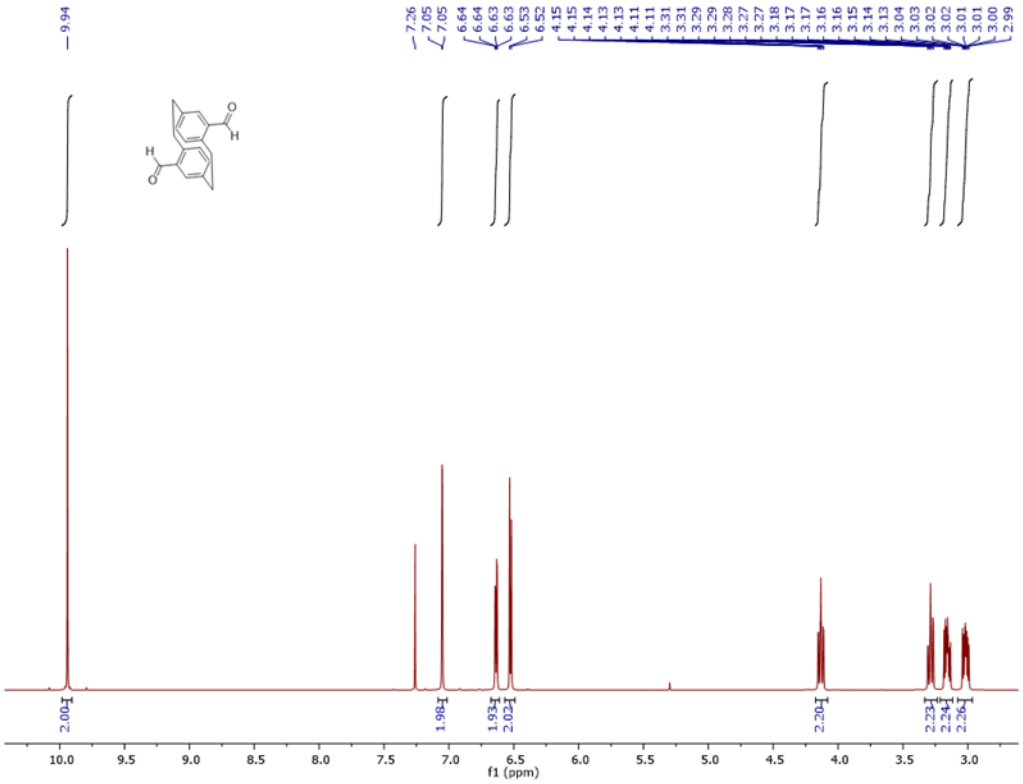
9.94
7.26
7.05
7.05
6.64
6.64
6.63
6.63
6.53
6.52
4.15
4.15
4.14
4.13
4.13
4.11
4.11
3.31
3.31
3.29
3.29
3.28
3.27
3.27
3.18
3.17
3.17
3.16
3.16
3.15
3.14
3.13
3.04
3.03
3.02
3.02
3.01
3.01
3.00
2.99
2.00
1.98
1.93
2.03
2.20
2.23
2.24
2.26
f1 (ppm)

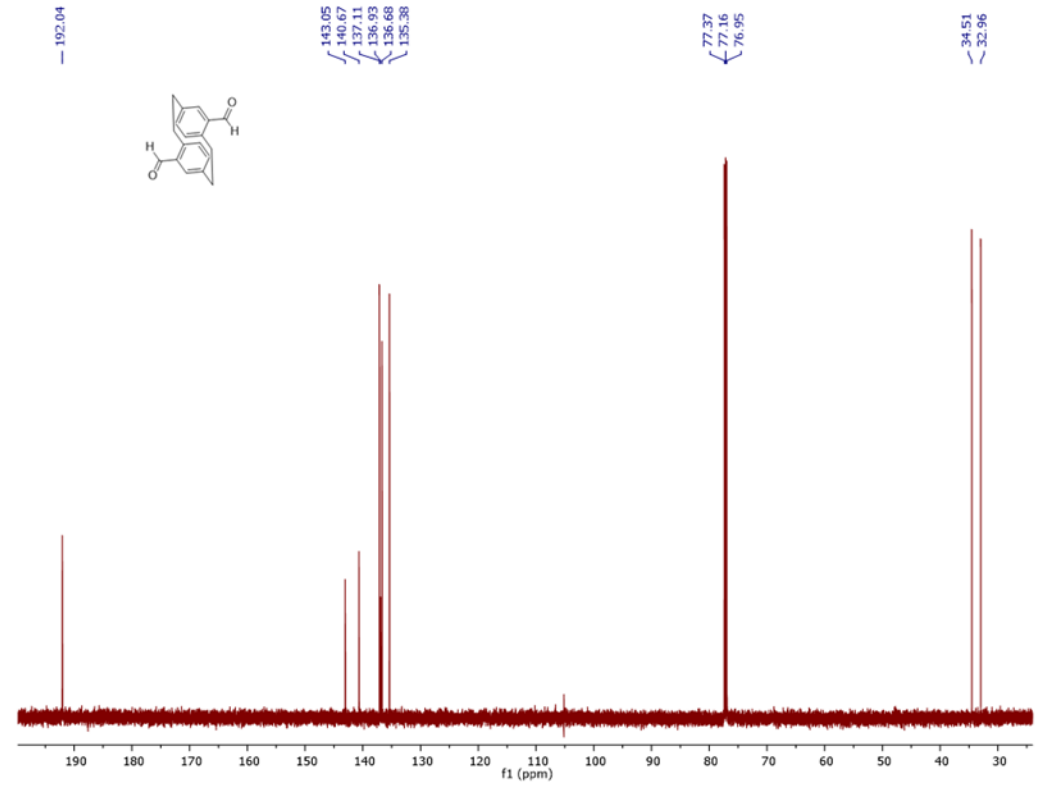
192.04
143.05
140.67
137.11
136.93
136.68
135.38
77.37
77.16
76.95
34.51
32.96
f1 (ppm)

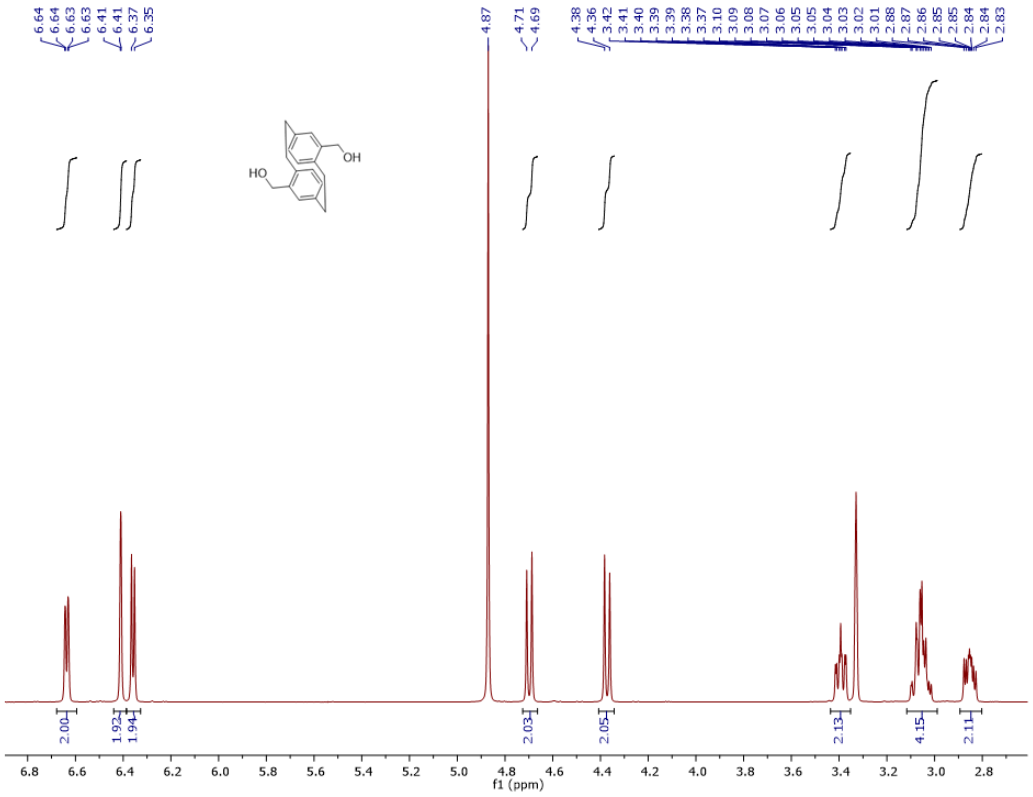
6.64
6.64
6.63
6.63
6.41
6.41
6.37
6.35
4.87
4.71
4.69
4.38
4.36
3.42
3.41
3.40
3.39
3.39
3.38
3.37
3.10
3.09
3.08
3.07
3.06
3.05
3.05
3.04
3.03
3.02
3.01
2.88
2.87
2.86
2.85
2.85
2.84
2.84
2.83
OH
HO
2.00
1.92
1.94
2.03
2.05
2.13
4.15
2.11
f1 (ppm)

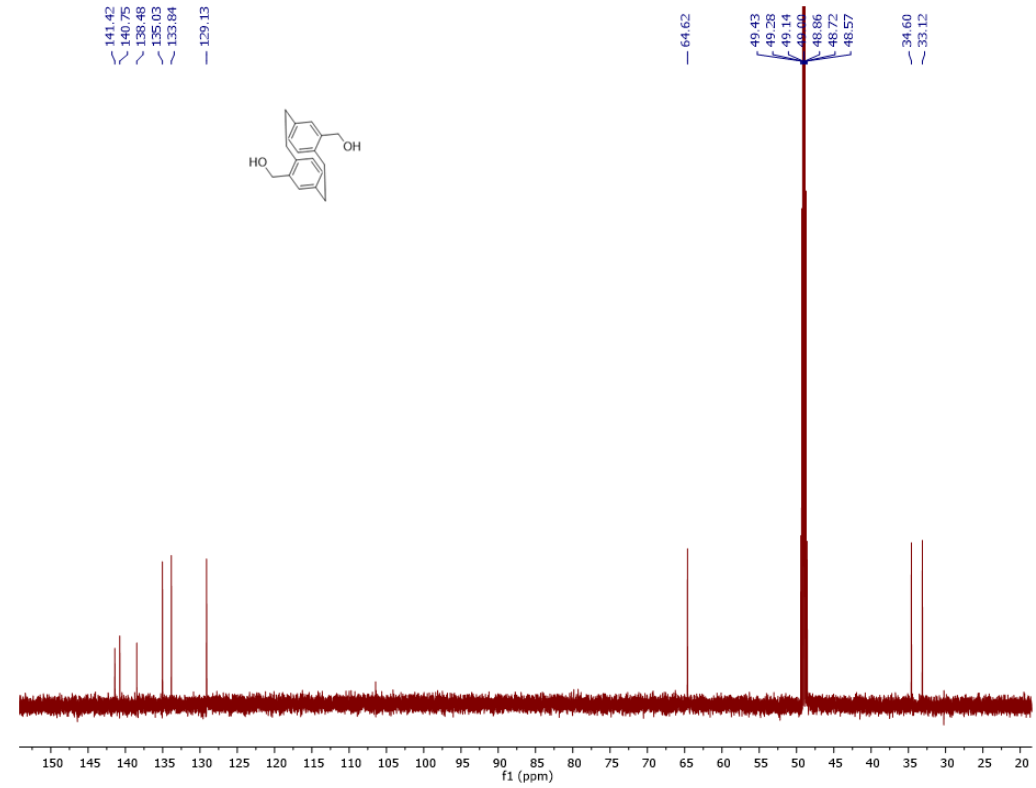
141.42
140.75
138.48
135.03
133.84
129.13
64.62
49.43
49.28
49.14
49.00
48.86
48.72
48.57
34.60
33.12
OH
HO
f1 (ppm)

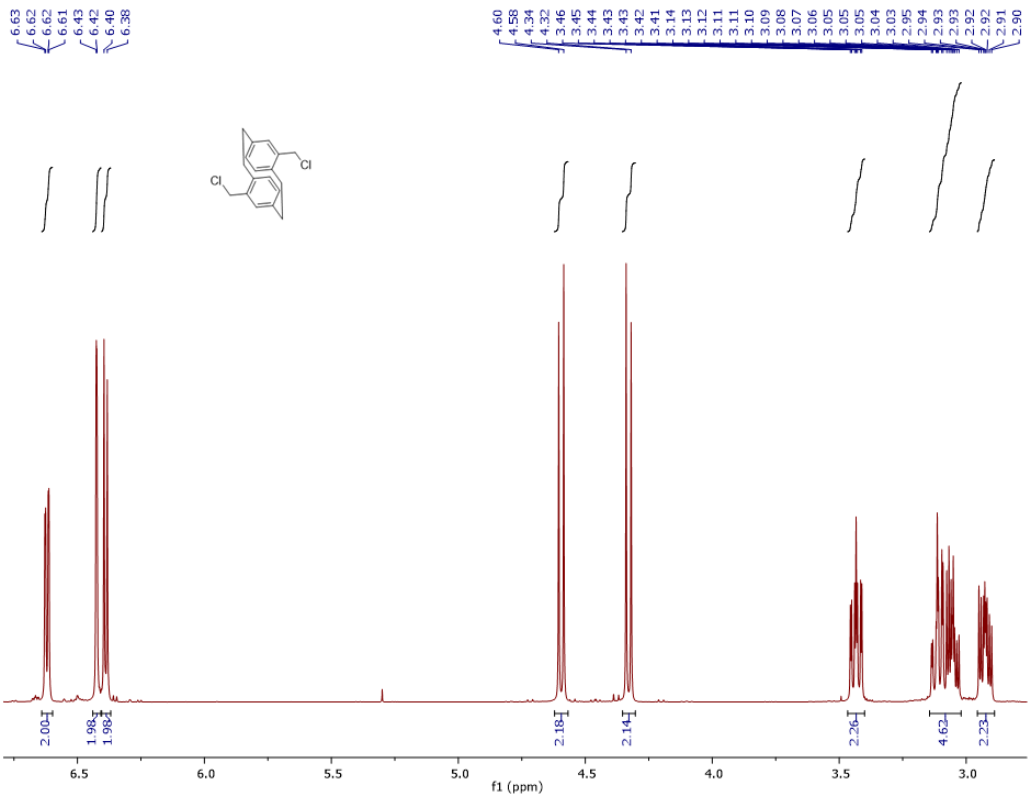
6.63
6.62
6.62
6.61
6.43
6.42
6.40
6.38
4.60
4.58
4.34
4.32
3.46
3.45
3.44
3.43
3.42
3.41
3.14
3.13
3.12
3.11
3.11
3.10
3.09
3.08
3.07
3.06
3.05
3.05
3.05
3.04
3.03
2.95
2.94
2.93
2.93
2.92
2.92
2.91
2.90
Cl
Cl
2.00
1.98
1.98
2.18
2.14
2.26
4.62
2.23
6.5
6.0
5.5
5.0
4.5
4.0
3.5
3.0
f1 (ppm)

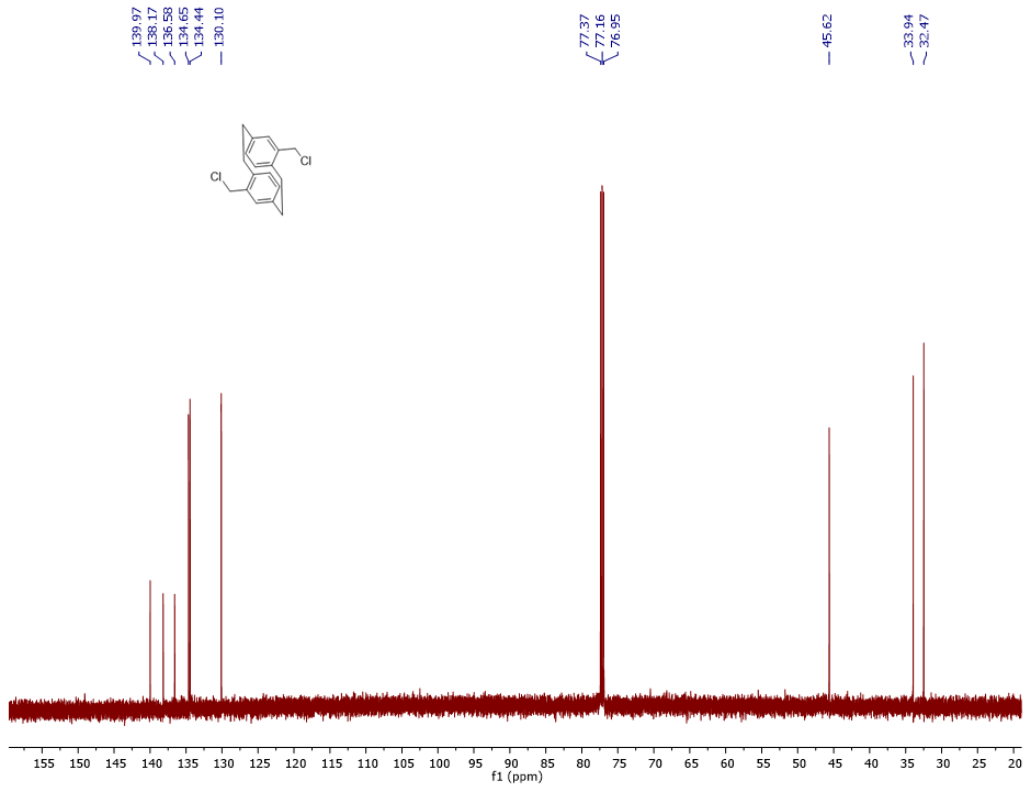
139.97
138.17
136.58
134.65
134.44
130.10
77.37
77.16
76.95
45.62
33.94
32.47
Cl
Cl
155 150 145 140 135 130 125 120 115 110 105 100 95 90 85 80 75 70 65 60 55 50 45 40 35 30 25 20
f1 (ppm)

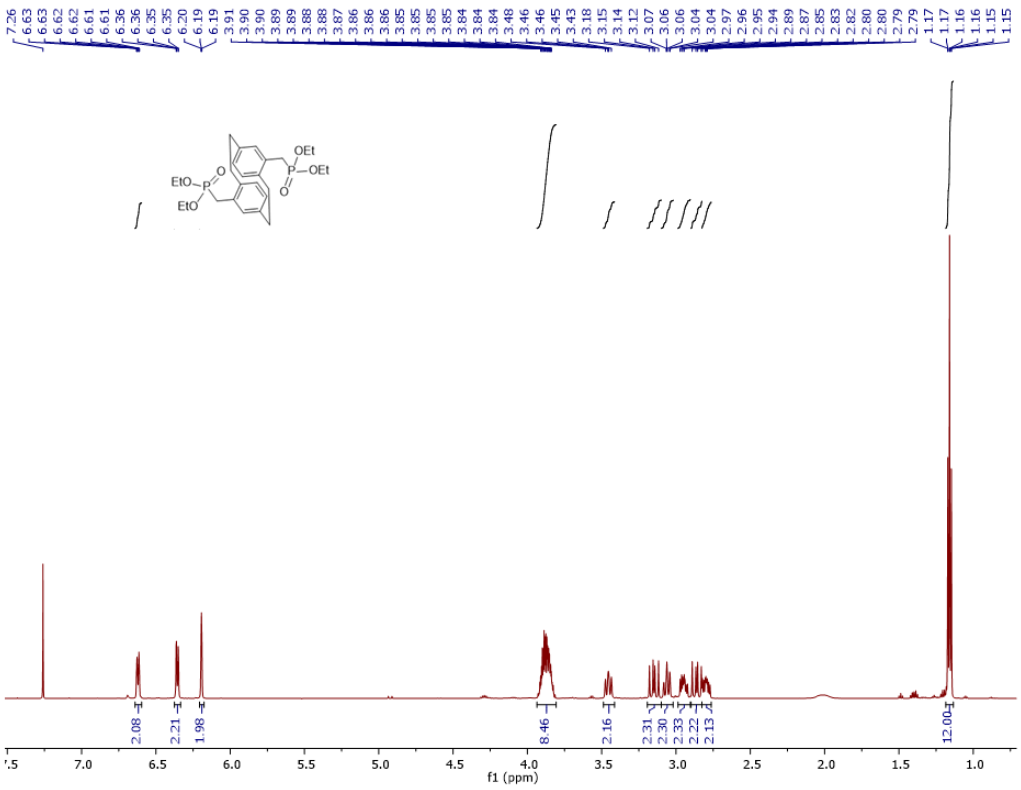
7.26 6.63 6.63 6.62 6.62 6.62 6.61 6.61 6.36 6.36 6.35 6.35 6.20 6.19 6.19 3.91 3.90 3.90 3.89 3.89 3.88 3.88 3.87 3.86 3.86 3.86 3.85 3.85 3.85 3.85 3.85 3.84 3.84 3.84 3.48 3.46 3.46 3.45 3.43 3.18 3.15 3.14 3.12 3.07 3.06 3.06 3.04 3.04 2.97 2.96 2.95 2.94 2.89 2.87 2.85 2.83 2.82 2.80 2.80 2.79 2.79 1.17 1.17 1.16 1.16 1.15 1.15
OEt
EtO
P
O
EtO
P
OEt
O
2.08
2.21
1.98
8.46
2.16
2.31
2.30
2.33
2.22
2.13
12.00
f1 (ppm)

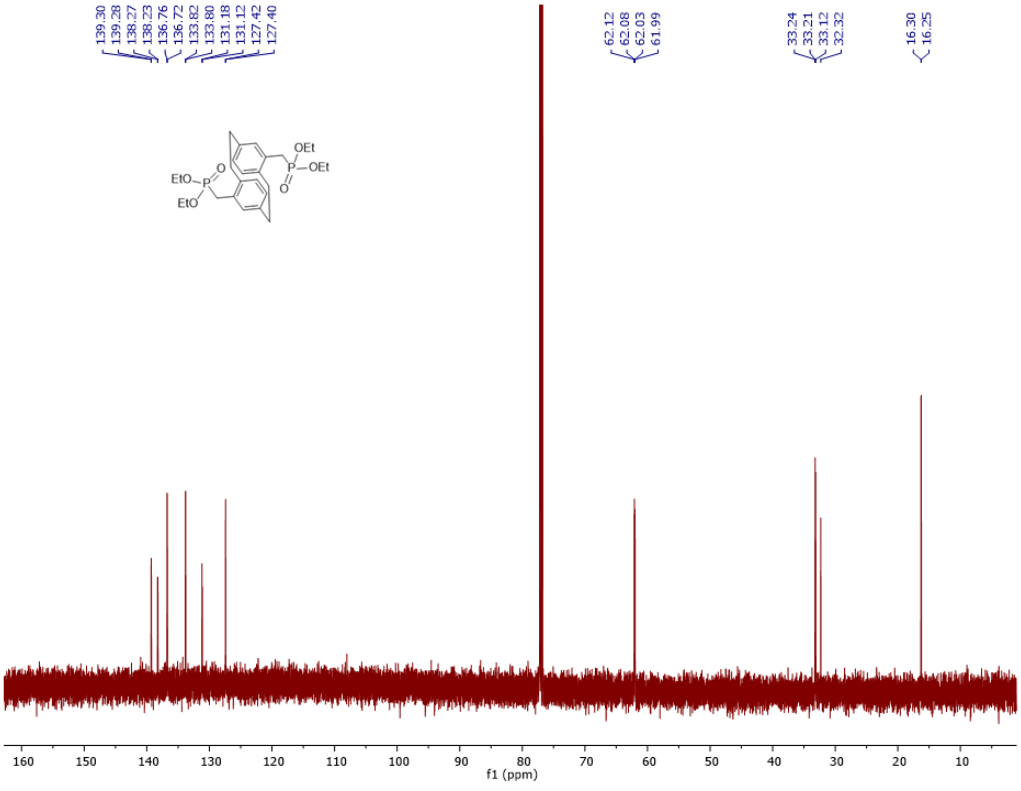
139.30 139.28 138.27 138.23 136.76 136.72 133.82 133.80 131.18 131.12 127.42 127.40
62.12 62.08 62.03 61.99
33.24 33.21 33.12 32.32
16.30 16.25
OEt
EtO
P
O
EtO
P
OEt
O
f1 (ppm)

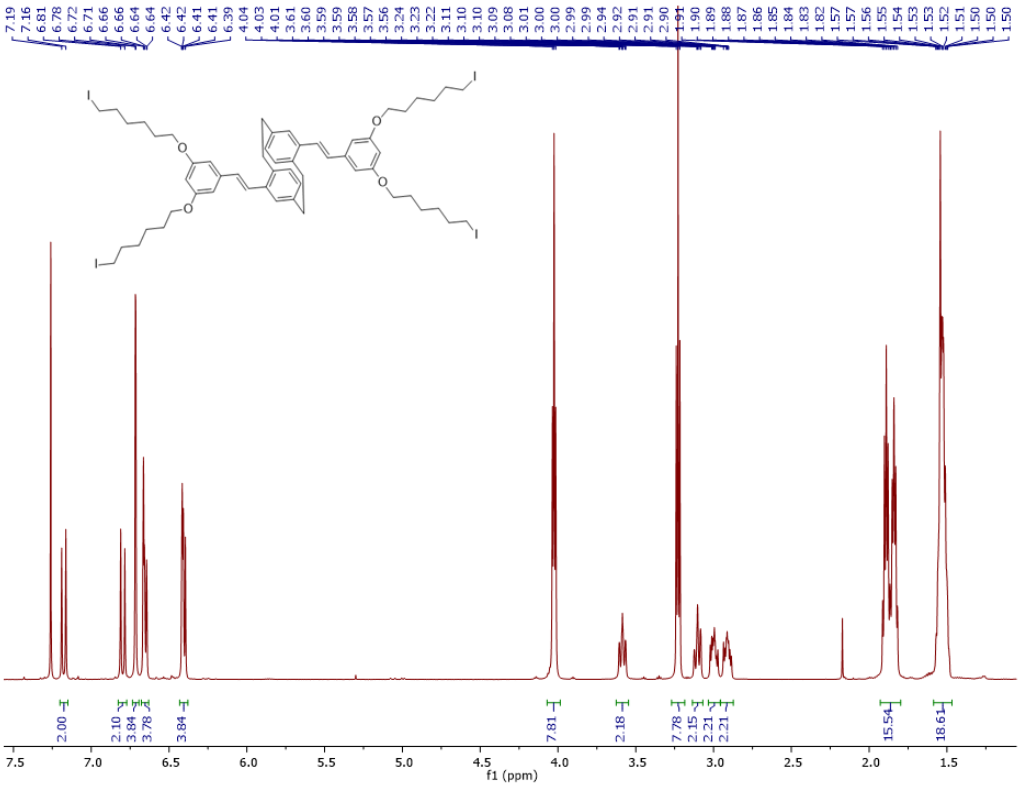
7.19 7.16 6.81 6.78 6.72 6.71 6.66 6.66 6.64 6.64 6.42 6.42 6.41 6.41 6.39 4.04 4.03 4.01 3.61 3.60 3.59 3.59 3.58 3.57 3.56 3.24 3.23 3.22 3.11 3.10 3.10 3.09 3.08 3.01 3.00 3.00 2.99 2.99 2.94 2.92 2.91 2.91 2.90 1.91 1.90 1.89 1.88 1.87 1.86 1.85 1.84 1.83 1.82 1.57 1.57 1.56 1.55 1.54 1.53 1.52 1.51 1.50 1.50 1.50
2.00 2.10 3.84 3.78 3.84 7.81 2.18 7.78 2.15 2.21 2.21 15.54 18.61
7.5 7.0 6.5 6.0 5.5 5.0 4.5 4.0 3.5 3.0 2.5 2.0 1.5
f1 (ppm)

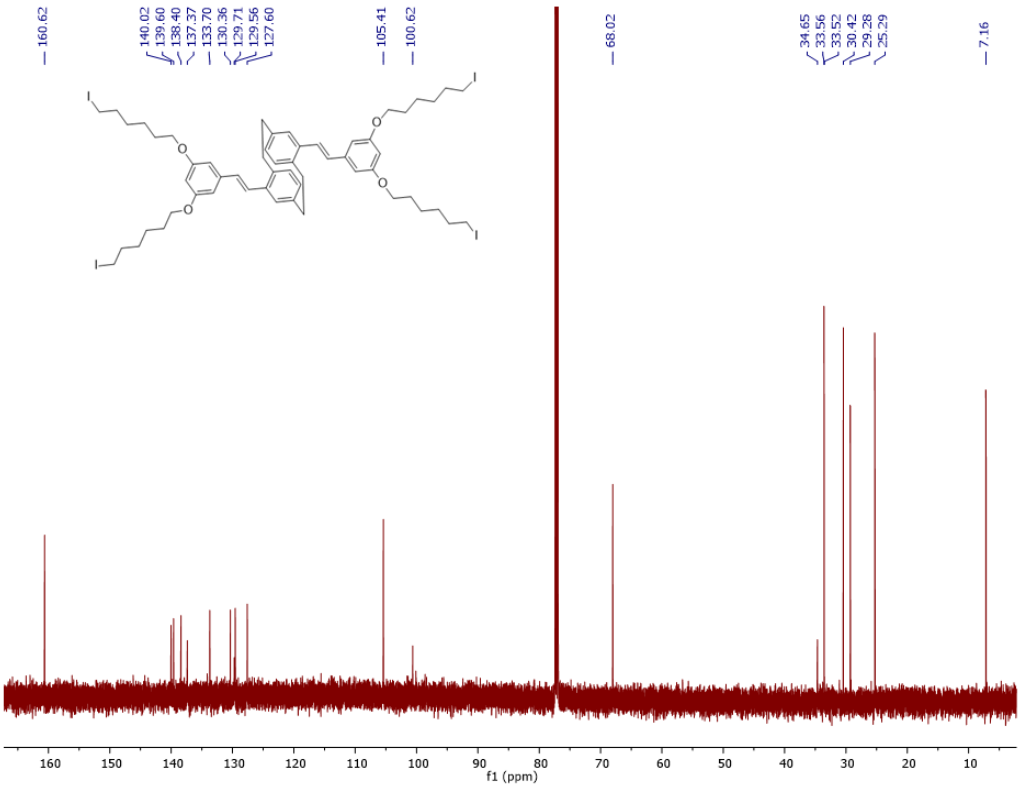
160.62 140.02 139.60 138.40 137.37 133.70 130.36 129.71 129.56 127.60 105.41 100.62 68.02 34.65 33.56 33.52 30.42 29.28 25.29 7.16
160 150 140 130 120 110 100 90 80 70 60 50 40 30 20 10
f1 (ppm)

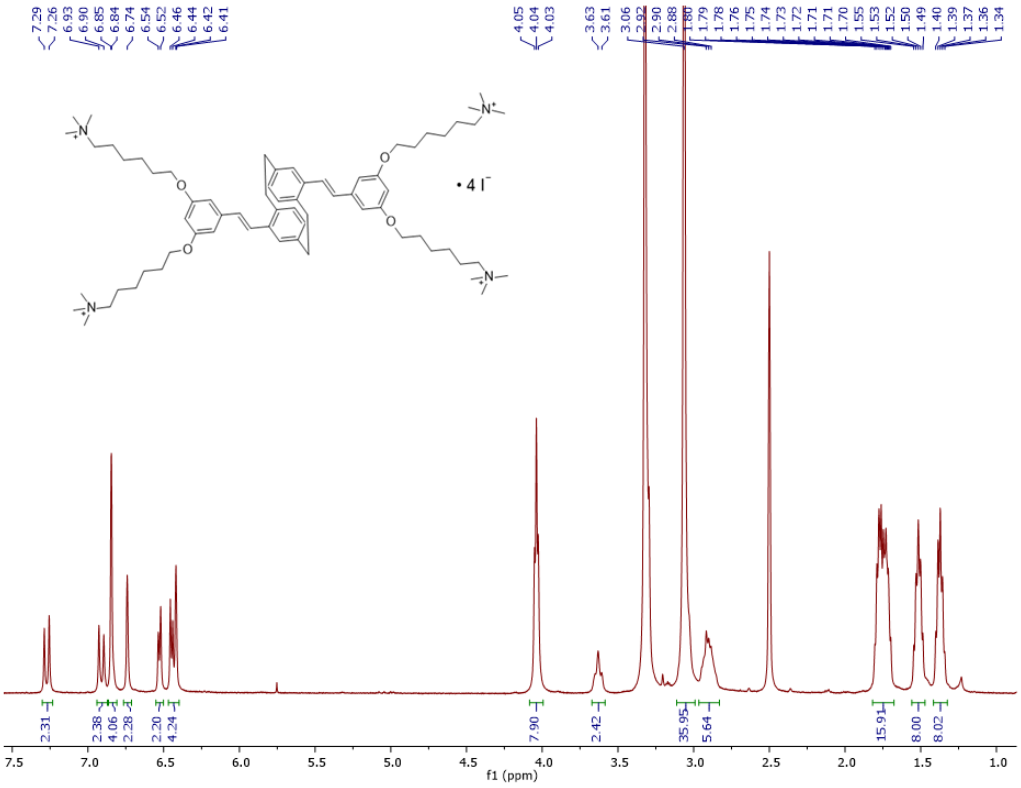
7.29
7.26
6.93
6.90
6.85
6.84
6.74
6.54
6.52
6.46
6.44
6.42
6.41
4.05
4.04
4.03
3.63
3.61
3.06
2.92
2.90
2.88
1.88
1.79
1.78
1.76
1.75
1.74
1.73
1.72
1.71
1.71
1.70
1.55
1.53
1.52
1.50
1.49
1.40
1.39
1.37
1.36
1.34
• 4 I⁻
2.31
2.38
4.06
2.28
2.20
4.24
7.90
2.42
35.95
5.64
15.91
8.00
8.02
f1 (ppm)

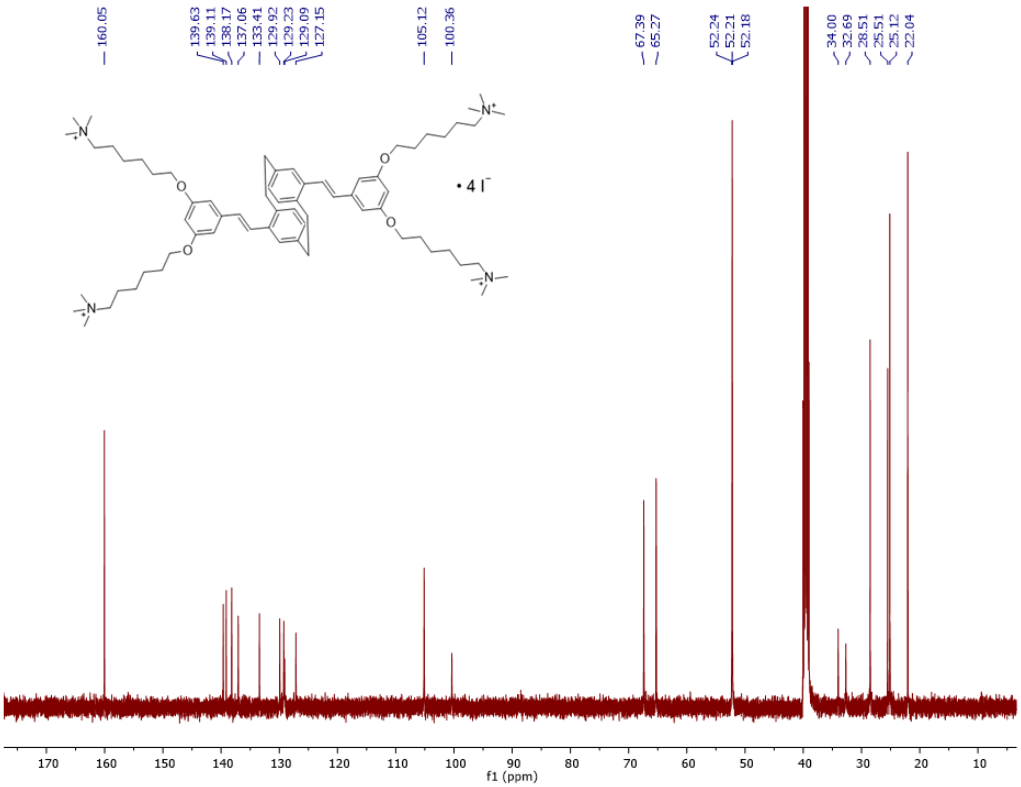
160.05
139.63
139.11
138.17
137.06
133.41
129.92
129.23
129.09
127.15
105.12
100.36
67.39
65.27
52.24
52.21
52.18
34.00
32.69
28.51
25.51
25.12
22.04
• 4 I⁻
f1 (ppm)

Chapter 3

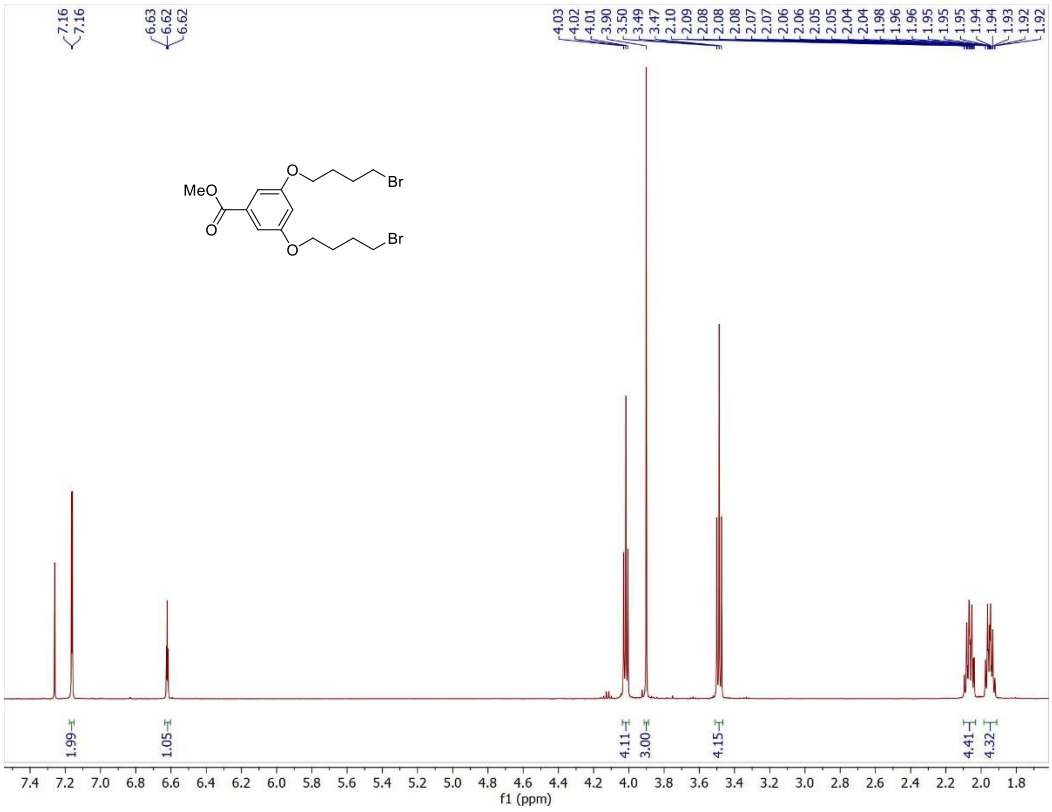
7.16
7.16
6.63
6.62
6.62
4.03
4.02
4.01
3.90
3.50
3.49
3.47
2.10
2.09
2.08
2.08
2.08
2.07
2.07
2.06
2.06
2.05
2.05
2.04
2.04
1.98
1.96
1.96
1.95
1.95
1.95
1.94
1.94
1.93
1.92
1.92
MeO
O
O
Br
O
Br
1.99
1.05
4.11
3.00
4.15
4.41
4.32
7.4 7.2 7.0 6.8 6.6 6.4 6.2 6.0 5.8 5.6 5.4 5.2 5.0 4.8 4.6 4.4 4.2 4.0 3.8 3.6 3.4 3.2 3.0 2.8 2.6 2.4 2.2 2.0 1.8
f1 (ppm)

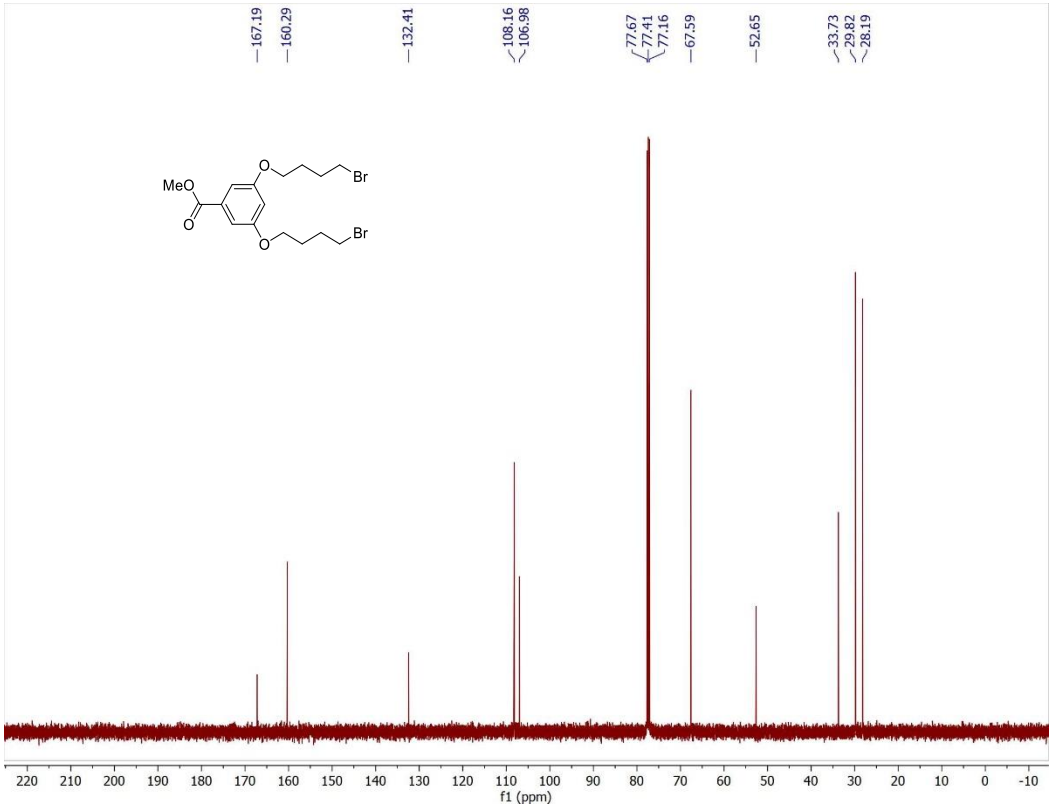
167.19
160.29
132.41
108.16
106.98
77.67
77.41
77.16
67.59
52.65
33.73
29.82
28.19
MeO
O
O
Br
O
Br
220 210 200 190 180 170 160 150 140 130 120 110 100 90 80 70 60 50 40 30 20 10 0 -10
f1 (ppm)

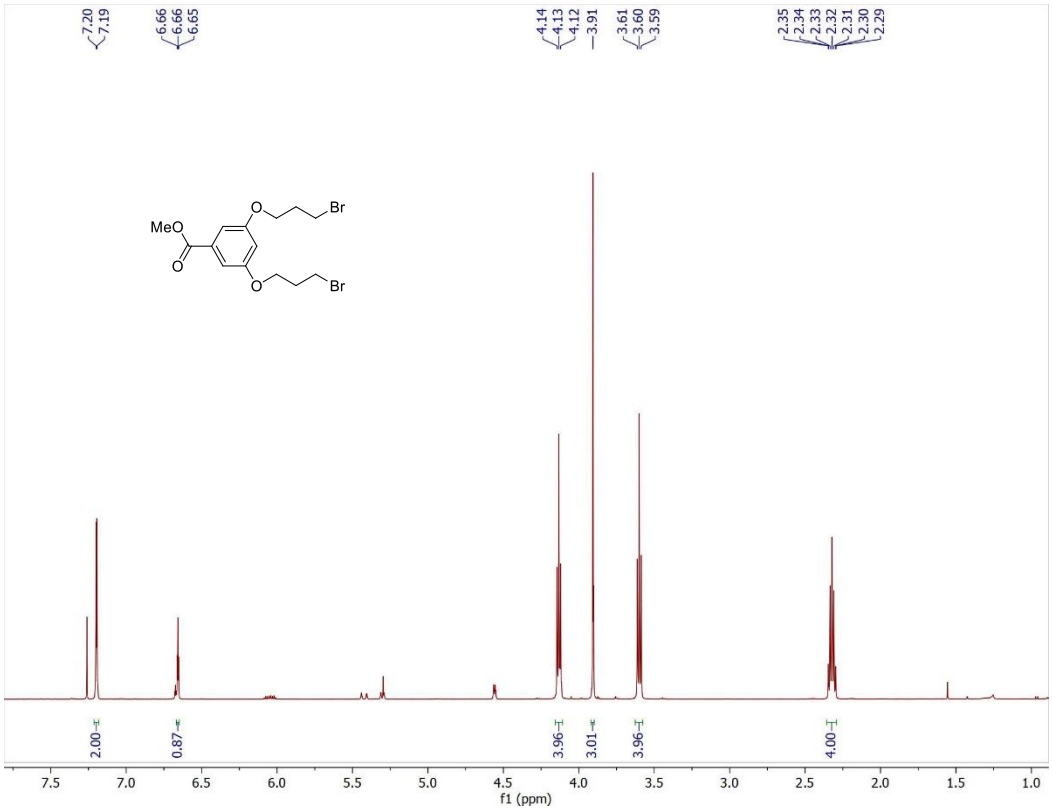
7.20
7.19
6.66
6.66
6.65
4.14
4.13
4.12
3.91
3.61
3.60
3.59
2.35
2.34
2.33
2.32
2.31
2.30
2.29
MeO
O
O
Br
O
Br
2.00
0.87
3.96
3.01
3.96
4.00
7.5
7.0
6.5
6.0
5.5
5.0
4.5
4.0
3.5
3.0
2.5
2.0
1.5
1.0
f1 (ppm)

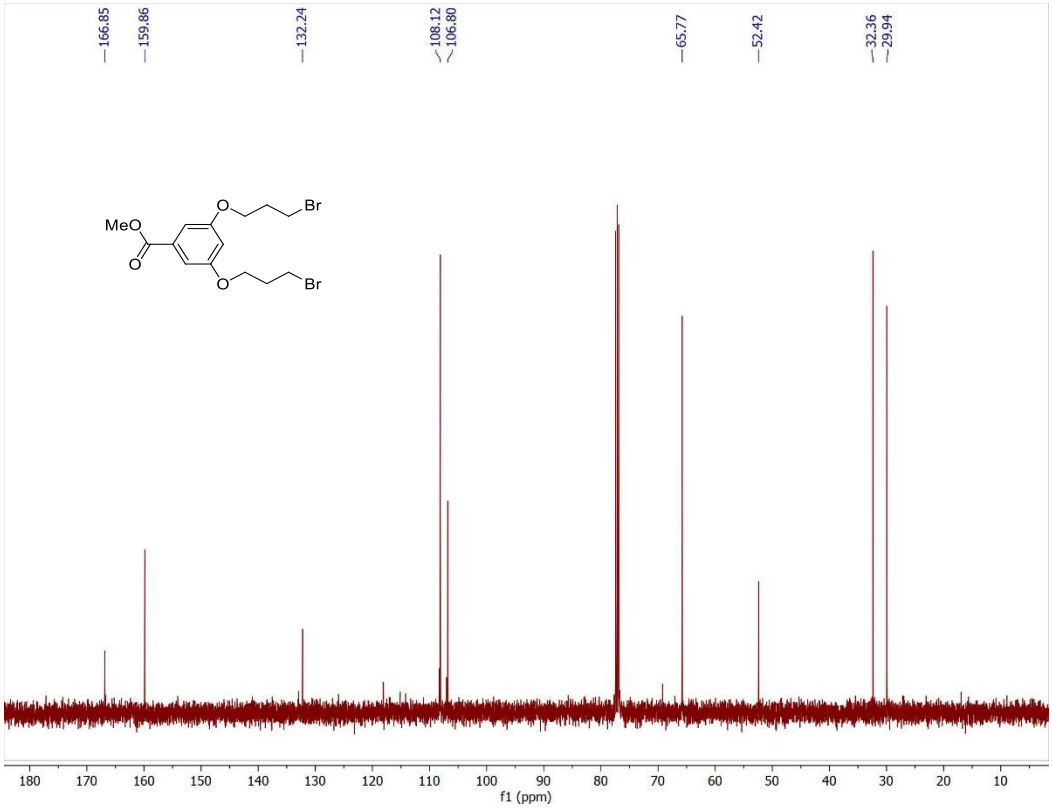
166.85
159.86
132.24
108.12
106.80
65.77
52.42
32.36
29.94
MeO
O
O
Br
O
Br
180
170
160
150
140
130
120
110
100
90
80
70
60
50
40
30
20
10
f1 (ppm)

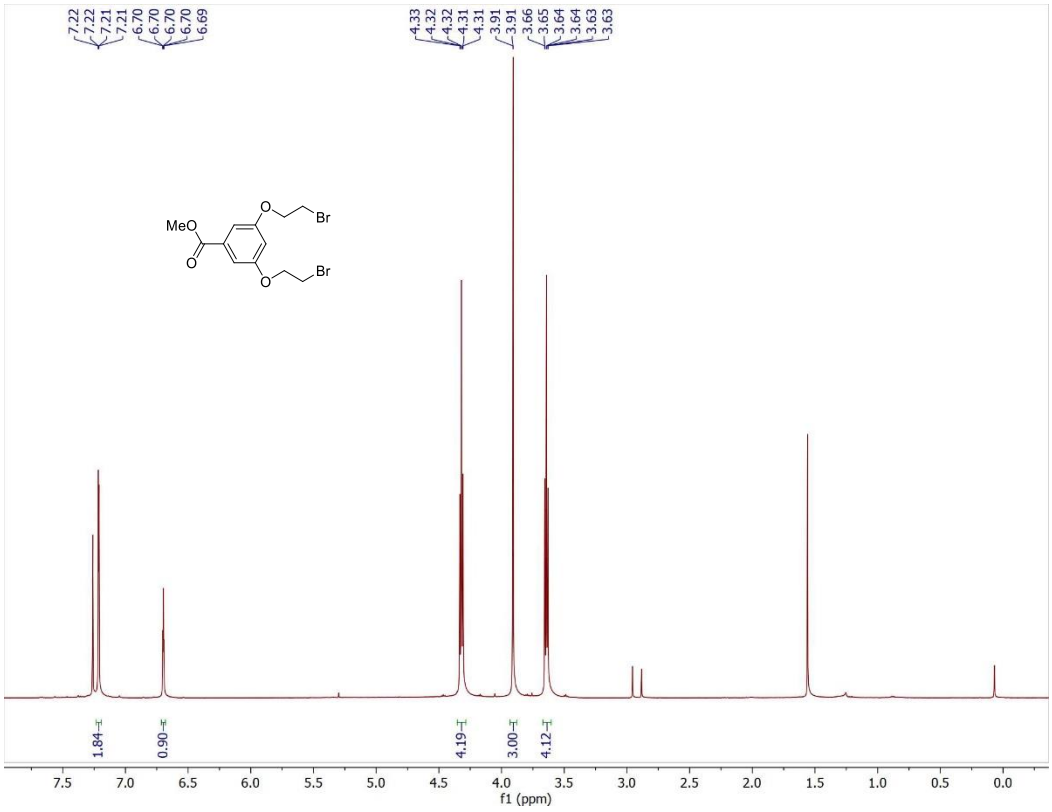
7.22
7.22
7.21
7.21
6.70
6.70
6.70
6.70
6.69
4.33
4.32
4.32
4.31
4.31
3.91
3.91
3.66
3.65
3.64
3.64
3.63
3.63
MeO
O
O
Br
O
Br
1.84
0.90
4.19
3.00
4.12
7.5
7.0
6.5
6.0
5.5
5.0
4.5
4.0
3.5
3.0
2.5
2.0
1.5
1.0
0.5
0.0
f1 (ppm)

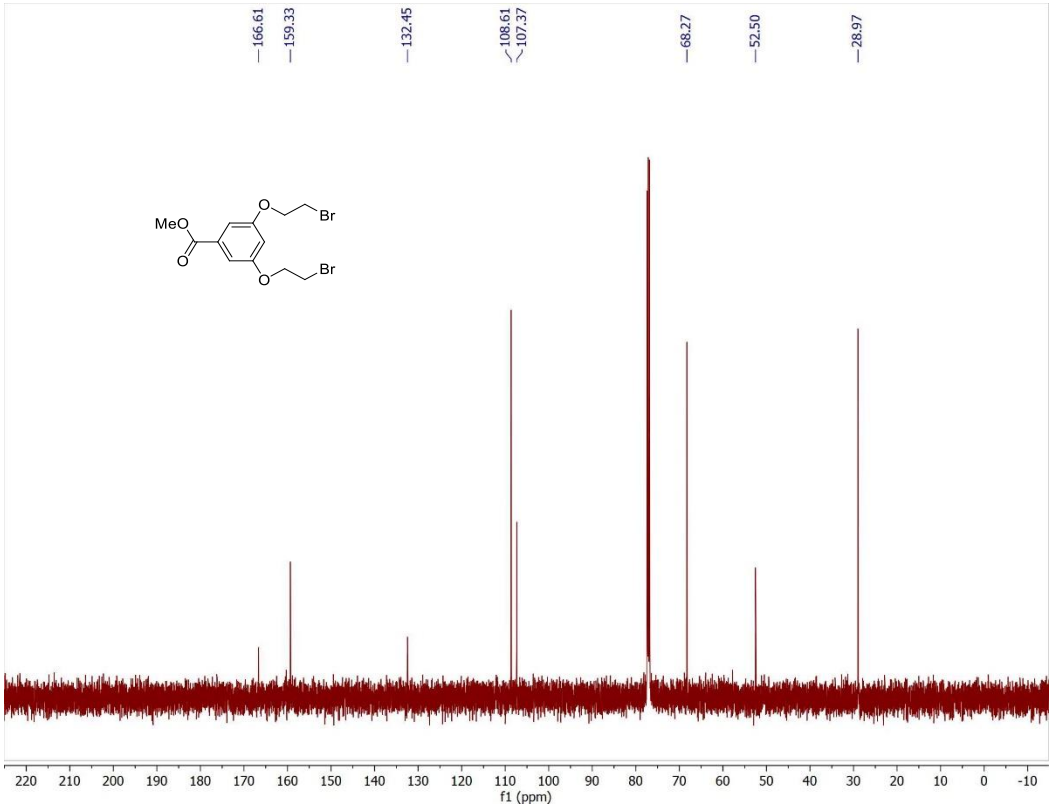
166.61
159.33
132.45
108.61
107.37
68.27
52.50
28.97
MeO
O
O
Br
O
Br
220
210
200
190
180
170
160
150
140
130
120
110
100
90
80
70
60
50
40
30
20
10
0
-10
f1 (ppm)

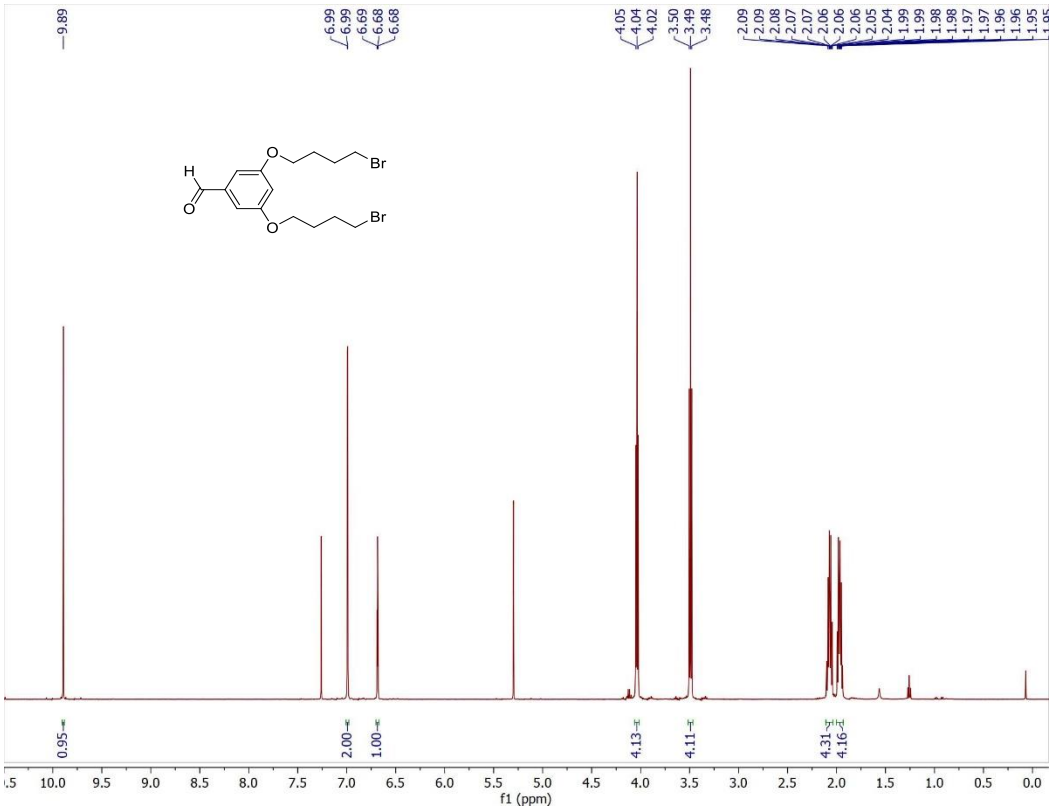
9.89
6.99
6.99
6.69
6.68
6.68
4.05
4.04
4.02
3.50
3.49
3.48
2.09
2.09
2.08
2.07
2.07
2.06
2.06
2.06
2.05
2.04
1.99
1.99
1.98
1.98
1.97
1.97
1.96
1.96
1.95
0.95
2.00
1.00
4.13
4.11
4.31
4.16
f1 (ppm)

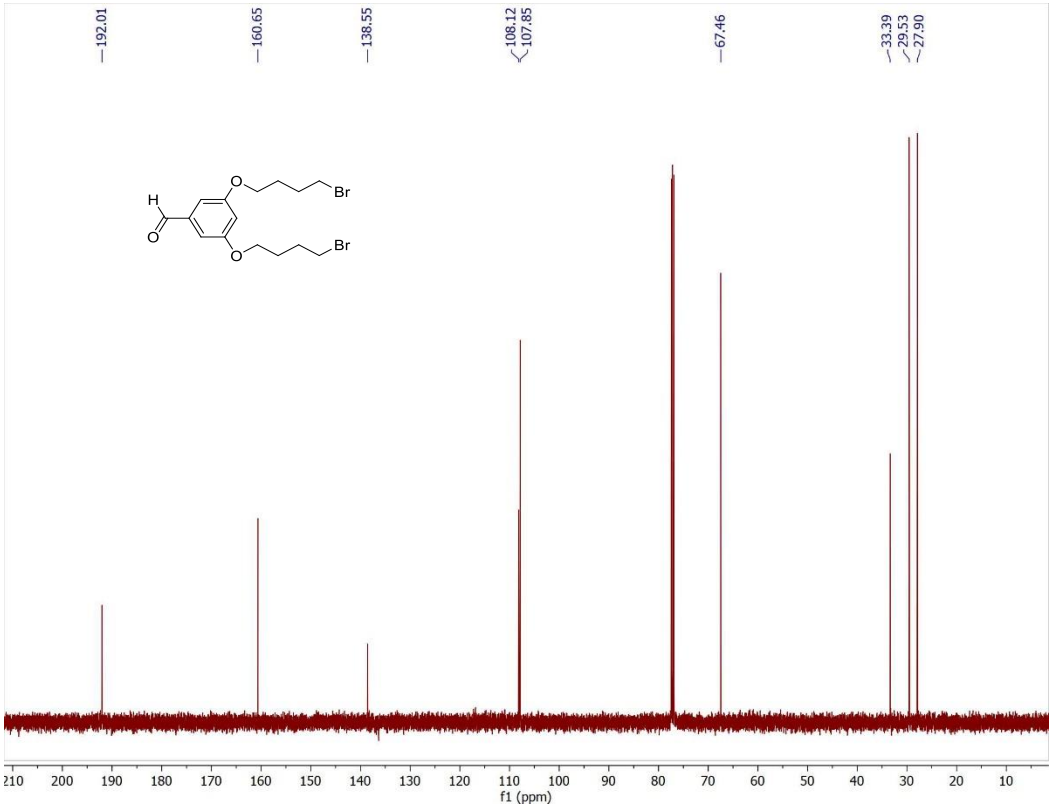
192.01
160.65
138.55
108.12
107.85
67.46
33.39
29.53
27.90
f1 (ppm)

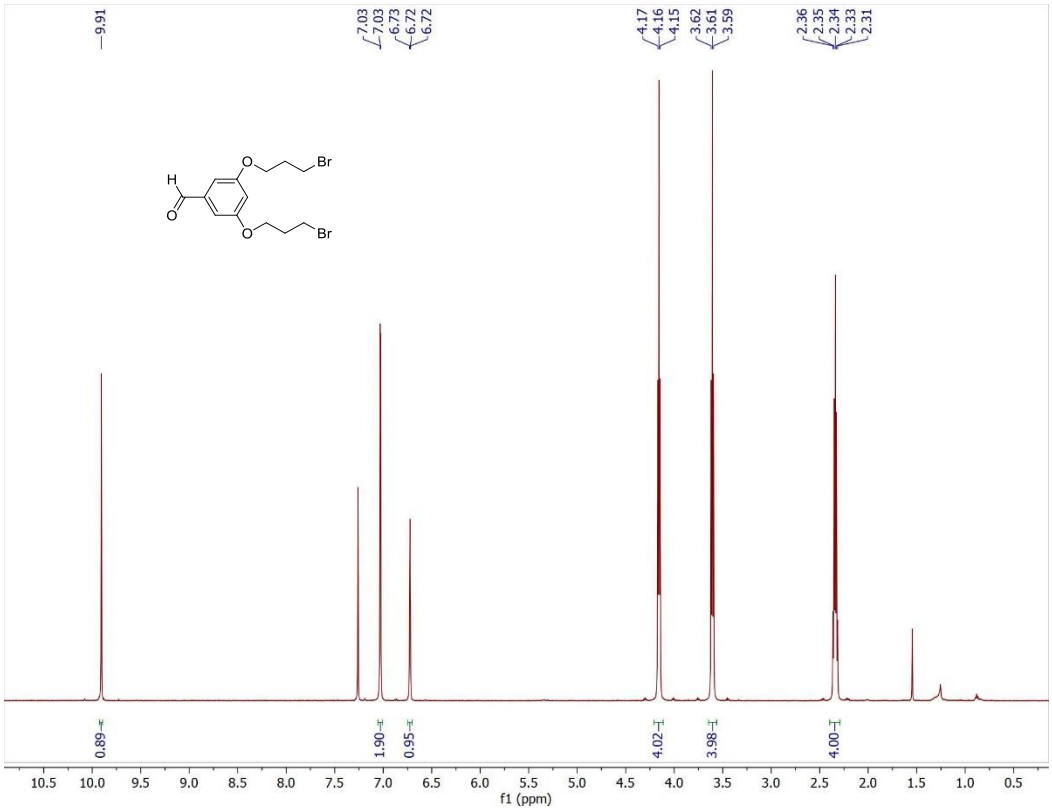
9.91
7.03
7.03
6.73
6.72
6.72
4.17
4.16
4.15
3.62
3.61
3.59
2.36
2.35
2.34
2.33
2.31
0.89
1.90
0.95
4.02
3.98
4.00
f1 (ppm)

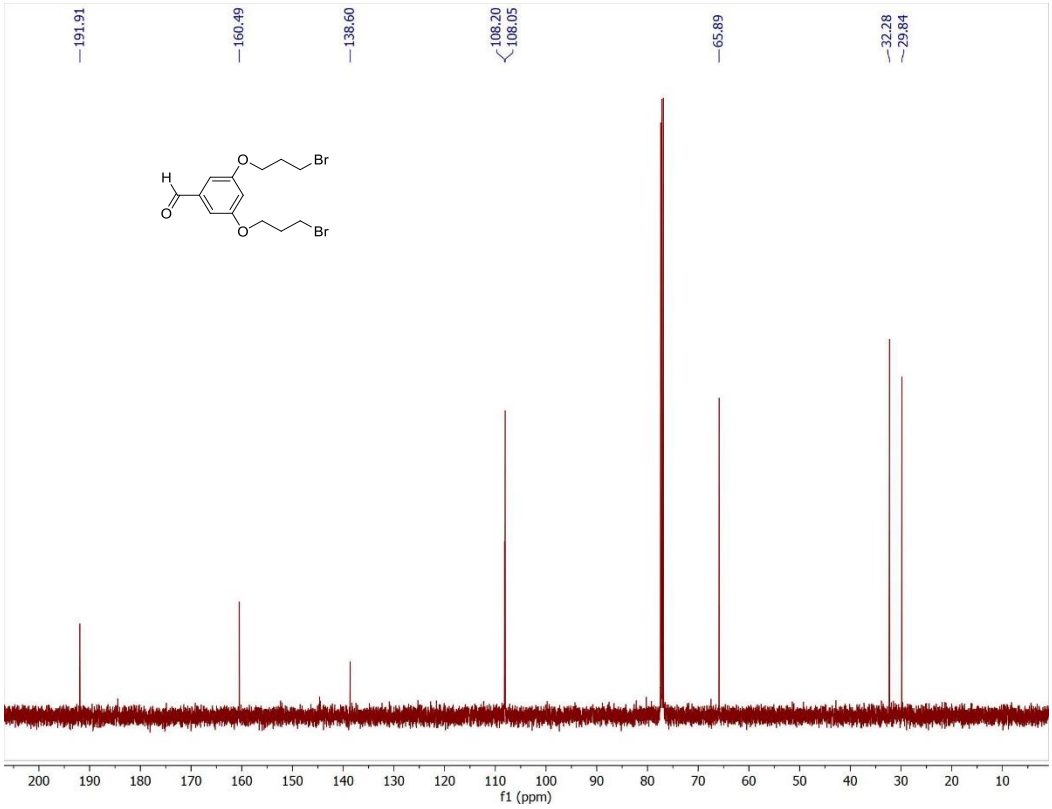
191.91
160.49
138.60
108.20
108.05
65.89
32.28
29.84
f1 (ppm)

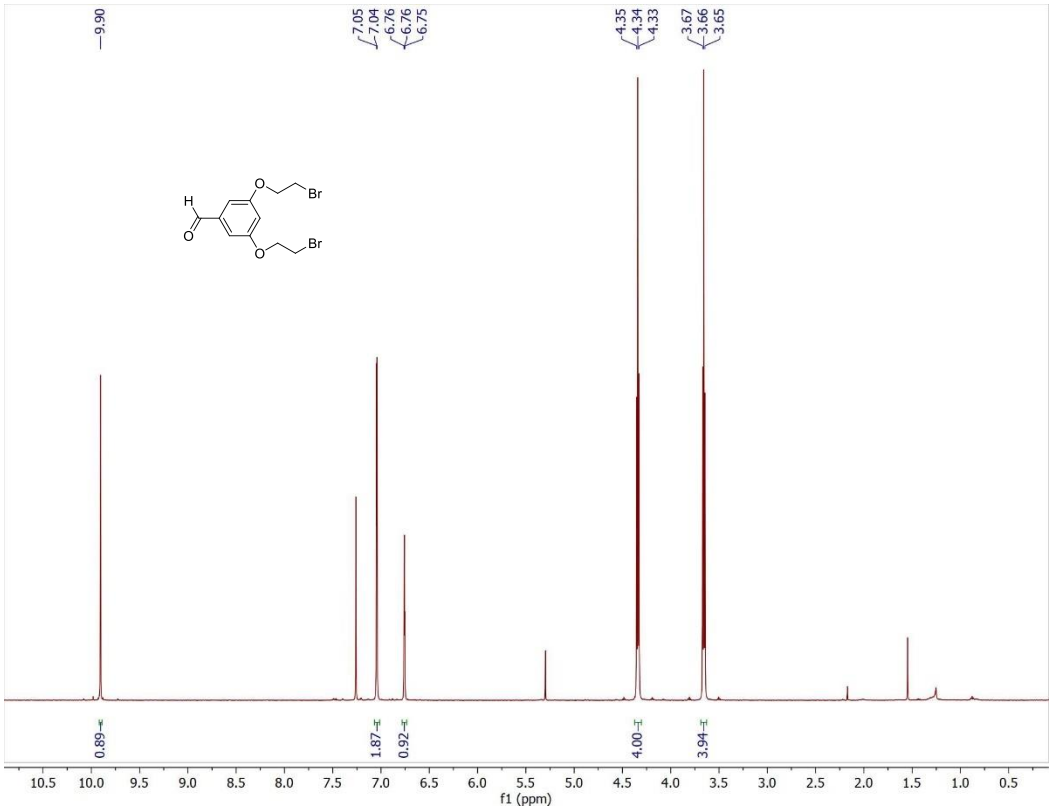
9.90
7.05
7.04
6.76
6.76
6.75
4.35
4.34
4.33
3.67
3.66
3.65
Br
Br
O
H
O
O
O
0.89
1.87
0.92
4.00
3.94
10.5 10.0 9.5 9.0 8.5 8.0 7.5 7.0 6.5 6.0 5.5 5.0 4.5 4.0 3.5 3.0 2.5 2.0 1.5 1.0 0.5
f1 (ppm)

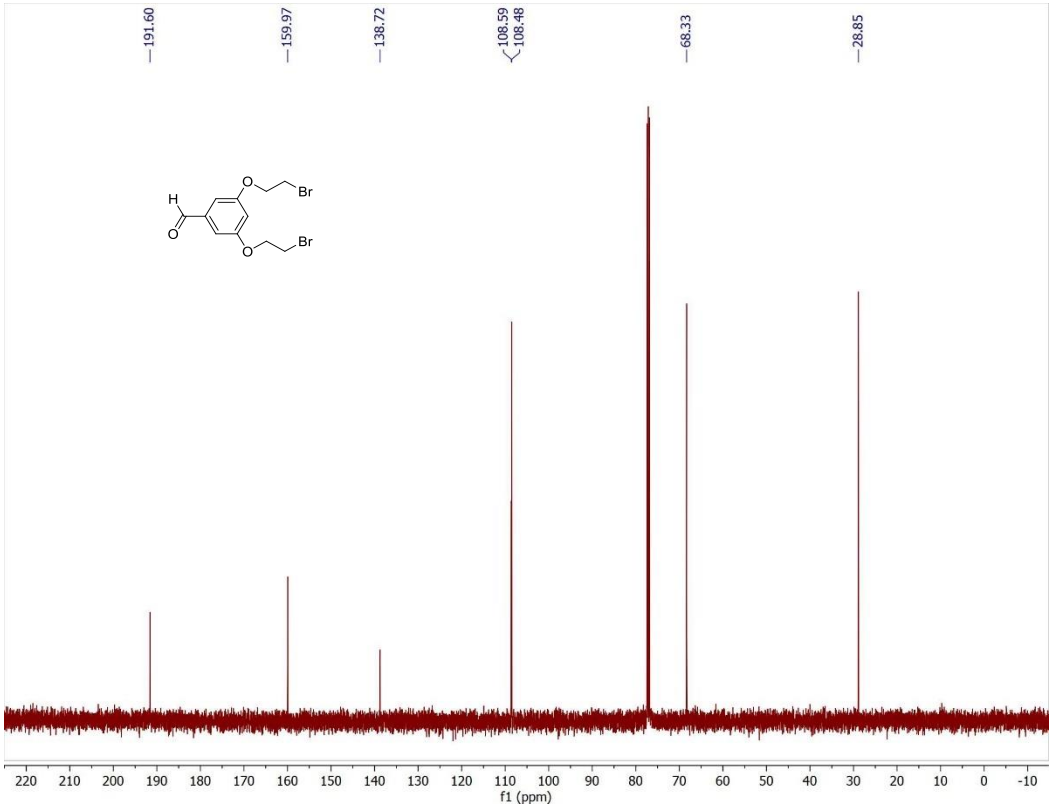
191.60
159.97
138.72
108.59
108.48
68.33
28.85
Br
Br
O
H
O
O
O
220 210 200 190 180 170 160 150 140 130 120 110 100 90 80 70 60 50 40 30 20 10 0 -10
f1 (ppm)

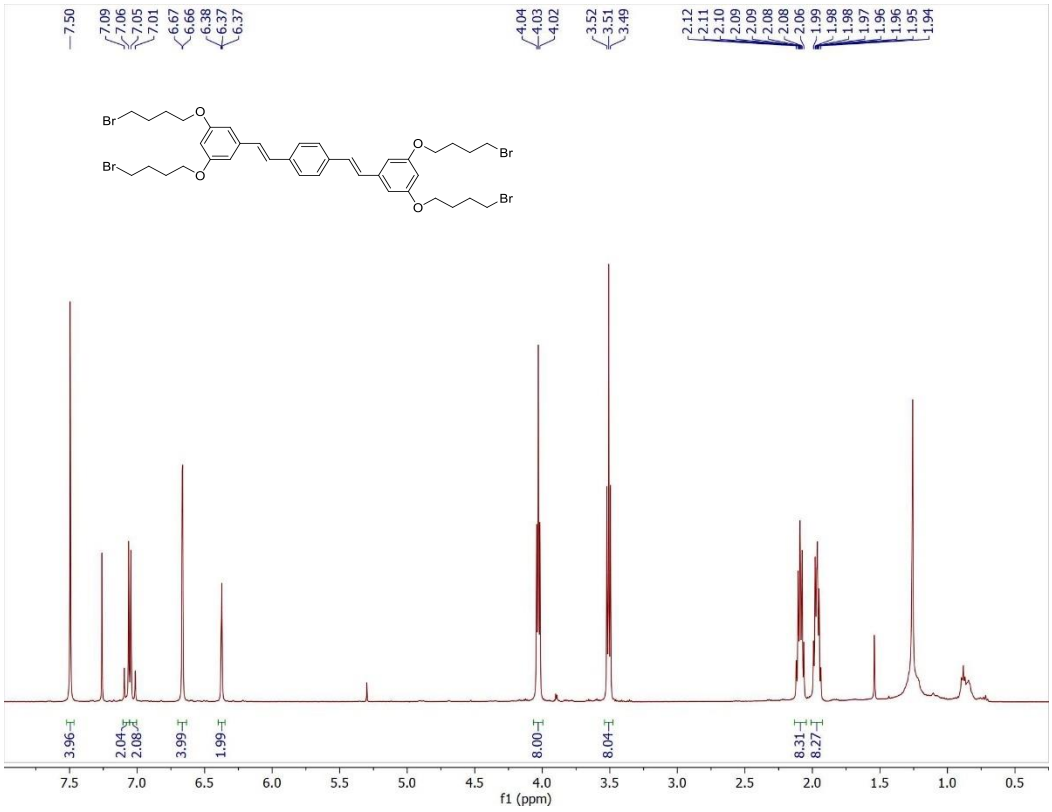
7.50
7.09
7.06
7.05
7.01
6.67
6.66
6.38
6.37
6.37
4.04
4.03
4.02
3.52
3.51
3.49
2.12
2.11
2.10
2.09
2.09
2.08
2.08
2.06
1.99
1.98
1.98
1.97
1.96
1.96
1.95
1.94
Br
Br
Br
Br
3.96
2.04
2.08
3.99
1.99
8.00
8.04
8.31
8.27
f1 (ppm)

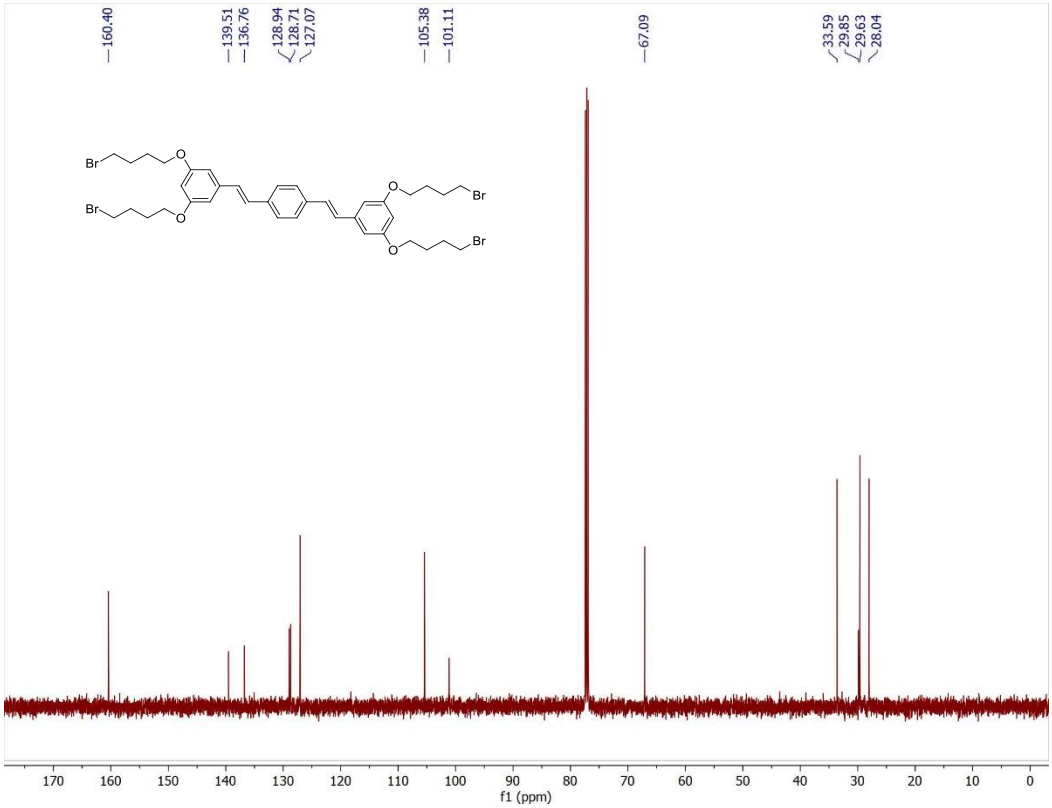
160.40
139.51
136.76
128.94
128.71
127.07
105.38
101.11
67.09
33.59
29.85
29.63
28.04
Br
Br
Br
Br
f1 (ppm)

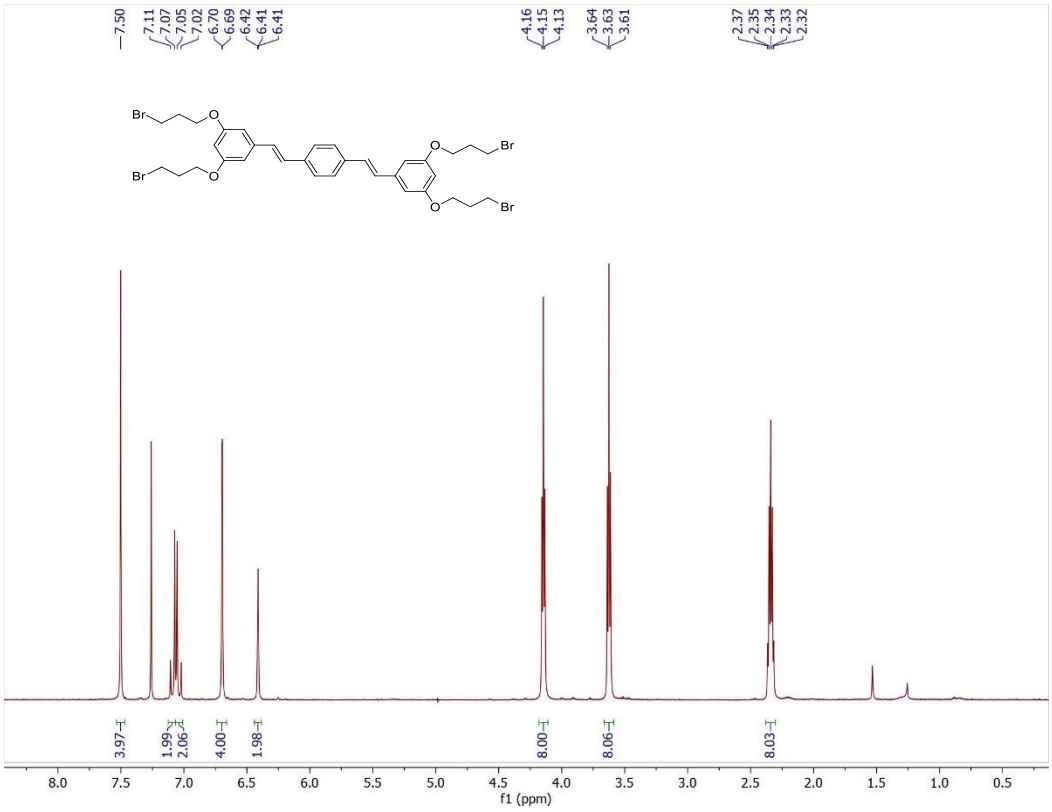
7.50
7.11
7.07
7.05
7.02
6.70
6.69
6.42
6.41
6.41
4.16
4.15
4.13
3.64
3.63
3.61
2.37
2.35
2.34
2.33
2.32
Br
O
Br
O
O
Br
O
Br
3.97
1.99
2.06
4.00
1.98
8.00
8.06
8.03
f1 (ppm)

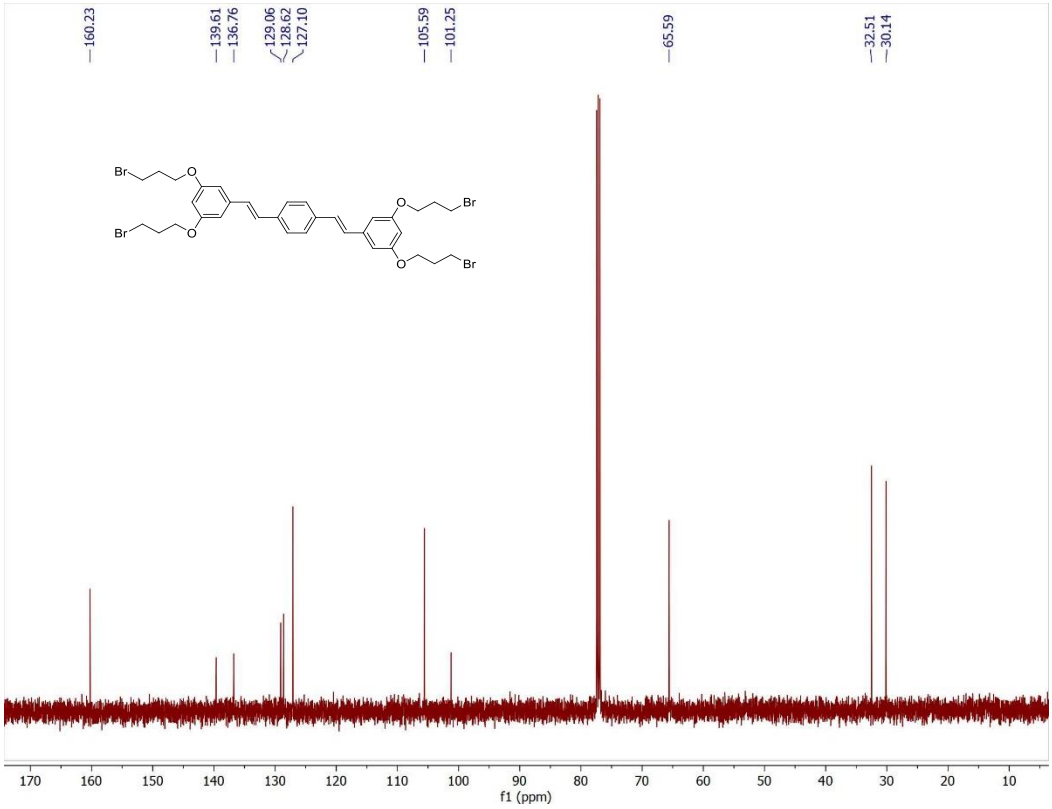
160.23
139.61
136.76
129.06
128.62
127.10
105.59
101.25
65.59
32.51
30.14
Br
O
Br
O
O
Br
O
Br
f1 (ppm)

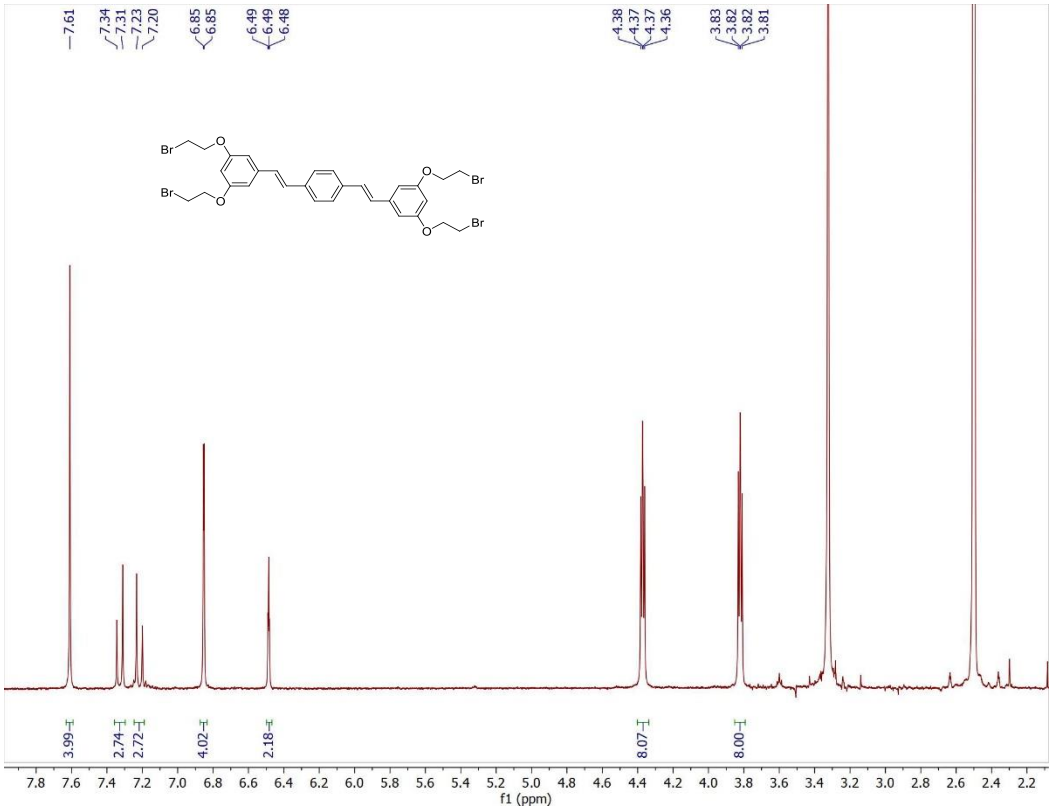
7.61
7.34
7.31
7.23
7.20
6.85
6.85
6.49
6.49
6.48
4.38
4.37
4.37
4.36
3.83
3.82
3.82
3.81
Br
Br
Br
Br
3.99
2.74
2.72
4.02
2.18
8.07
8.00
f1 (ppm)

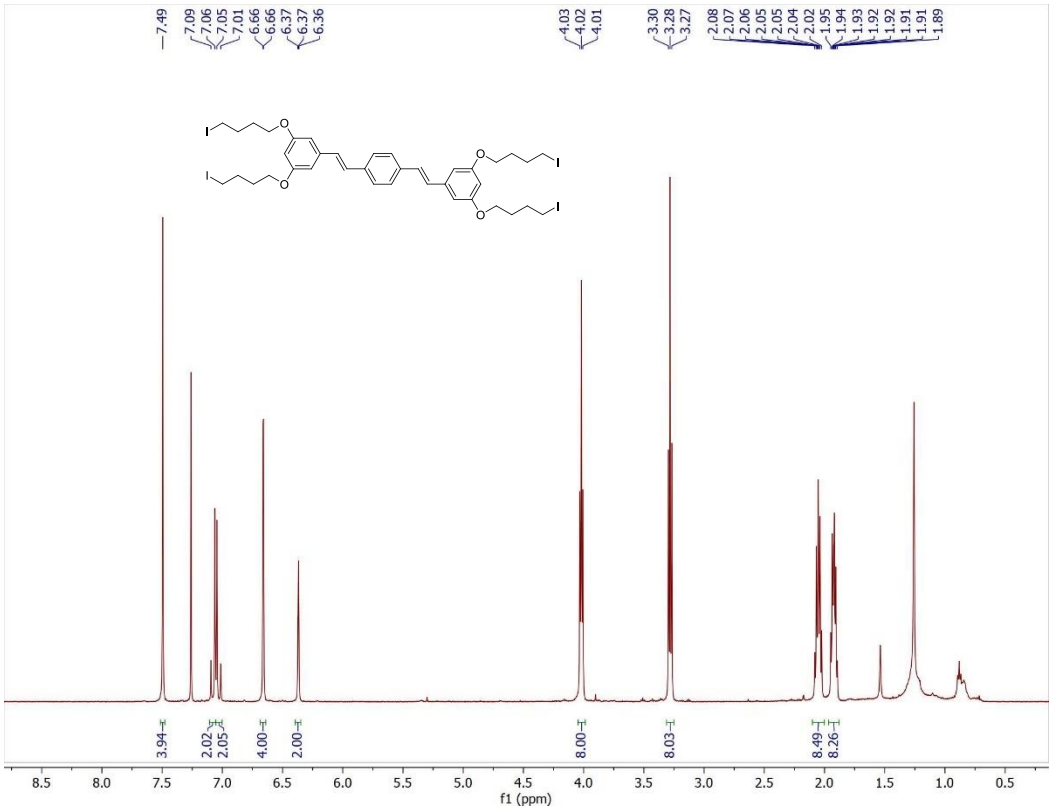
7.49
7.09
7.06
7.05
7.01
6.66
6.66
6.37
6.37
6.36
4.03
4.02
4.01
3.30
3.28
3.27
2.08
2.07
2.06
2.05
2.05
2.04
2.02
1.95
1.94
1.93
1.92
1.92
1.91
1.91
1.89
3.94
2.02
2.05
4.00
2.00
8.00
8.03
8.49
8.26
f1 (ppm)

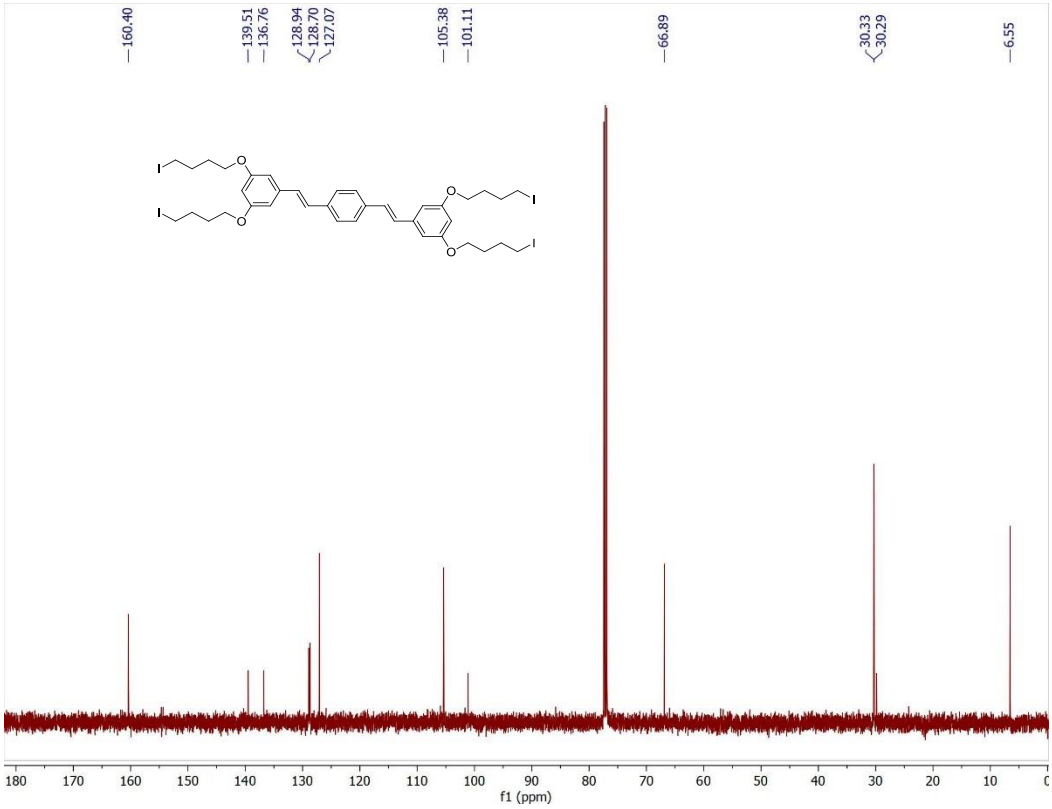
160.40
139.51
136.76
128.94
128.70
127.07
105.38
101.11
66.89
30.33
30.29
6.55
f1 (ppm)

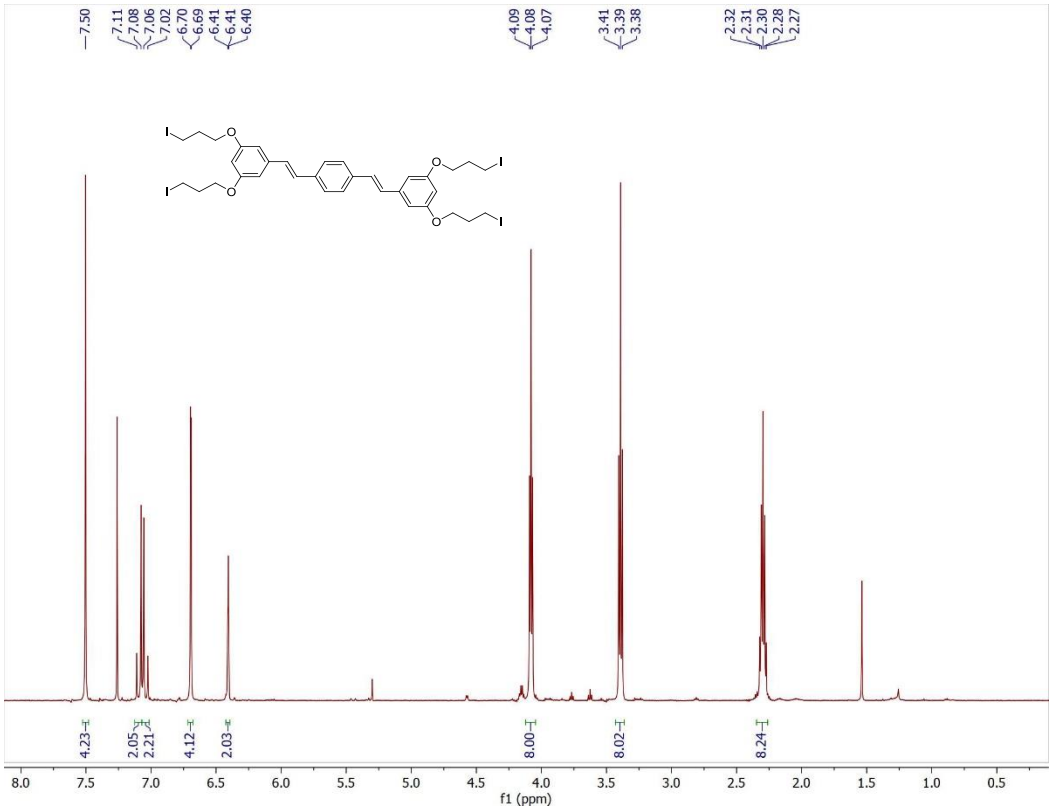
7.50
7.11
7.08
7.06
7.02
6.70
6.69
6.41
6.41
6.40
4.09
4.08
4.07
3.41
3.39
3.38
2.32
2.31
2.30
2.28
2.27
4.23
2.05
2.21
4.12
2.03
8.00
8.02
8.24
f1 (ppm)

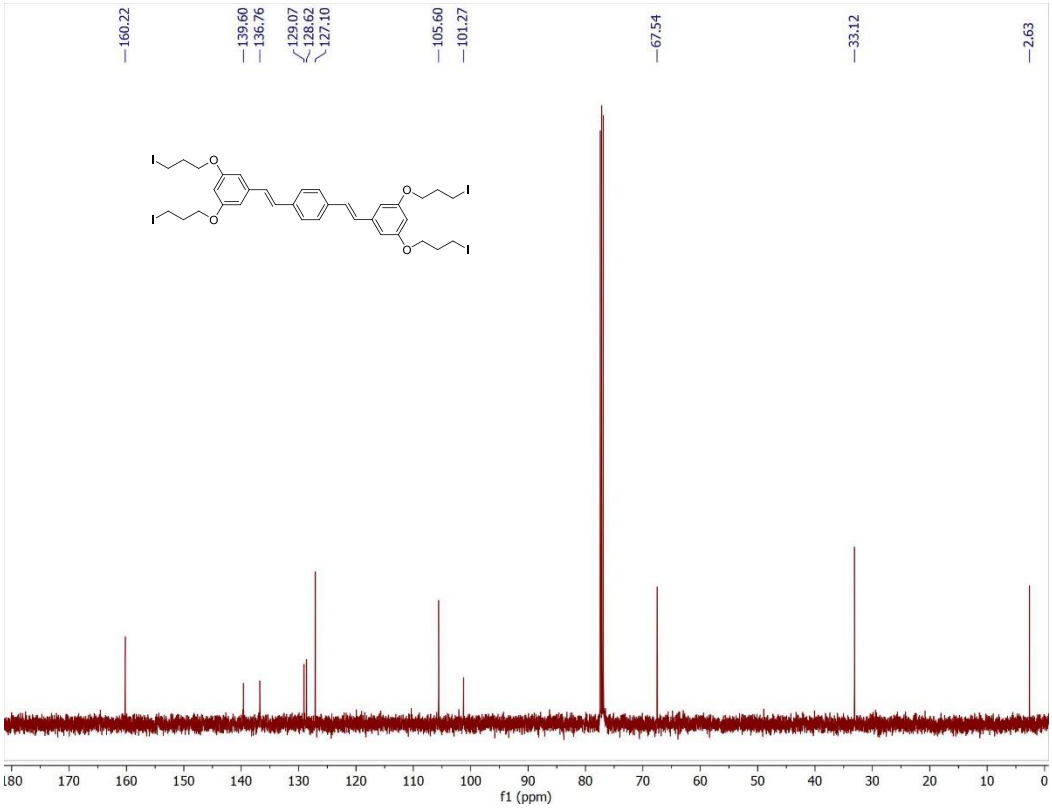
160.22
139.60
136.76
129.07
128.62
127.10
105.60
101.27
67.54
33.12
2.63
f1 (ppm)

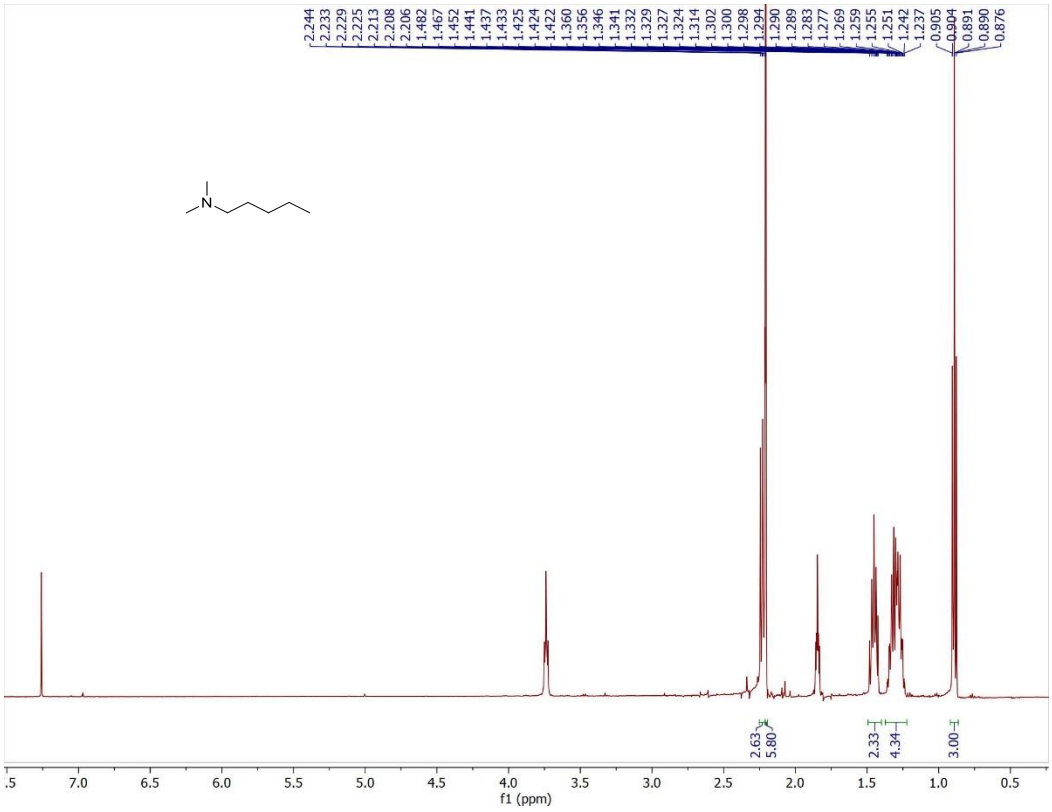
2.244
2.233
2.229
2.225
2.213
2.208
2.206
1.482
1.467
1.452
1.441
1.437
1.433
1.425
1.424
1.422
1.360
1.356
1.346
1.341
1.332
1.329
1.327
1.324
1.314
1.302
1.300
1.298
1.294
1.290
1.289
1.283
1.277
1.269
1.259
1.255
1.251
1.242
1.237
0.905
0.904
0.891
0.890
0.876
2.63
5.80
2.33
4.34
3.00
f1 (ppm)

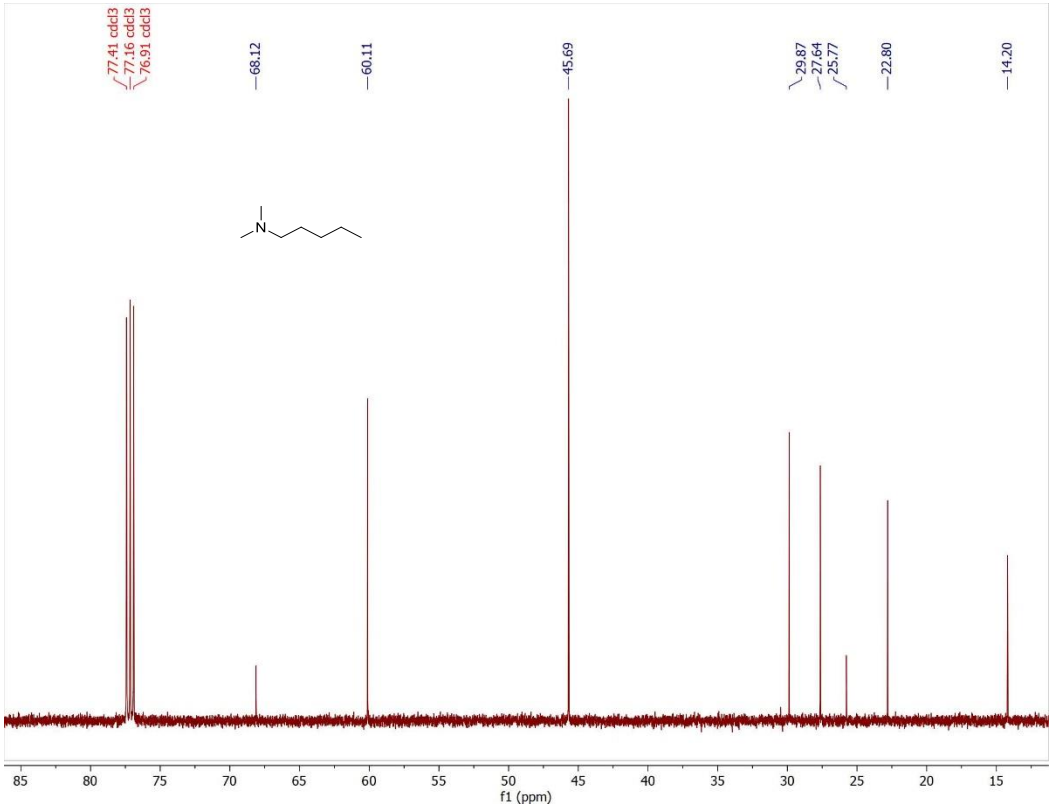
77.41 cdcl3
77.16 cdcl3
76.91 cdcl3
68.12
60.11
45.69
29.87
27.64
25.77
22.80
14.20
f1 (ppm)

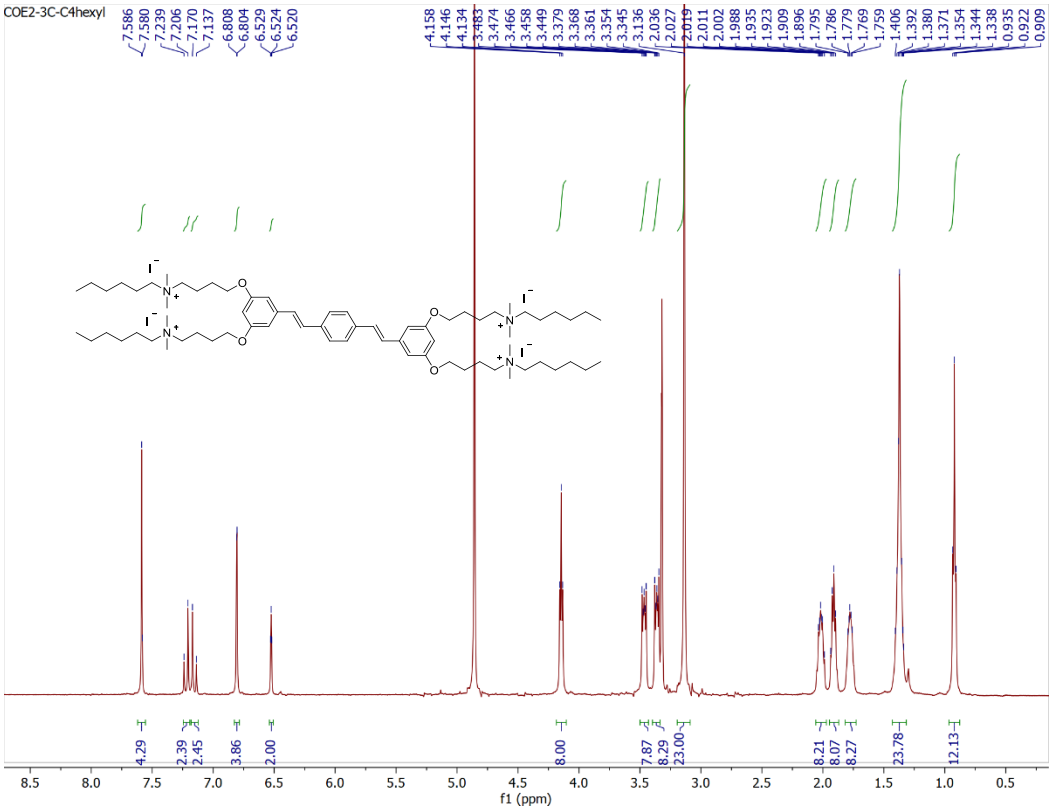
COE2-3C-C4hexyl
f1 (ppm)

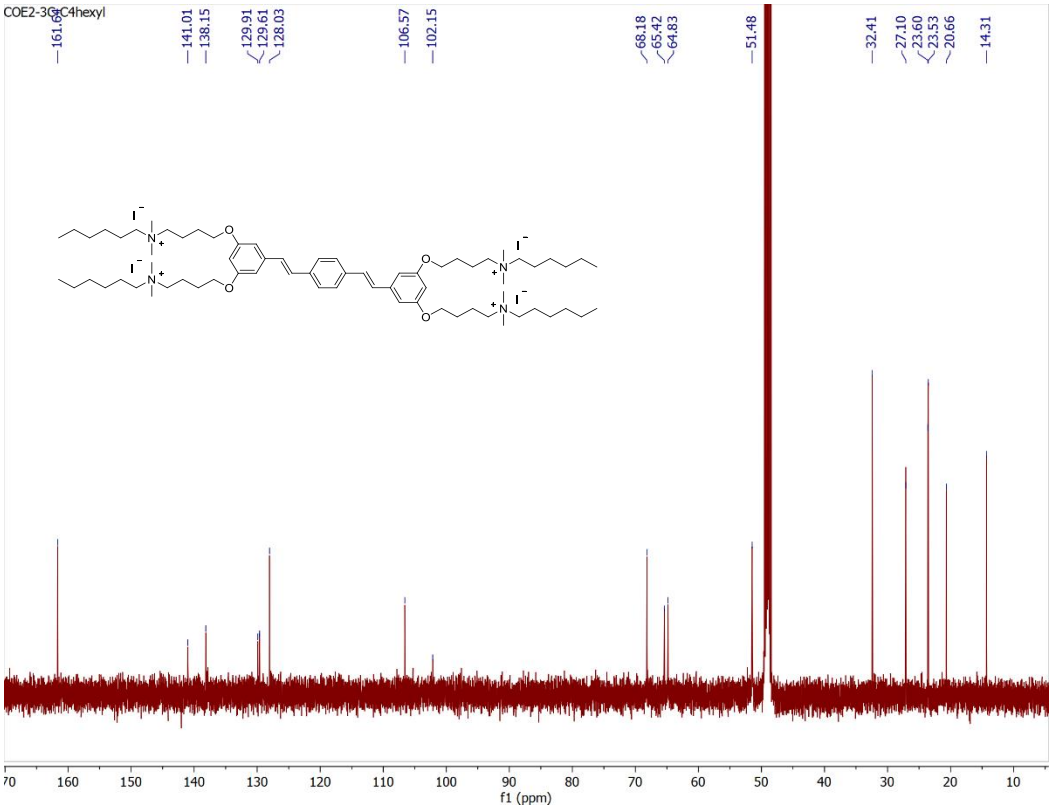
COE2-3C-C4hexyl
f1 (ppm)

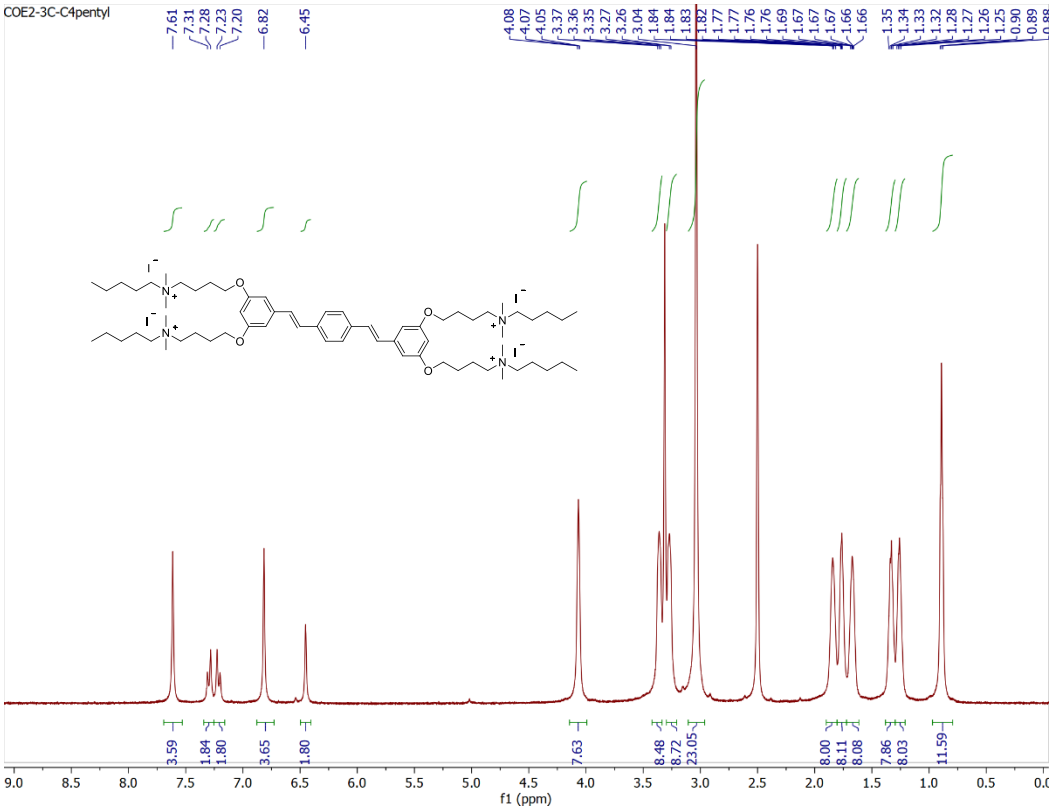
COE2-3C-C4pentyl
7.61
7.31
7.28
7.23
7.20
6.82
6.45
4.08
4.07
4.05
3.37
3.36
3.35
3.27
3.26
3.04
1.84
1.84
1.83
1.82
1.77
1.77
1.76
1.76
1.69
1.67
1.67
1.67
1.66
1.66
1.35
1.34
1.33
1.32
1.28
1.27
1.26
1.25
0.90
0.89
3.59
1.84
1.80
3.65
1.80
7.63
8.48
8.72
23.05
8.00
8.11
8.08
7.86
8.03
11.59
f1 (ppm)

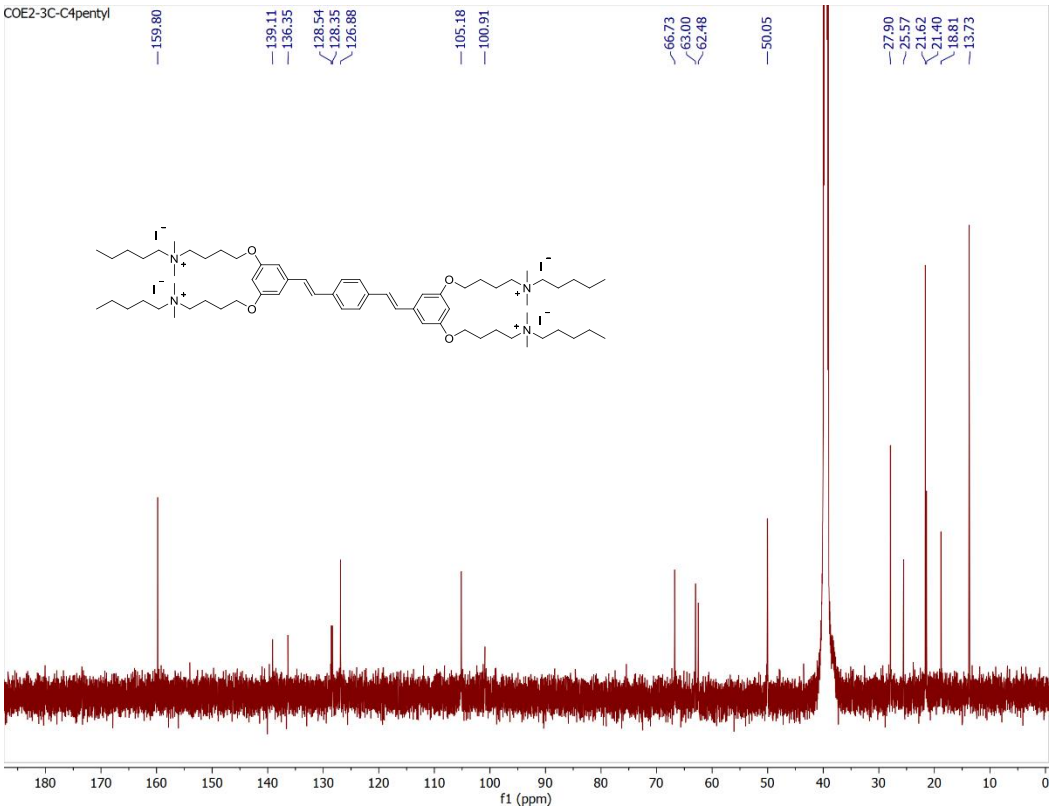
COE2-3C-C4pentyl
159.80
139.11
136.35
128.54
128.35
126.88
105.18
100.91
66.73
63.00
62.48
50.05
27.90
25.57
21.62
21.40
18.81
13.73
f1 (ppm)

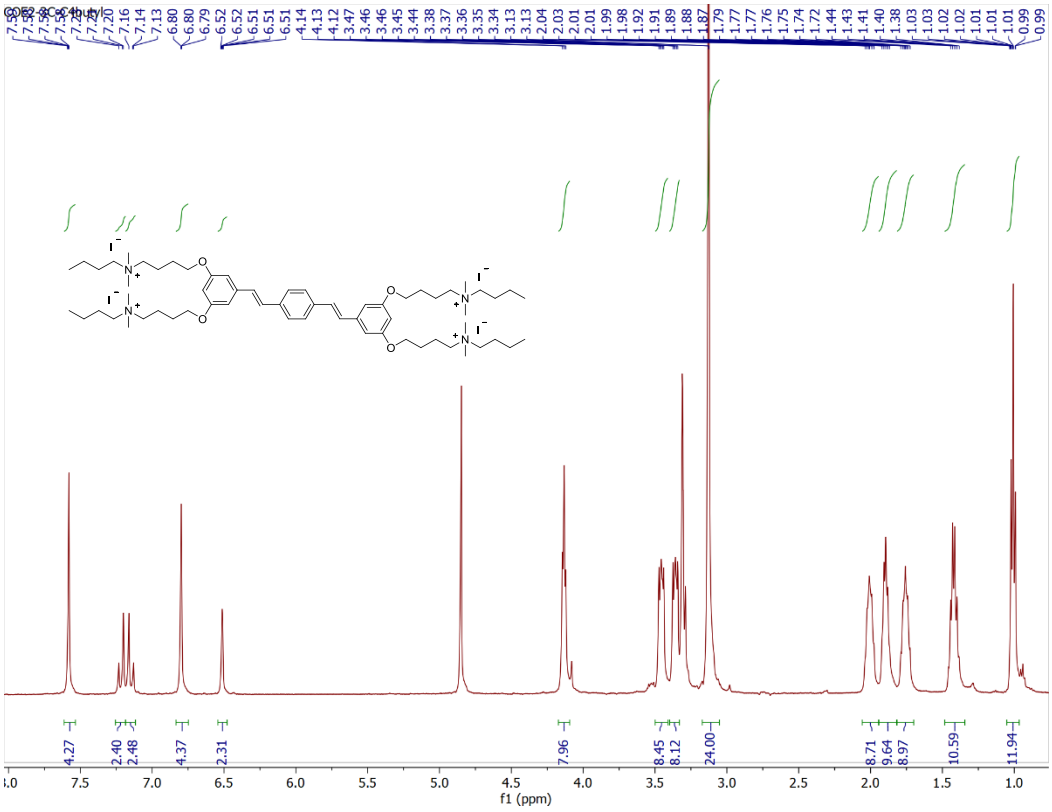
4.27
2.40
2.48
4.37
2.31
7.96
8.45
8.12
24.00
8.71
9.64
8.97
10.59
11.94
f1 (ppm)

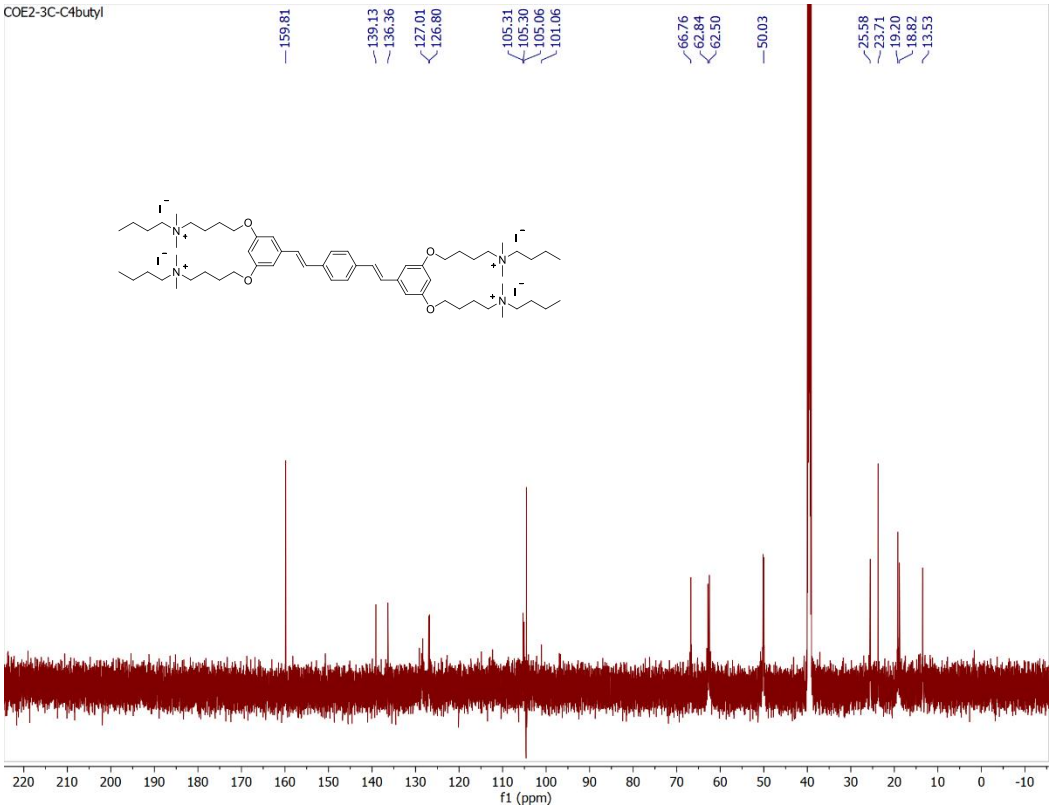
COE2-3C-C4butyl
159.81
139.13
136.36
127.01
126.80
105.31
105.30
105.06
101.06
66.76
62.84
62.50
50.03
25.58
23.71
19.20
18.82
13.53
f1 (ppm)

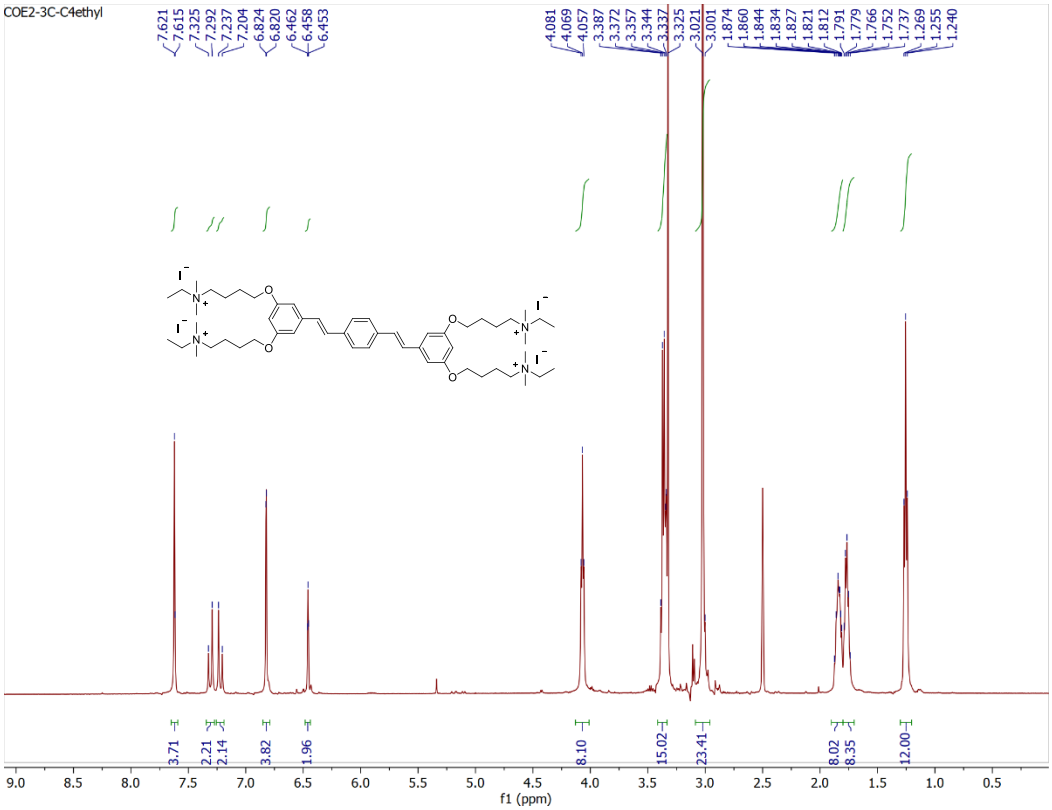
COE2-3C-C4ethyl
7.621
7.615
7.325
7.292
7.237
7.204
6.824
6.820
6.462
6.458
6.453
4.081
4.069
4.057
3.387
3.372
3.357
3.344
3.332
3.325
3.021
3.001
1.874
1.860
1.844
1.834
1.827
1.821
1.812
1.791
1.779
1.766
1.752
1.737
1.269
1.255
1.240
3.71
2.21
2.14
3.82
1.96
8.10
15.02
23.41
8.02
8.35
12.00
f1 (ppm)

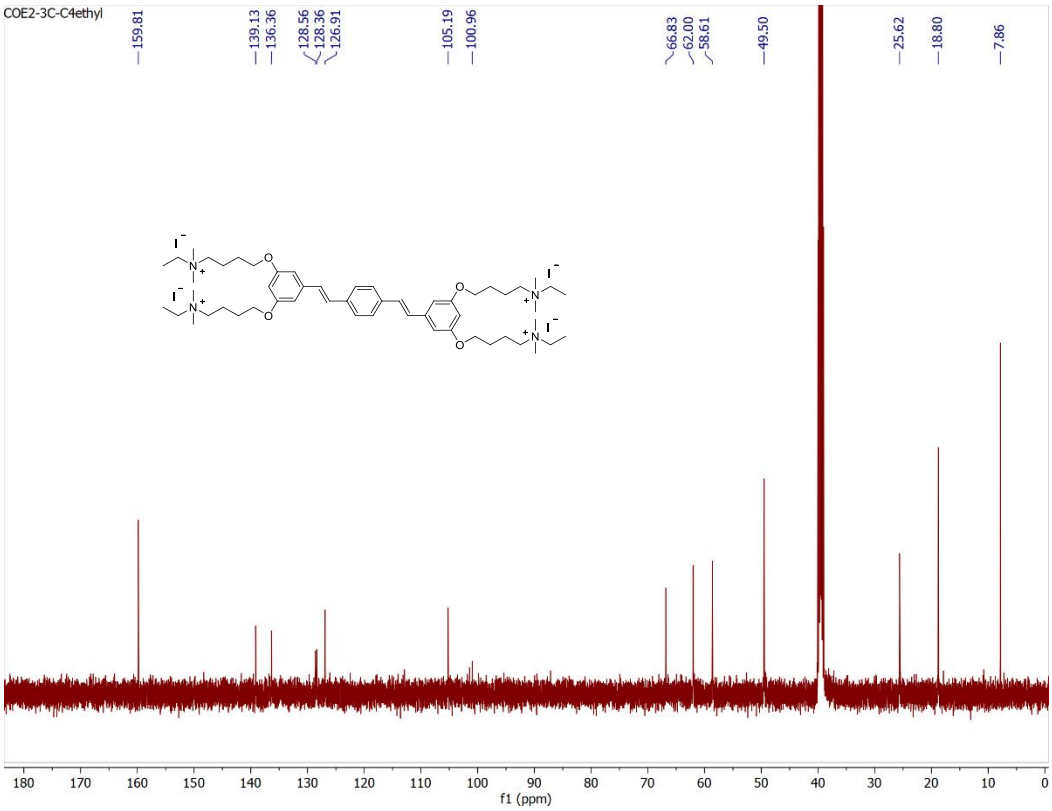
COE2-3C-C4ethyl
159.81
139.13
136.36
128.56
128.36
126.91
105.19
100.96
66.83
62.00
58.61
49.50
25.62
18.80
7.86
f1 (ppm)

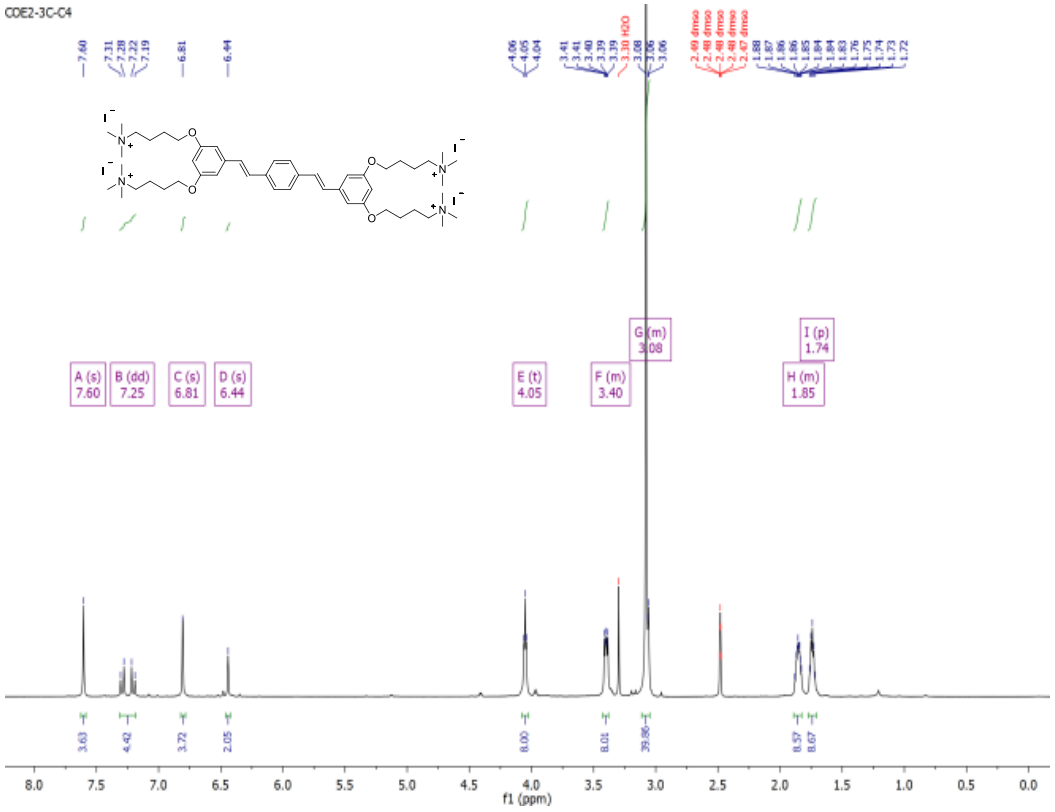
CDE2-3C-C4
A (s) 7.60
B (dd) 7.25
C (s) 6.81
D (s) 6.44
E (t) 4.05
F (m) 3.40
G (m) 3.08
H (m) 1.85
I (p) 1.74
f1 (ppm)

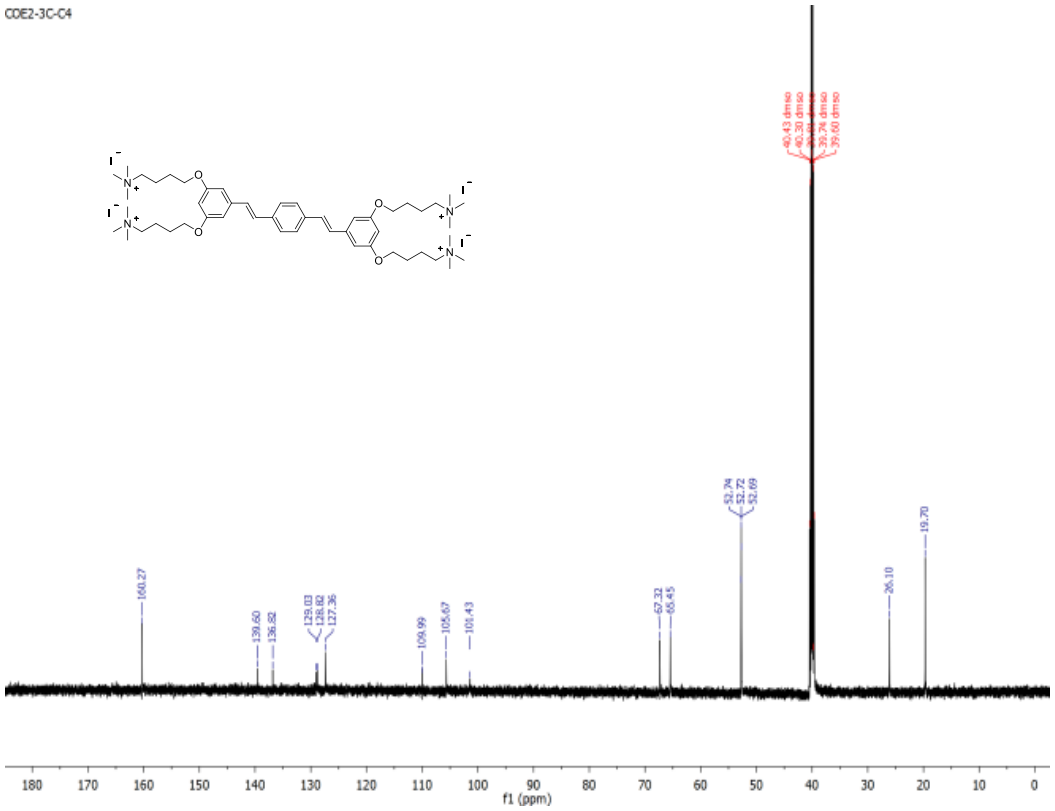
CDE2-3C-C4
160.27
139.60
136.82
129.03
128.82
127.36
109.99
105.67
101.43
67.32
65.45
52.74
52.72
52.69
26.10
19.70
f1 (ppm)

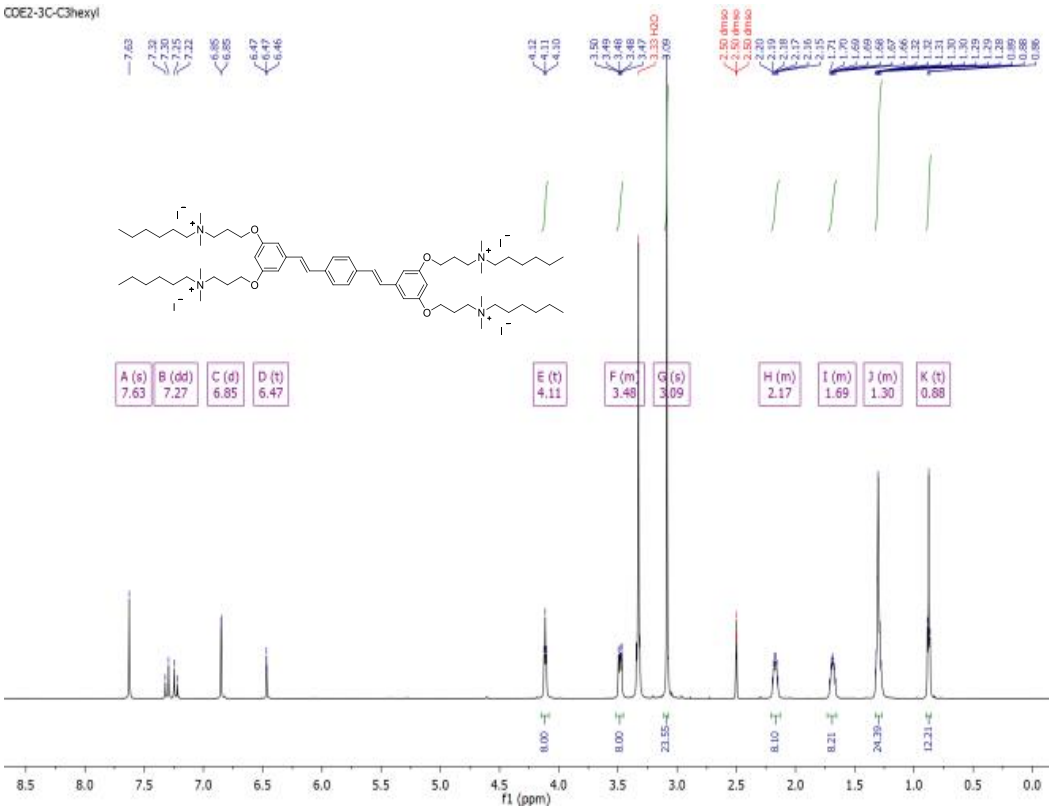
CDE2-3C-C3hexyl
A (s) 7.63
B (dd) 7.27
C (d) 6.85
D (t) 6.47
E (t) 4.11
F (m) 3.48
G (s) 3.09
H (m) 2.17
I (m) 1.69
J (m) 1.30
K (t) 0.88
f1 (ppm)

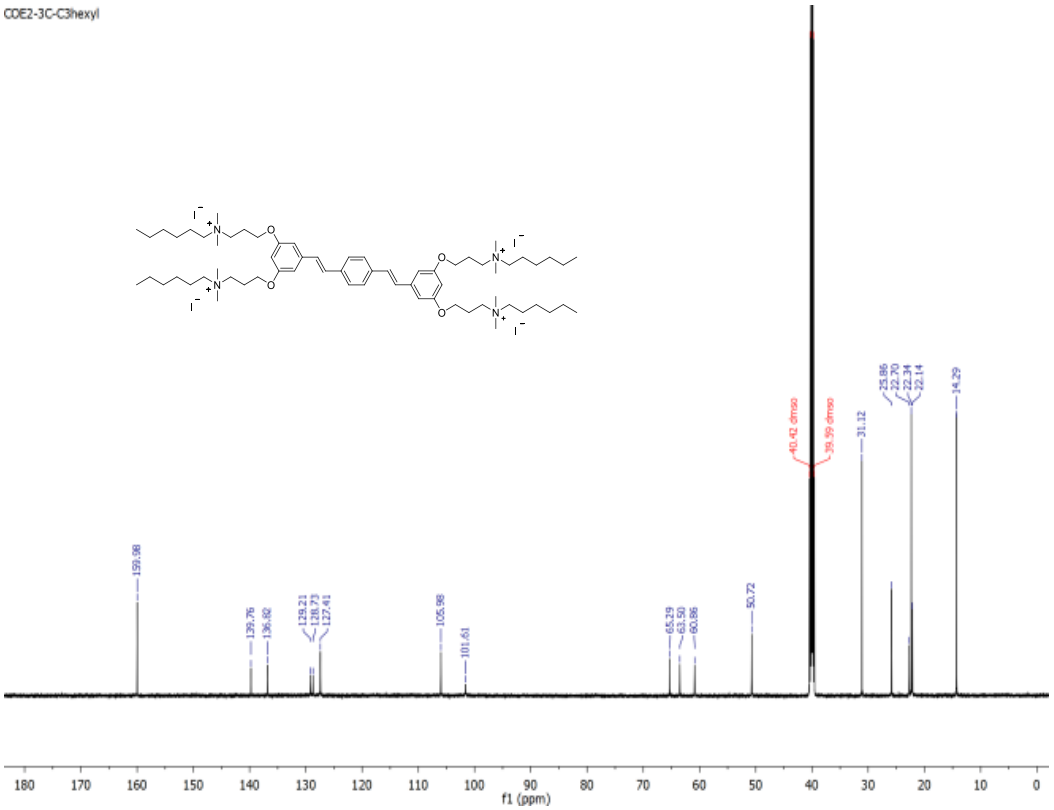
CDE2-3C-C3hexyl
159.98
139.76
136.82
129.21
128.73
127.41
105.98
101.61
65.29
63.50
60.86
50.72
40.42 dmso
39.99 dmso
31.12
25.86
22.70
22.34
22.14
14.29
f1 (ppm)

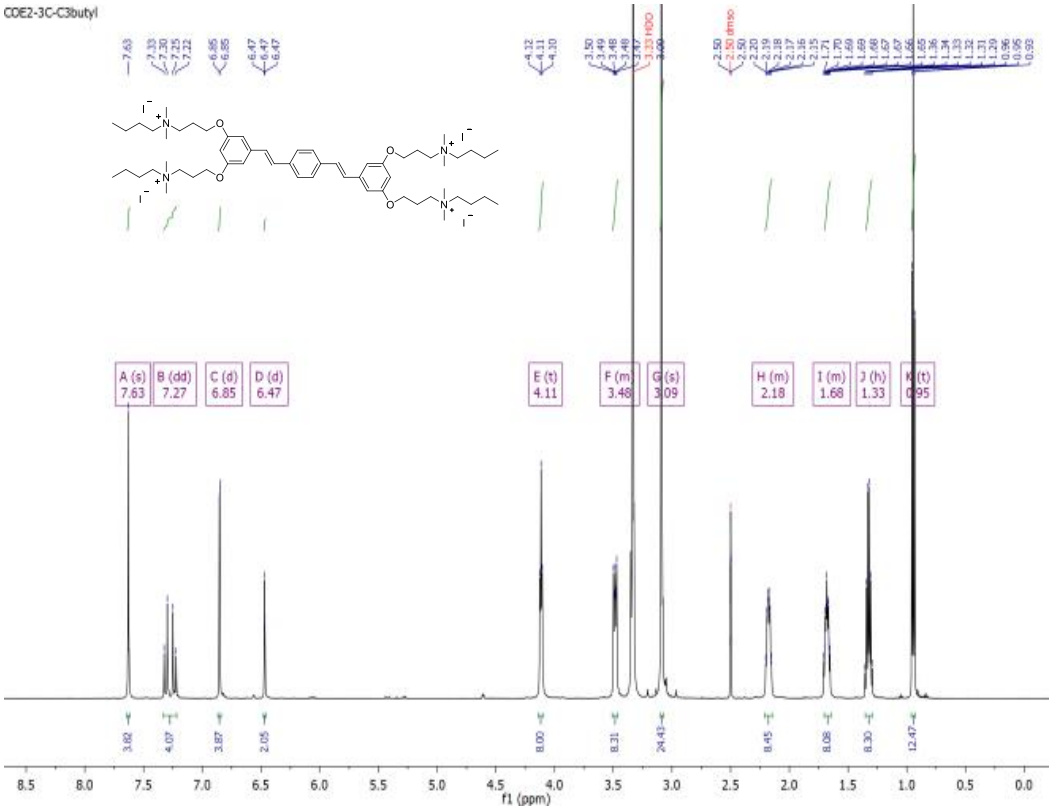
CDE2-3C-C3butyl
A (s) 7.63
B (dd) 7.27
C (d) 6.85
D (d) 6.47
E (t) 4.11
F (m) 3.48
G (s) 3.09
H (m) 2.18
I (m) 1.68
J (h) 1.33
K (t) 0.95
f1 (ppm)

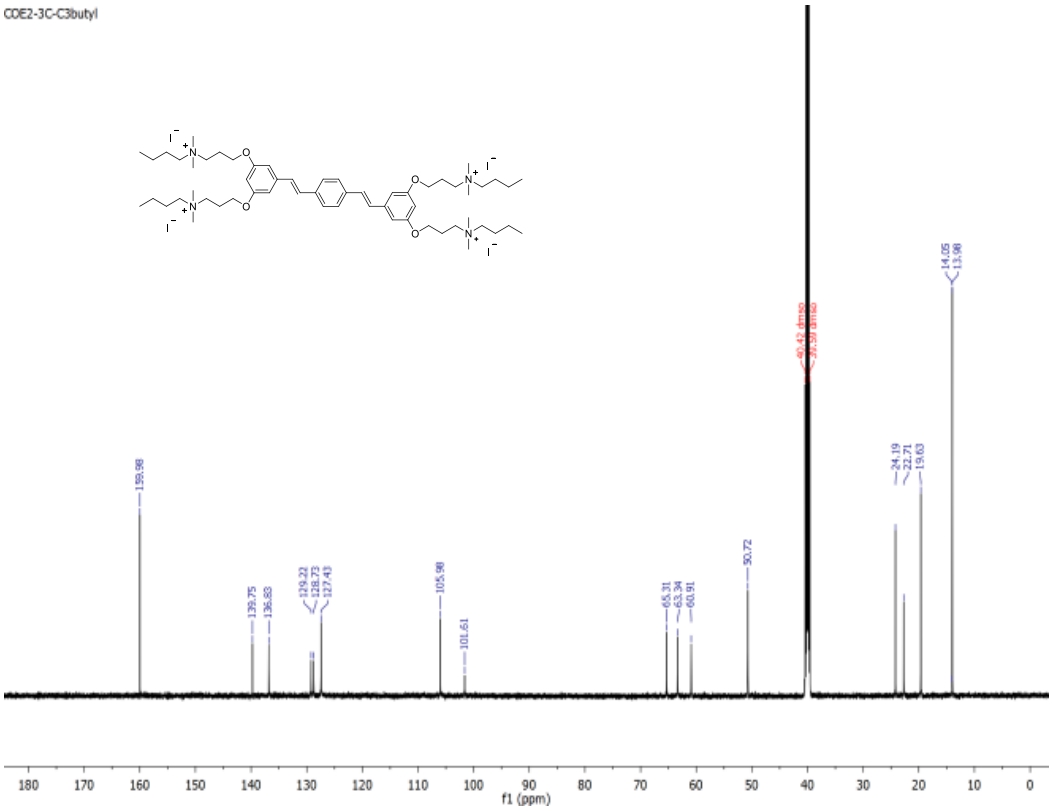
CDE2-3C-C3butyl
159.98
139.75
136.83
129.22
128.73
127.43
105.98
101.61
65.31
63.34
60.91
50.72
40.47 dmso
24.19
22.71
19.63
14.05
13.98
f1 (ppm)

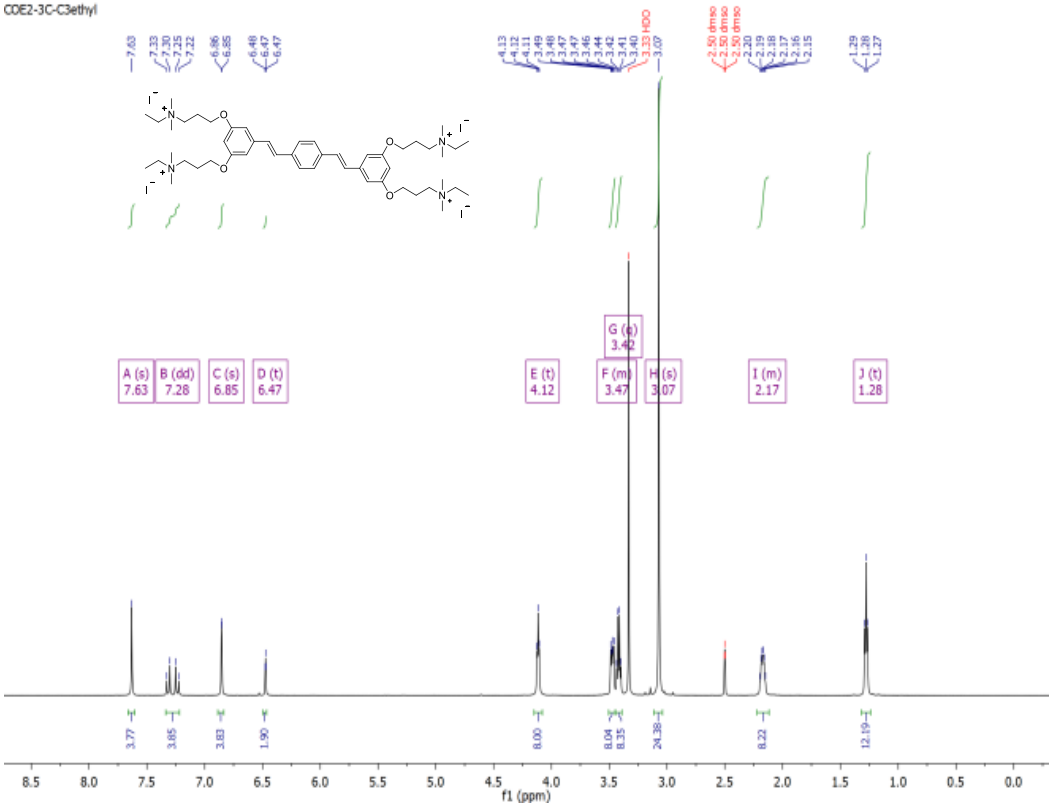
CDE2-3C-C3ethyl
A (s) 7.63
B (dd) 7.28
C (s) 6.85
D (t) 6.47
E (t) 4.12
G (q) 3.42
F (m) 3.47
H (s) 3.07
I (m) 2.17
J (t) 1.28
f1 (ppm)

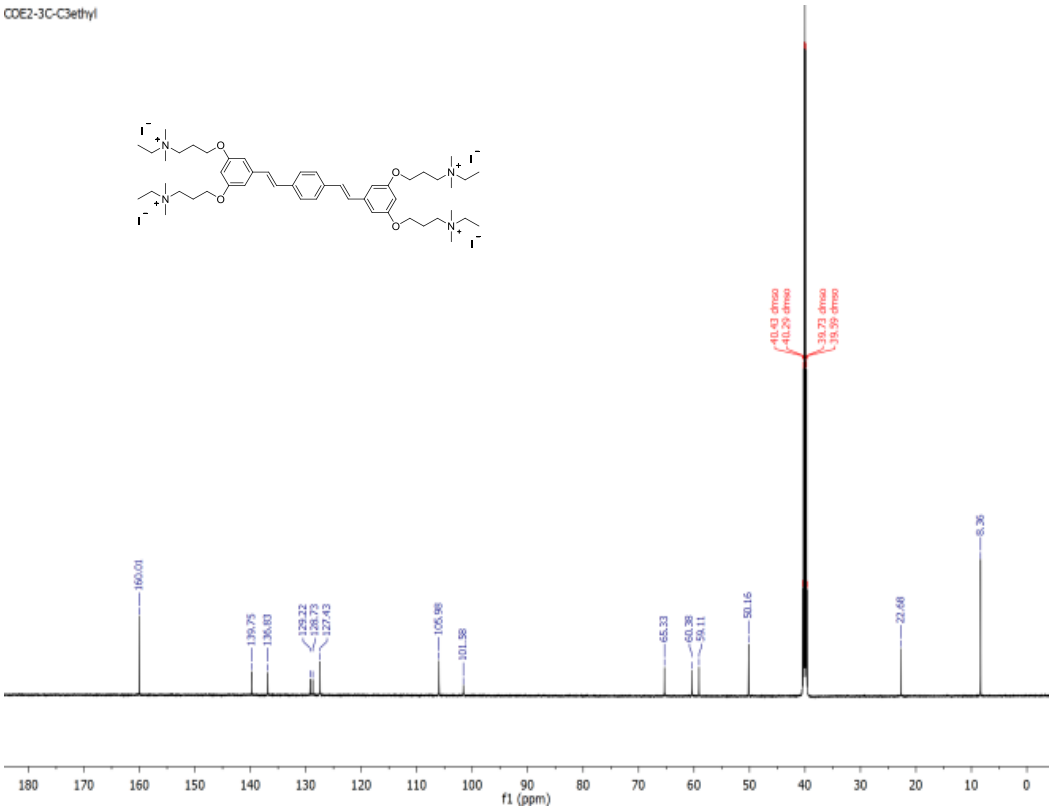
CDE2-3C-C3ethyl
160.01
139.75
136.83
129.22
128.73
127.43
105.98
101.58
65.53
60.38
59.11
50.16
40.43 dmso
40.29 dmso
39.73 dmso
39.59 dmso
22.68
8.36
f1 (ppm)

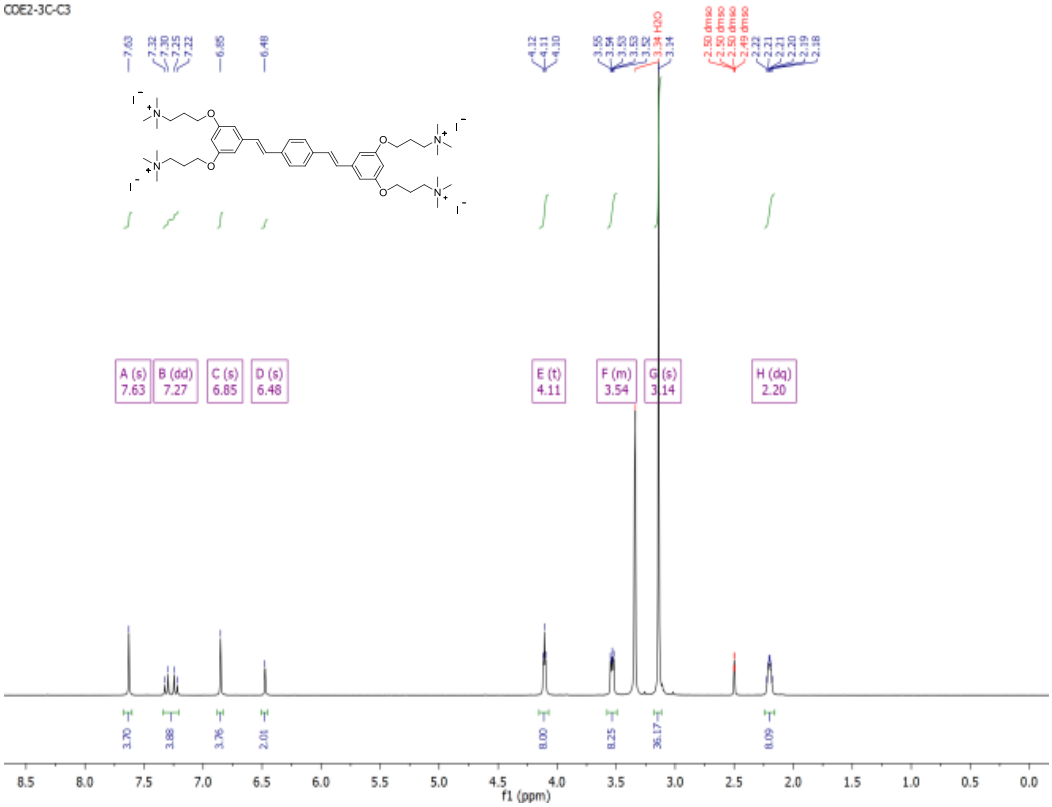
CDE2-3C-C3
A (s) 7.63
B (dd) 7.27
C (s) 6.85
D (s) 6.48
E (t) 4.11
F (m) 3.54
G (s) 3.14
H (dq) 2.20
f1 (ppm)

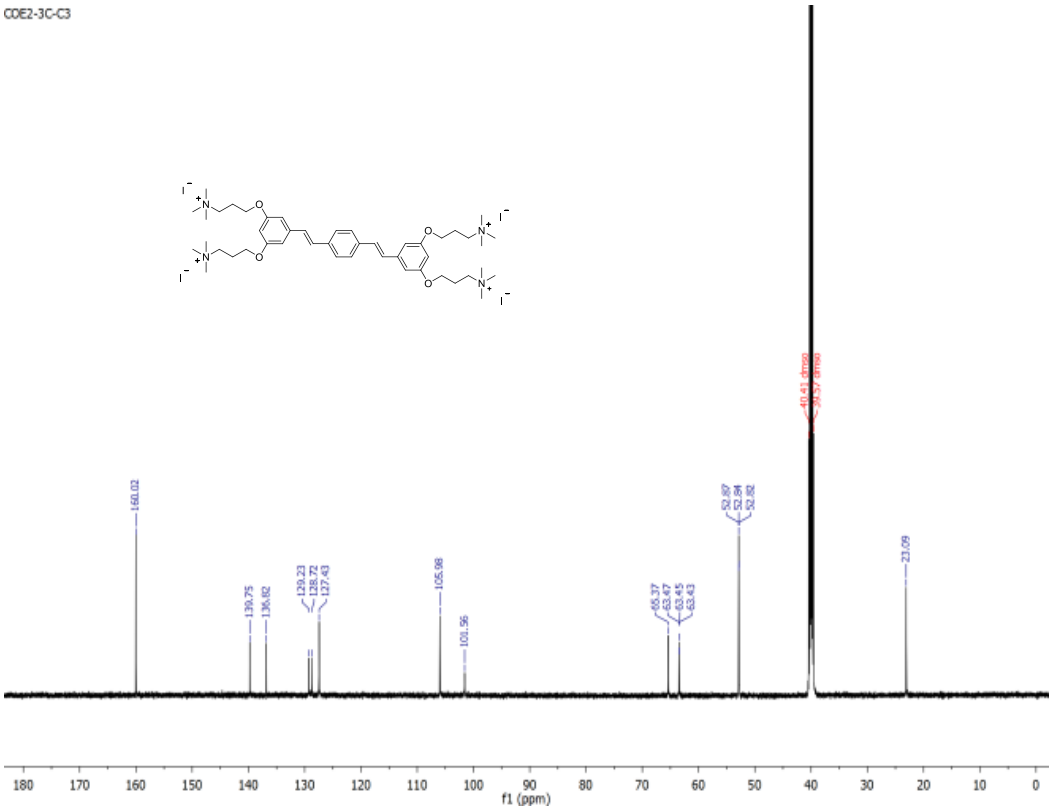
CDE2-3C-C3
f1 (ppm)

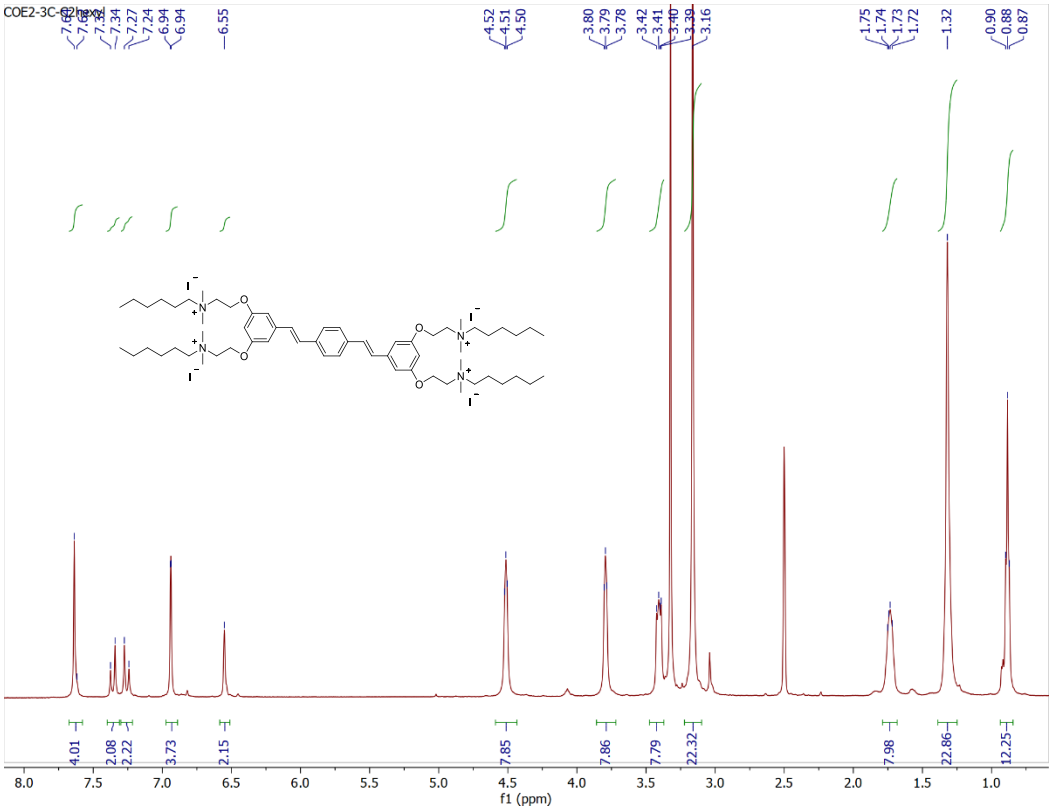
7.68
7.67
7.34
7.34
7.27
7.24
6.94
6.94
6.55
4.52
4.51
4.50
3.80
3.79
3.78
3.42
3.41
3.40
3.39
3.16
1.75
1.74
1.73
1.72
1.32
0.90
0.88
0.87
4.01
2.08
2.22
3.73
2.15
7.85
7.86
7.79
22.32
7.98
22.86
12.25
f1 (ppm)

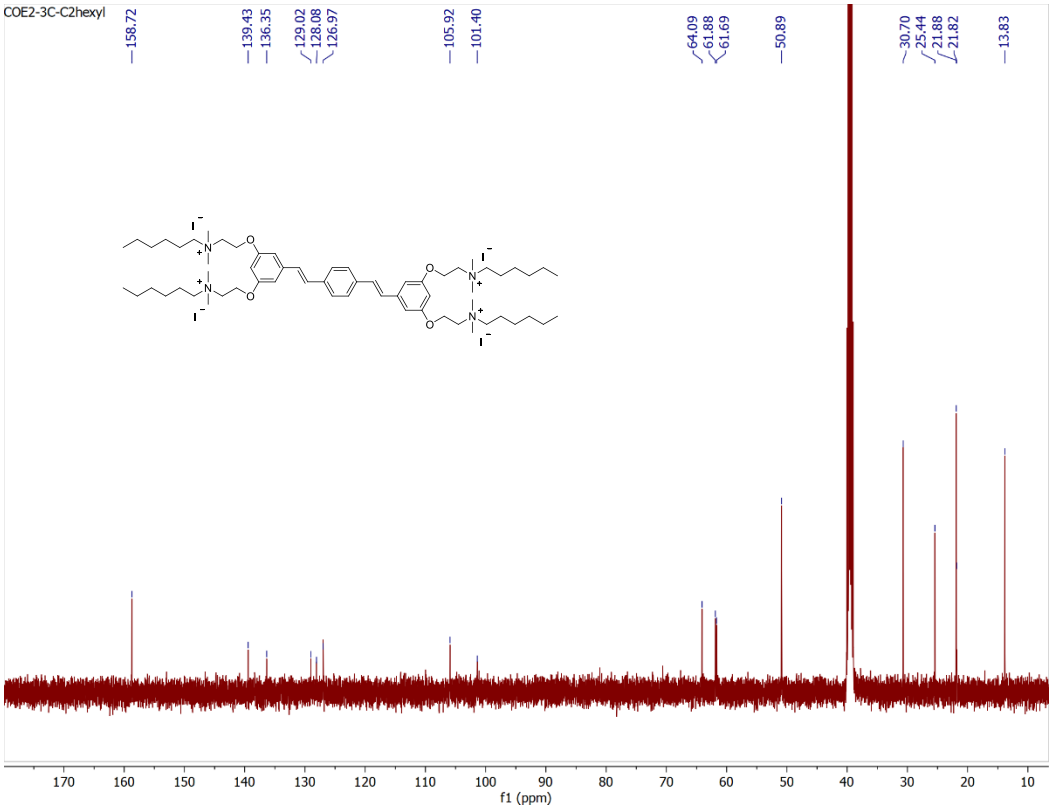
COE2-3C-C2hexyl
158.72
139.43
136.35
129.02
128.08
126.97
105.92
101.40
64.09
61.88
61.69
50.89
30.70
25.44
21.88
21.82
13.83
f1 (ppm)

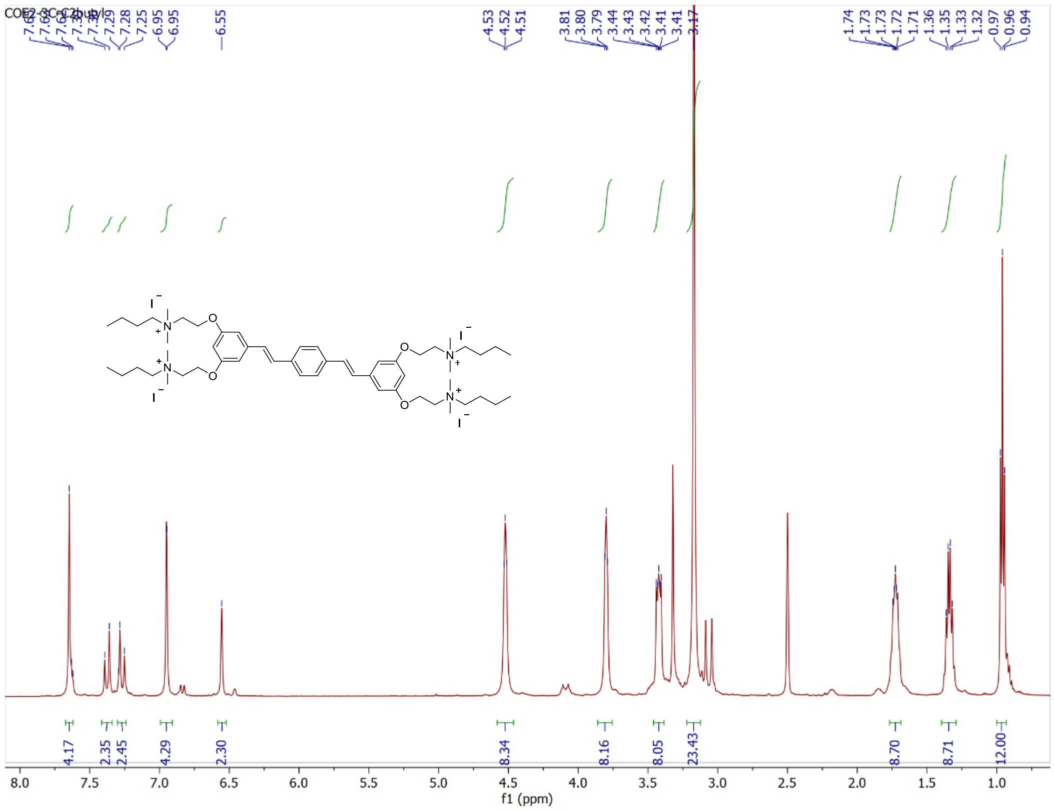

COE2-3C-C2butyl
7.62
7.60
7.38
7.29
7.28
7.25
6.95
6.95
6.55
4.53
4.52
4.51
3.81
3.80
3.79
3.44
3.43
3.42
3.41
3.41
3.17
1.74
1.73
1.73
1.72
1.71
1.36
1.35
1.33
1.32
0.97
0.96
0.94
4.17
2.35
2.45
4.29
2.30
8.34
8.16
8.05
23.43
8.70
8.71
12.00
f1 (ppm)

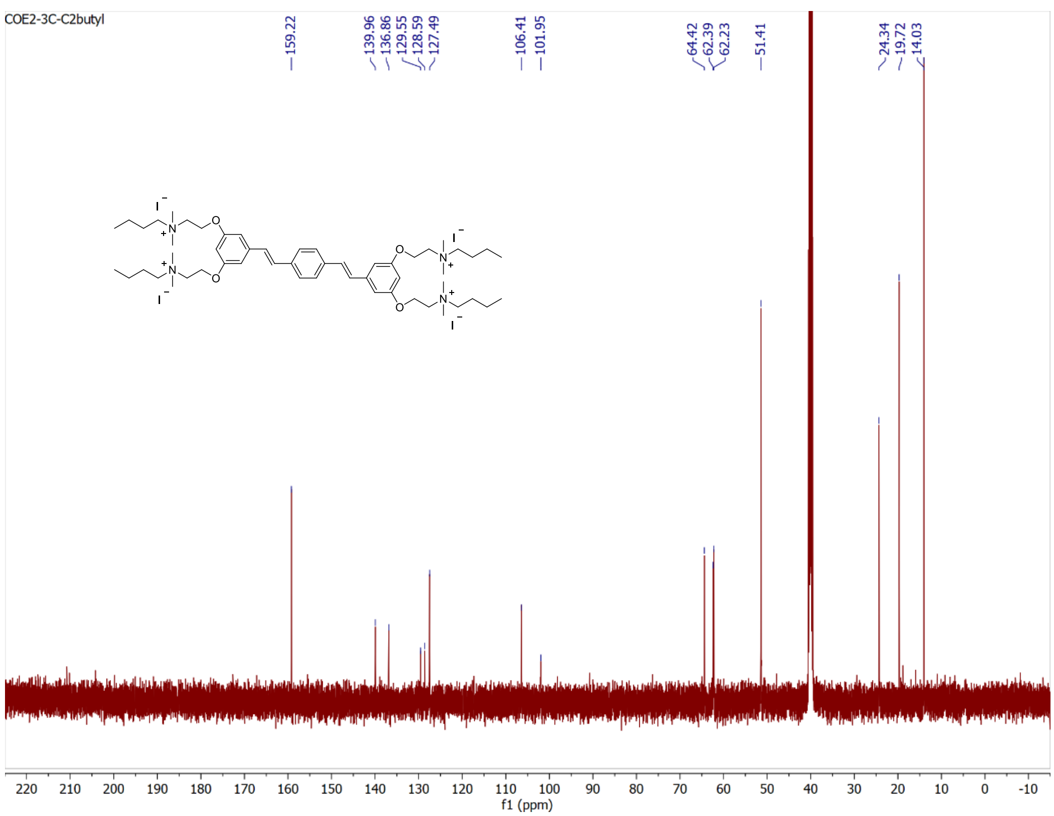

COE2-3C-C2butyl
159.22
139.96
136.86
129.55
128.59
127.49
106.41
101.95
64.42
62.39
62.23
51.41
24.34
19.72
14.03
f1 (ppm)

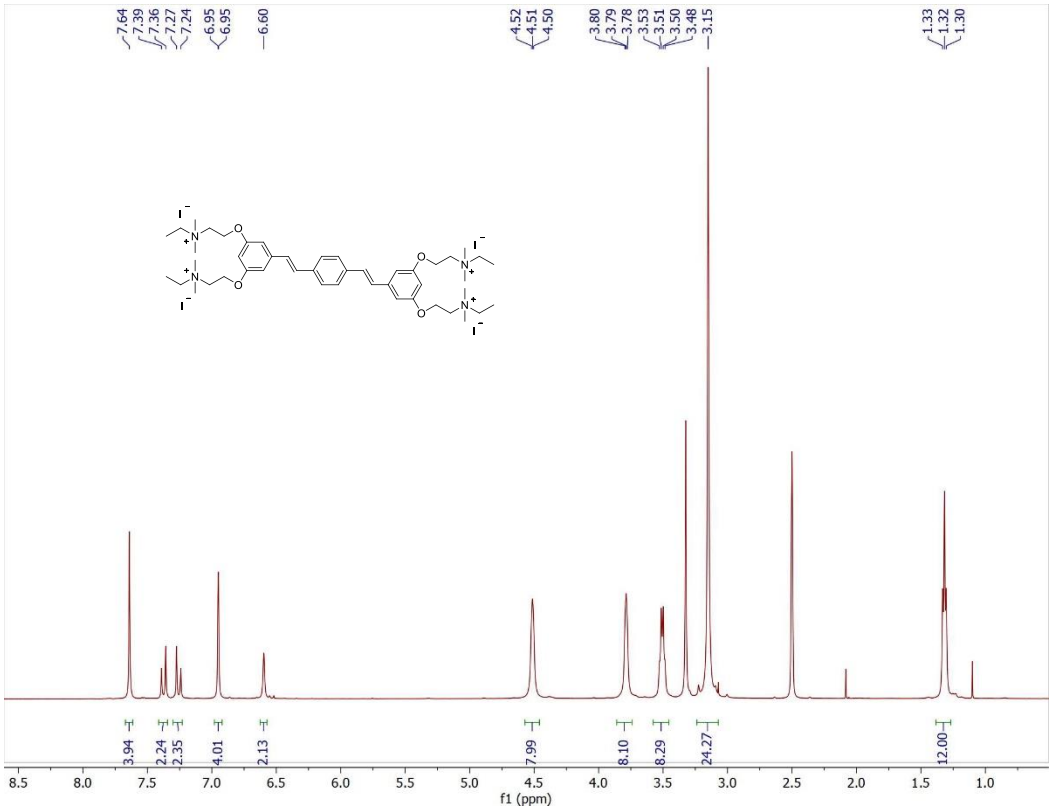
7.64
7.39
7.36
7.27
7.24
6.95
6.95
6.60
4.52
4.51
4.50
3.80
3.79
3.78
3.53
3.51
3.50
3.48
3.15
1.33
1.32
1.30
3.94
2.24
2.35
4.01
2.13
7.99
8.10
8.29
24.27
12.00
f1 (ppm)

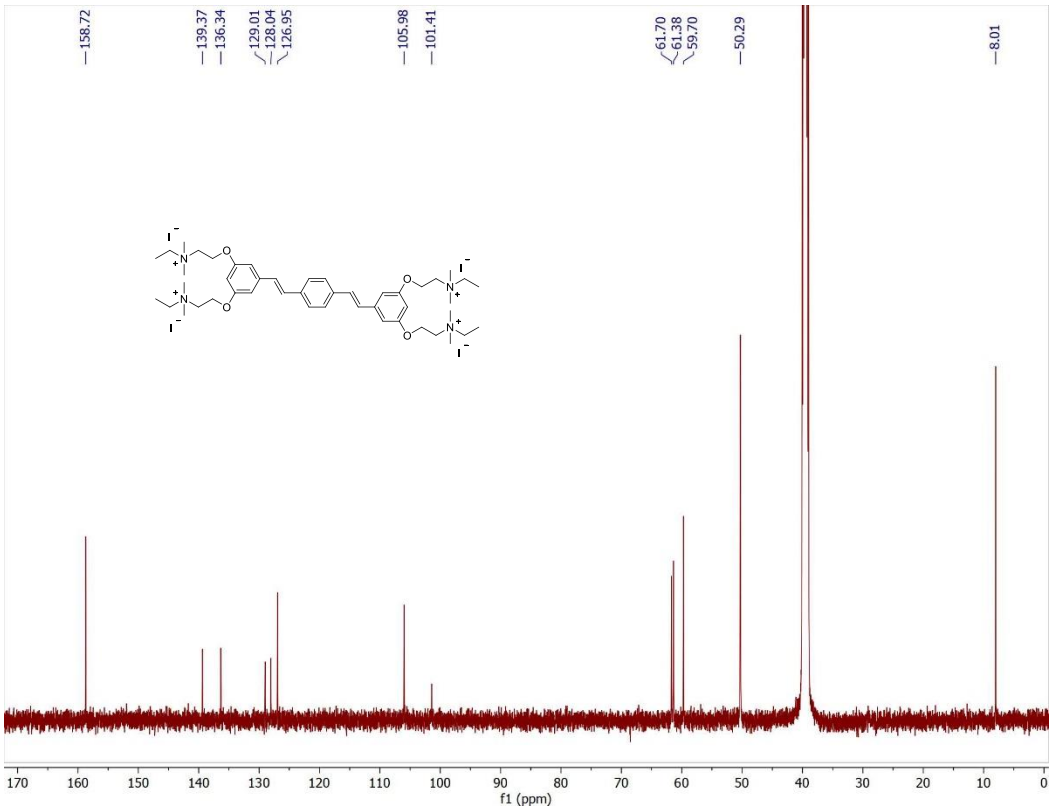
158.72
139.37
136.34
129.01
128.04
126.95
105.98
101.41
61.70
61.38
59.70
50.29
8.01
f1 (ppm)

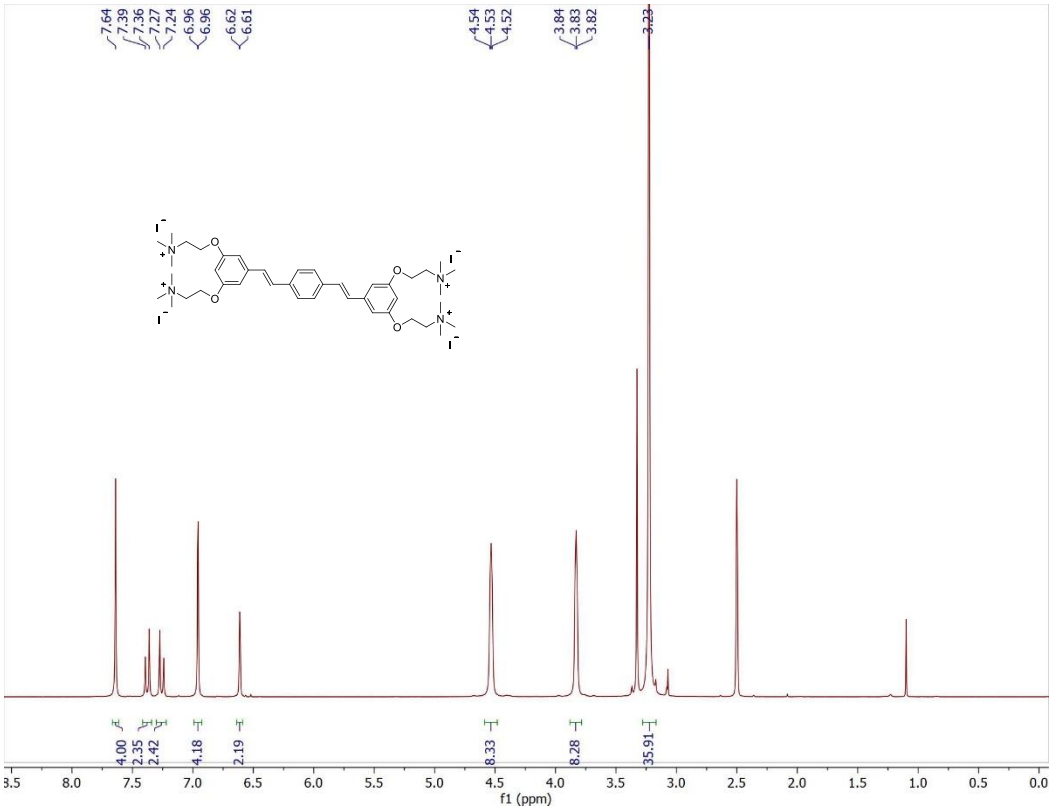
7.64
7.39
7.36
7.27
7.24
6.96
6.96
6.62
6.61
4.54
4.53
4.52
3.84
3.83
3.82
3.33
4.00
2.35
2.42
4.18
2.19
8.33
8.28
35.91
f1 (ppm)

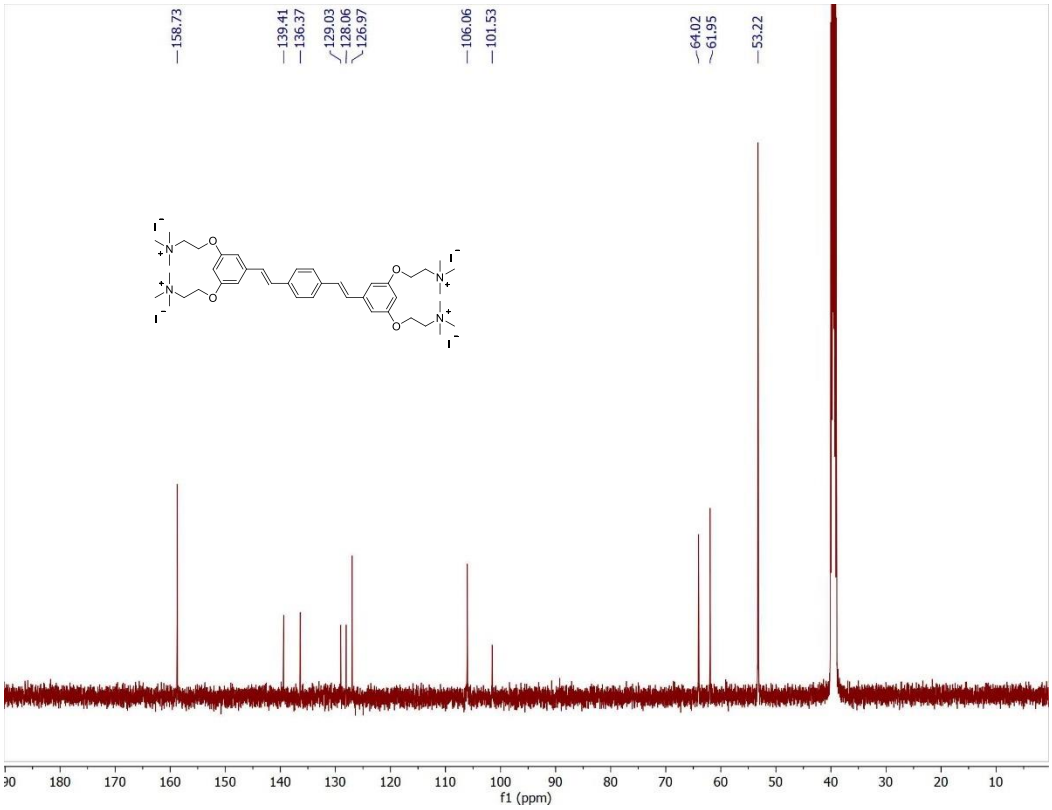
158.73
139.41
136.37
129.03
128.06
126.97
106.06
101.53
64.02
61.95
53.22
f1 (ppm)

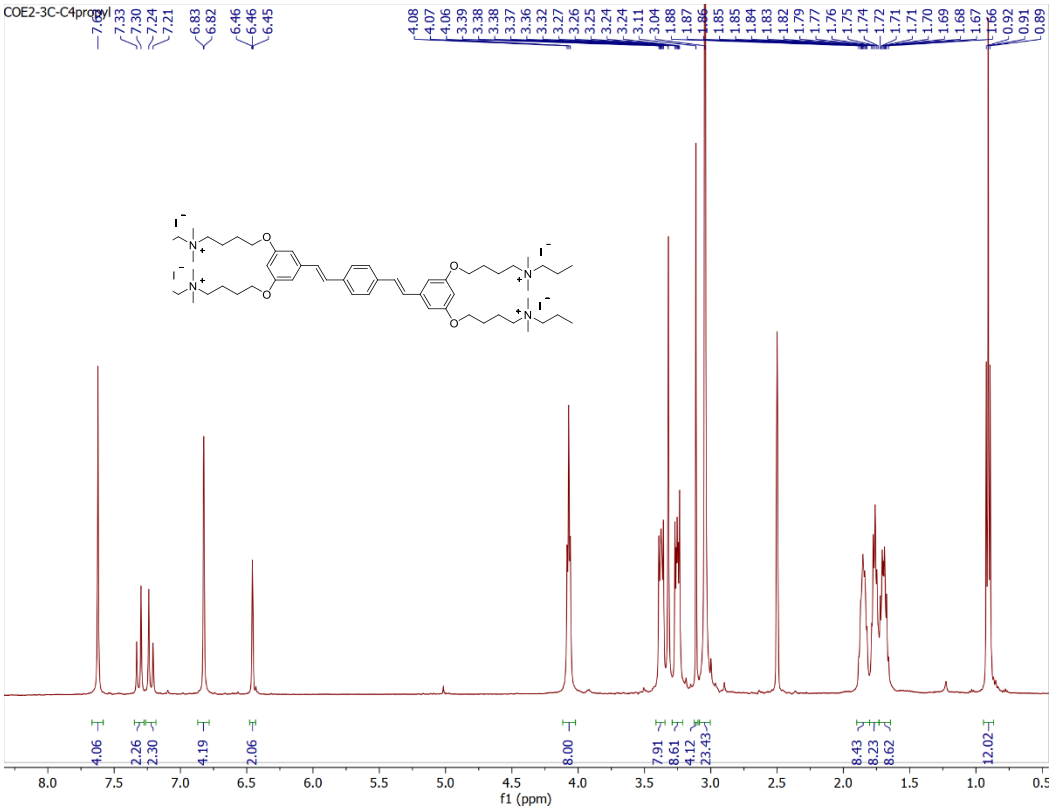
COE2-3C-C4propyl
f1 (ppm)

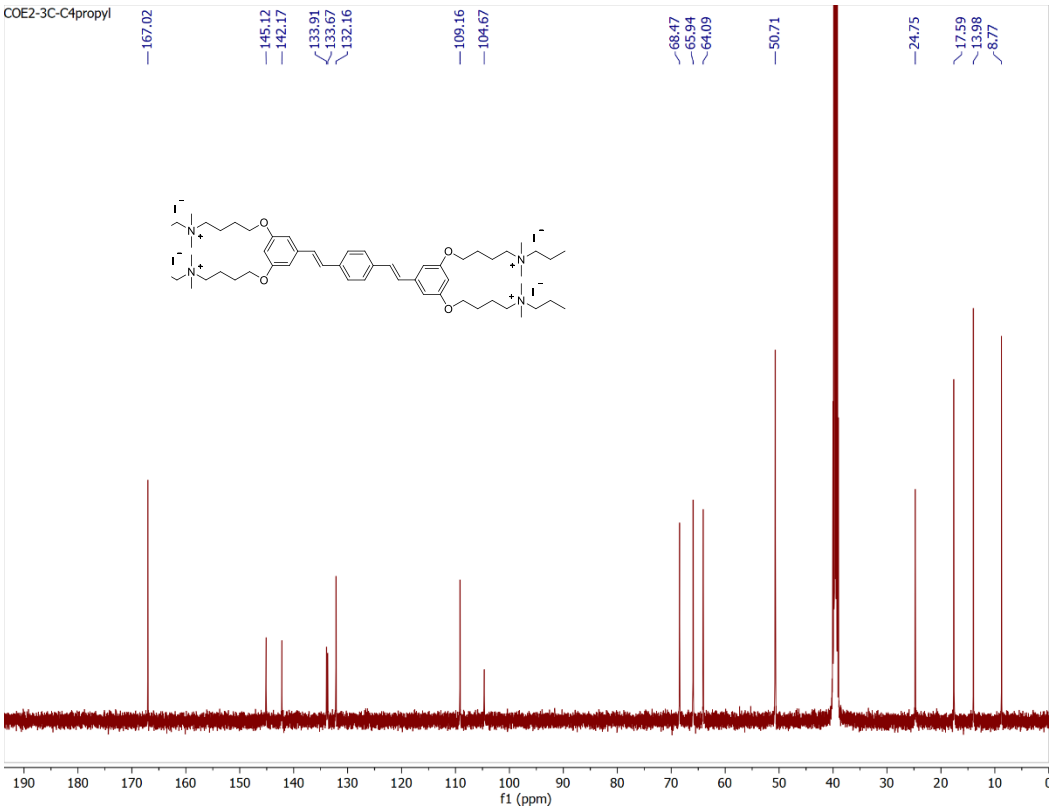
COE2-3C-C4propyl
f1 (ppm)

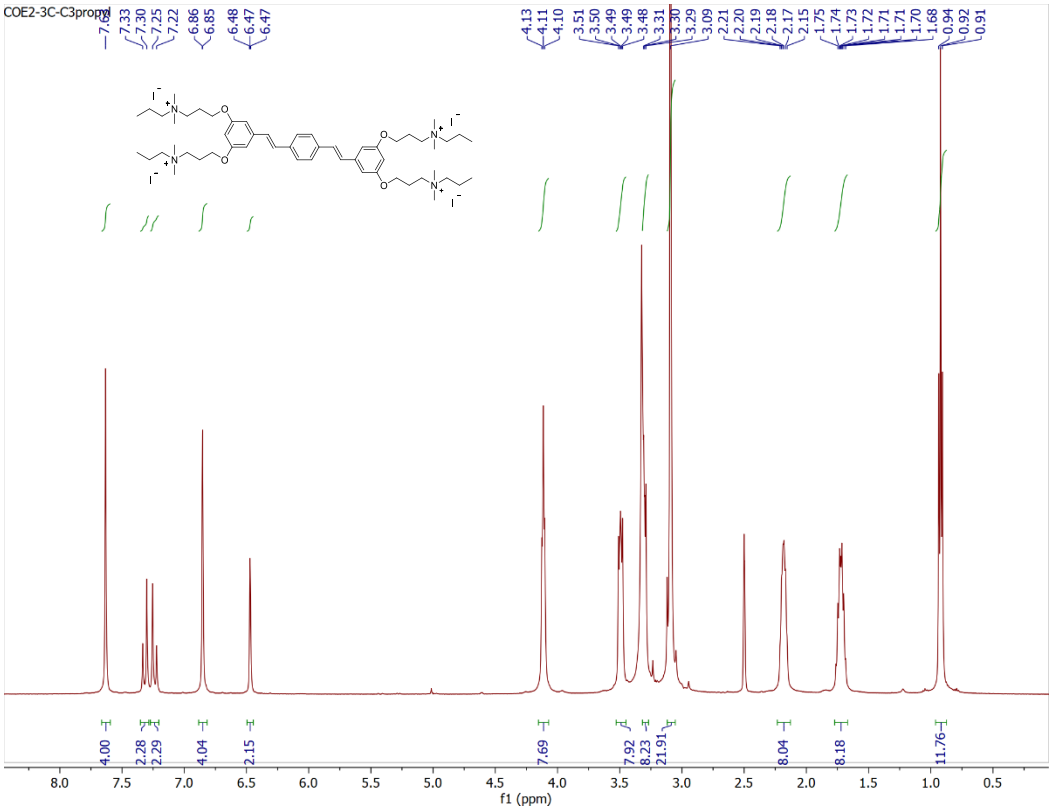
COE2-3C-C3propyl
7.33
7.30
7.25
7.22
6.86
6.85
6.48
6.47
6.47
4.13
4.11
4.10
3.51
3.50
3.49
3.49
3.48
3.31
3.30
3.29
3.09
2.21
2.20
2.19
2.18
2.17
2.15
1.75
1.74
1.73
1.72
1.71
1.71
1.70
1.68
0.94
0.92
0.91
4.00
2.28
2.29
4.04
2.15
7.69
7.92
8.23
21.91
8.04
8.18
11.76
f1 (ppm)

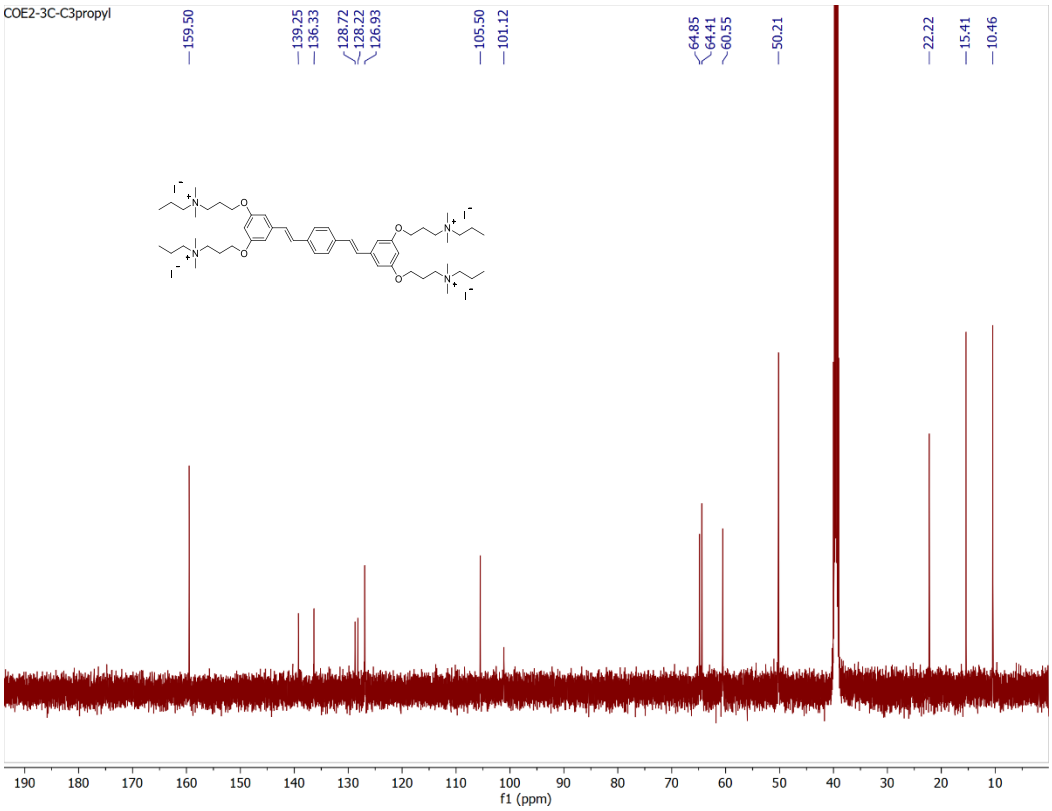
COE2-3C-C3propyl
159.50
139.25
136.33
128.72
128.22
126.93
105.50
101.12
64.85
64.41
60.55
50.21
22.22
15.41
10.46
f1 (ppm)

Chapter 4

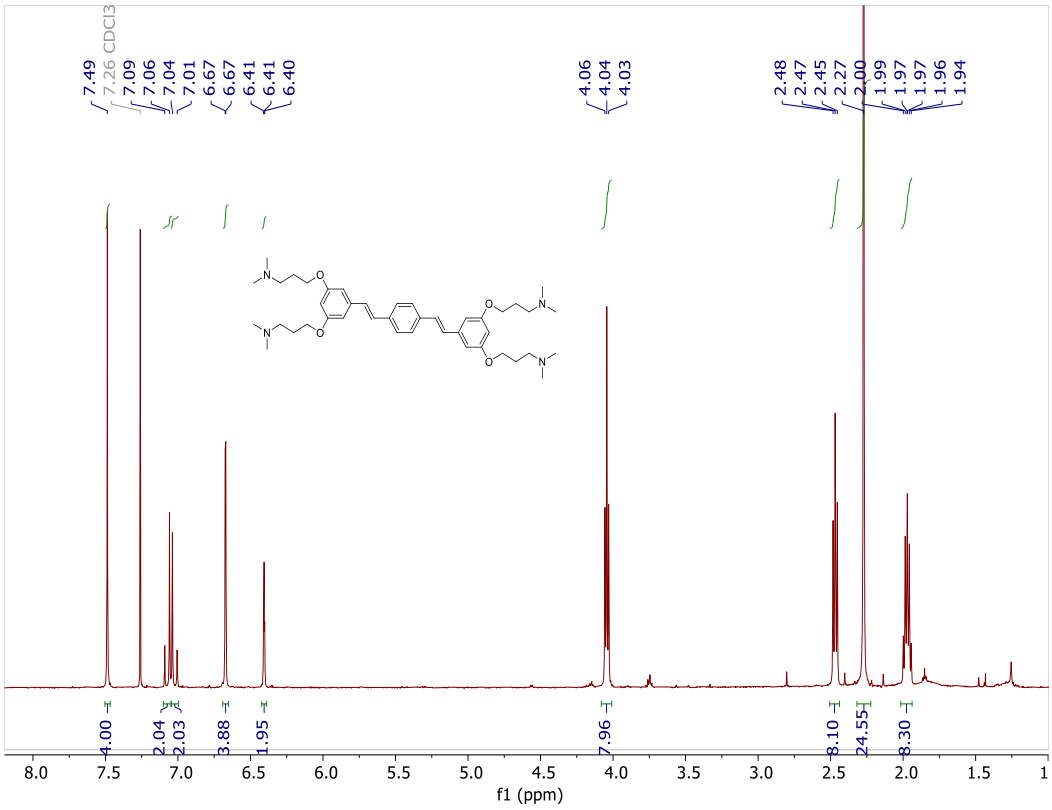
7.49
7.26 CDCl3
7.09
7.06
7.04
7.01
6.67
6.67
6.41
6.41
6.40
4.06
4.04
4.03
2.48
2.47
2.45
2.27
2.00
1.99
1.97
1.97
1.96
1.94
4.00
2.04
2.03
3.88
1.95
7.96
8.10
24.55
8.30
f1 (ppm)

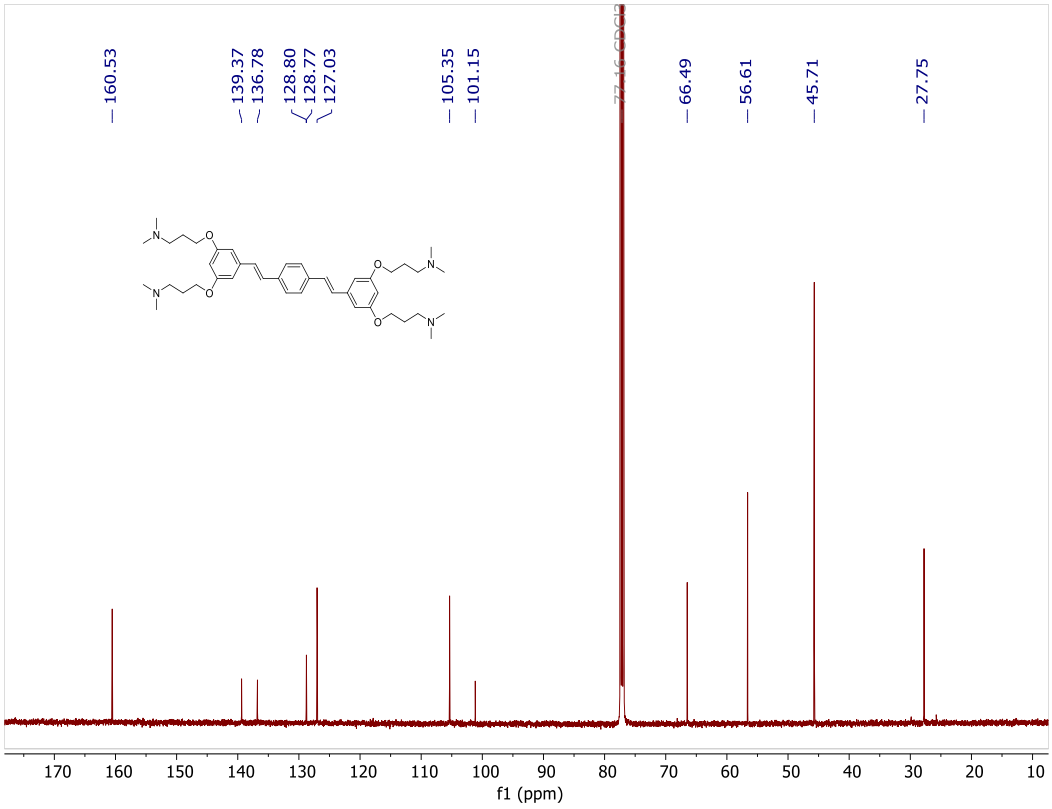
160.53
139.37
136.78
128.80
128.77
127.03
105.35
101.15
77.16 CDCl3
66.49
56.61
45.71
27.75
f1 (ppm)

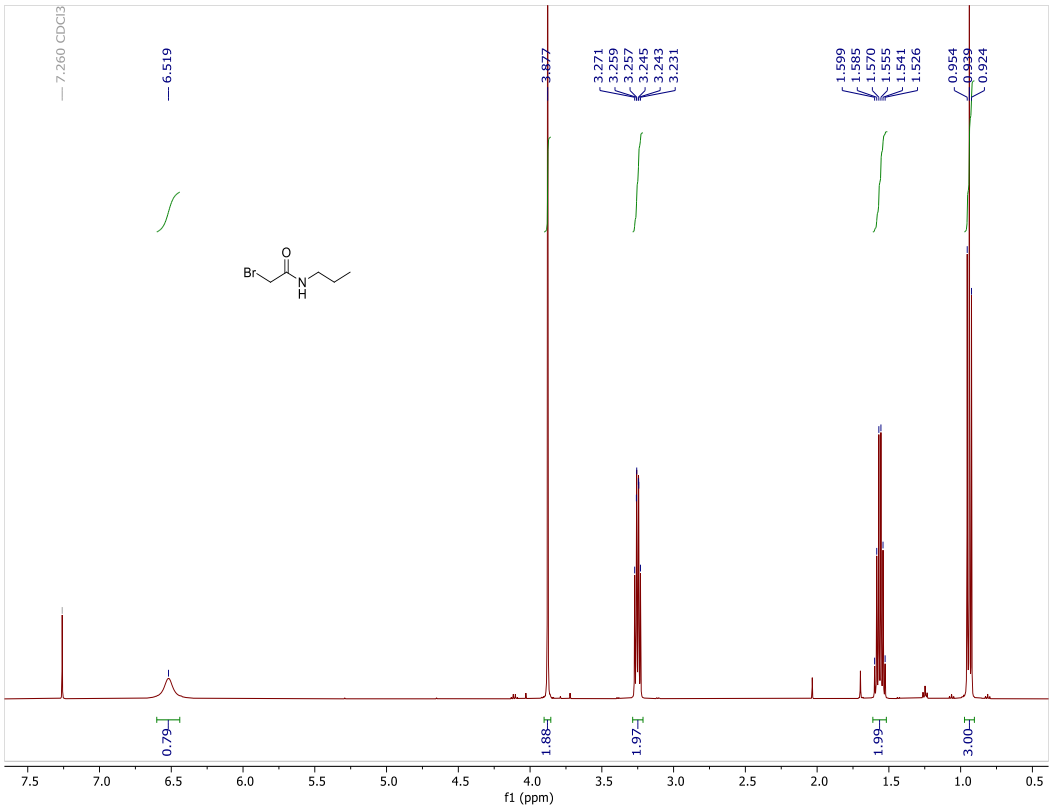
7.260 CDCl3
6.519
3.877
3.271
3.259
3.257
3.245
3.243
3.231
1.599
1.585
1.570
1.555
1.541
1.526
0.954
0.939
0.924
Br
O
N
H
0.79
1.88
1.97
1.99
3.00
f1 (ppm)

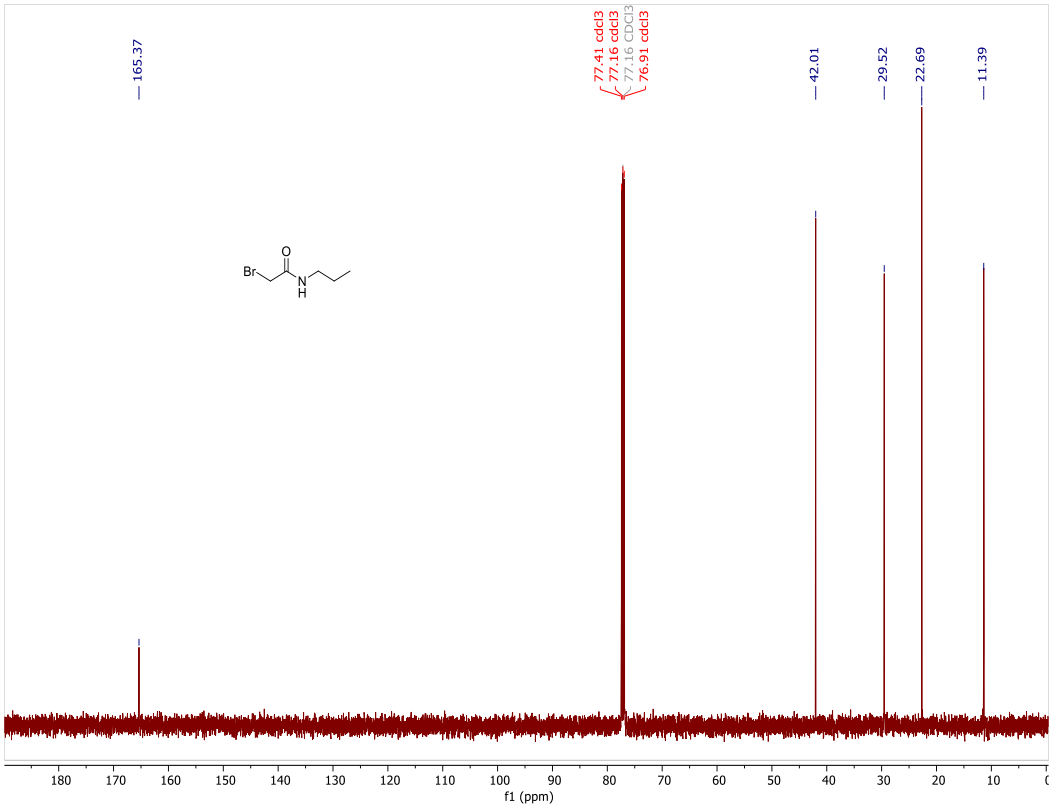
165.37
77.41 cdcl3
77.16 cdcl3
77.16 CDCl3
76.91 cdcl3
42.01
29.52
22.69
11.39
Br
O
N
H
f1 (ppm)

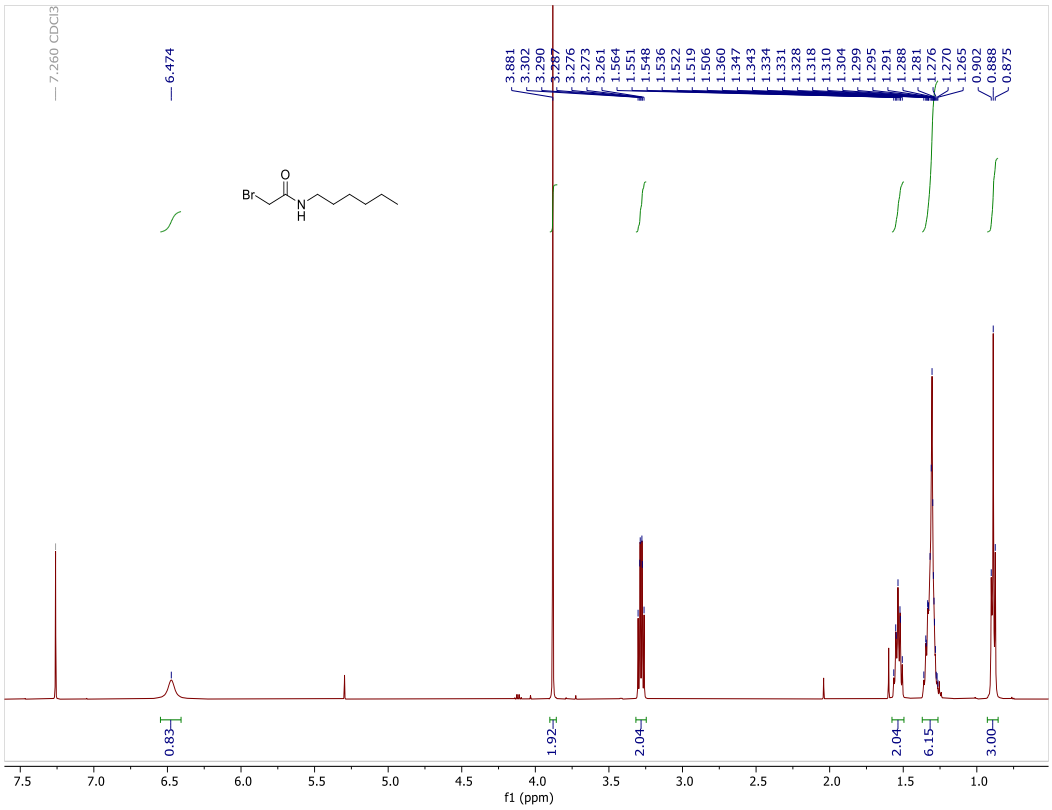
7.260 CDCl3
6.474
3.881
3.302
3.290
3.287
3.276
3.273
3.261
1.564
1.551
1.548
1.536
1.522
1.519
1.506
1.360
1.347
1.343
1.334
1.331
1.328
1.318
1.310
1.304
1.299
1.295
1.291
1.288
1.281
1.276
1.270
1.265
0.902
0.888
0.875
Br
O
N
H
0.83
1.92
2.04
2.04
6.15
3.00
7.5
7.0
6.5
6.0
5.5
5.0
4.5
4.0
3.5
3.0
2.5
2.0
1.5
1.0
f1 (ppm)

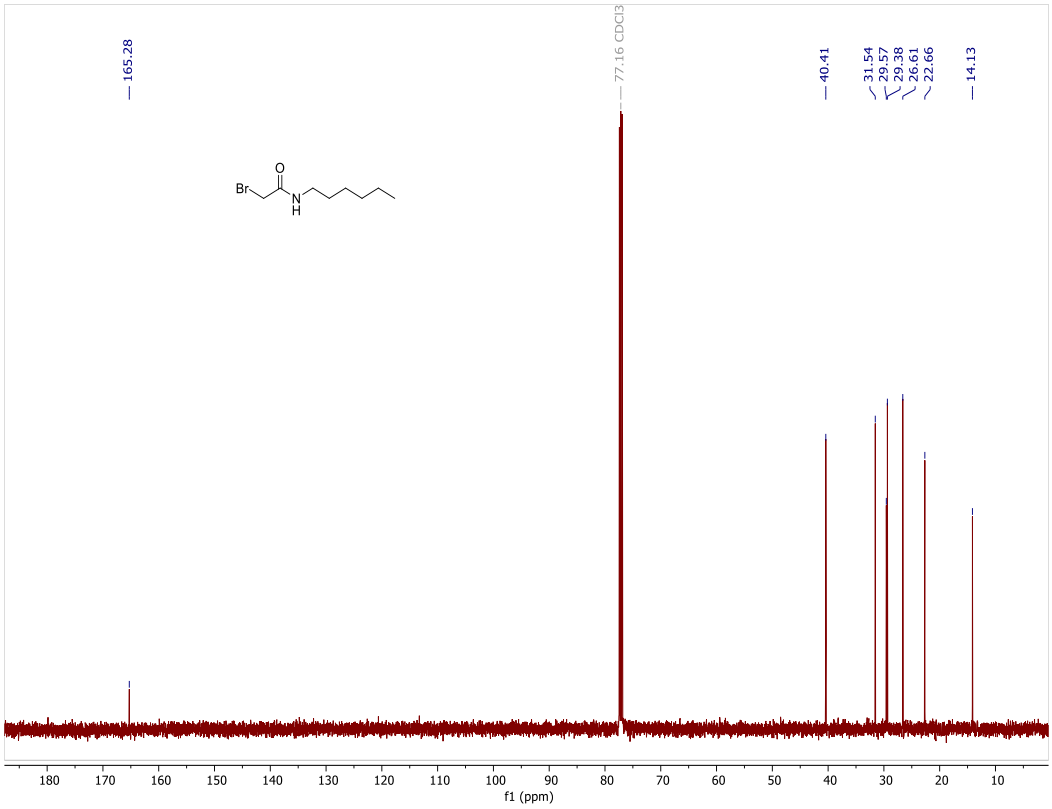
165.28
77.16 CDCl3
40.41
31.54
29.57
29.38
26.61
22.66
14.13
Br
O
N
H
180
170
160
150
140
130
120
110
100
90
80
70
60
50
40
30
20
10
f1 (ppm)

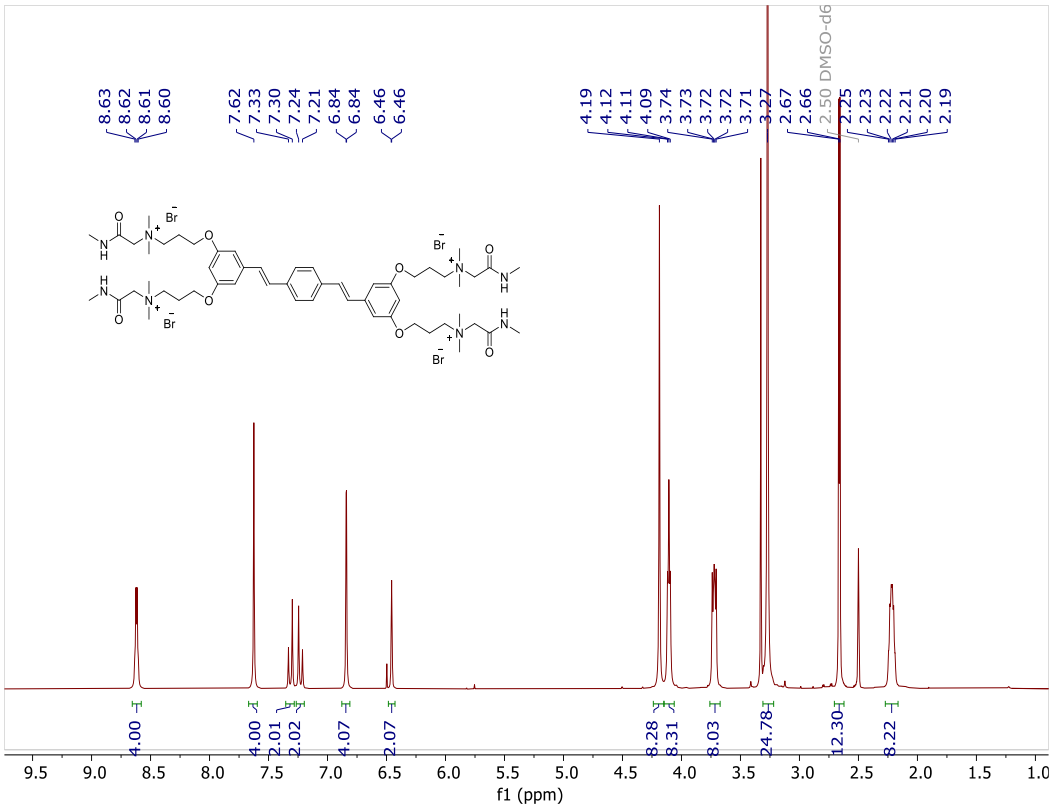
8.63
8.62
8.61
8.60
7.62
7.33
7.30
7.24
7.21
6.84
6.84
6.46
6.46
4.19
4.12
4.11
4.09
3.74
3.73
3.72
3.71
3.27
2.67
2.66
2.50 DMSO-d6
2.25
2.23
2.22
2.21
2.20
2.19
4.00
4.00
2.01
2.02
4.07
2.07
8.28
8.31
8.03
24.78
12.30
8.22
f1 (ppm)

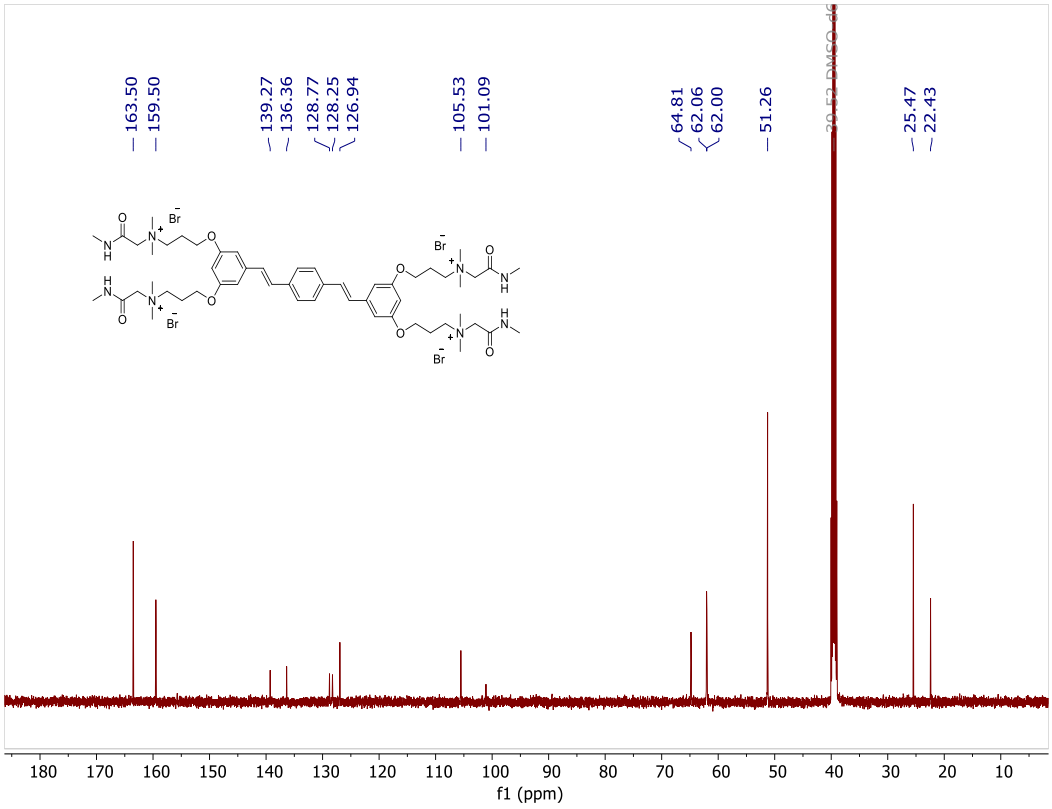
163.50
159.50
139.27
136.36
128.77
128.25
126.94
105.53
101.09
64.81
62.06
62.00
51.26
39.52 DMSO-d6
25.47
22.43
f1 (ppm)

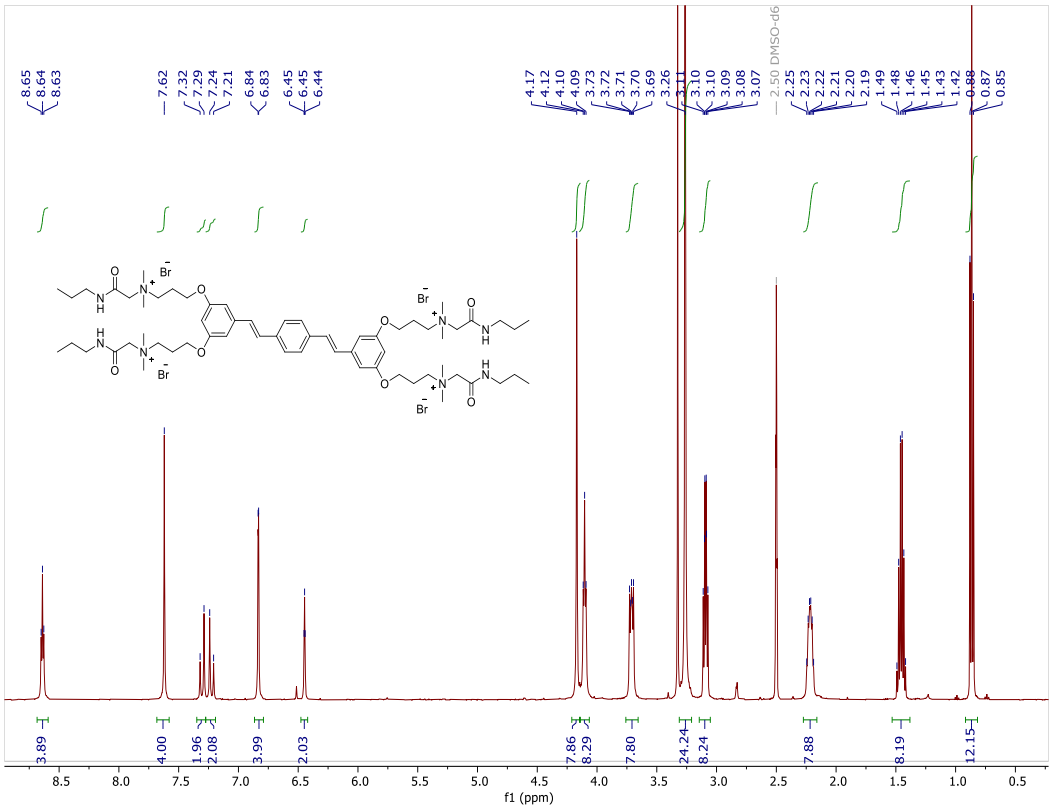
8.65
8.64
8.63
7.62
7.32
7.29
7.24
7.21
6.84
6.83
6.45
6.45
6.44
4.17
4.12
4.10
4.09
3.73
3.72
3.71
3.70
3.69
3.26
3.11
3.10
3.10
3.09
3.08
3.07
2.50 DMSO-d6
2.25
2.23
2.22
2.21
2.20
2.19
1.49
1.48
1.46
1.45
1.43
1.42
0.88
0.87
0.85
3.89
4.00
1.96
2.08
3.99
2.03
7.86
8.29
7.80
24.24
8.24
7.88
8.19
12.15
f1 (ppm)

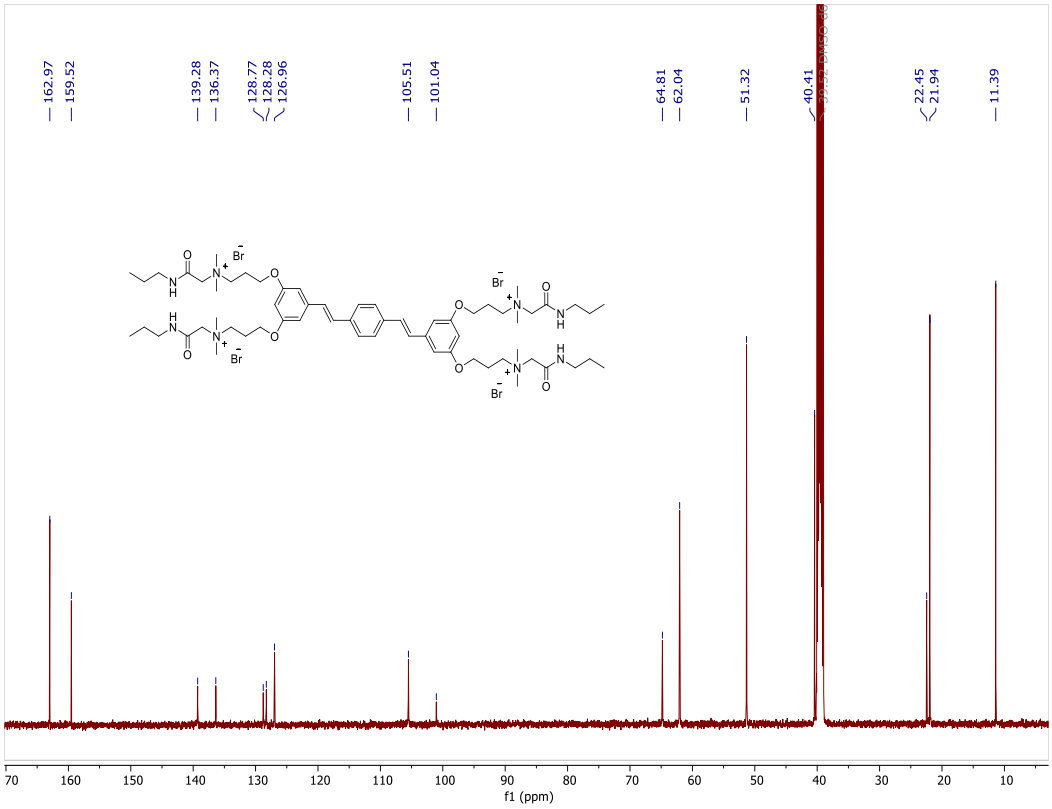
162.97
159.52
139.28
136.37
128.77
128.28
126.96
105.51
101.04
64.81
62.04
51.32
40.41
22.45
21.94
11.39
f1 (ppm)

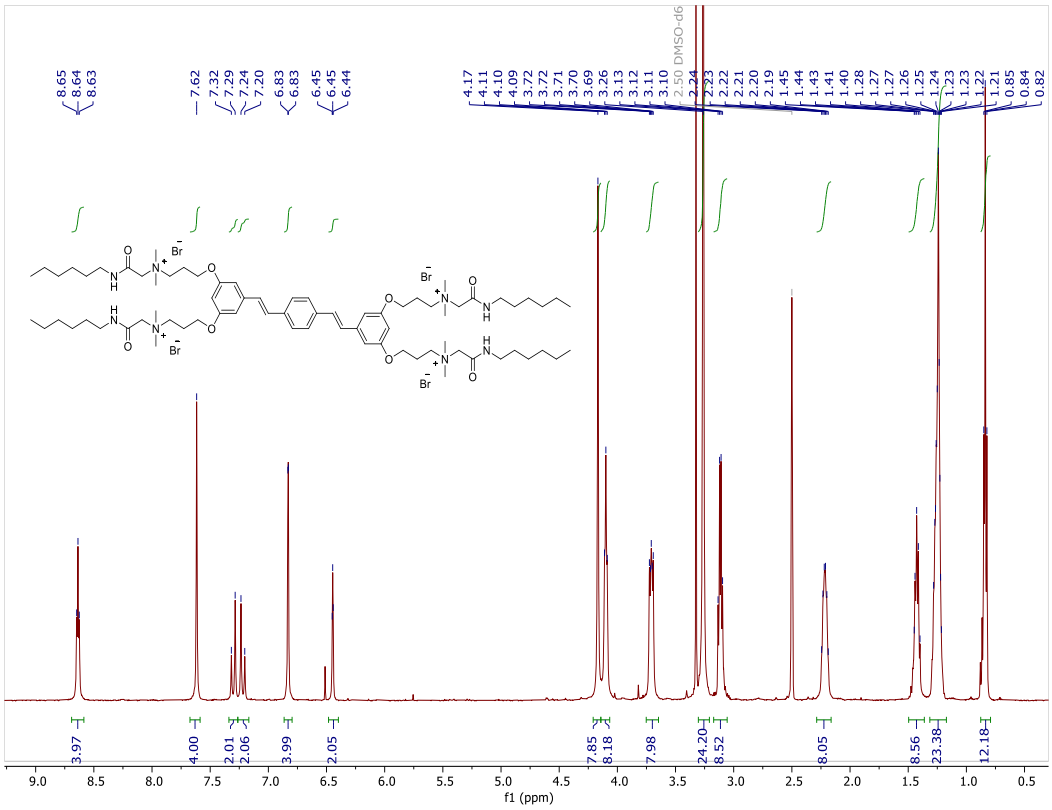
8.65
8.64
8.63
7.62
7.32
7.29
7.24
7.20
6.83
6.83
6.45
6.45
6.44
4.17
4.11
4.10
4.09
3.72
3.72
3.71
3.70
3.69
3.26
3.13
3.12
3.11
3.10
2.50 DMSO-d6
2.24
2.23
2.22
2.21
2.20
2.19
1.45
1.44
1.43
1.41
1.40
1.28
1.27
1.27
1.26
1.25
1.24
1.23
1.23
1.22
1.21
0.85
0.84
0.82
3.97
4.00
2.01
2.06
3.99
2.05
7.85
8.18
7.98
24.20
8.52
8.05
8.56
23.38
12.18
f1 (ppm)

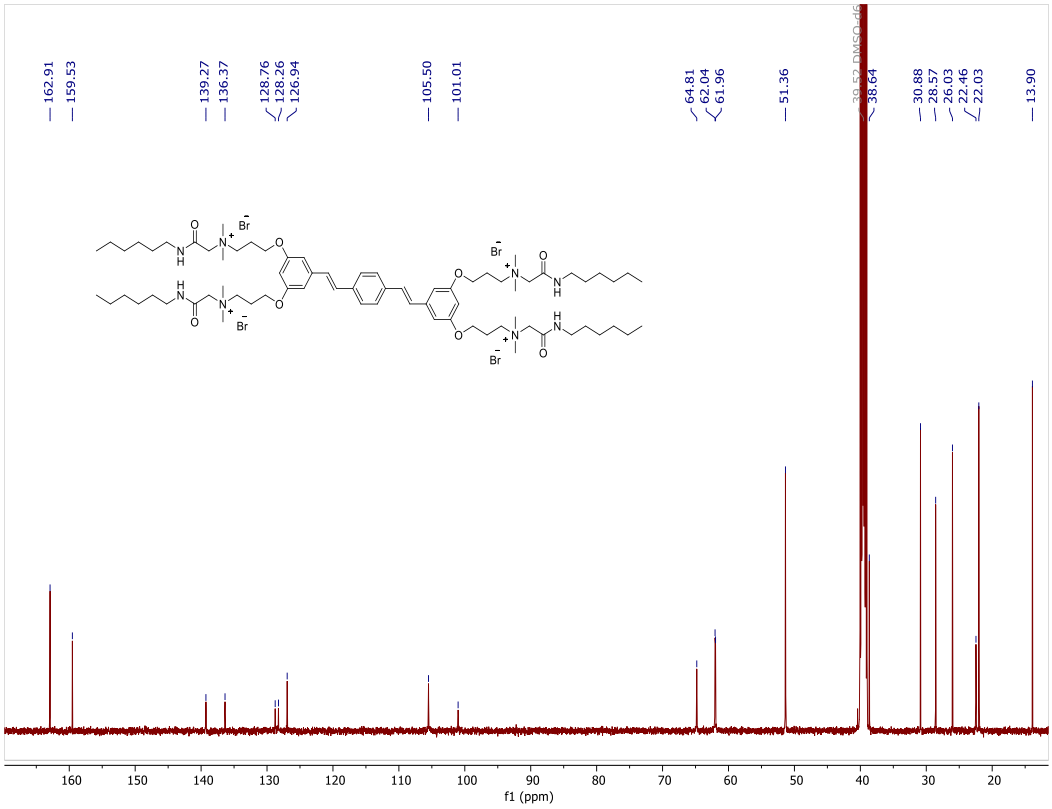
162.91
159.53
139.27
136.37
128.76
128.26
126.94
105.50
101.01
64.81
62.04
61.96
51.36
39.52 DMSO-d6
38.64
30.88
28.57
26.03
22.46
22.03
13.90
f1 (ppm)

Chapter 5

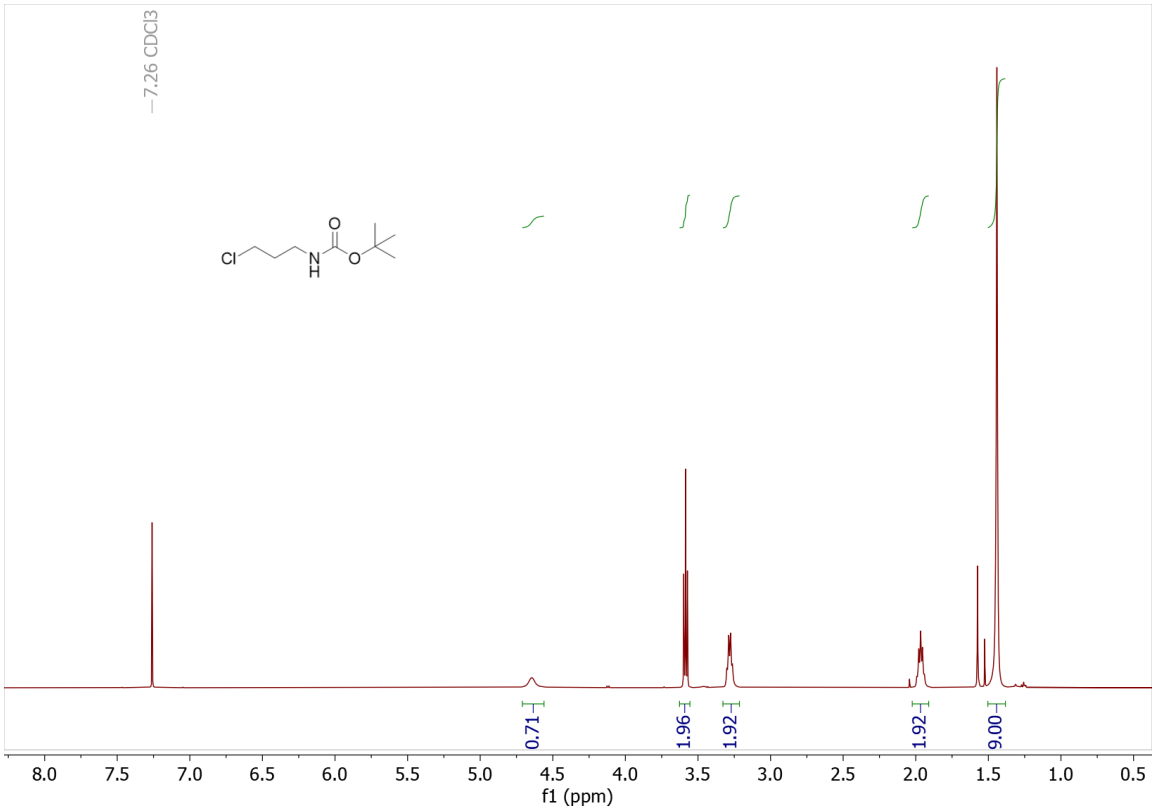
7.26 CDCl3
Cl
N
H
O
O
0.71
1.96
1.92
1.92
9.00
8.0 7.5 7.0 6.5 6.0 5.5 5.0 4.5 4.0 3.5 3.0 2.5 2.0 1.5 1.0 0.5
f1 (ppm)

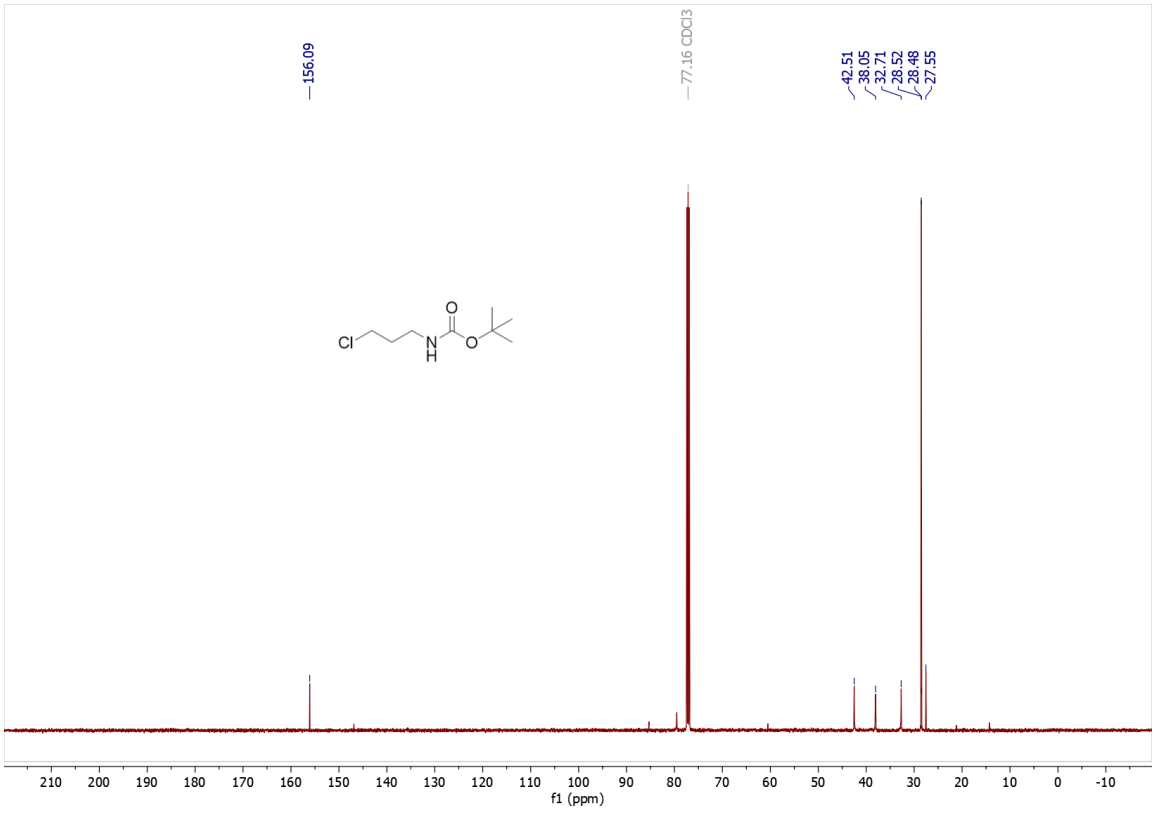
156.09
77.16 CDCl3
42.51
38.05
32.71
28.52
28.48
27.55
Cl
N
H
O
O
210 200 190 180 170 160 150 140 130 120 110 100 90 80 70 60 50 40 30 20 10 0 -10
f1 (ppm)

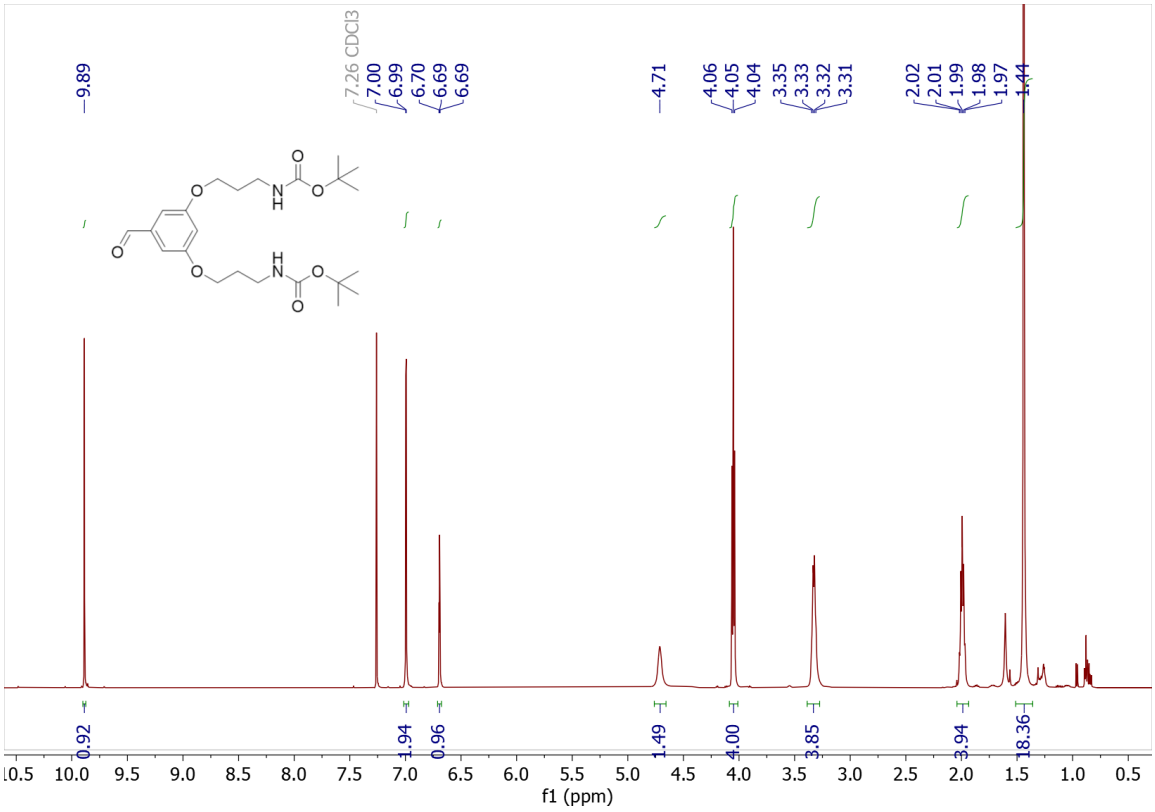
9.89
7.26 CDCl3
7.00
6.99
6.70
6.69
6.69
4.71
4.06
4.05
4.04
3.35
3.33
3.32
3.31
2.02
2.01
1.99
1.98
1.97
1.44
0.92
1.94
0.96
1.49
4.00
3.85
3.94
18.36
f1 (ppm)

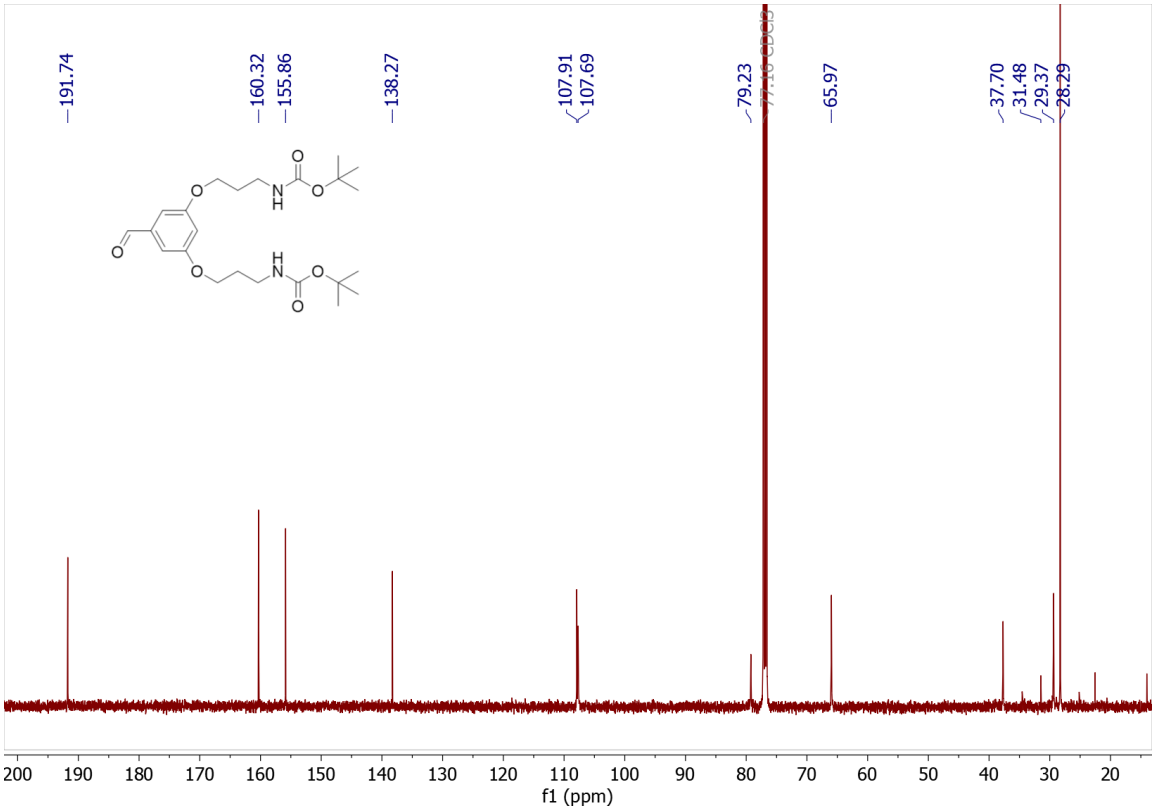
191.74
160.32
155.86
138.27
107.91
107.69
79.23
77.16 CDCl3
65.97
37.70
31.48
29.37
28.29
f1 (ppm)

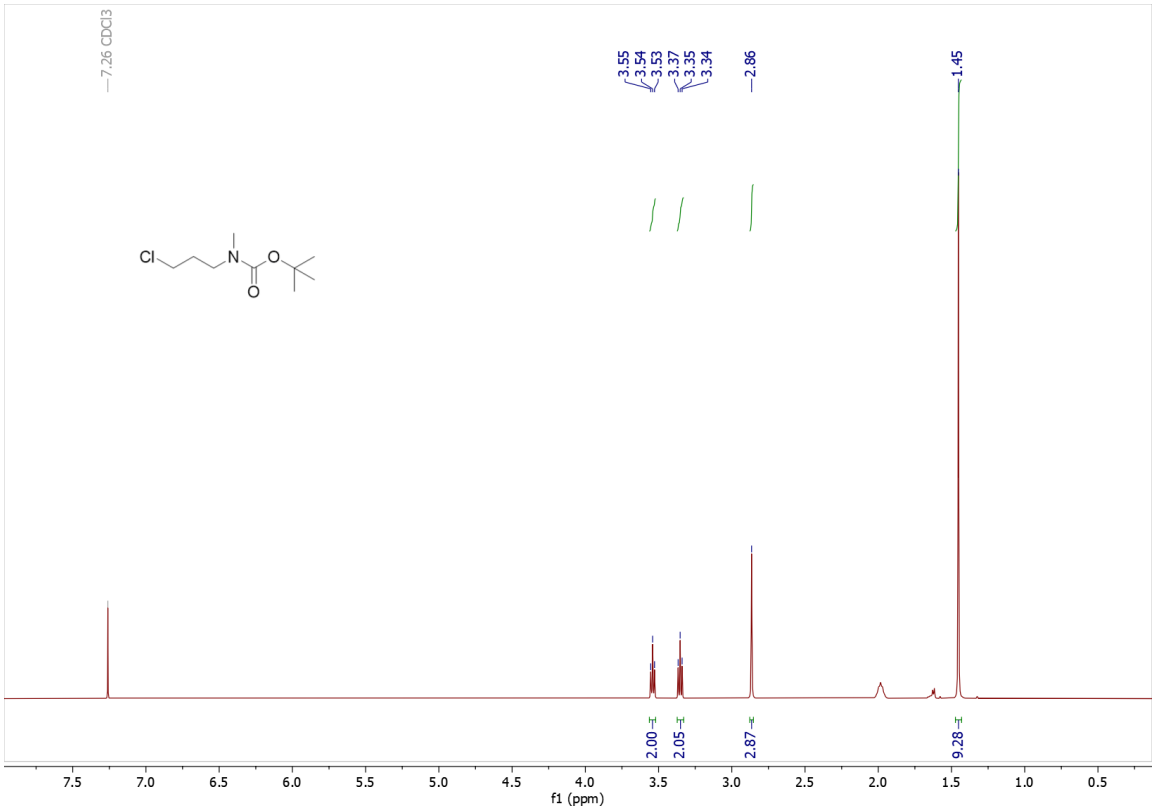
7.26 CDCl3
3.55
3.54
3.53
3.37
3.35
3.34
2.86
1.45
Cl
N
O
O
2.00
2.05
2.87
9.28
7.5
7.0
6.5
6.0
5.5
5.0
4.5
4.0
3.5
3.0
2.5
2.0
1.5
1.0
0.5
f1 (ppm)

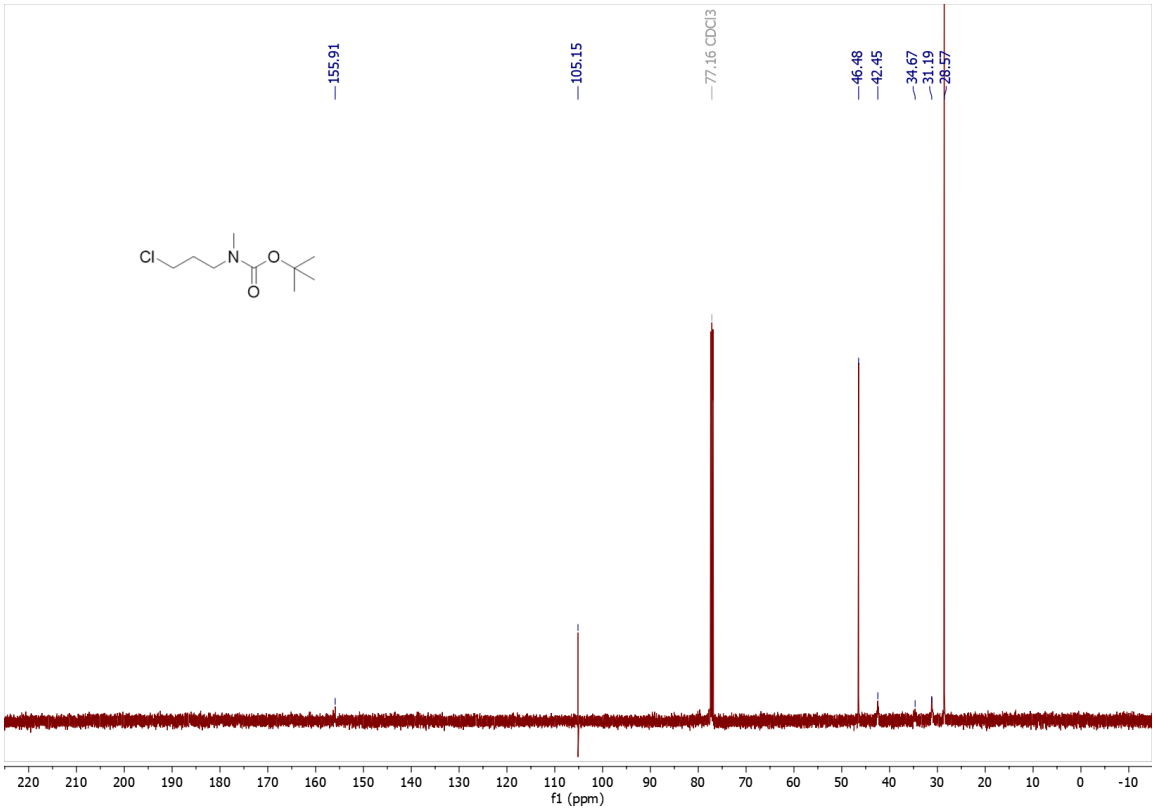
155.91
105.15
77.16 CDCl3
46.48
42.45
34.67
31.19
28.57
Cl
N
O
O
220
210
200
190
180
170
160
150
140
130
120
110
100
90
80
70
60
50
40
30
20
10
0
-10
f1 (ppm)

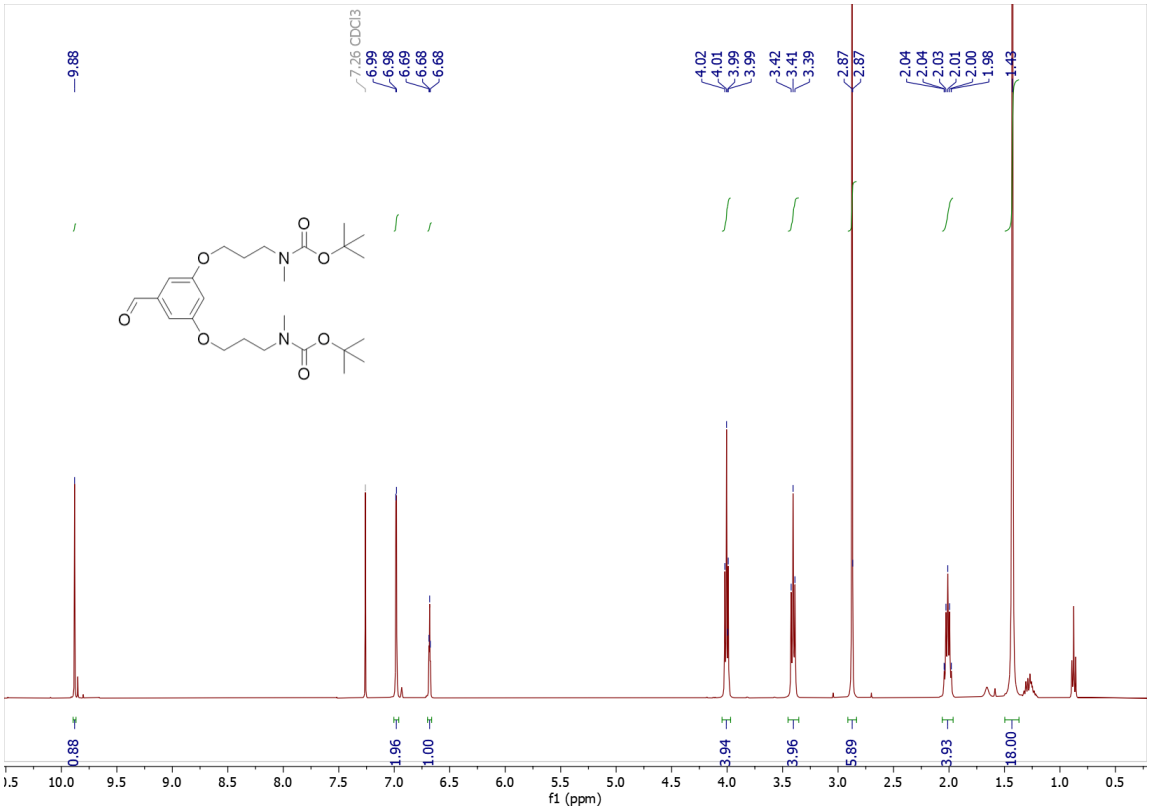
9.88
7.26 CDCl3
6.99
6.98
6.69
6.68
6.68
4.02
4.01
3.99
3.99
3.42
3.41
3.39
2.87
2.87
2.04
2.04
2.03
2.01
2.00
1.98
1.43
0.88
1.96
1.00
3.94
3.96
5.89
3.93
18.00
f1 (ppm)

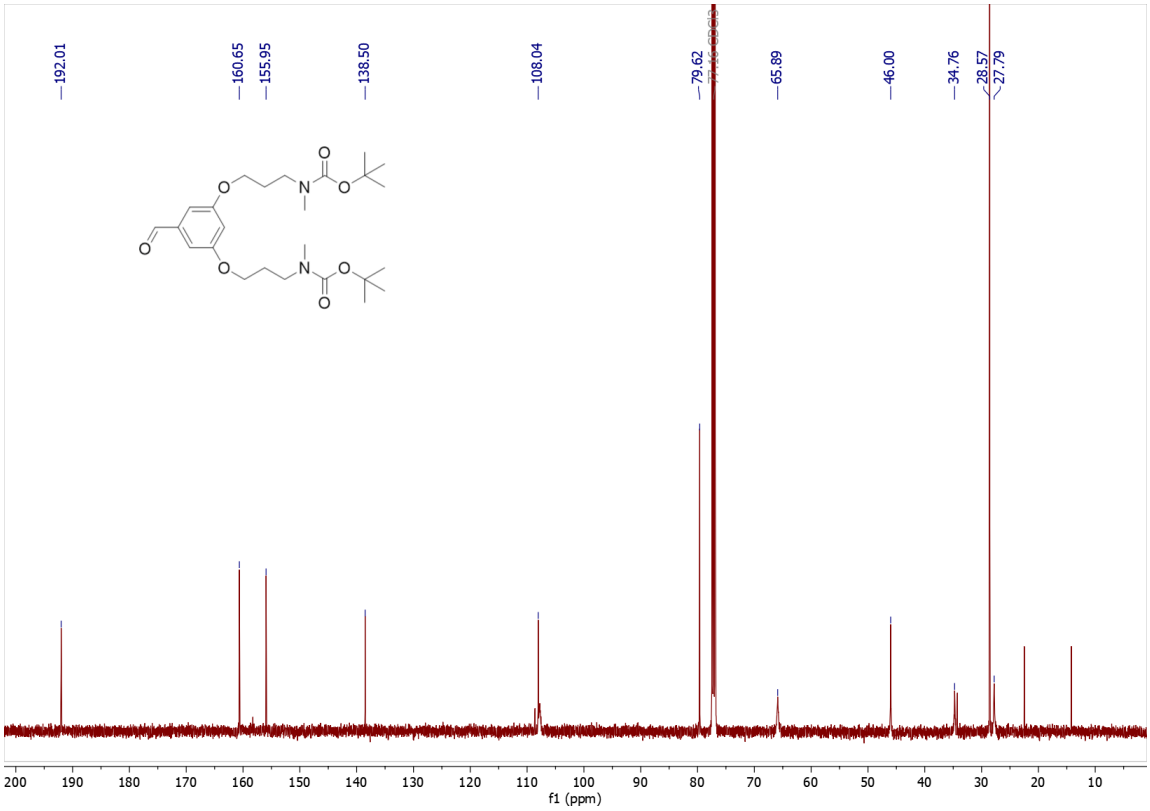
192.01
160.65
155.95
138.50
108.04
79.62
77.16 CDCl3
65.89
46.00
34.76
28.57
27.79
f1 (ppm)

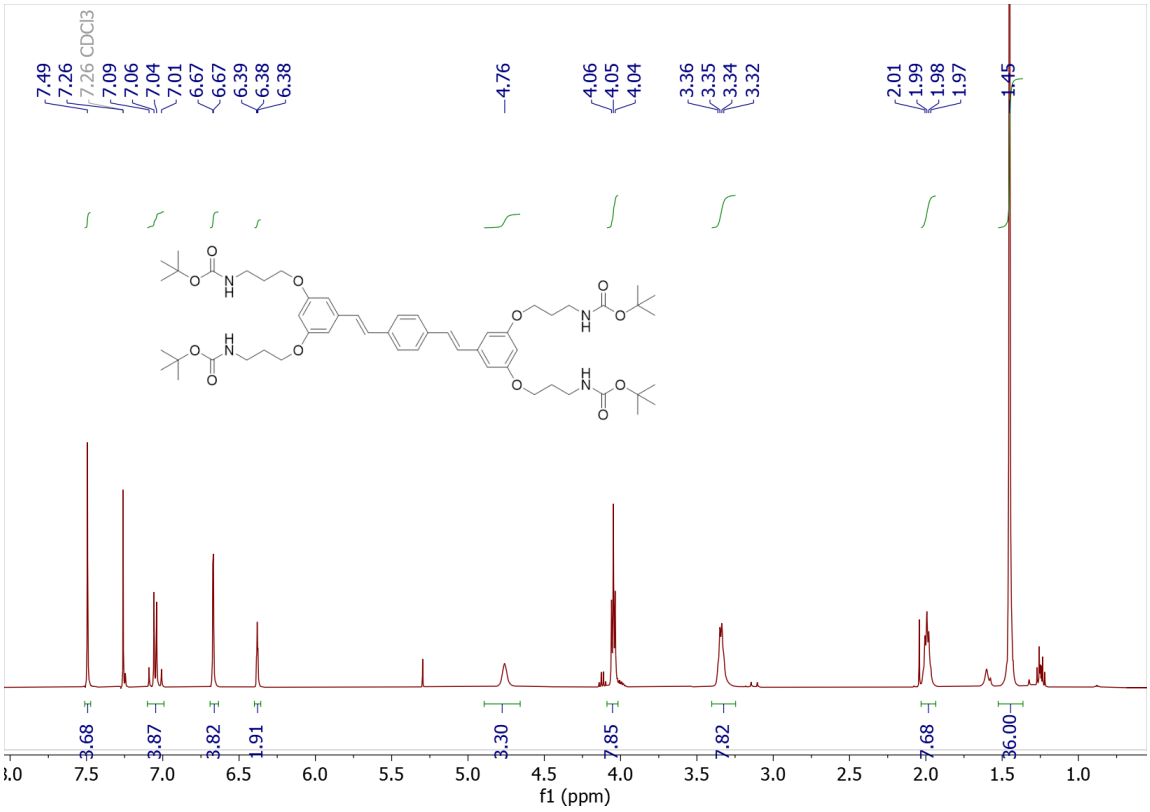
7.49
7.26
7.26 CDCl3
7.09
7.06
7.04
7.01
6.67
6.67
6.39
6.38
6.38
4.76
4.06
4.05
4.04
3.36
3.35
3.34
3.32
2.01
1.99
1.98
1.97
1.45
3.68
3.87
3.82
1.91
3.30
7.85
7.82
7.68
36.00
f1 (ppm)

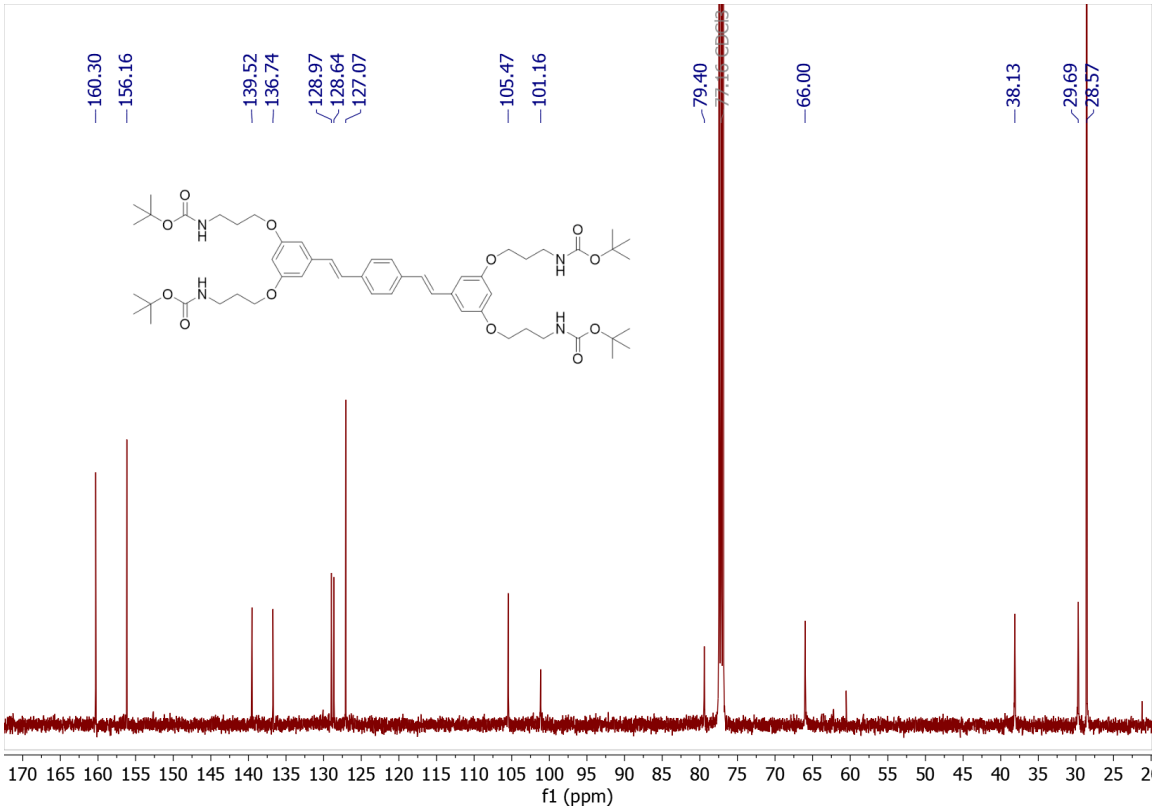
160.30
156.16
139.52
136.74
128.97
128.64
127.07
105.47
101.16
79.40
66.00
38.13
29.69
28.57
f1 (ppm)

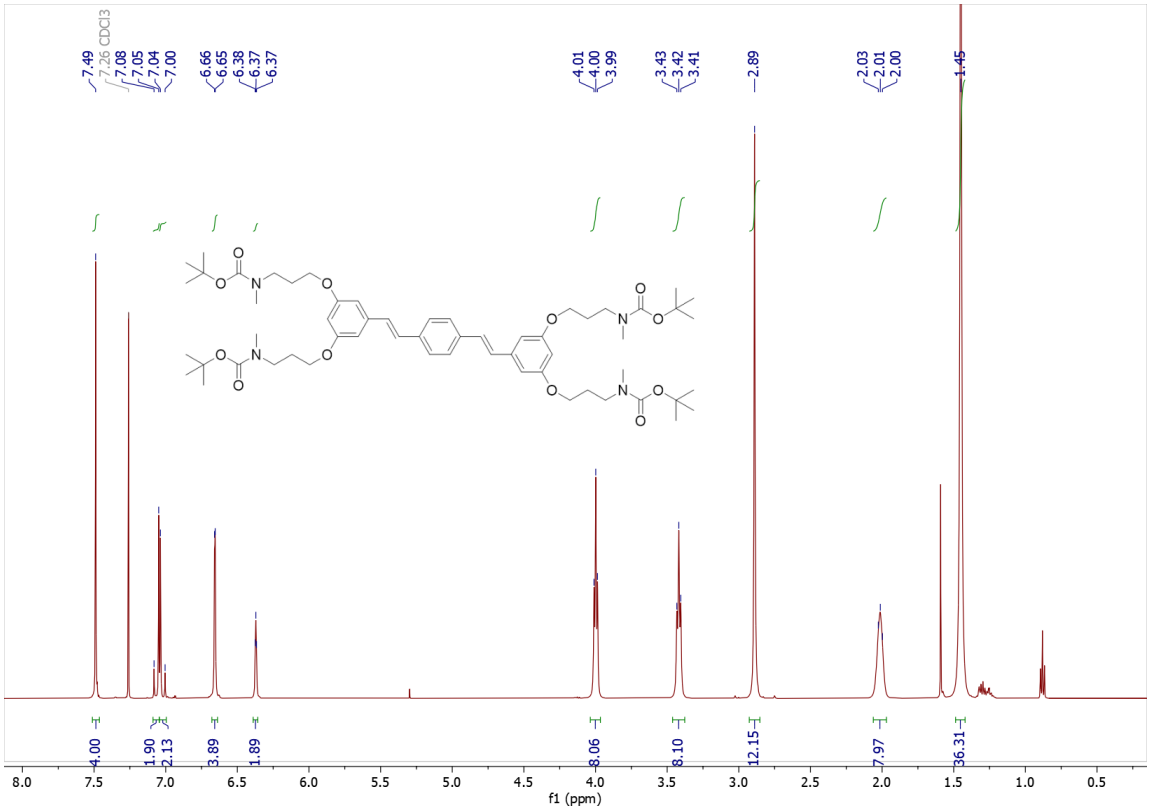
7.49
7.26 CDCl3
7.08
7.05
7.04
7.00
6.66
6.65
6.38
6.37
6.37
4.01
4.00
3.99
3.43
3.42
3.41
2.89
2.03
2.01
2.00
1.45
4.00
1.90
2.13
3.89
1.89
8.06
8.10
12.15
7.97
36.31
f1 (ppm)

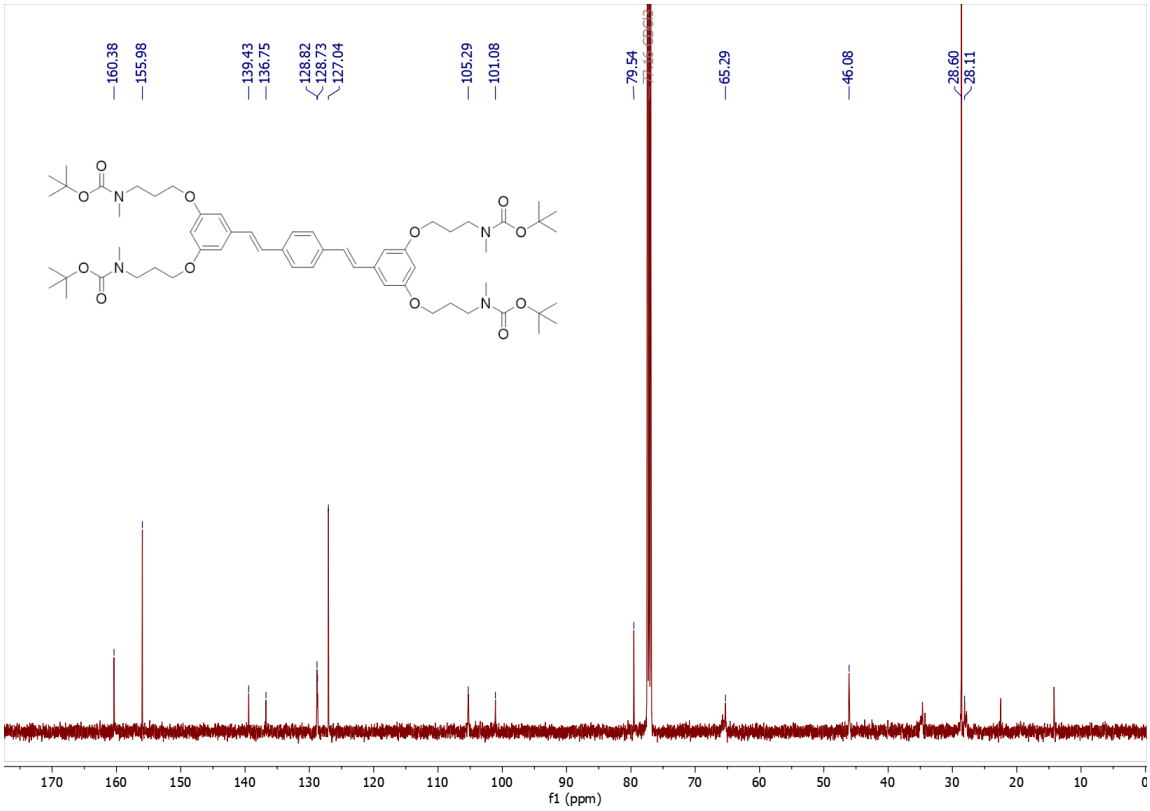
160.38
155.98
139.43
136.75
128.82
128.73
127.04
105.29
101.08
79.54
77.16 CDCl3
65.29
46.08
28.60
28.11
f1 (ppm)

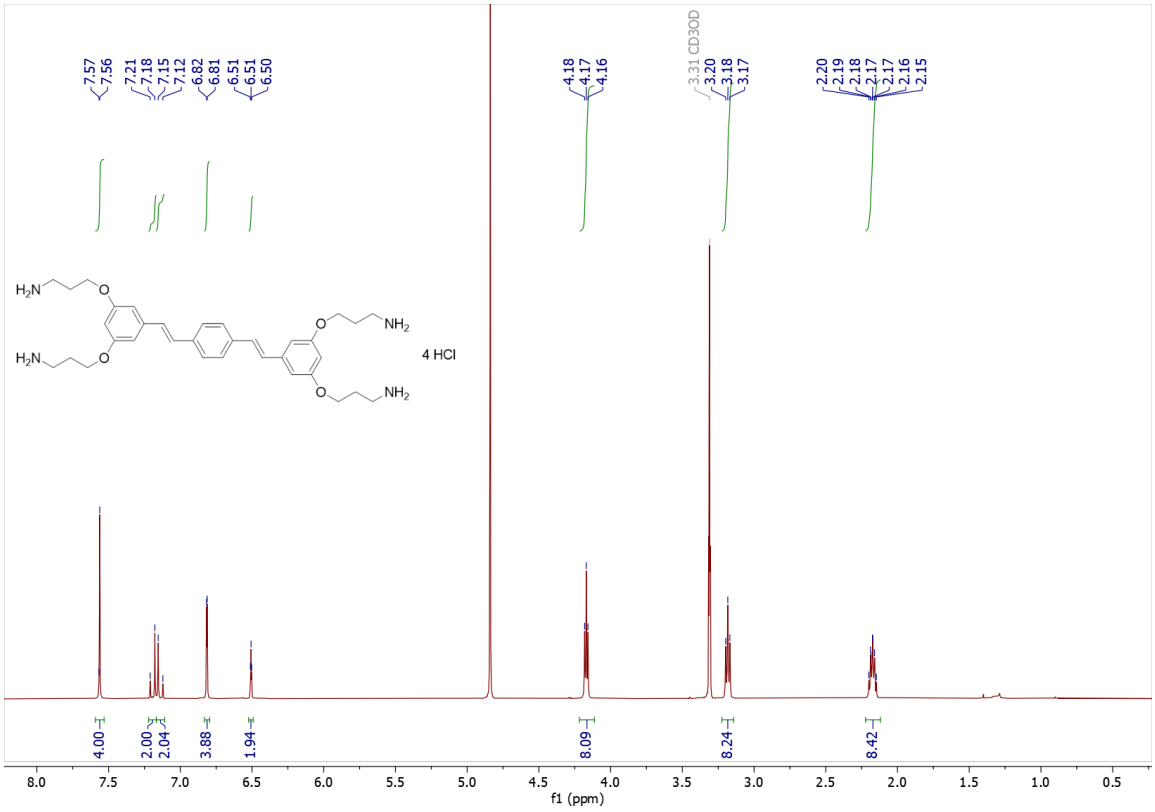
7.57
7.56
7.21
7.18
7.15
7.12
6.82
6.81
6.51
6.51
6.50
4.18
4.17
4.16
3.31 CD3OD
3.20
3.18
3.17
2.20
2.19
2.18
2.17
2.17
2.16
2.15
4 HCl
4.00
2.00
2.04
3.88
1.94
8.09
8.24
8.42
f1 (ppm)

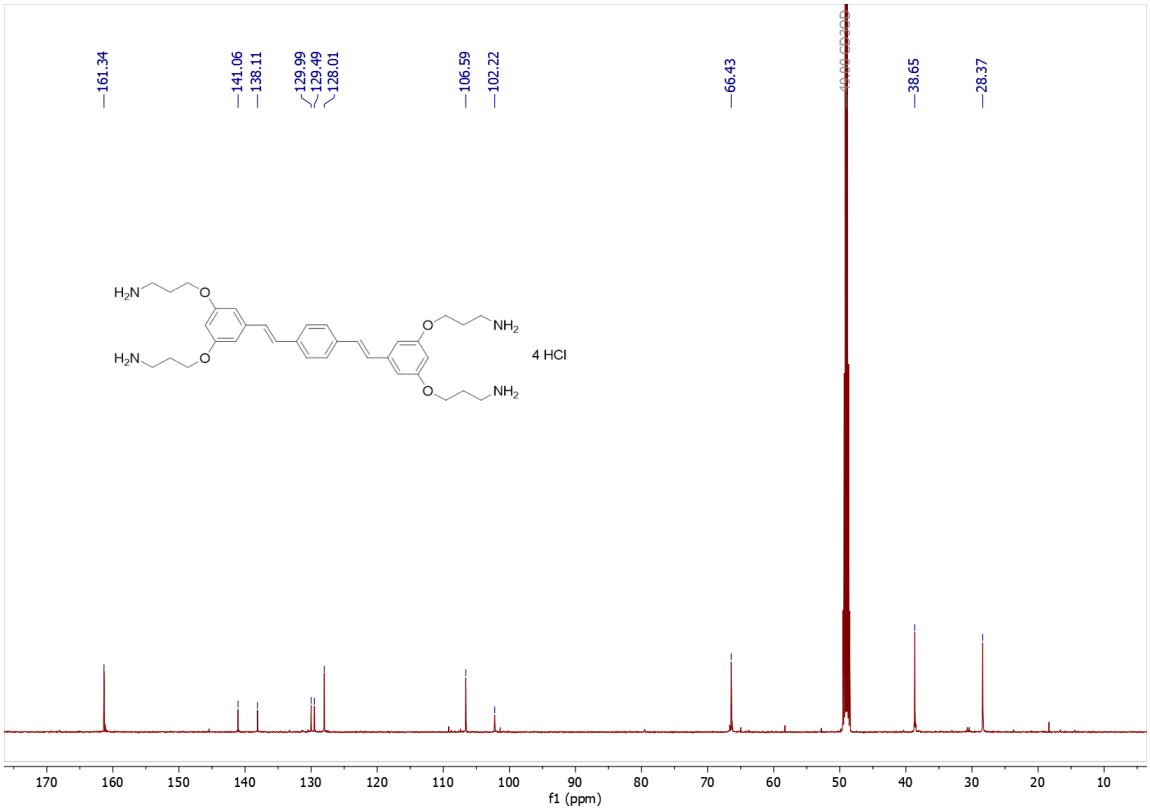
161.34
141.06
138.11
129.99
129.49
128.01
106.59
102.22
66.43
49.00 CD3OD
38.65
28.37
4 HCl
f1 (ppm)

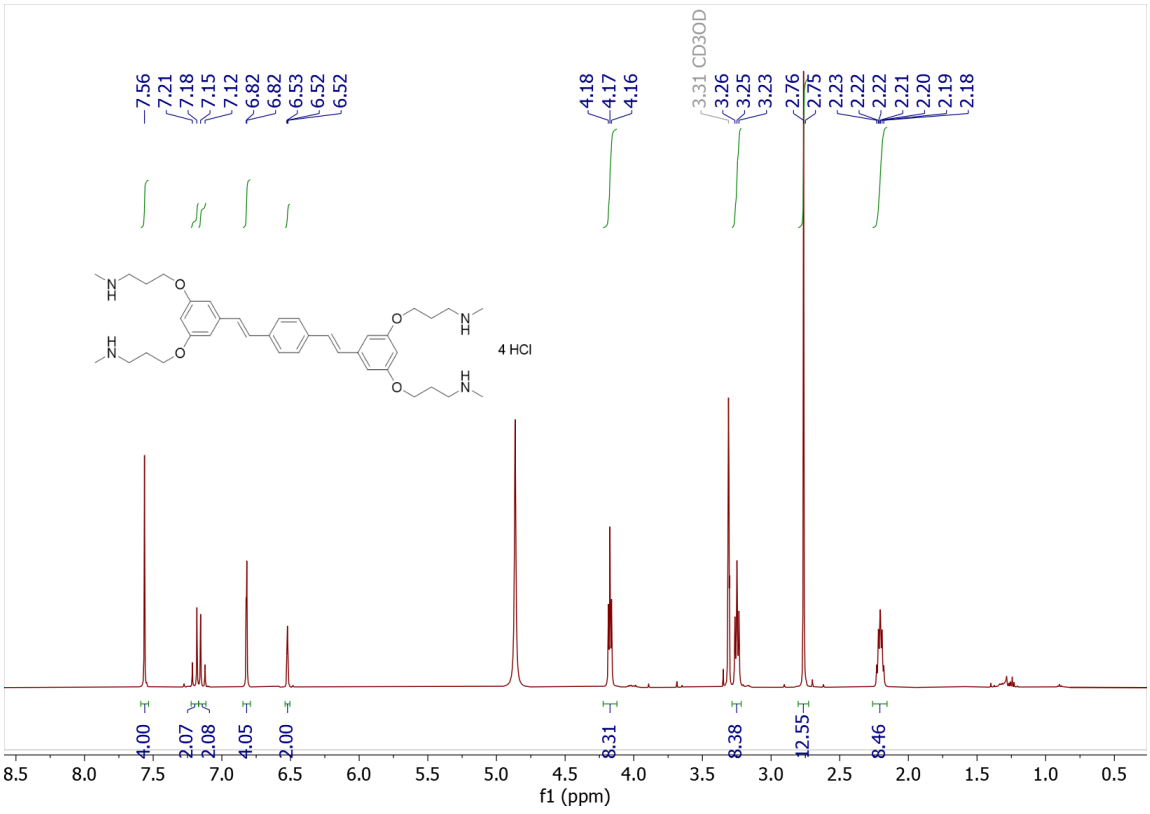
7.56
7.21
7.18
7.15
7.12
6.82
6.82
6.53
6.52
6.52
4.18
4.17
4.16
3.31 CD3OD
3.26
3.25
3.23
2.76
2.75
2.23
2.22
2.22
2.21
2.20
2.19
2.18
4 HCl
4.00
2.07
2.08
4.05
2.00
8.31
8.38
12.55
8.46
f1 (ppm)

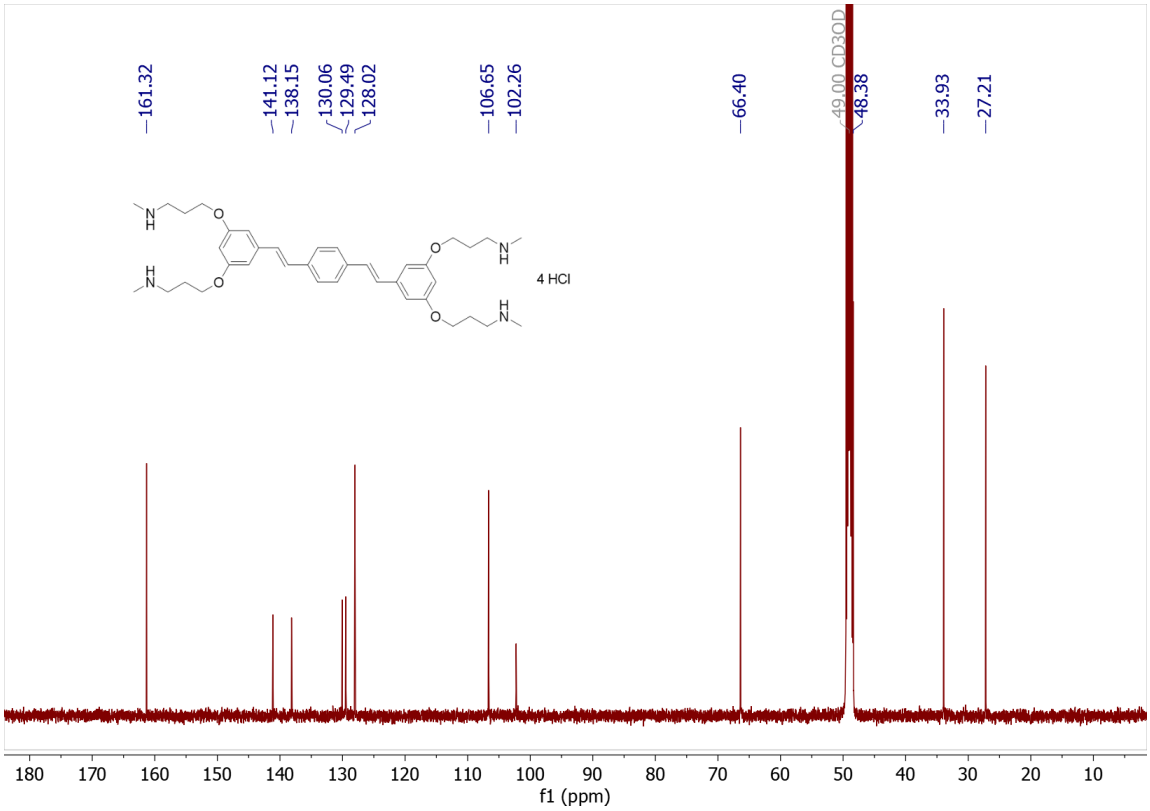
161.32
141.12
138.15
130.06
129.49
128.02
106.65
102.26
66.40
49.00 CD3OD
48.38
33.93
27.21
4 HCl
f1 (ppm)

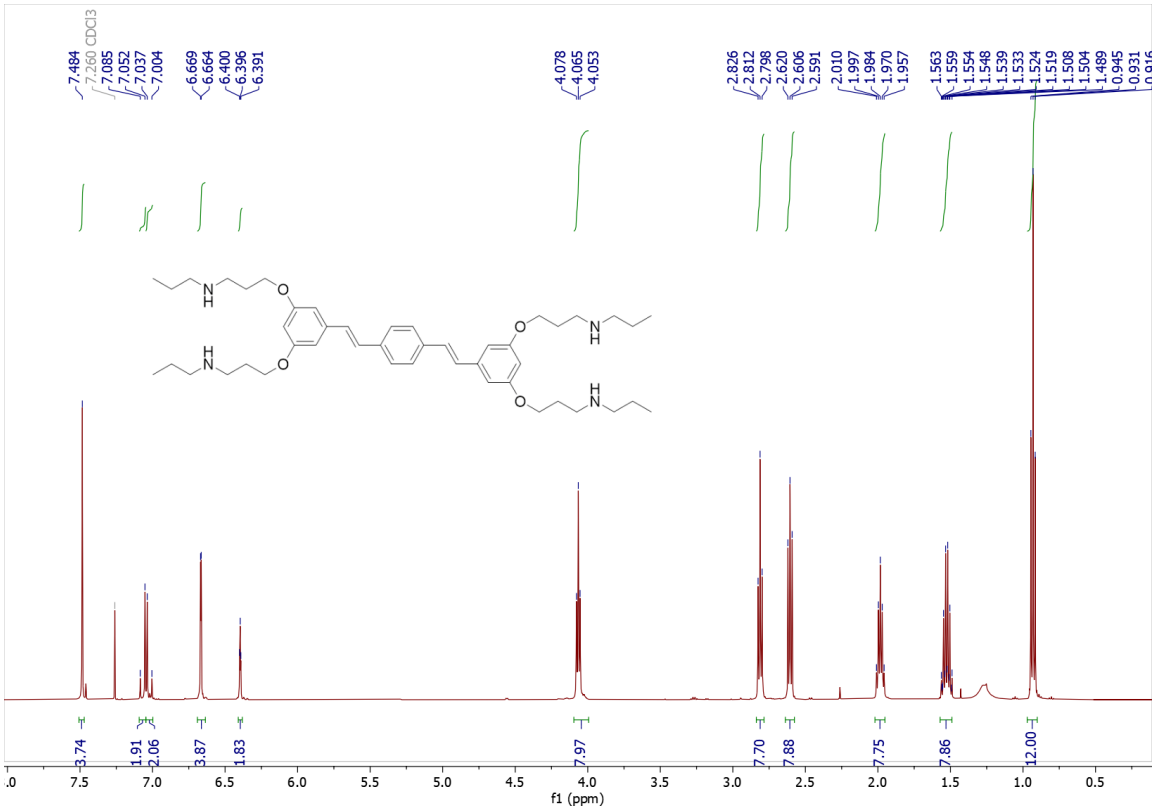
7.484
7.260 CDCl3
7.085
7.052
7.037
7.004
6.669
6.664
6.400
6.396
6.391
4.078
4.065
4.053
2.826
2.812
2.798
2.620
2.606
2.591
2.010
1.997
1.984
1.970
1.957
1.563
1.559
1.554
1.548
1.539
1.533
1.524
1.519
1.508
1.504
1.489
0.945
0.931
3.74
1.91
2.06
3.87
1.83
7.97
7.70
7.88
7.75
7.86
12.00
f1 (ppm)

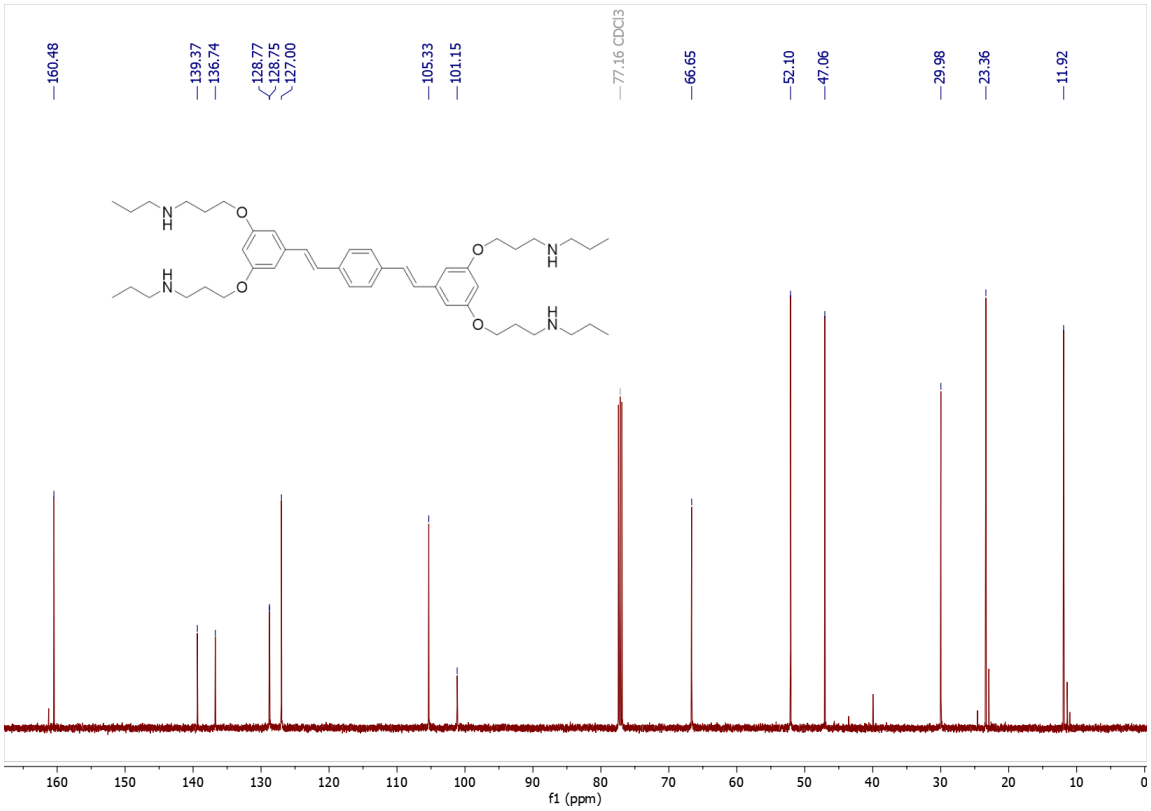
160.48
139.37
136.74
128.77
128.75
127.00
105.33
101.15
77.16 CDCl3
66.65
52.10
47.06
29.98
23.36
11.92
f1 (ppm)

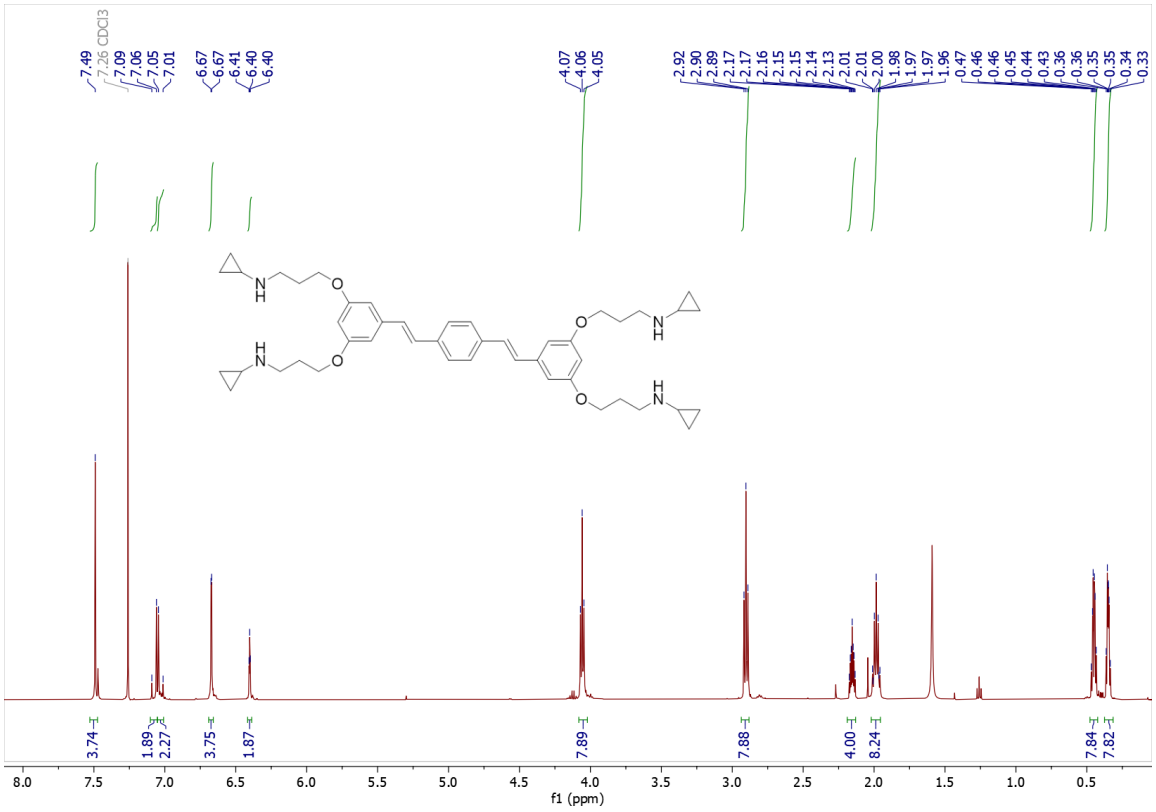
7.49
7.26 CDCl3
7.09
7.06
7.05
7.01
6.67
6.67
6.41
6.40
6.40
4.07
4.06
4.05
2.92
2.90
2.89
2.17
2.16
2.15
2.15
2.14
2.13
2.01
2.01
2.00
1.98
1.97
1.97
1.96
0.47
0.46
0.46
0.45
0.44
0.43
0.36
0.36
0.35
0.35
0.34
0.33
3.74
1.89
2.27
3.75
1.87
7.89
7.88
4.00
8.24
7.84
7.82
f1 (ppm)

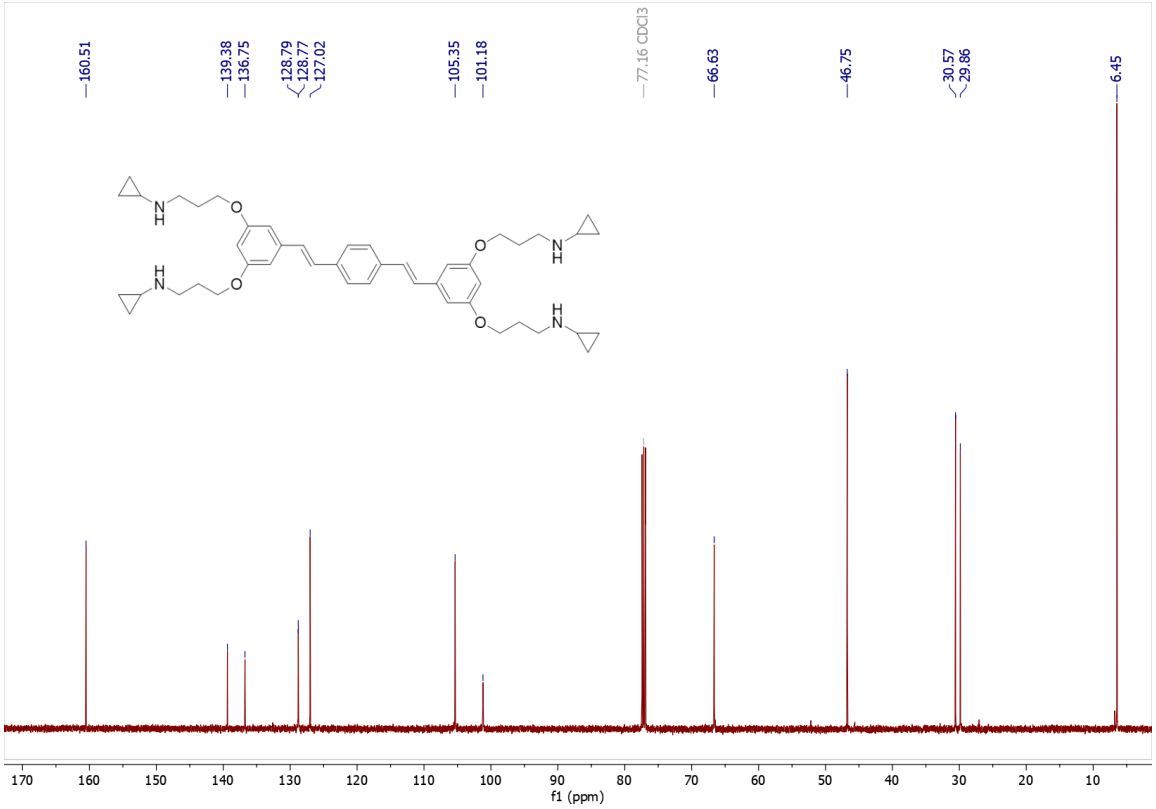
160.51
139.38
136.75
128.79
128.77
127.02
105.35
101.18
77.16 CDCl3
66.63
46.75
30.57
29.86
6.45
f1 (ppm)

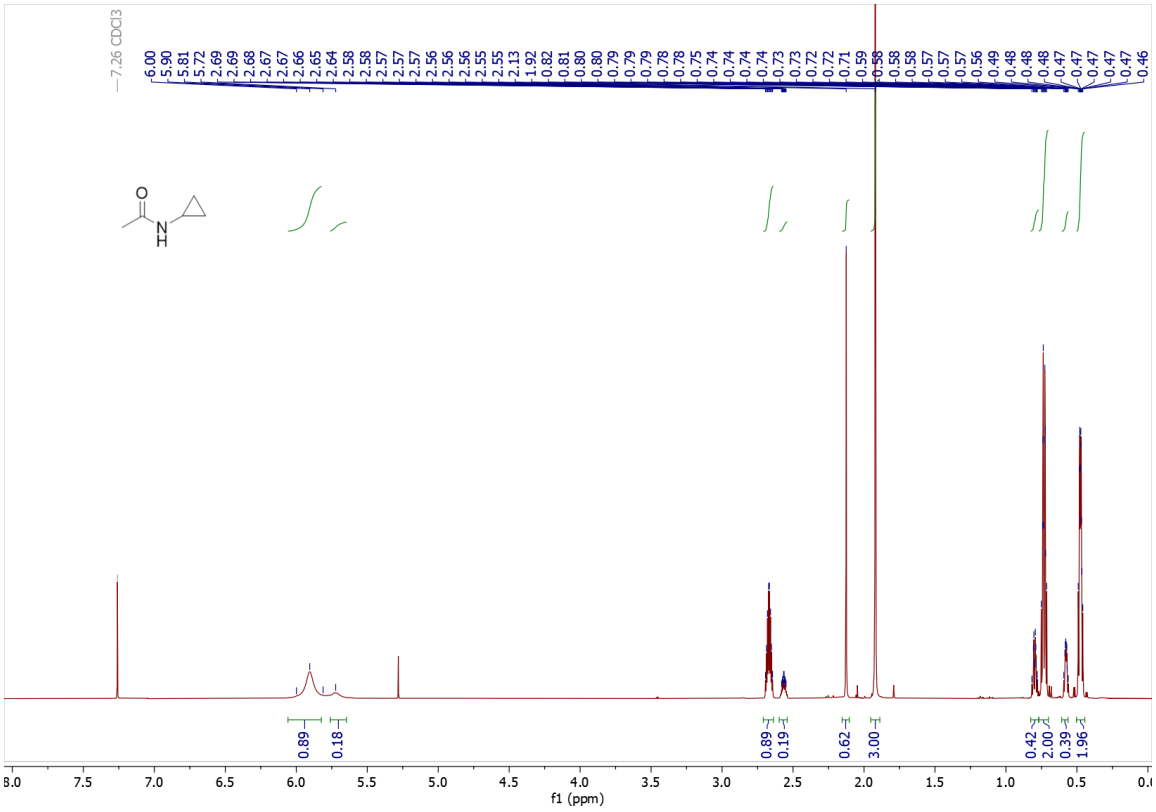
7.26 CDCl3
6.00
5.90
5.81
5.72
2.69
2.69
2.68
2.67
2.67
2.66
2.65
2.64
2.58
2.58
2.57
2.57
2.57
2.56
2.56
2.56
2.55
2.55
2.13
1.92
0.82
0.81
0.80
0.80
0.79
0.79
0.79
0.78
0.78
0.75
0.74
0.74
0.74
0.74
0.73
0.73
0.72
0.72
0.71
0.59
0.58
0.58
0.58
0.57
0.57
0.57
0.56
0.49
0.48
0.48
0.48
0.47
0.47
0.47
0.47
0.47
0.46
O
N
H
0.89
0.18
0.89
0.19
0.62
3.00
0.42
2.00
0.39
1.96
8.0
7.5
7.0
6.5
6.0
5.5
5.0
4.5
4.0
3.5
3.0
2.5
2.0
1.5
1.0
0.5
f1 (ppm)

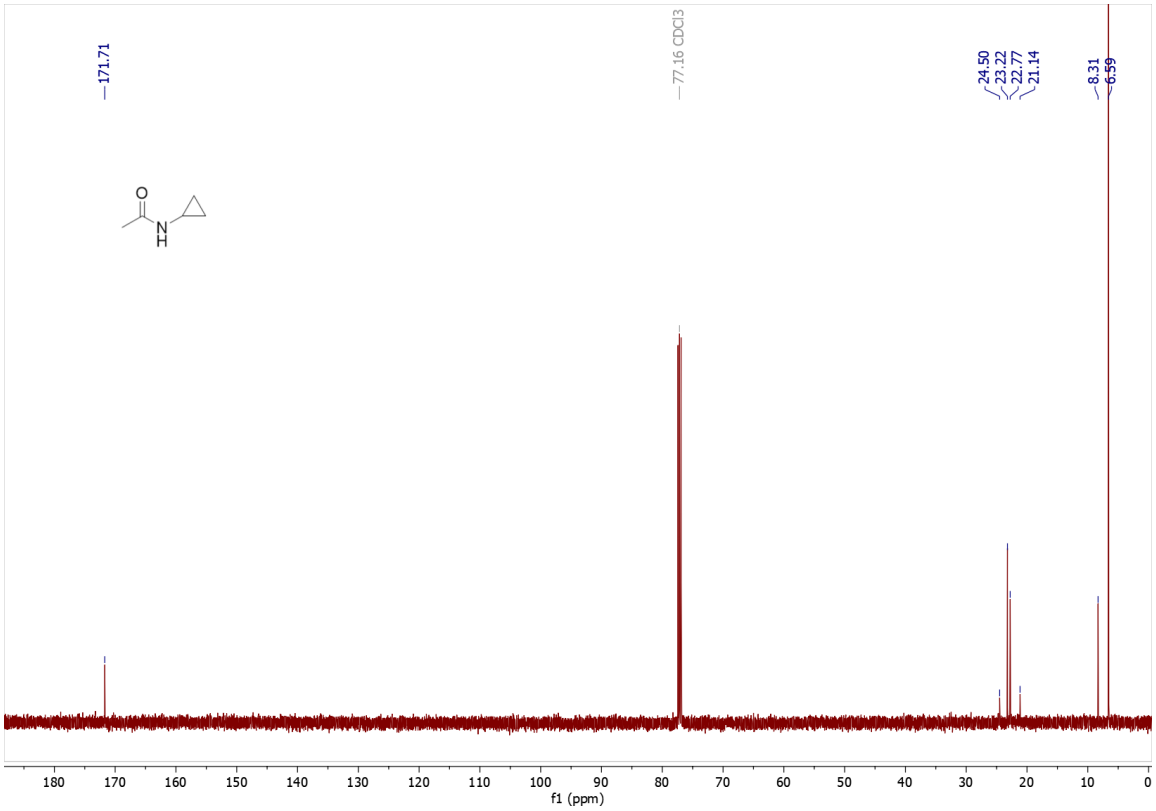
171.71
77.16 CDCl3
24.50
23.22
22.77
21.14
8.31
6.59
O
N
H
180
170
160
150
140
130
120
110
100
90
80
70
60
50
40
30
20
10
0
f1 (ppm)

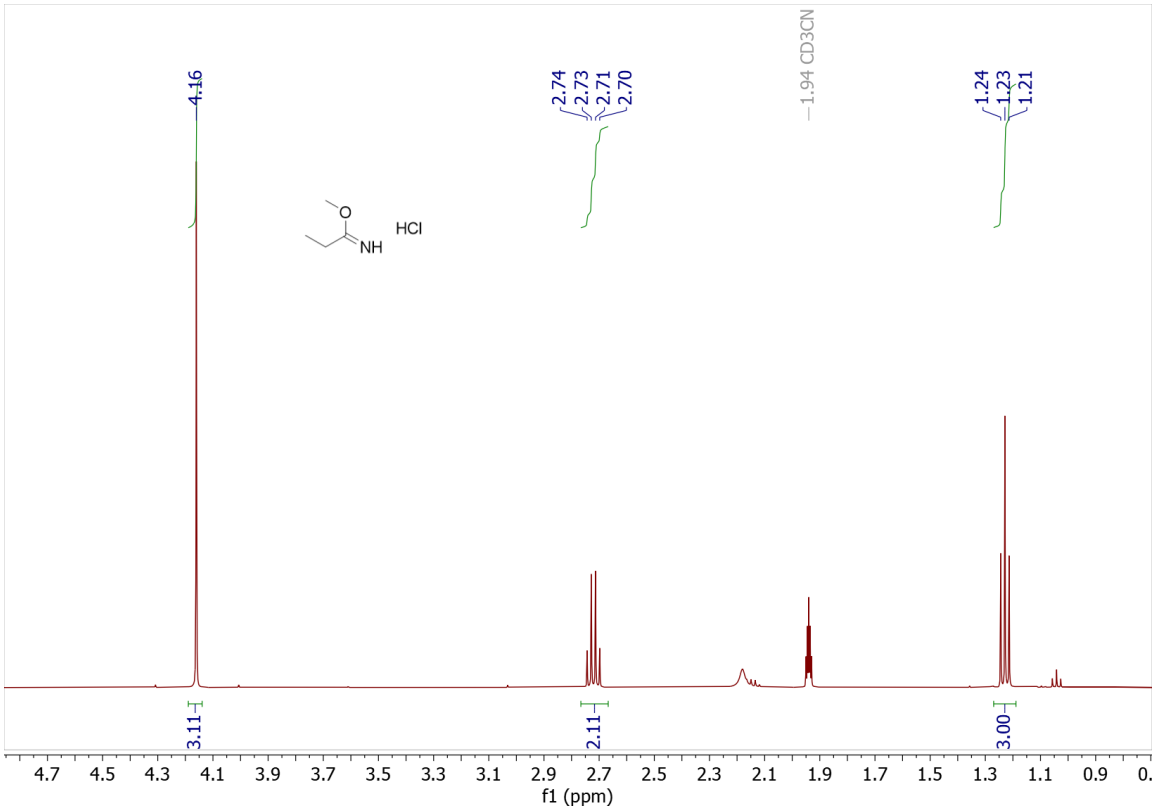
4.16
2.74
2.73
2.71
2.70
1.94 CD3CN
1.24
1.23
1.21
HCl
NH
3.11
2.11
3.00
f1 (ppm)

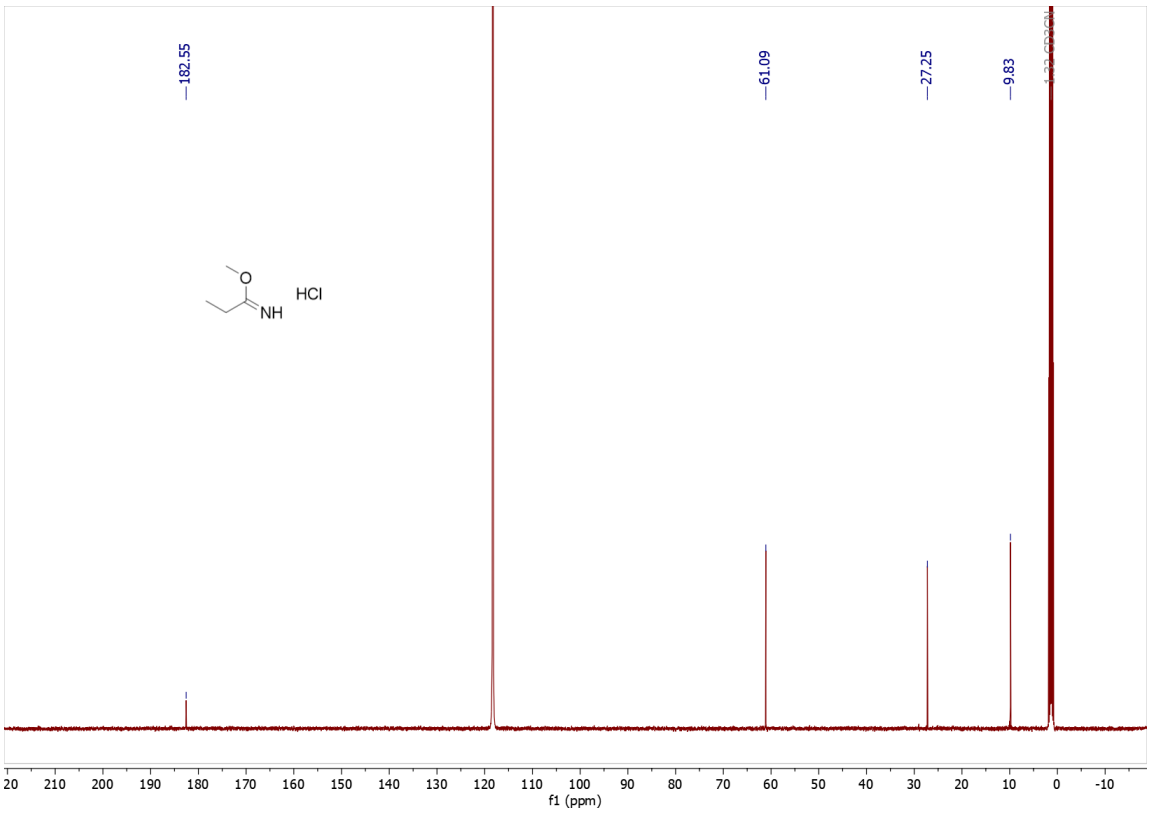
182.55
61.09
27.25
9.83
HCl
NH
f1 (ppm)

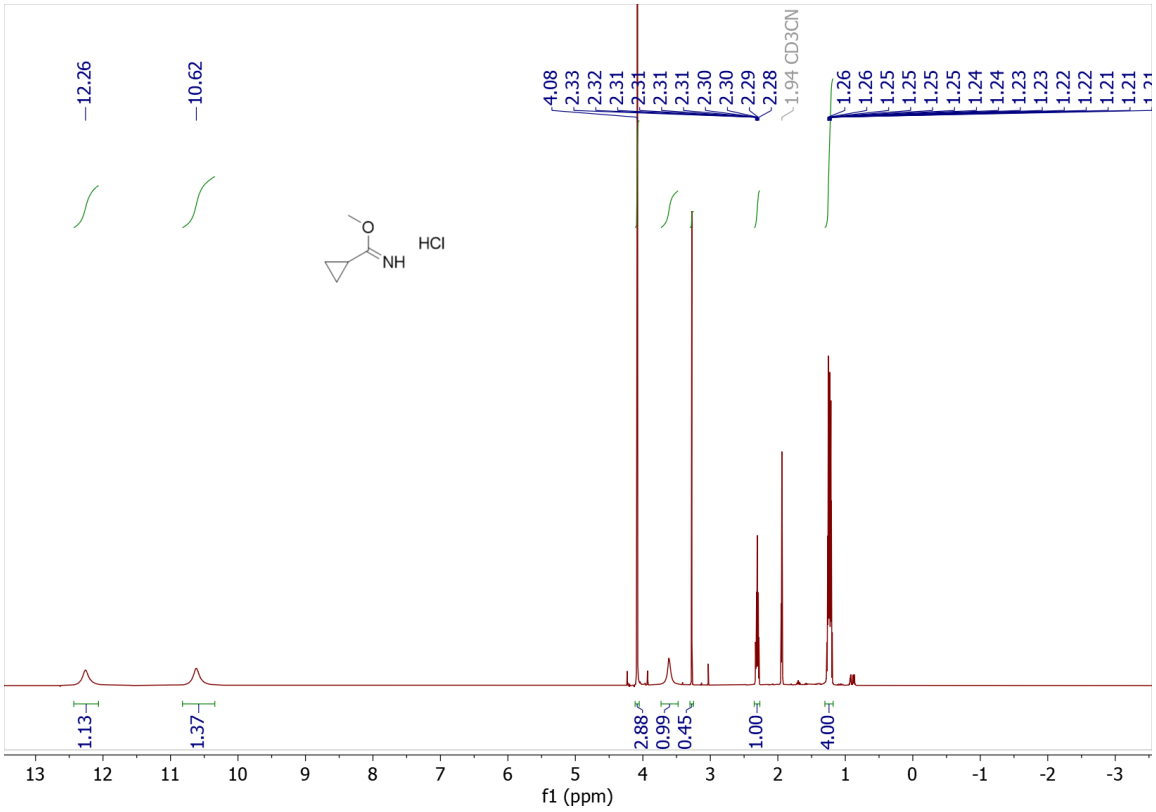
12.26
10.62
4.08
2.33
2.32
2.31
2.31
2.31
2.31
2.30
2.30
2.29
2.28
1.94 CD3CN
1.26
1.26
1.25
1.25
1.25
1.25
1.24
1.24
1.23
1.23
1.22
1.22
1.21
1.21
HCl
1.13
1.37
2.88
0.99
0.45
1.00
4.00
f1 (ppm)

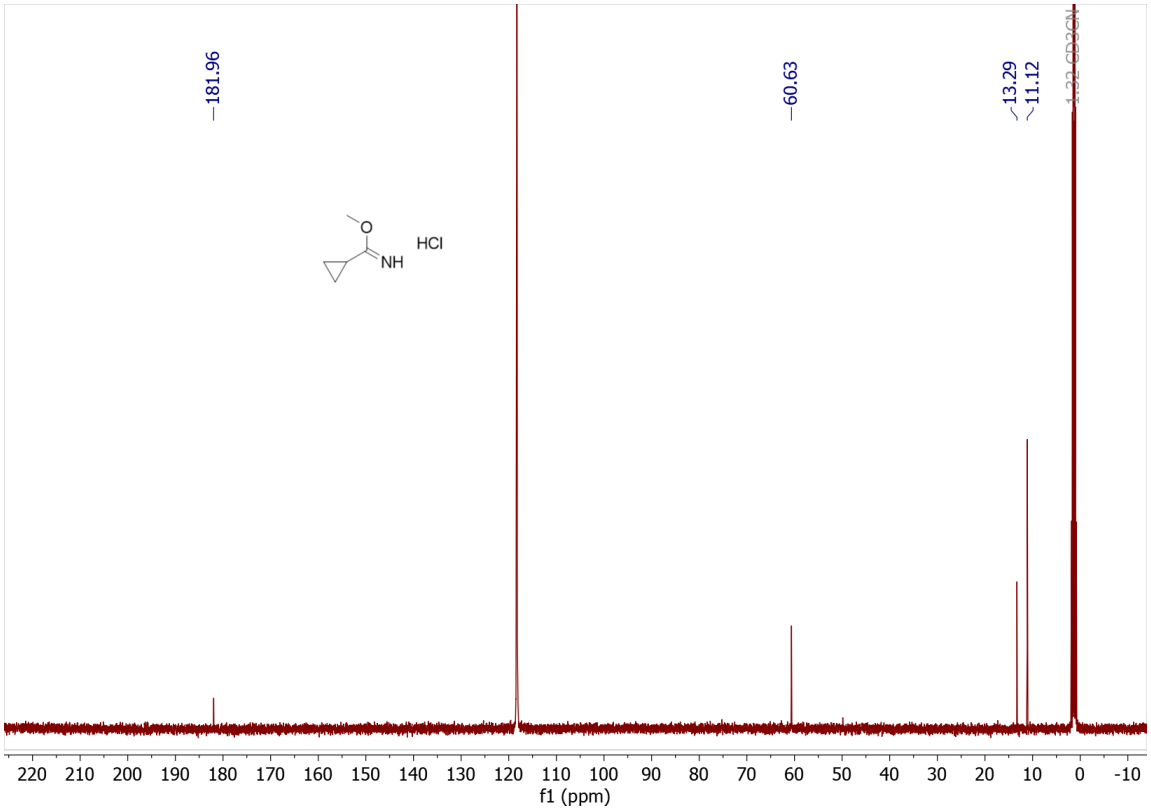
181.96
60.63
13.29
11.12
HCl
f1 (ppm)

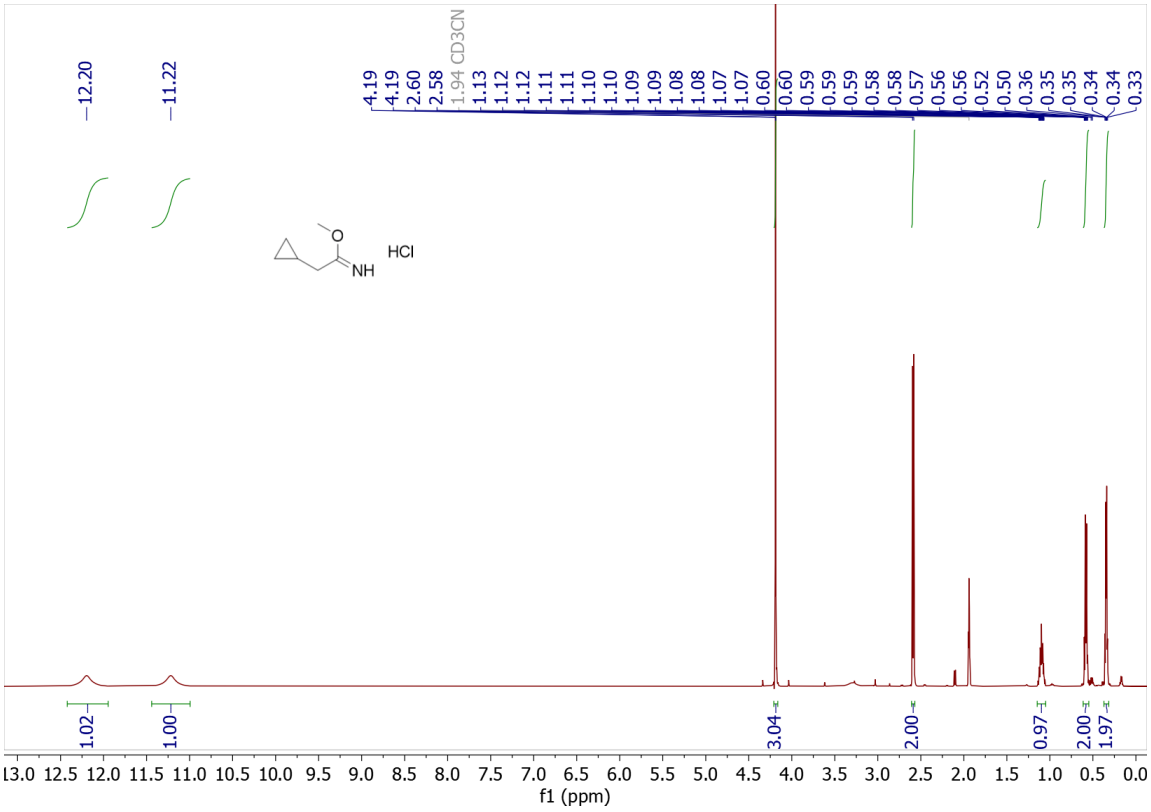
12.20
11.22
4.19
4.19
2.60
2.58
1.94 CD3CN
1.13
1.12
1.12
1.11
1.11
1.10
1.10
1.09
1.09
1.08
1.08
1.07
1.07
0.60
0.60
0.59
0.59
0.59
0.58
0.58
0.57
0.56
0.56
0.52
0.50
0.36
0.35
0.35
0.34
0.34
0.33
HCl
NH
1.02
1.00
3.04
2.00
0.97
2.00
1.97
f1 (ppm)

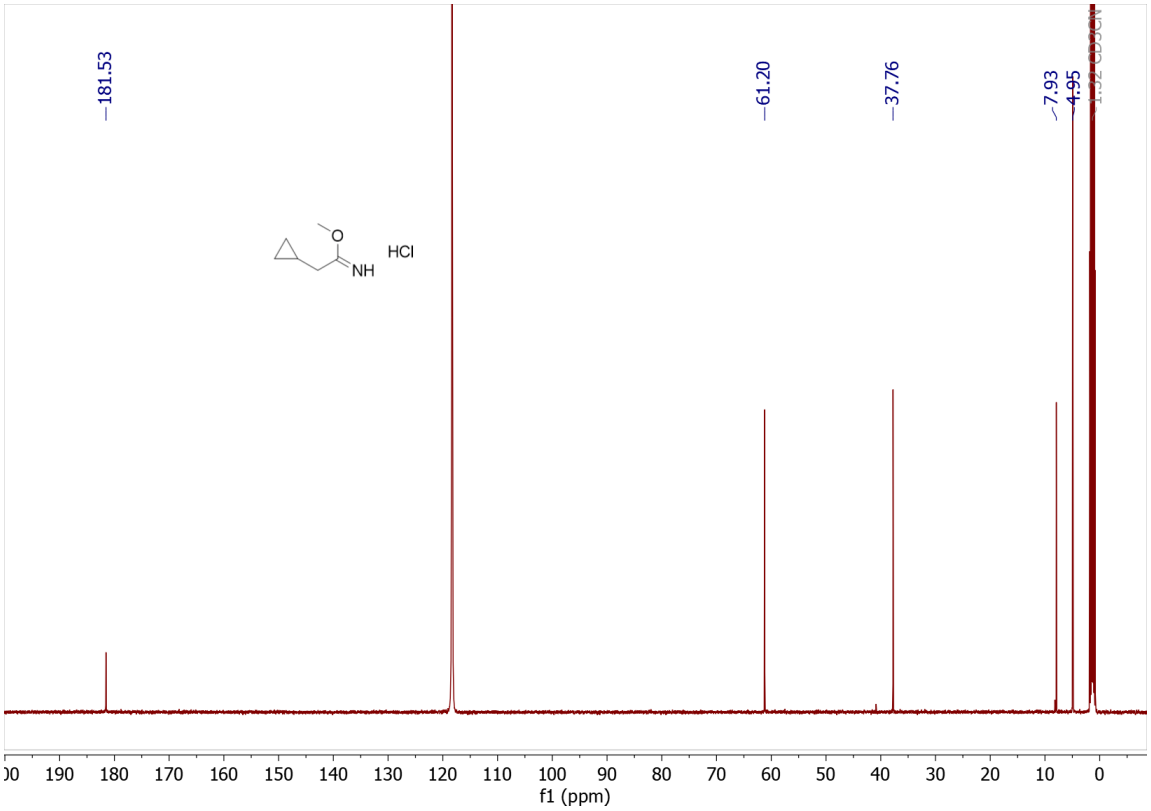
181.53
61.20
37.76
7.93
4.95
1.92 CD3CN
HCl
NH
f1 (ppm)

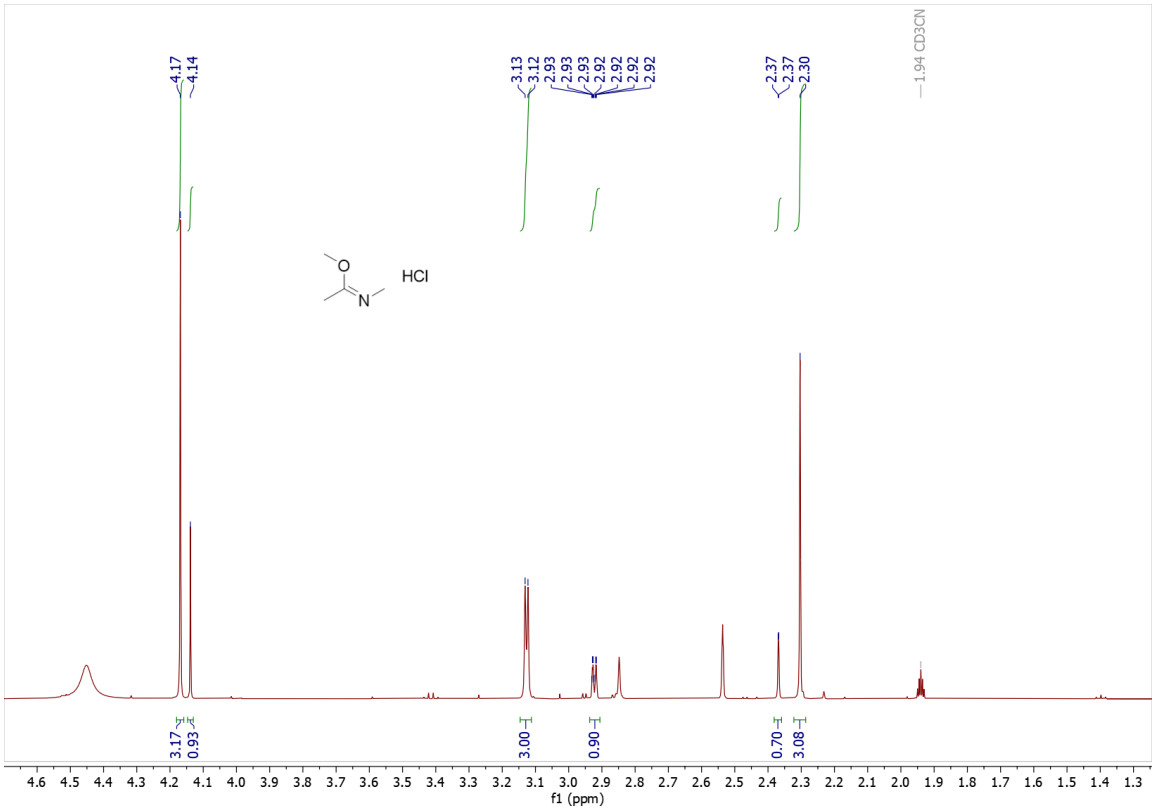
4.17
4.14
3.13
3.12
2.93
2.93
2.93
2.92
2.92
2.92
2.92
2.37
2.37
2.30
1.94 CD3CN
HCl
3.17
0.93
3.00
0.90
0.70
3.08
f1 (ppm)

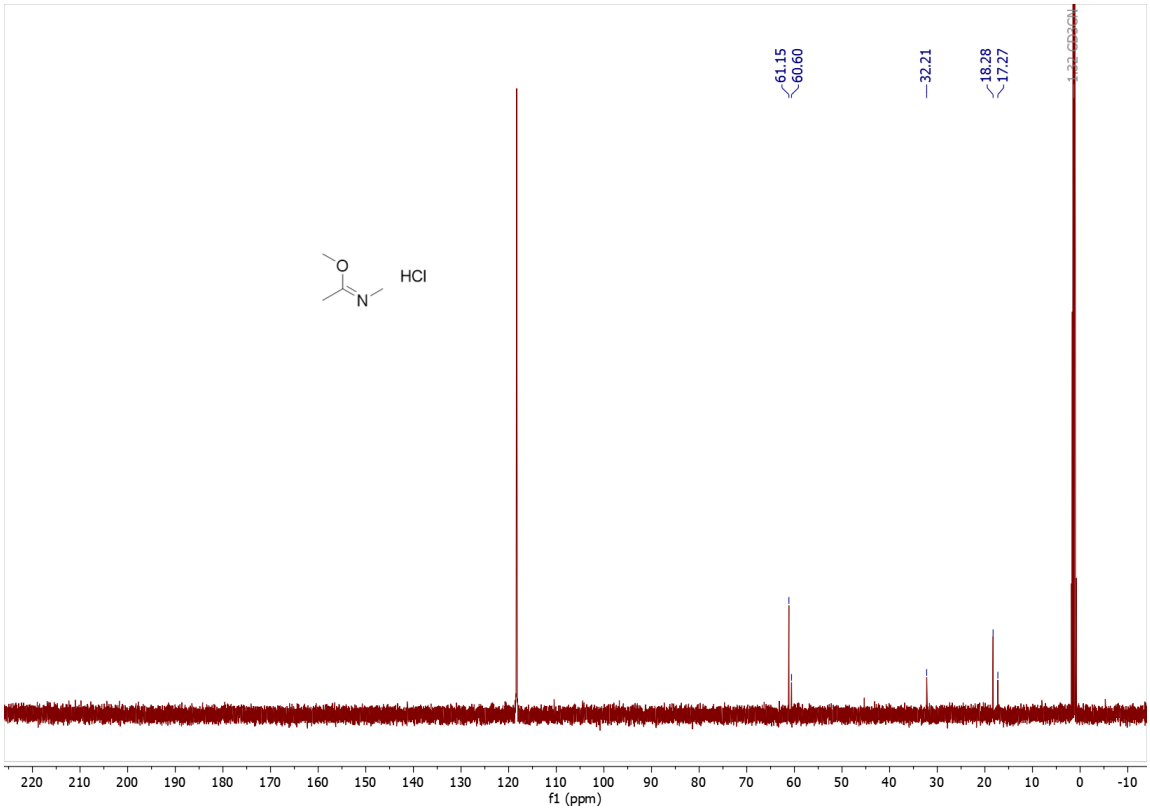
61.15
60.60
32.21
18.28
17.27
1.32 CD3CN
HCl
f1 (ppm)

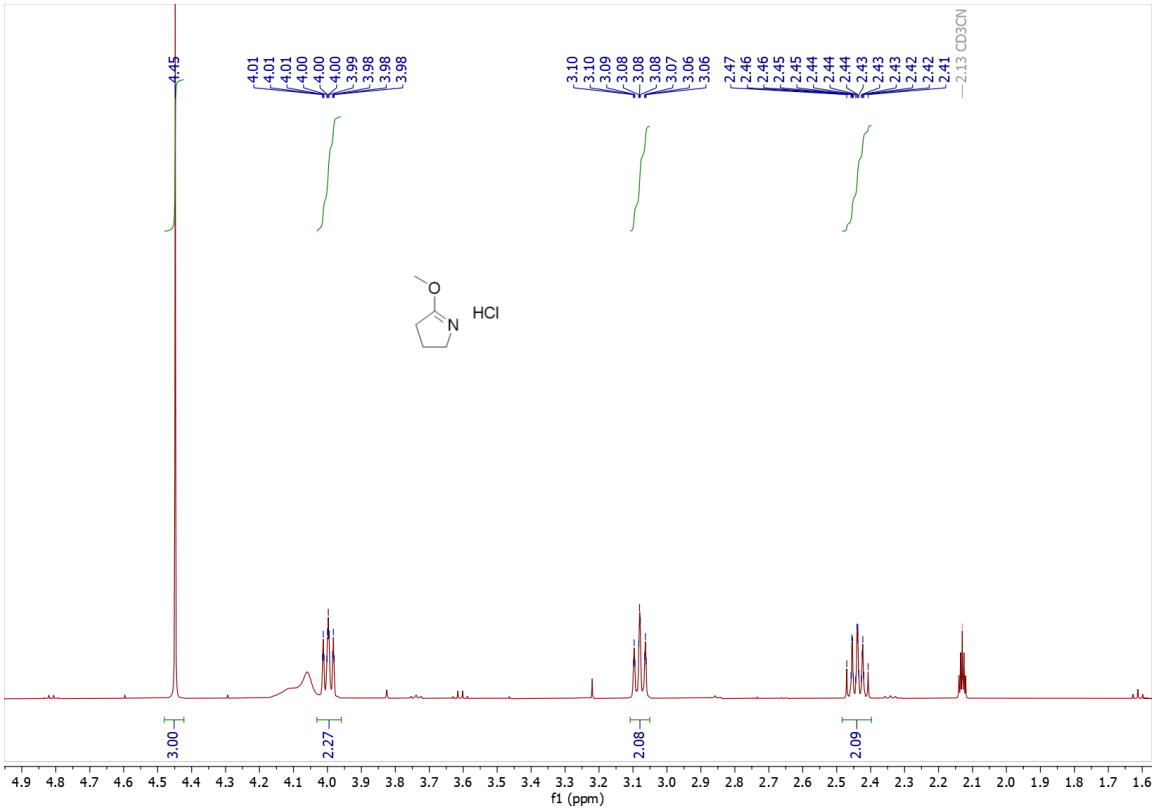
4.45
4.01
4.01
4.01
4.00
4.00
4.00
3.99
3.98
3.98
3.98
3.10
3.10
3.09
3.08
3.08
3.08
3.07
3.06
3.06
2.47
2.46
2.46
2.45
2.45
2.44
2.44
2.44
2.43
2.43
2.43
2.42
2.42
2.41
2.13 CD3CN
O
N
HCl
3.00
2.27
2.08
2.09
4.9 4.8 4.7 4.6 4.5 4.4 4.3 4.2 4.1 4.0 3.9 3.8 3.7 3.6 3.5 3.4 3.3 3.2 3.1 3.0 2.9 2.8 2.7 2.6 2.5 2.4 2.3 2.2 2.1 2.0 1.9 1.8 1.7 1.6
f1 (ppm)

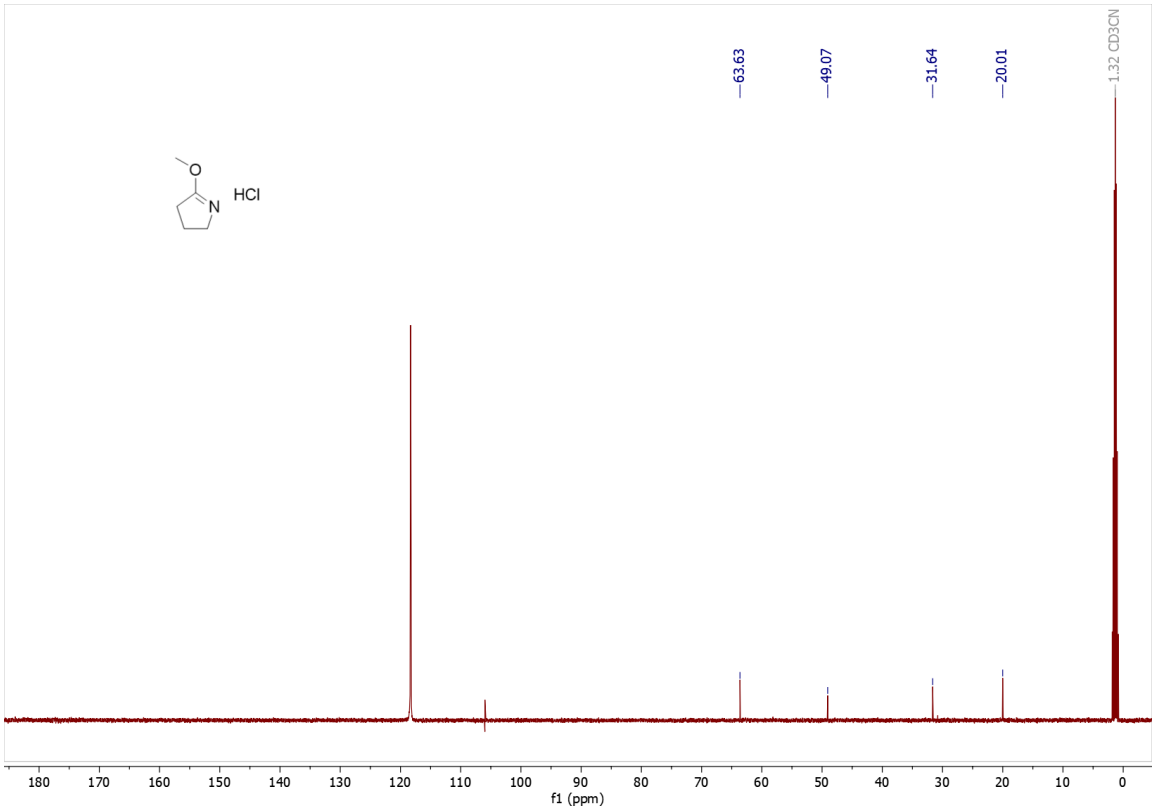
63.63
49.07
31.64
20.01
1.32 CD3CN
O
N
HCl
180 170 160 150 140 130 120 110 100 90 80 70 60 50 40 30 20 10 0
f1 (ppm)

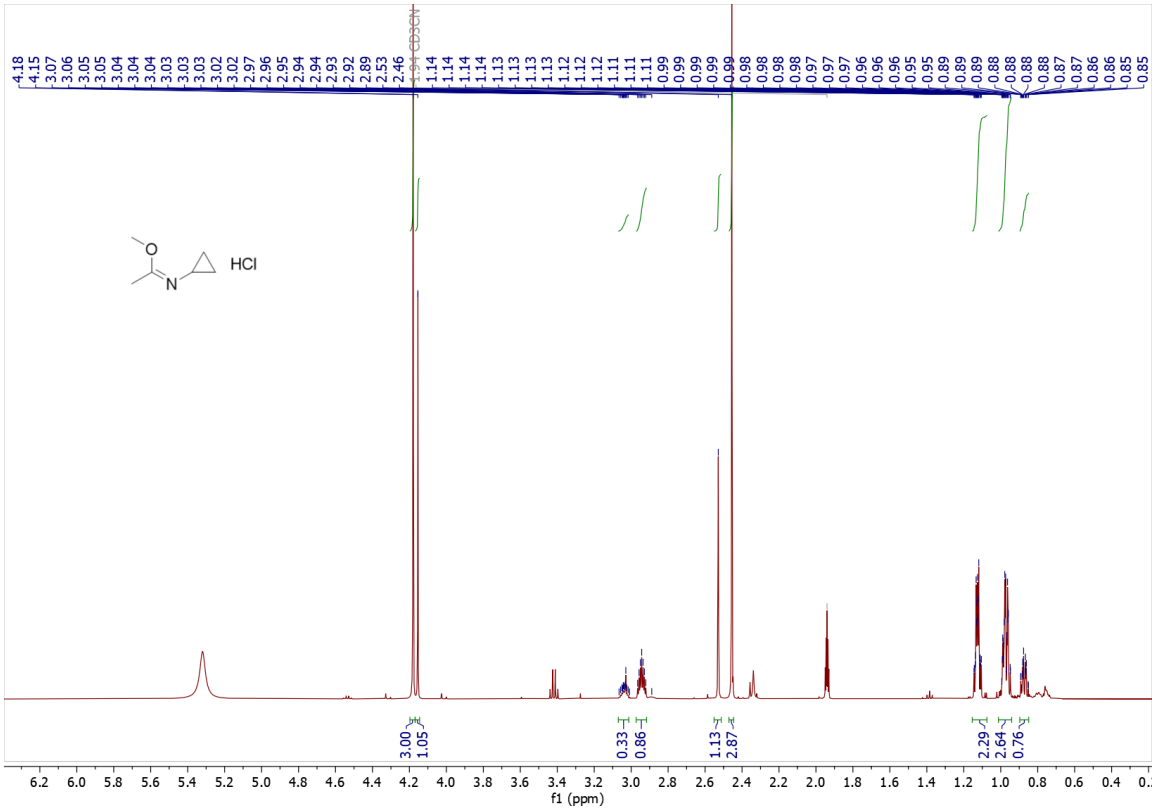
HCl
3.00
1.05
0.33
0.86
1.13
2.87
2.29
2.64
0.76
f1 (ppm)

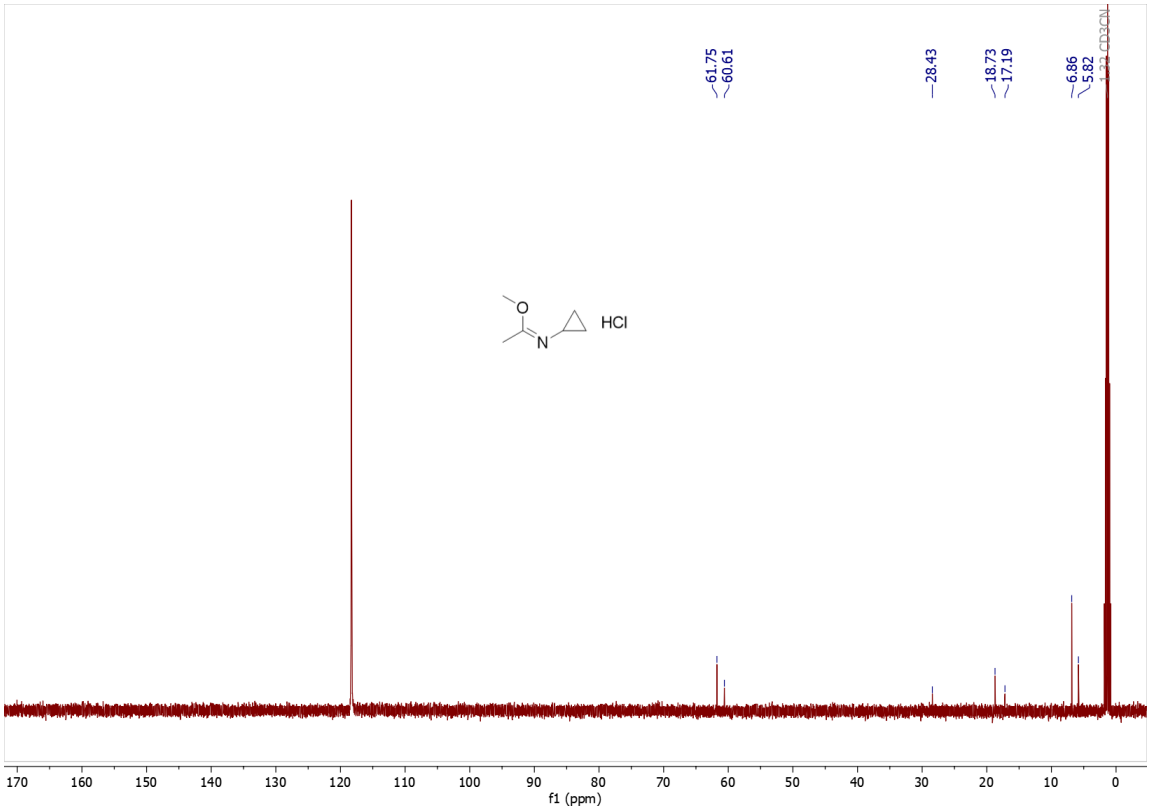
61.75
60.61
28.43
18.73
17.19
6.86
5.82
HCl
f1 (ppm)

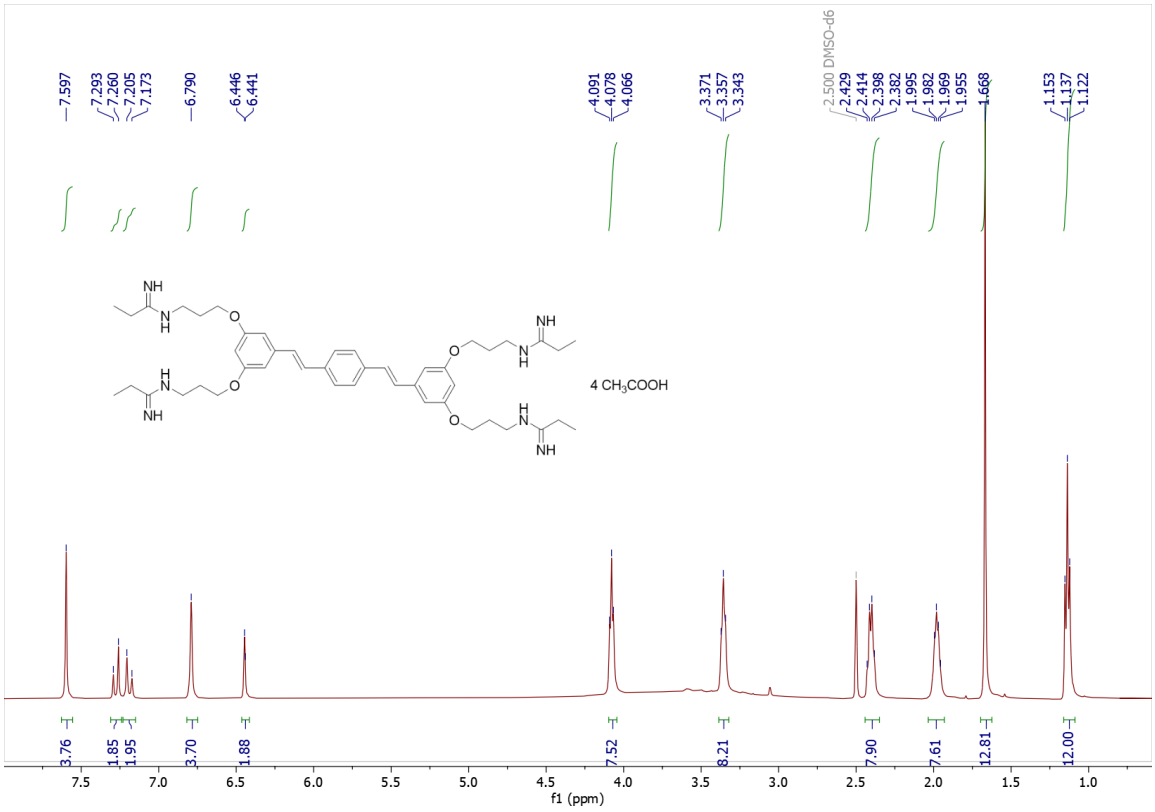
7.597
7.293
7.260
7.205
7.173
6.790
6.446
6.441
4.091
4.078
4.066
3.371
3.357
3.343
2.500 DMSO-d6
2.429
2.414
2.398
2.382
1.995
1.982
1.969
1.955
1.668
1.153
1.137
1.122
4 CH3COOH
3.76
1.85
1.95
3.70
1.88
7.52
8.21
7.90
7.61
12.81
12.00
f1 (ppm)

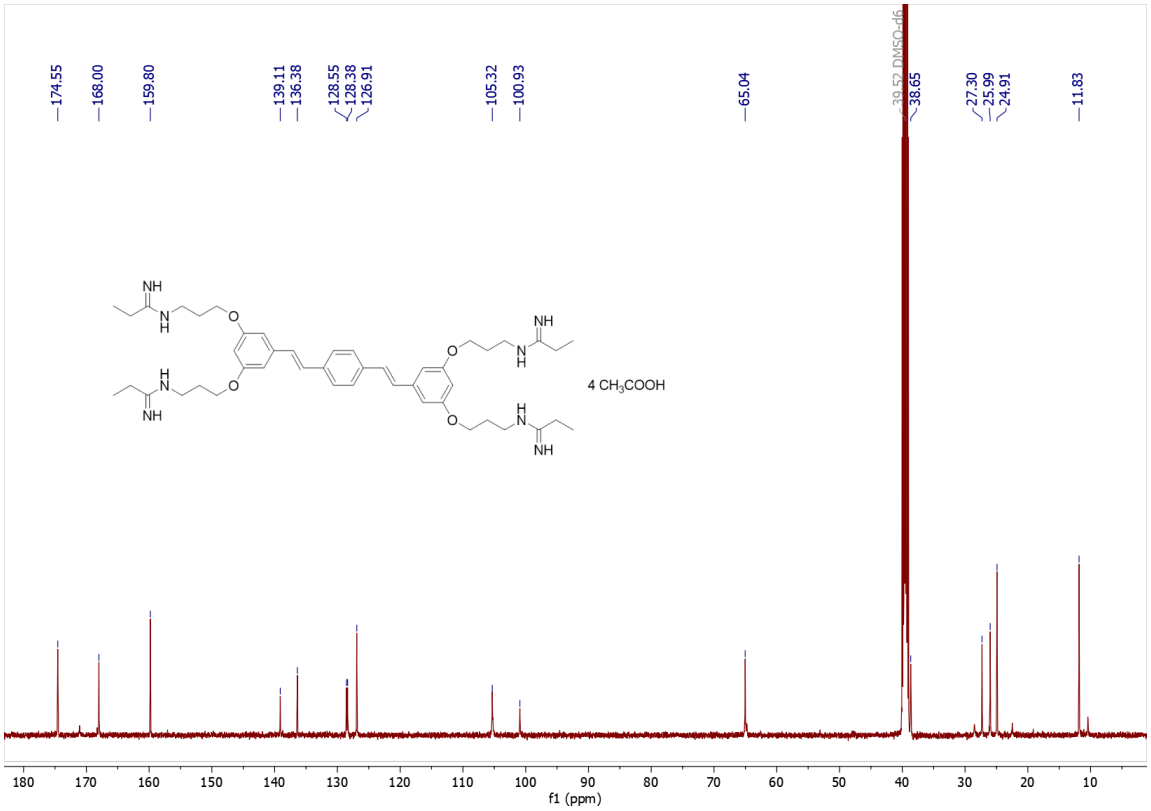
174.55
168.00
159.80
139.11
136.38
128.55
128.38
126.91
105.32
100.93
65.04
39.52 DMSO-d6
38.65
27.30
25.99
24.91
11.83
4 CH3COOH
f1 (ppm)

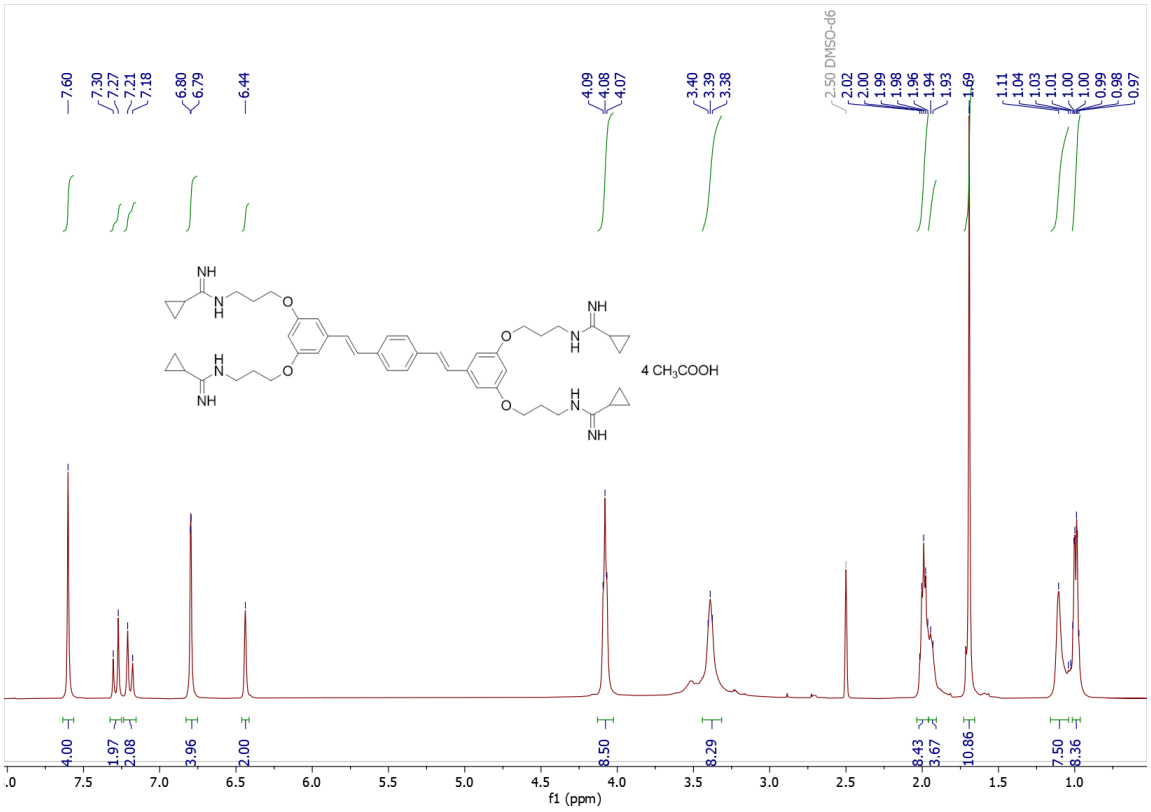
7.60
7.30
7.27
7.21
7.18
6.80
6.79
6.44
4.09
4.08
4.07
3.40
3.39
3.38
2.50 DMSO-d6
2.02
2.00
1.99
1.98
1.96
1.94
1.93
1.69
1.11
1.04
1.03
1.01
1.00
1.00
0.99
0.98
0.97
4 CH3COOH
4.00
1.97
2.08
3.96
2.00
8.50
8.29
8.43
3.67
10.86
7.50
8.36
f1 (ppm)

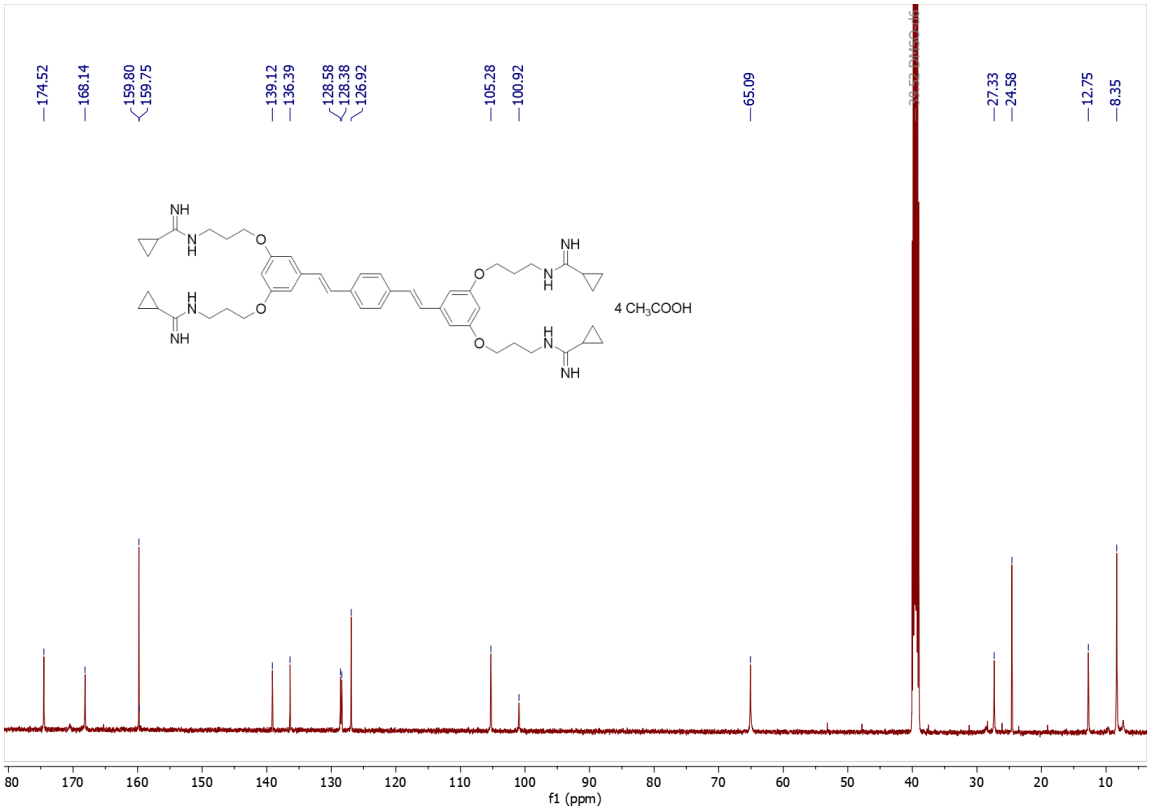
174.52
168.14
159.80
159.75
139.12
136.39
128.58
128.38
126.92
105.28
100.92
65.09
39.52 DMSO-d6
27.33
24.58
12.75
8.35
4 CH3COOH
f1 (ppm)

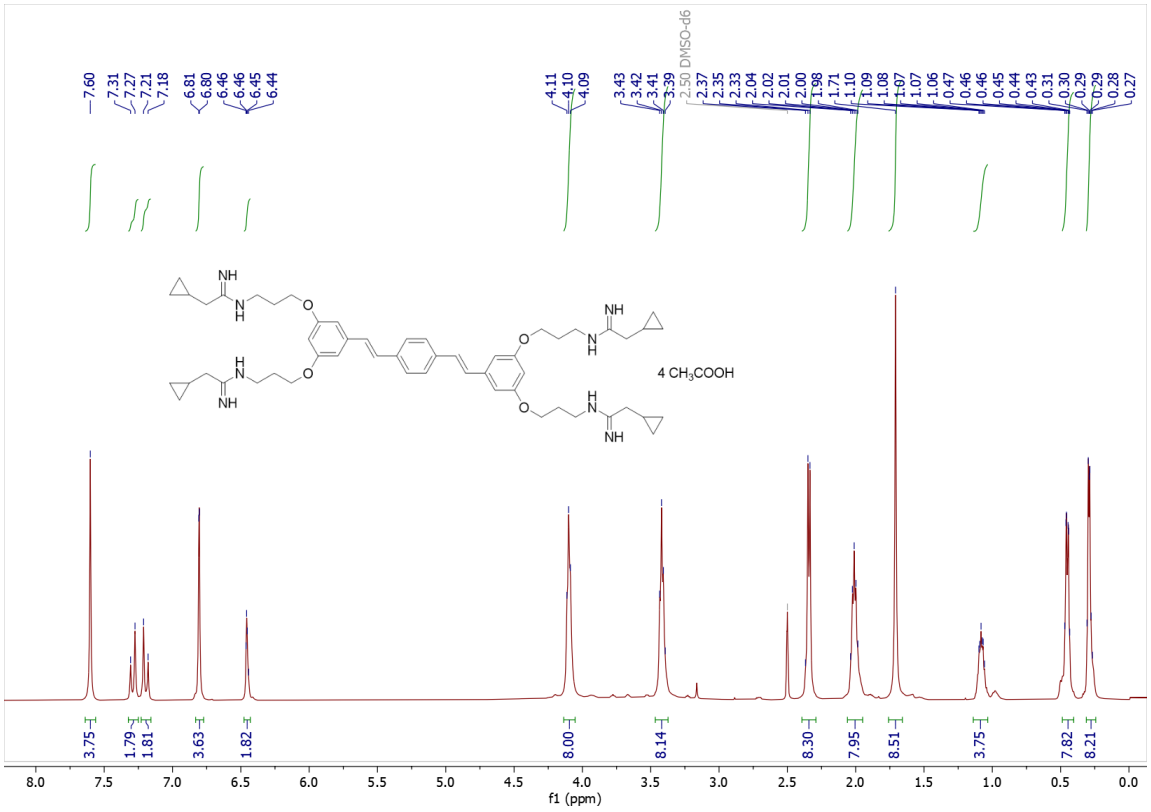
7.60
7.31
7.27
7.21
7.18
6.81
6.80
6.46
6.46
6.45
6.44
4.11
4.10
4.09
3.43
3.42
3.41
3.39
2.50 DMSO-d6
2.37
2.35
2.33
2.04
2.02
2.01
2.00
1.98
1.71
1.10
1.09
1.08
1.07
1.07
1.06
0.47
0.46
0.46
0.45
0.44
0.43
0.31
0.30
0.29
0.29
0.28
0.27
4 CH3COOH
3.75
1.79
1.81
3.63
1.82
8.00
8.14
8.30
7.95
8.51
3.75
7.82
8.21
f1 (ppm)

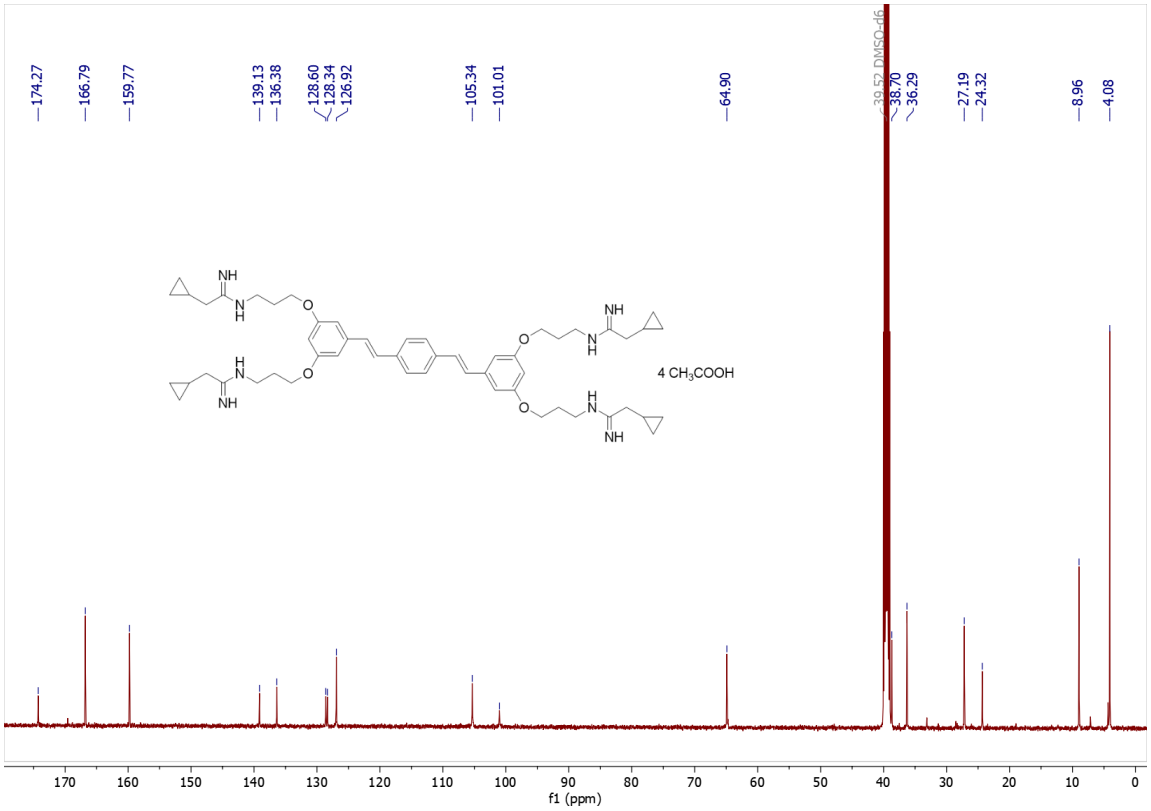
174.27
166.79
159.77
139.13
136.38
128.60
128.34
126.92
105.34
101.01
64.90
39.52 DMSO-d6
38.70
36.29
27.19
24.32
8.96
4.08
4 CH3COOH
f1 (ppm)

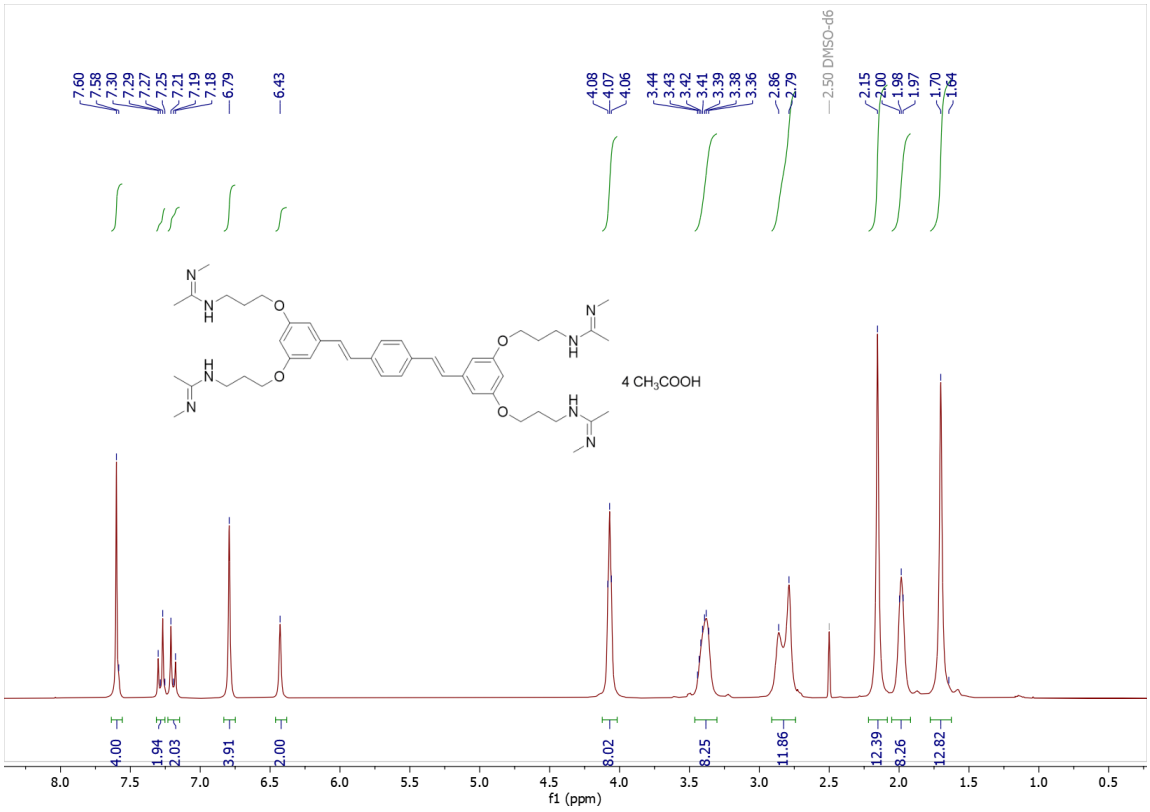
7.60
7.58
7.30
7.29
7.27
7.25
7.21
7.19
7.18
6.79
6.43
4.08
4.07
4.06
3.44
3.43
3.42
3.41
3.39
3.38
3.36
2.86
2.79
2.50 DMSO-d6
2.15
2.00
1.98
1.97
1.70
1.64
4 CH3COOH
4.00
1.94
2.03
3.91
2.00
8.02
8.25
11.86
12.39
8.26
12.82
f1 (ppm)

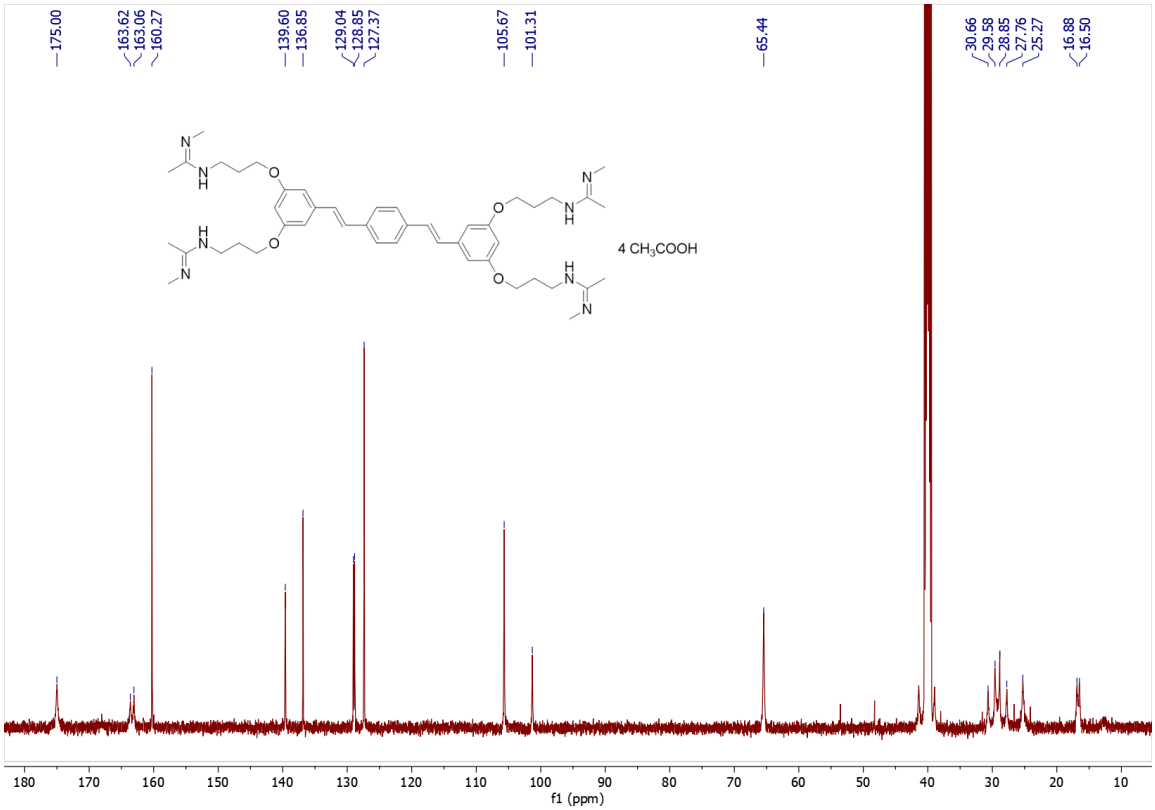
175.00
163.62
163.06
160.27
139.60
136.85
129.04
128.85
127.37
105.67
101.31
65.44
30.66
29.58
28.85
27.76
25.27
16.88
16.50
4 CH3COOH
f1 (ppm)

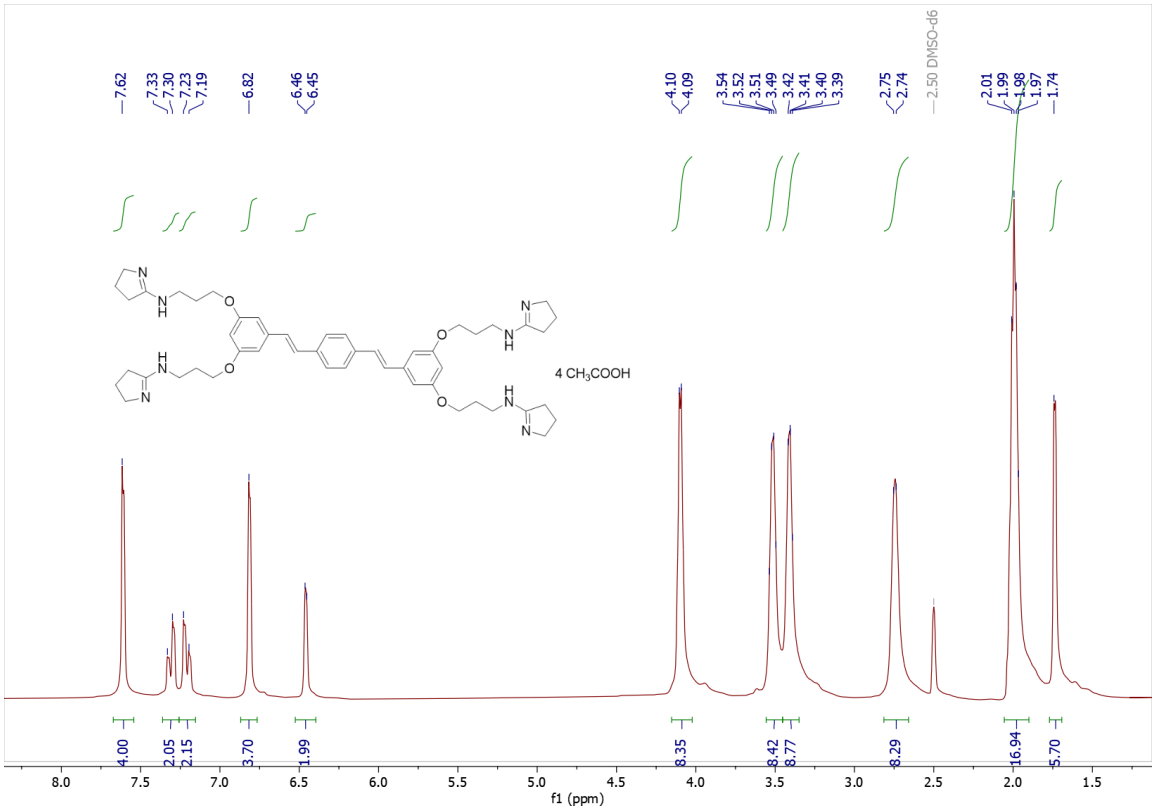
7.62
7.33
7.30
7.23
7.19
6.82
6.46
6.45
4.10
4.09
3.54
3.52
3.51
3.49
3.42
3.41
3.40
3.39
2.75
2.74
2.50 DMSO-d6
2.01
1.99
1.98
1.97
1.74
4 CH3COOH
4.00
2.05
2.15
3.70
1.99
8.35
8.42
8.77
8.29
16.94
5.70
f1 (ppm)

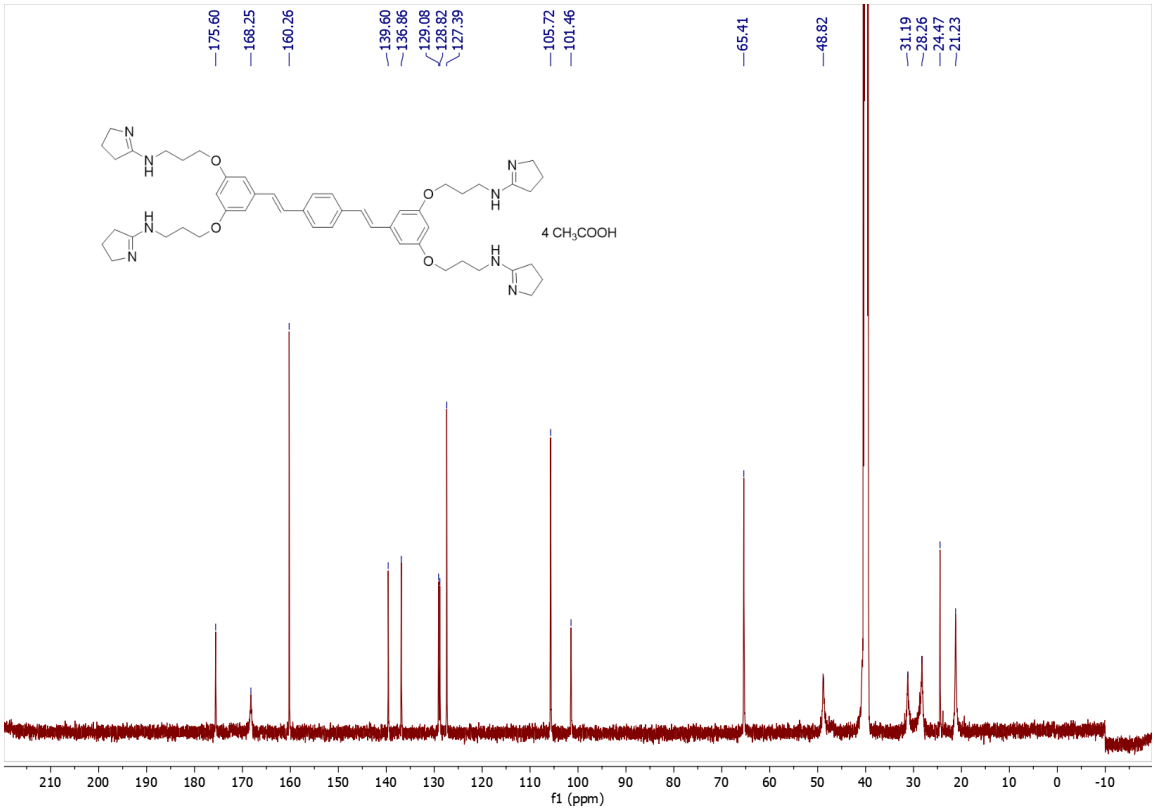
175.60
168.25
160.26
139.60
136.86
129.08
128.82
127.39
105.72
101.46
65.41
48.82
31.19
28.26
24.47
21.23
4 CH3COOH
f1 (ppm)

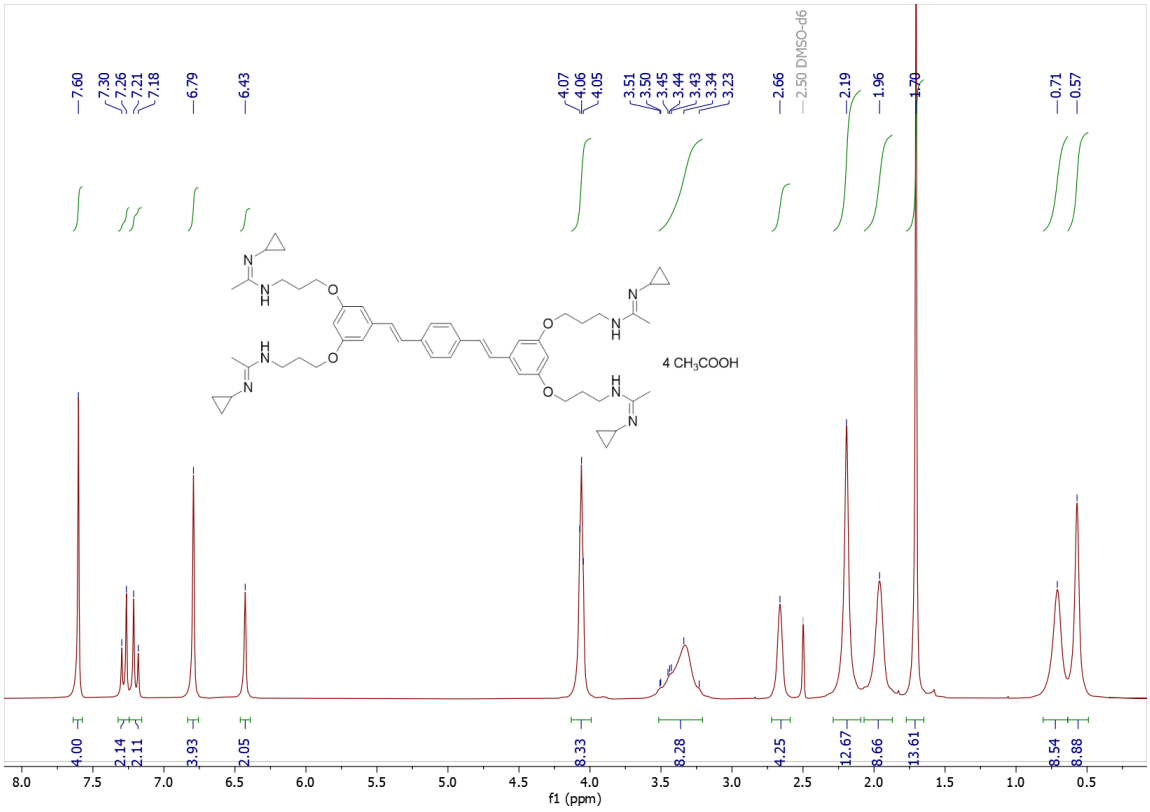
7.60
7.30
7.26
7.21
7.18
6.79
6.43
4.07
4.06
4.05
3.51
3.50
3.45
3.44
3.43
3.34
3.23
2.66
2.50 DMSO-d6
2.19
1.96
1.70
0.71
0.57
4 CH3COOH
4.00
2.14
2.11
3.93
2.05
8.33
8.28
4.25
12.67
8.66
13.61
8.54
8.88
f1 (ppm)

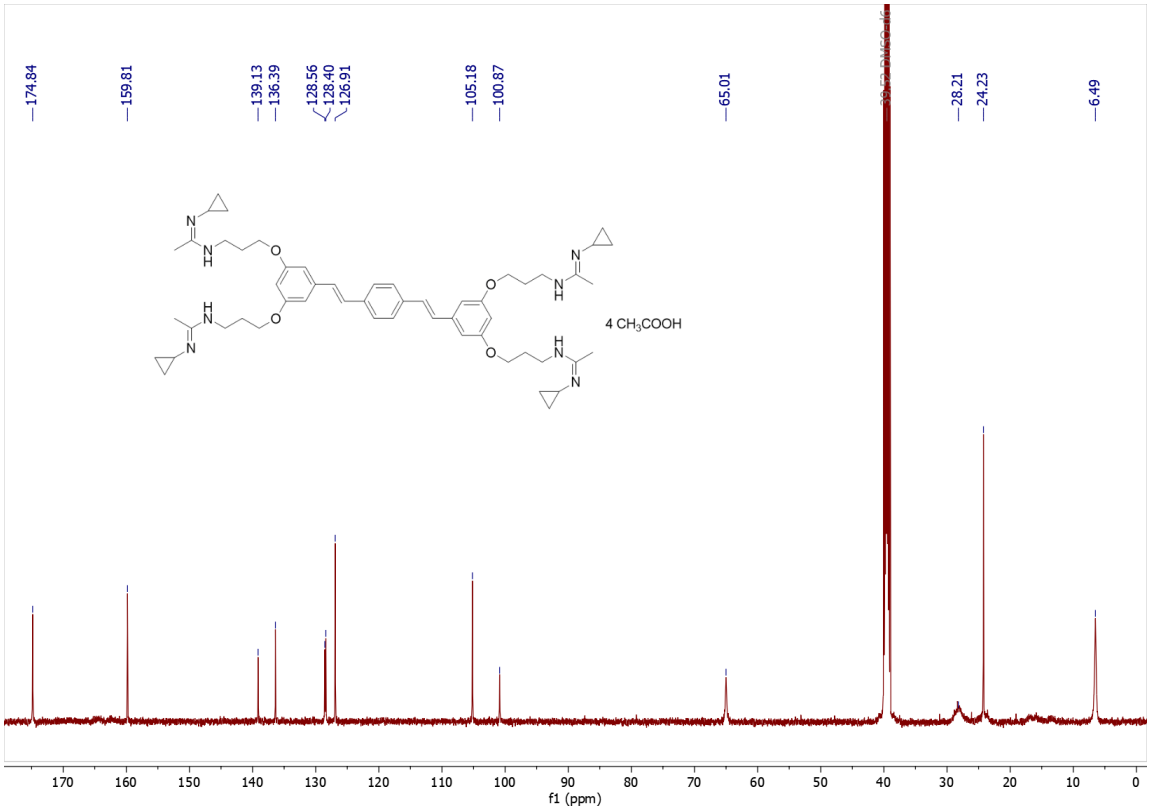
174.84
159.81
139.13
136.39
128.56
128.40
126.91
105.18
100.87
65.01
39.52 DMSO-d6
28.21
24.23
6.49
4 CH3COOH
f1 (ppm)

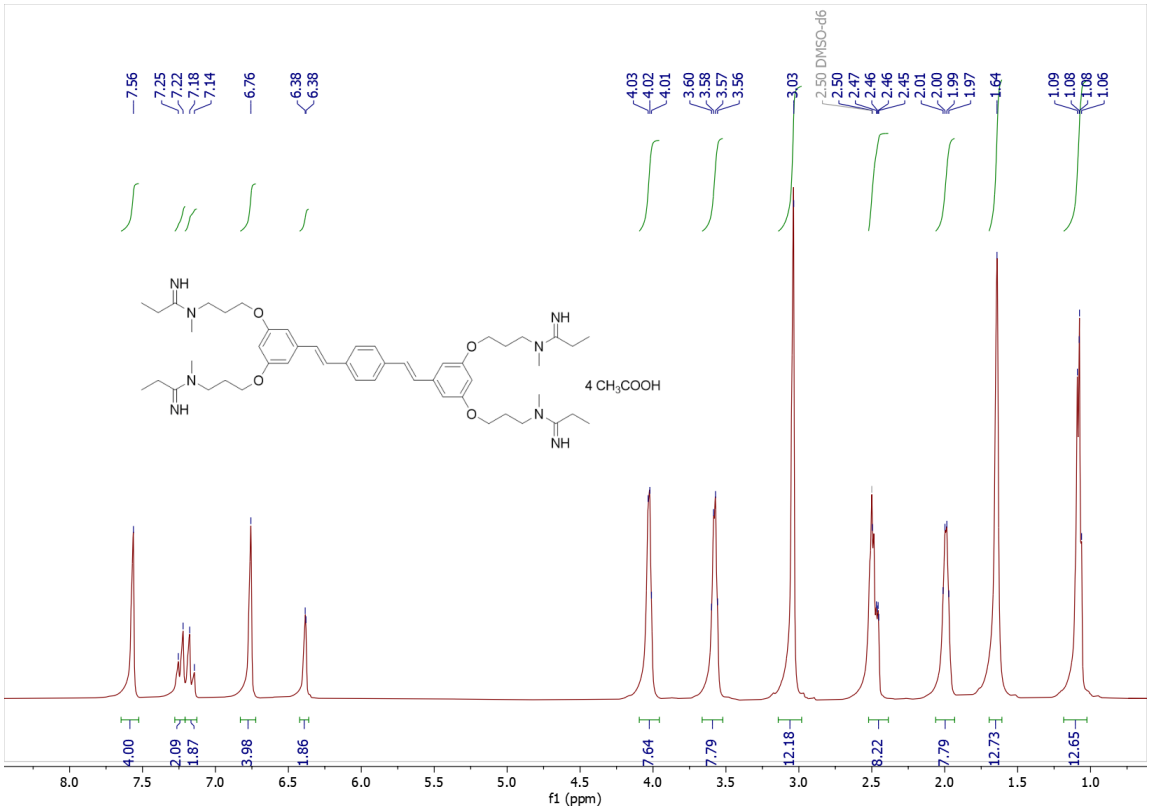
7.56
7.25
7.22
7.18
7.14
6.76
6.38
6.38
4.03
4.02
4.01
3.60
3.58
3.57
3.56
3.03
2.50 DMSO-d6
2.50
2.47
2.46
2.46
2.45
2.01
2.00
1.99
1.97
1.64
1.09
1.08
1.08
1.06
4 CH3COOH
4.00
2.09
1.87
3.98
1.86
7.64
7.79
12.18
8.22
7.79
12.73
12.65
f1 (ppm)

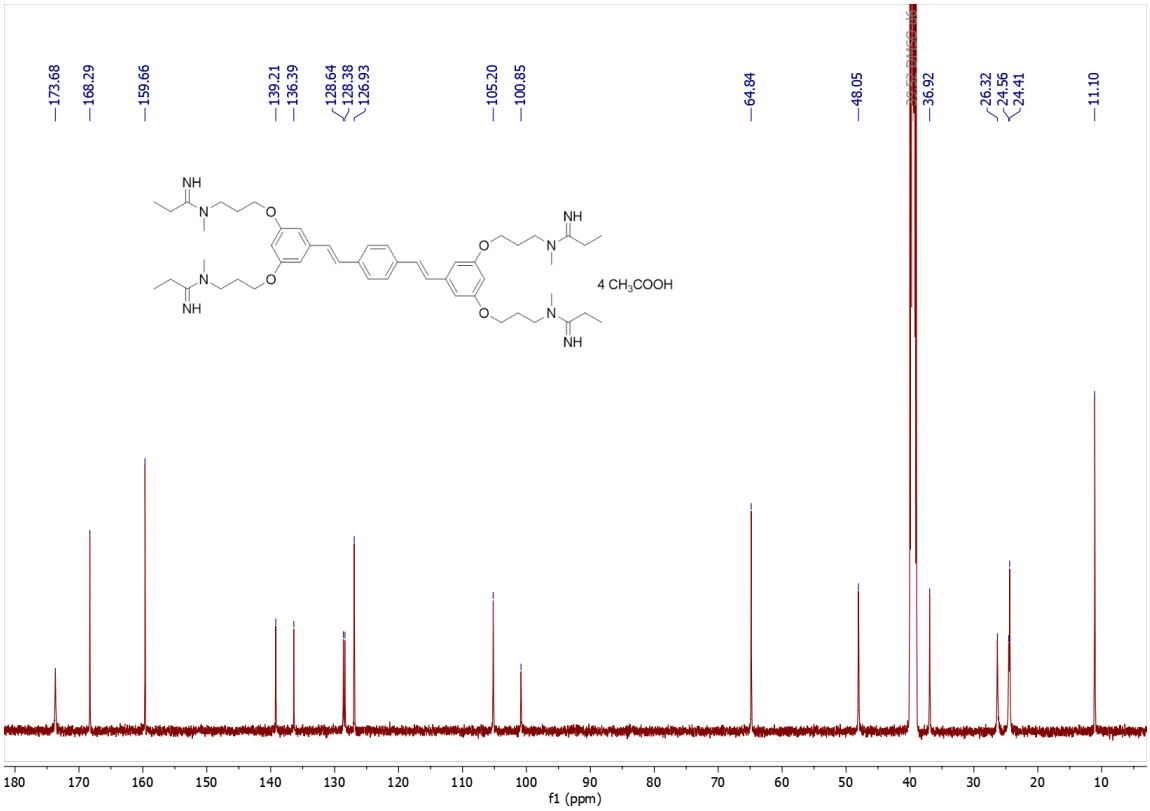
173.68
168.29
159.66
139.21
136.39
128.64
128.38
126.93
105.20
100.85
64.84
48.05
36.92
26.32
24.56
24.41
11.10
4 CH3COOH
f1 (ppm)

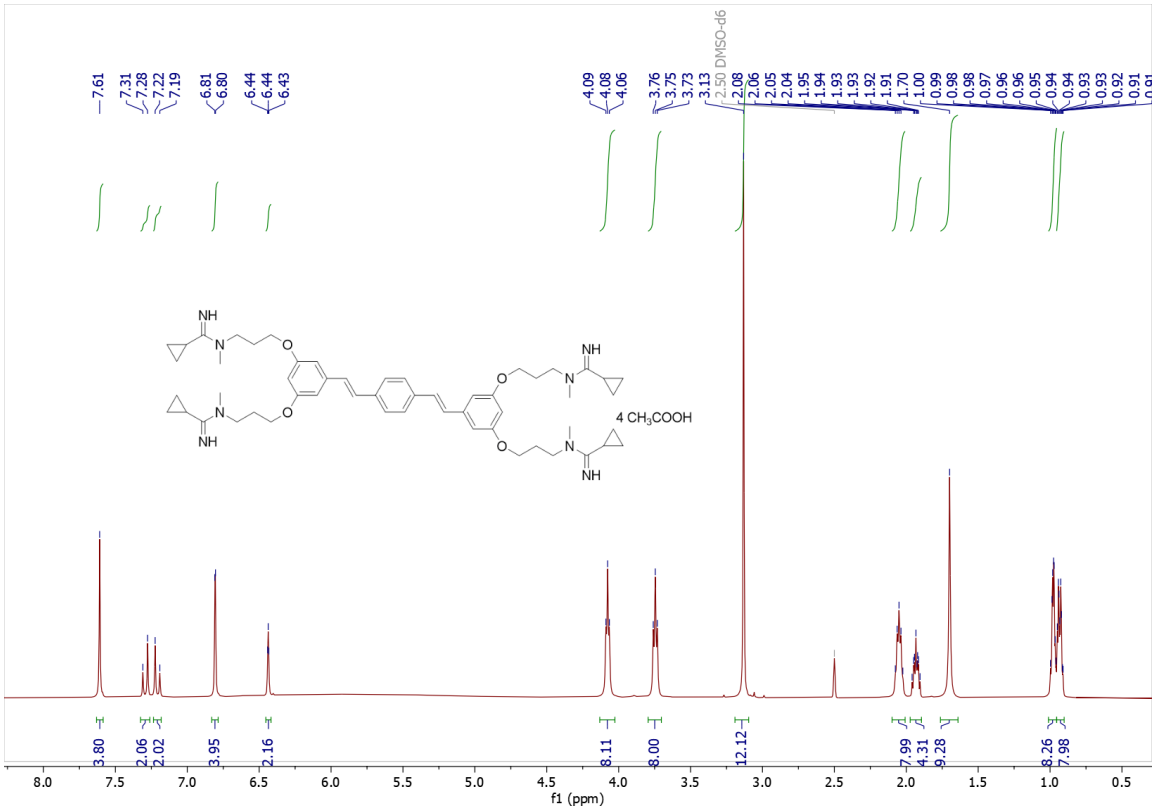
7.61
7.31
7.28
7.22
7.19
6.81
6.80
6.44
6.44
6.43
4.09
4.08
4.06
3.76
3.75
3.73
3.13
2.50 DMSO-d6
2.08
2.06
2.05
2.04
1.95
1.94
1.93
1.93
1.92
1.91
1.70
1.00
0.99
0.98
0.98
0.97
0.96
0.96
0.95
0.94
0.94
0.93
0.93
0.92
0.91
NH
N
O
NH
N
O
NH
N
O
NH
N
O
4 CH3COOH
3.80
2.06
2.02
3.95
2.16
8.11
8.00
12.12
7.99
4.31
9.28
8.26
7.98
8.0
7.5
7.0
6.5
6.0
5.5
5.0
4.5
4.0
3.5
3.0
2.5
2.0
1.5
1.0
0.5
f1 (ppm)

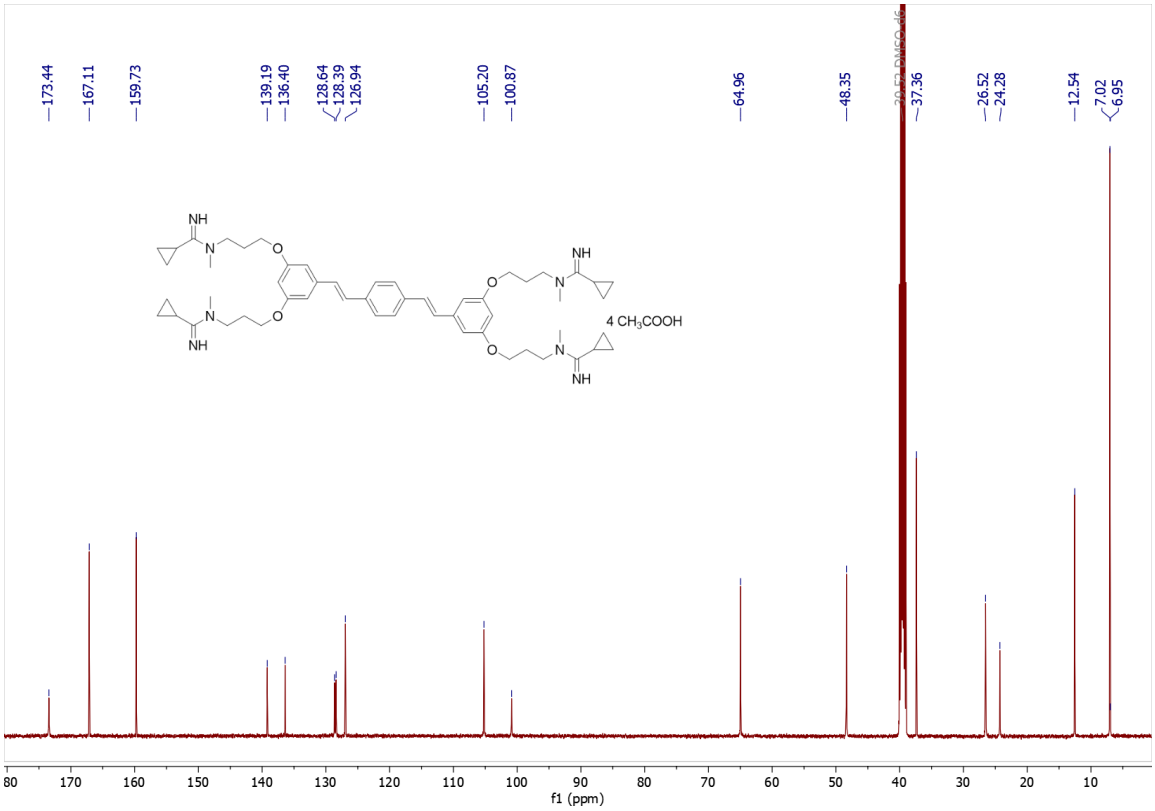
173.44
167.11
159.73
139.19
136.40
128.64
128.39
126.94
105.20
100.87
64.96
48.35
39.51 DMSO-d6
37.36
26.52
24.28
12.54
7.02
6.95
NH
N
O
NH
N
O
NH
N
O
NH
N
O
4 CH3COOH
80
170
160
150
140
130
120
110
100
90
80
70
60
50
40
30
20
10
f1 (ppm)

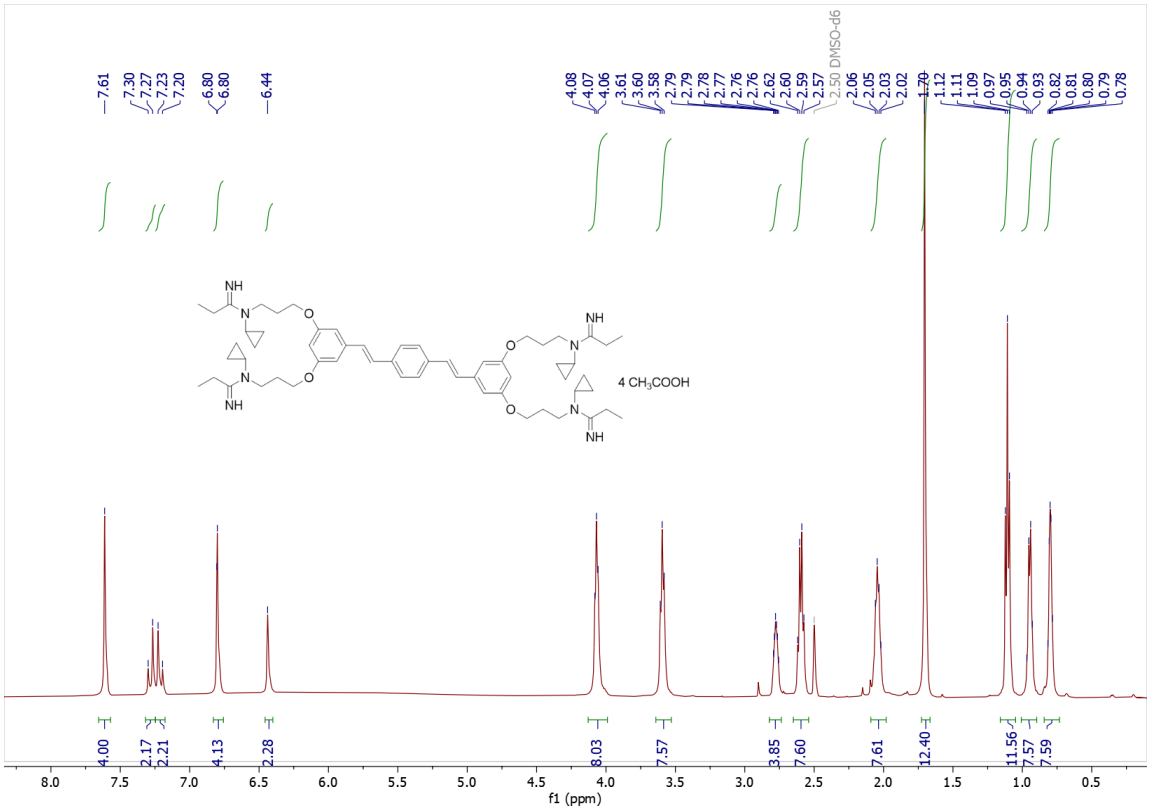
7.61
7.30
7.27
7.23
7.20
6.80
6.80
6.44
4.08
4.07
4.06
3.61
3.60
3.58
2.79
2.79
2.78
2.77
2.76
2.76
2.62
2.60
2.59
2.57
2.50 DMSO-d6
2.06
2.05
2.03
2.02
1.70
1.12
1.11
1.09
0.97
0.95
0.94
0.93
0.82
0.81
0.80
0.79
0.78
4 CH3COOH
4.00
2.17
2.21
4.13
2.28
8.03
7.57
3.85
7.60
7.61
12.40
11.56
7.57
7.59
f1 (ppm)

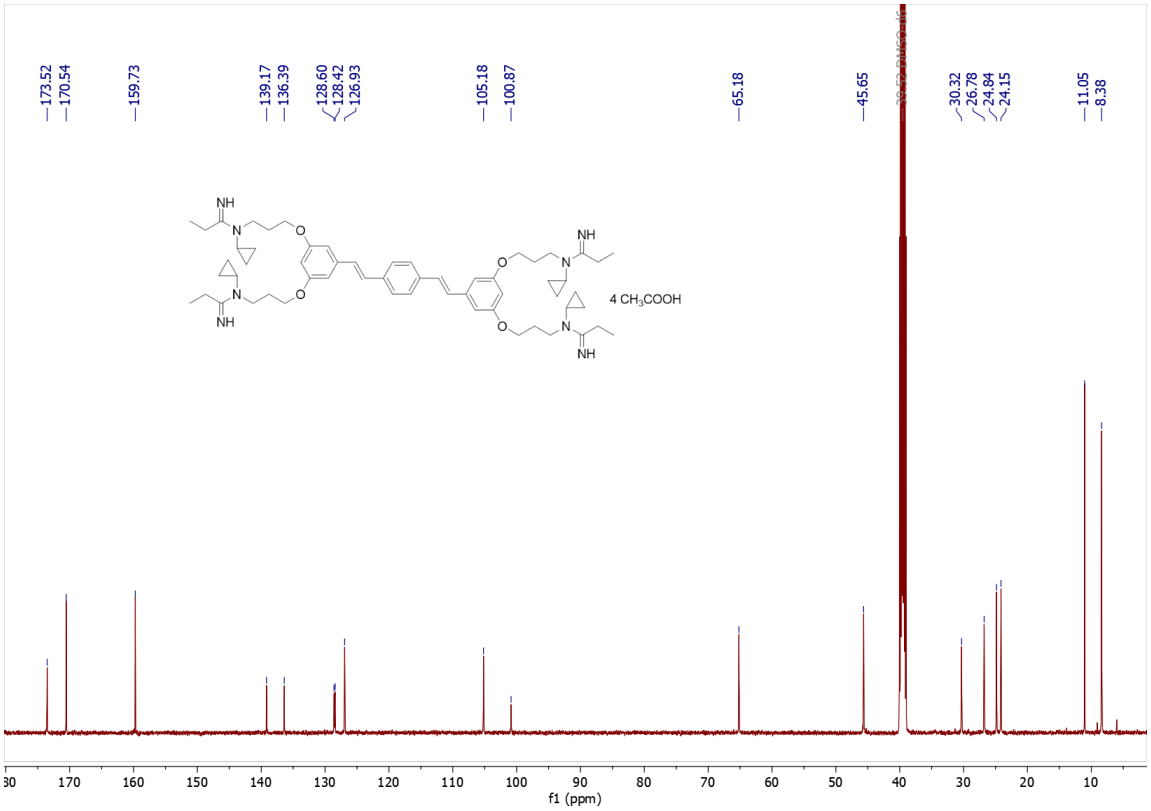
173.52
170.54
159.73
139.17
136.39
128.60
128.42
126.93
105.18
100.87
65.18
45.65
39.51 DMSO-d6
30.32
26.78
24.84
24.15
11.05
8.38
4 CH3COOH
f1 (ppm)

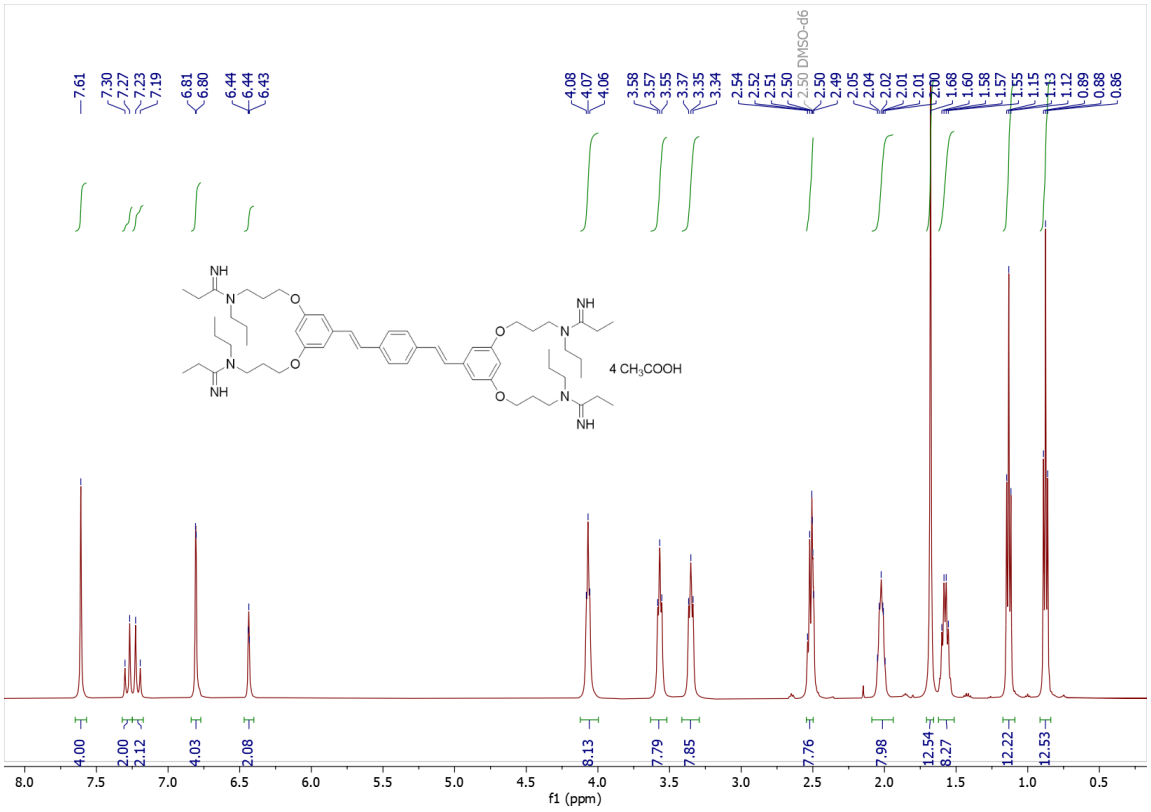
7.61
7.30
7.27
7.23
7.19
6.81
6.80
6.44
6.44
6.43
4.08
4.07
4.06
3.58
3.57
3.55
3.37
3.35
3.34
2.54
2.52
2.51
2.50 DMSO-d6
2.50
2.49
2.05
2.04
2.02
2.01
2.01
2.00
1.68
1.60
1.58
1.57
1.55
1.15
1.13
1.12
0.89
0.88
0.86
4 CH3COOH
4.00
2.00
2.12
4.03
2.08
8.13
7.79
7.85
7.76
7.98
12.54
8.27
12.22
12.53
f1 (ppm)

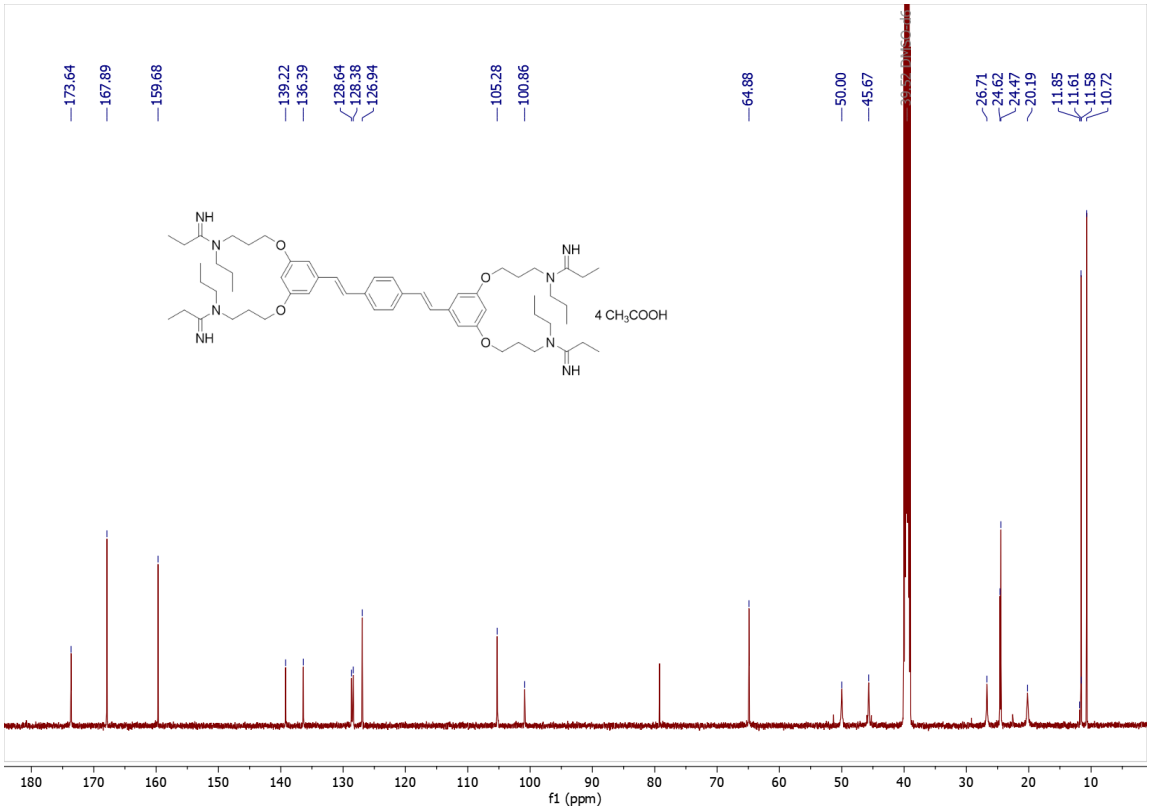
173.64
167.89
159.68
139.22
136.39
128.64
128.38
126.94
105.28
100.86
64.88
50.00
45.67
39.52 DMSO-d6
26.71
24.62
24.47
20.19
11.85
11.61
11.58
10.72
4 CH3COOH
f1 (ppm)

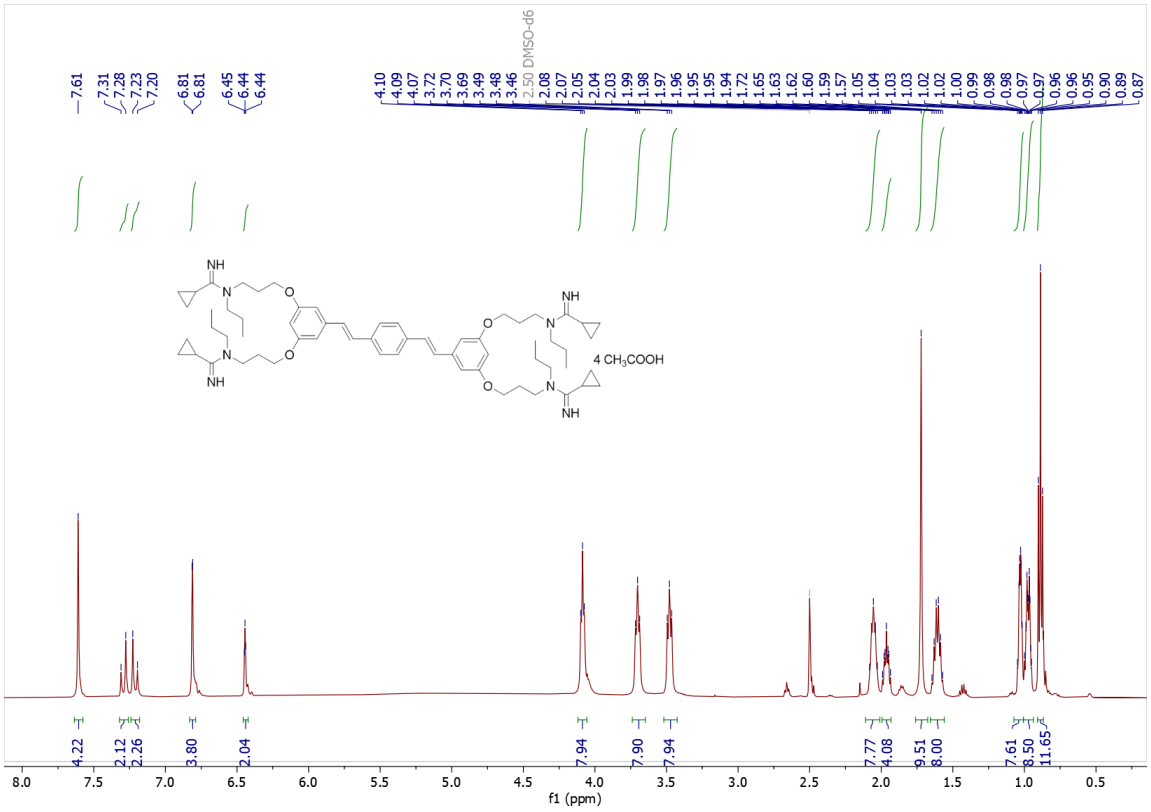
7.61
7.31
7.28
7.23
7.20
6.81
6.81
6.45
6.44
6.44
4.10
4.09
4.07
3.72
3.70
3.69
3.49
3.48
3.46
2.50 DMSO-d6
2.08
2.07
2.05
2.04
2.03
1.99
1.98
1.97
1.96
1.95
1.95
1.94
1.72
1.65
1.63
1.62
1.60
1.59
1.57
1.05
1.04
1.03
1.03
1.02
1.02
1.00
0.99
0.98
0.98
0.97
0.97
0.96
0.96
0.95
0.90
0.89
0.87
NH
NH
NH
NH
4 CH3COOH
4.22
2.12
2.26
3.80
2.04
7.94
7.90
7.94
7.77
4.08
9.51
8.00
7.61
8.50
11.65
8.0
7.5
7.0
6.5
6.0
5.5
5.0
4.5
4.0
3.5
3.0
2.5
2.0
1.5
1.0
0.5
f1 (ppm)

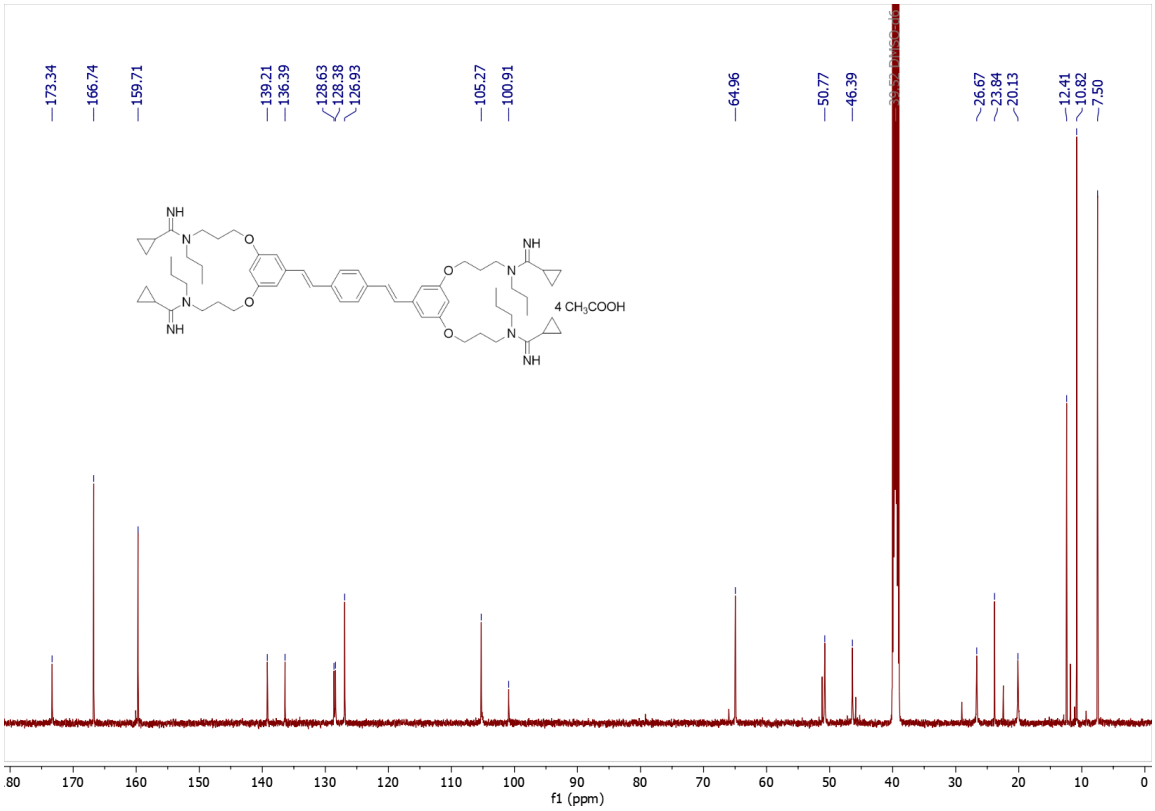
173.34
166.74
159.71
139.21
136.39
128.63
128.38
126.93
105.27
100.91
64.96
50.77
46.39
39.52 DMSO-d6
26.67
23.84
20.13
12.41
10.82
7.50
NH
NH
NH
NH
4 CH3COOH
80
170
160
150
140
130
120
110
100
90
80
70
60
50
40
30
20
10
0
f1 (ppm)

Chapter 6

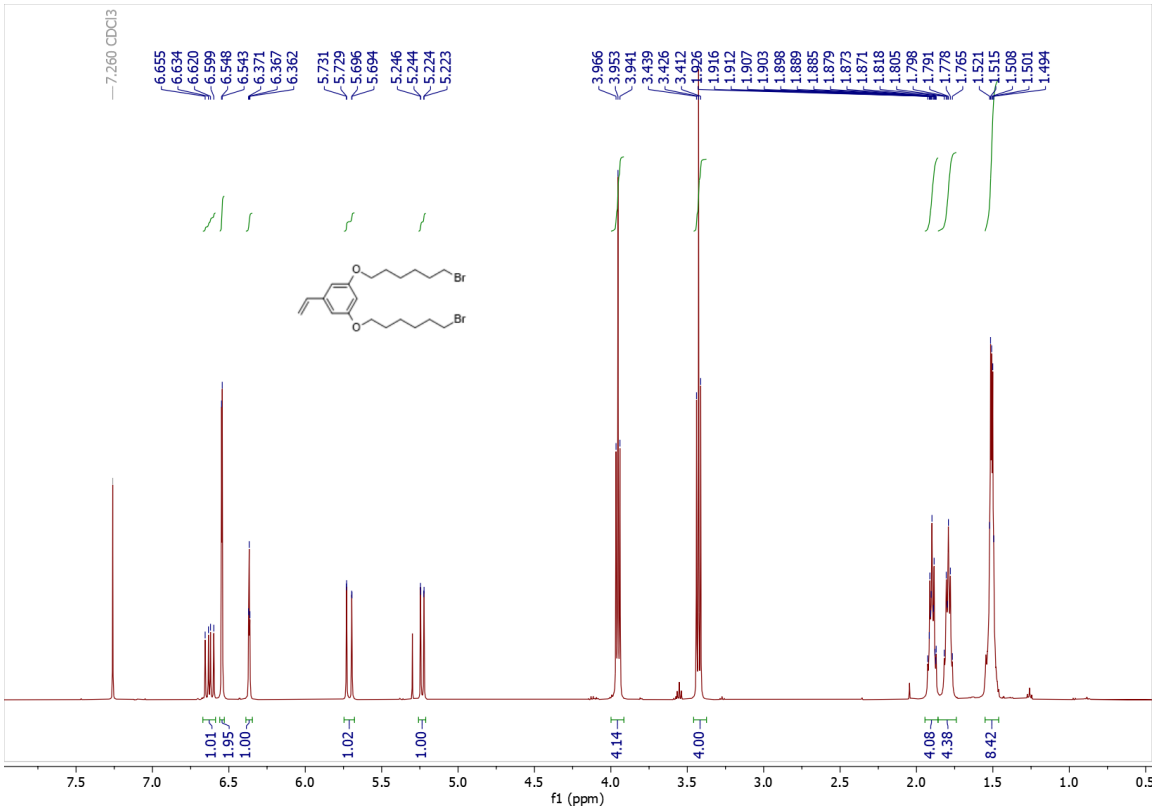
7.260 CDCl3
6.655
6.634
6.620
6.599
6.548
6.543
6.371
6.367
6.362
5.731
5.729
5.696
5.694
5.246
5.244
5.224
5.223
3.966
3.953
3.941
3.439
3.426
3.412
1.926
1.916
1.912
1.907
1.903
1.898
1.889
1.885
1.879
1.873
1.871
1.818
1.805
1.798
1.791
1.778
1.765
1.521
1.515
1.508
1.501
1.494
Br
Br
1.01
1.95
1.00
1.02
1.00
4.14
4.00
4.08
4.38
8.42
7.5
7.0
6.5
6.0
5.5
5.0
4.5
4.0
3.5
3.0
2.5
2.0
1.5
1.0
0.5
f1 (ppm)

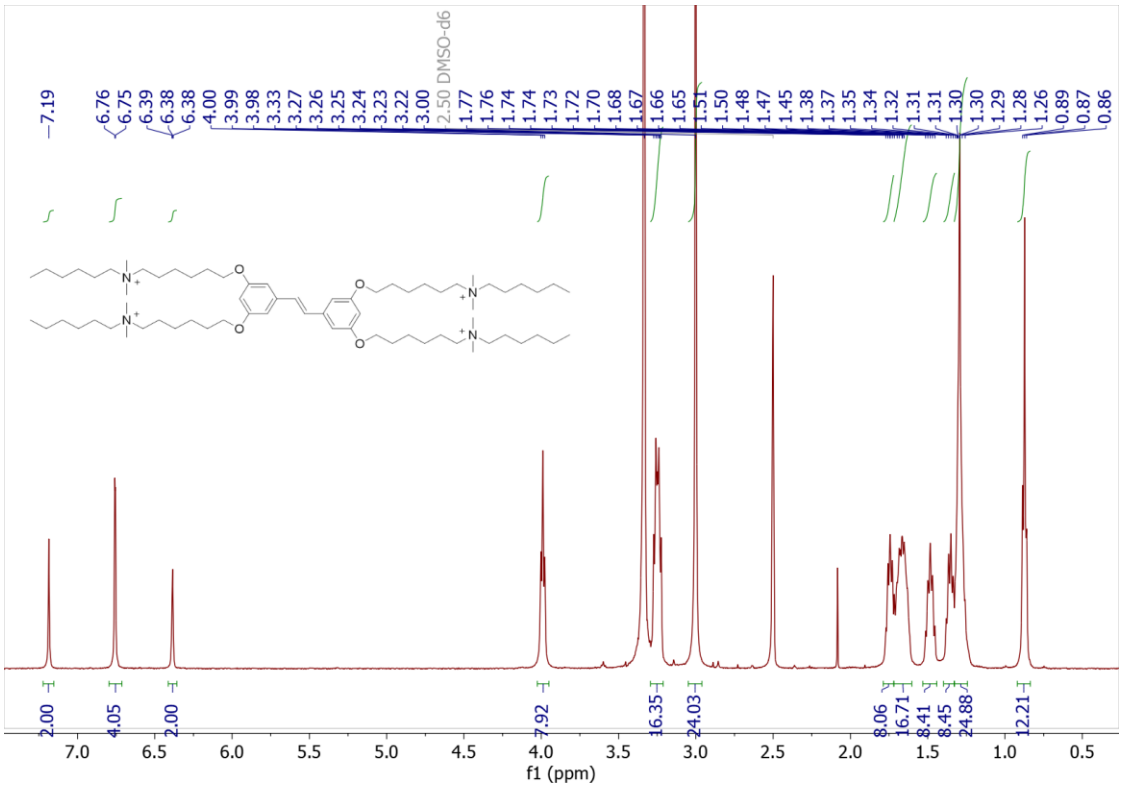
7.19
6.76
6.75
6.39
6.38
6.38
4.00
3.99
3.98
3.33
3.27
3.26
3.25
3.24
3.23
3.22
3.00
2.50 DMSO-d6
1.77
1.76
1.74
1.74
1.73
1.72
1.70
1.68
1.67
1.66
1.65
1.51
1.50
1.48
1.47
1.45
1.38
1.37
1.35
1.34
1.32
1.31
1.31
1.30
1.30
1.29
1.28
1.26
0.89
0.87
0.86
2.00
4.05
2.00
7.92
16.35
24.03
8.06
16.71
8.41
8.45
24.88
12.21
f1 (ppm)

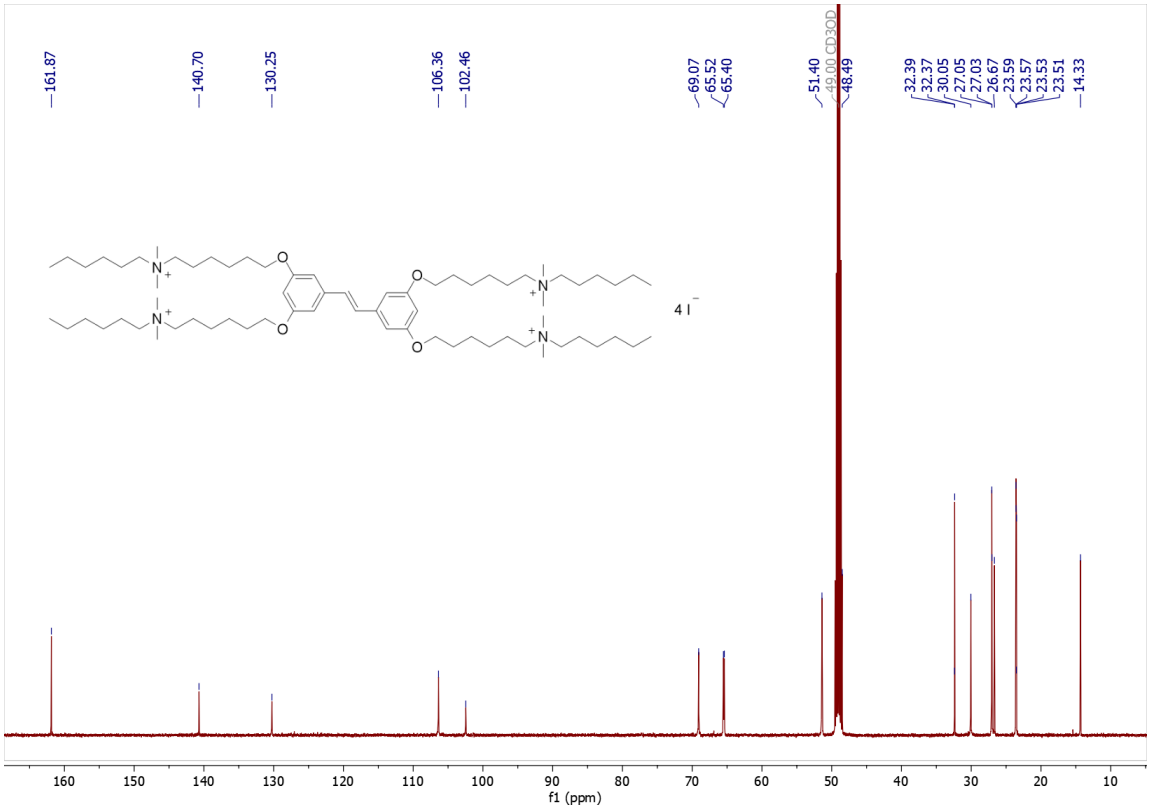
161.87
140.70
130.25
106.36
102.46
69.07
65.52
65.40
51.40
49.00 CD3OD
48.49
32.39
32.37
30.05
27.05
27.03
26.67
23.59
23.57
23.53
23.51
14.33
4 I⁻
f1 (ppm)

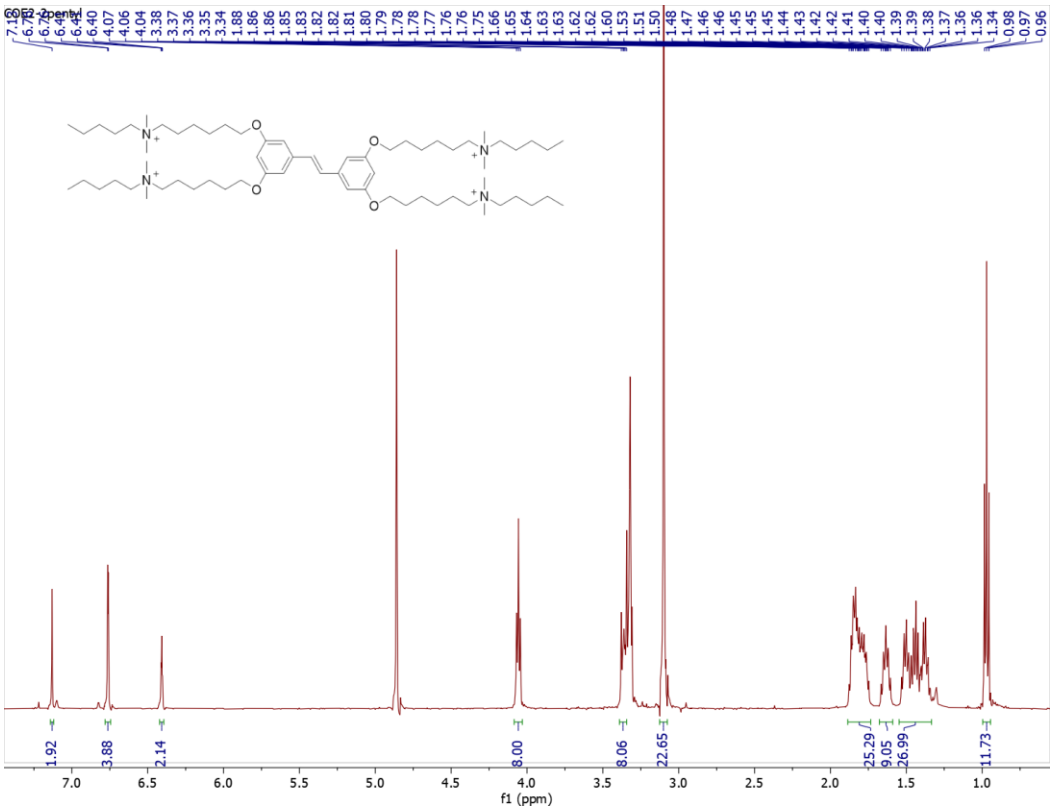
COE2-2pentyl
1.92
3.88
2.14
8.00
8.06
22.65
25.29
9.05
26.99
11.73
f1 (ppm)

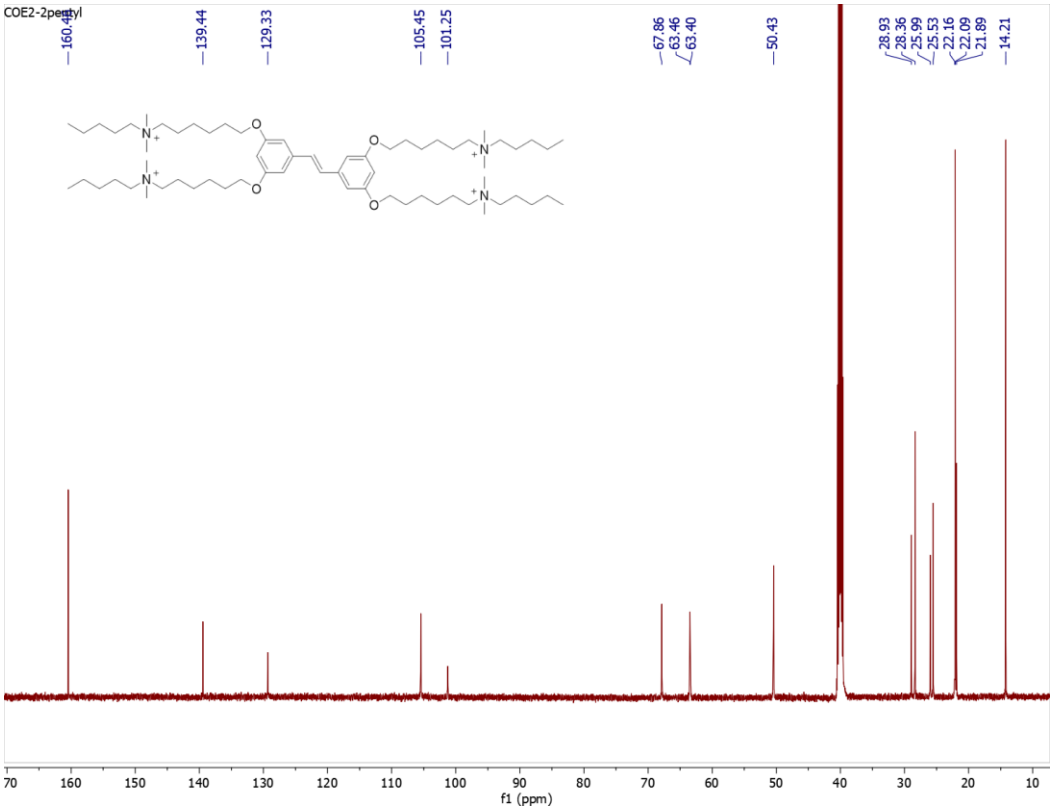
COE2-2pentyl
160.44
139.44
129.33
105.45
101.25
67.86
63.46
63.40
50.43
28.93
28.36
25.99
25.53
22.16
22.09
21.89
14.21
f1 (ppm)

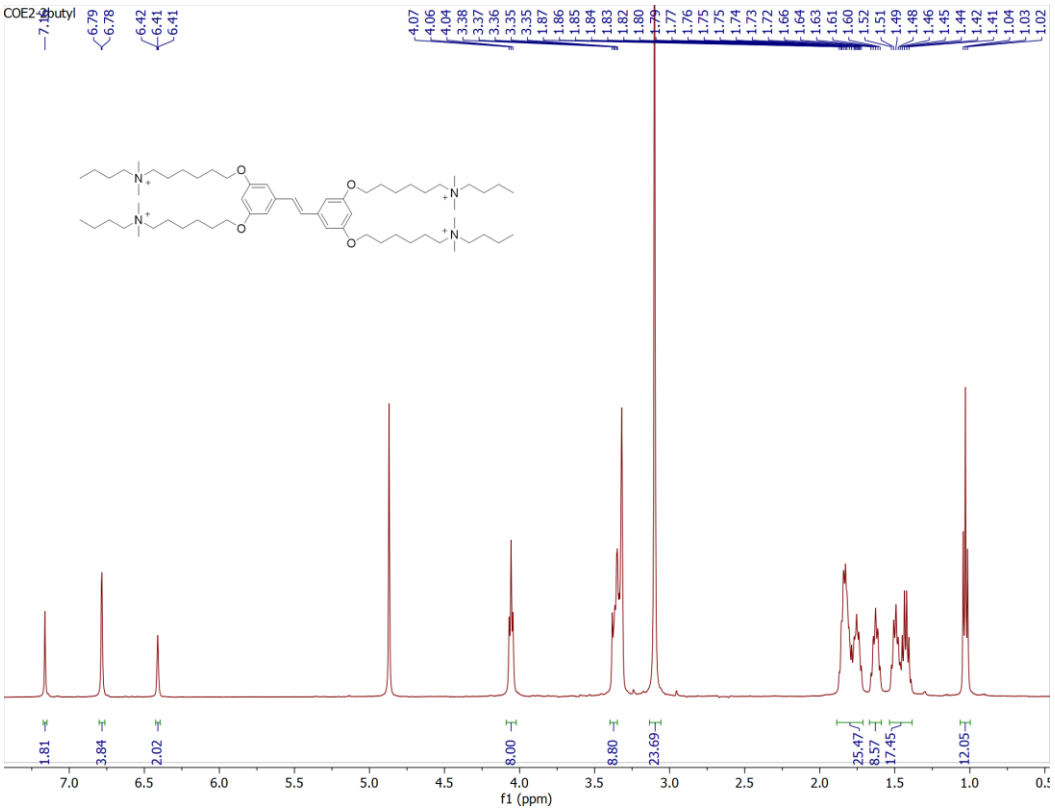
COE2-2butyl
7.41
6.79
6.78
6.42
6.41
6.41
4.07
4.06
4.04
3.38
3.37
3.36
3.35
3.35
1.87
1.86
1.85
1.84
1.83
1.82
1.80
1.79
1.77
1.76
1.75
1.75
1.74
1.73
1.72
1.66
1.64
1.63
1.61
1.60
1.52
1.51
1.49
1.48
1.46
1.45
1.44
1.42
1.41
1.04
1.03
1.02
1.81
3.84
2.02
8.00
8.80
23.69
25.47
8.57
17.45
12.05
7.0
6.5
6.0
5.5
5.0
4.5
4.0
3.5
3.0
2.5
2.0
1.5
1.0
f1 (ppm)

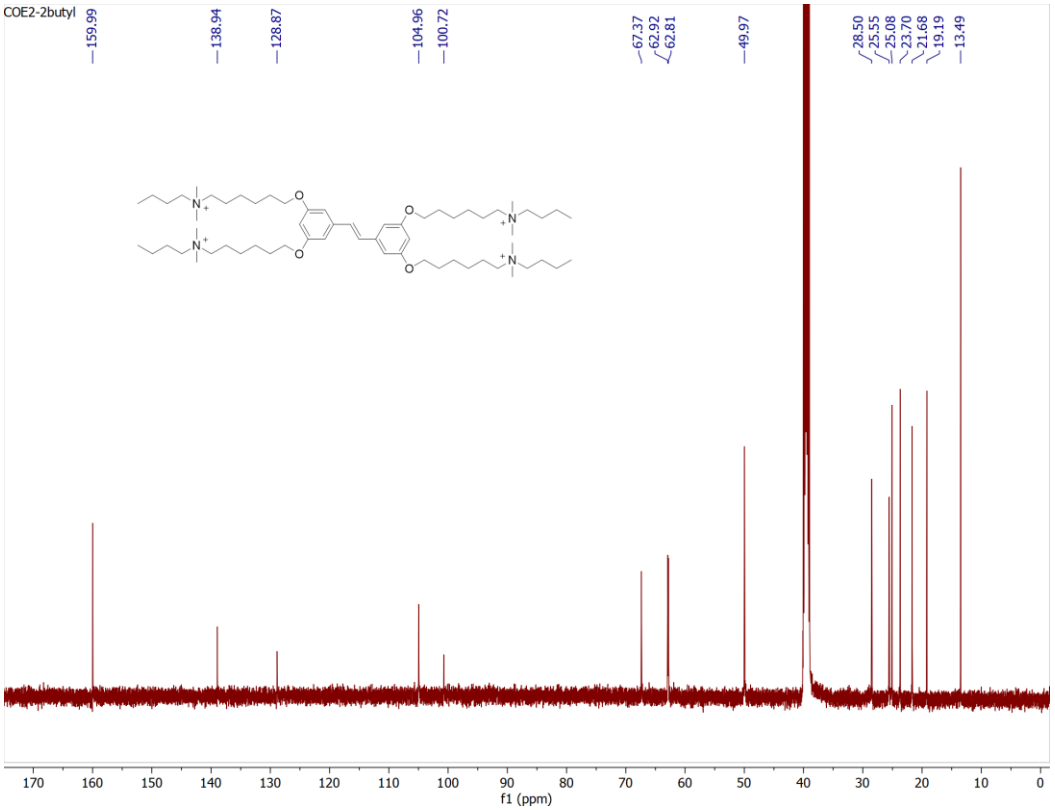
COE2-2butyl
159.99
138.94
128.87
104.96
100.72
67.37
62.92
62.81
49.97
28.50
25.55
25.08
23.70
21.68
19.19
13.49
170
160
150
140
130
120
110
100
90
80
70
60
50
40
30
20
10
0
f1 (ppm)

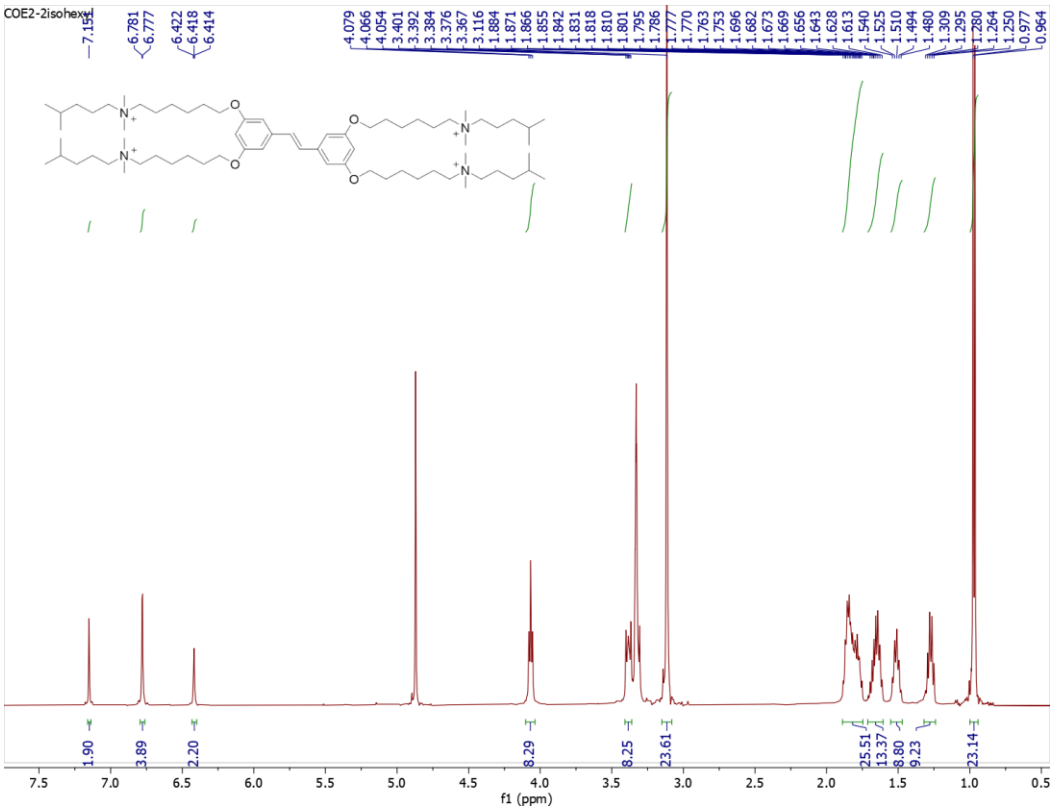
COE2-2isohexyl
7.151
6.781
6.777
6.422
6.418
6.414
4.079
4.066
4.054
3.401
3.392
3.384
3.376
3.367
3.116
1.884
1.871
1.866
1.855
1.842
1.831
1.818
1.810
1.801
1.795
1.786
1.777
1.770
1.763
1.753
1.696
1.682
1.673
1.669
1.656
1.643
1.628
1.613
1.540
1.525
1.510
1.494
1.480
1.309
1.295
1.280
1.264
1.250
0.977
0.964
1.90
3.89
2.20
8.29
8.25
23.61
25.51
13.37
8.80
9.23
23.14
f1 (ppm)

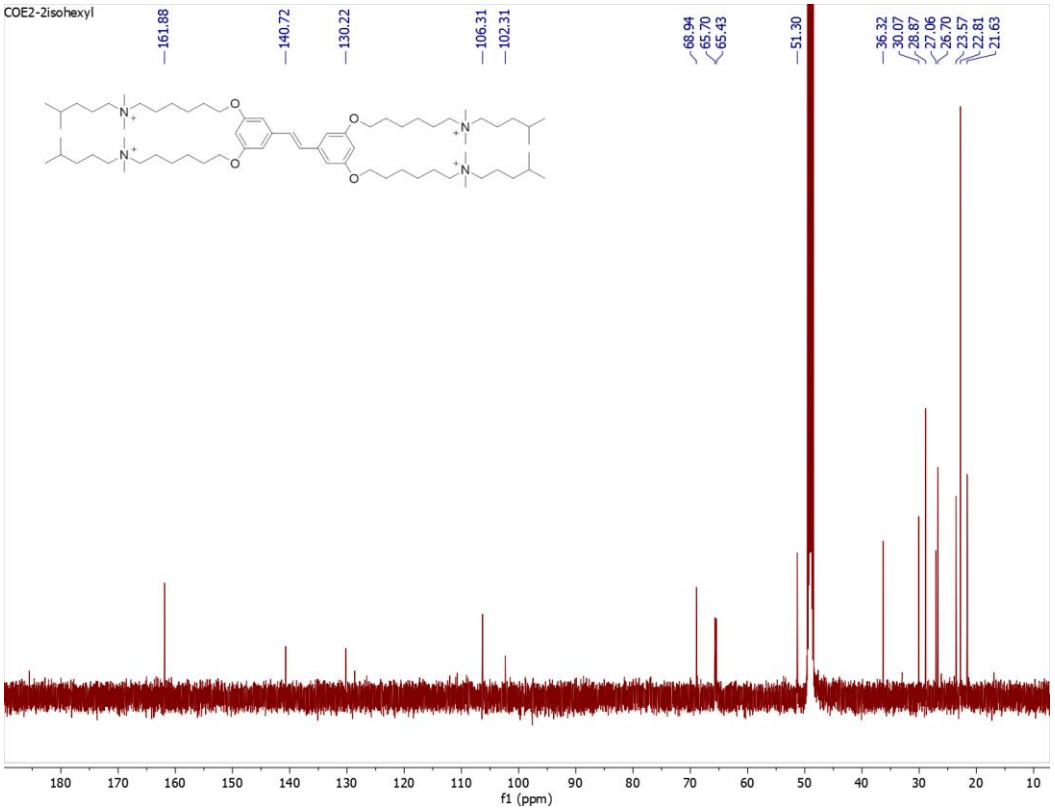
COE2-2isohexyl
161.88
140.72
130.22
106.31
102.31
68.94
65.70
65.43
51.30
36.32
30.07
28.87
27.06
26.70
23.57
22.81
21.63
f1 (ppm)

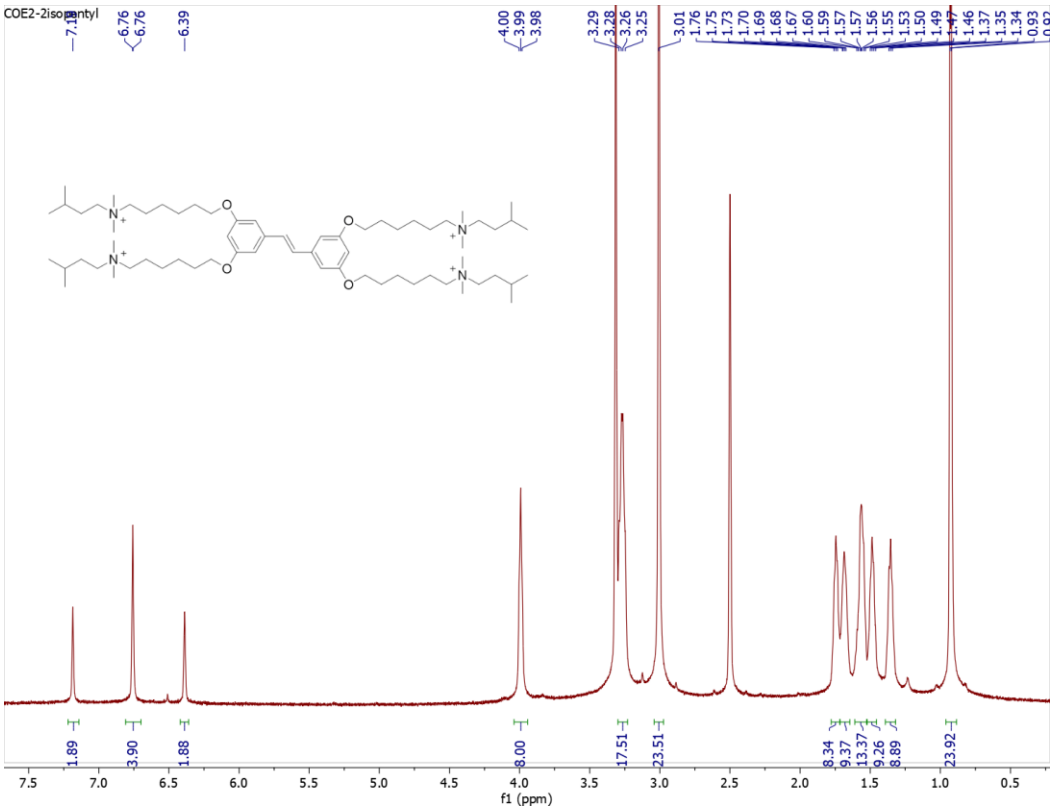
COE2-2isopentyl
f1 (ppm)

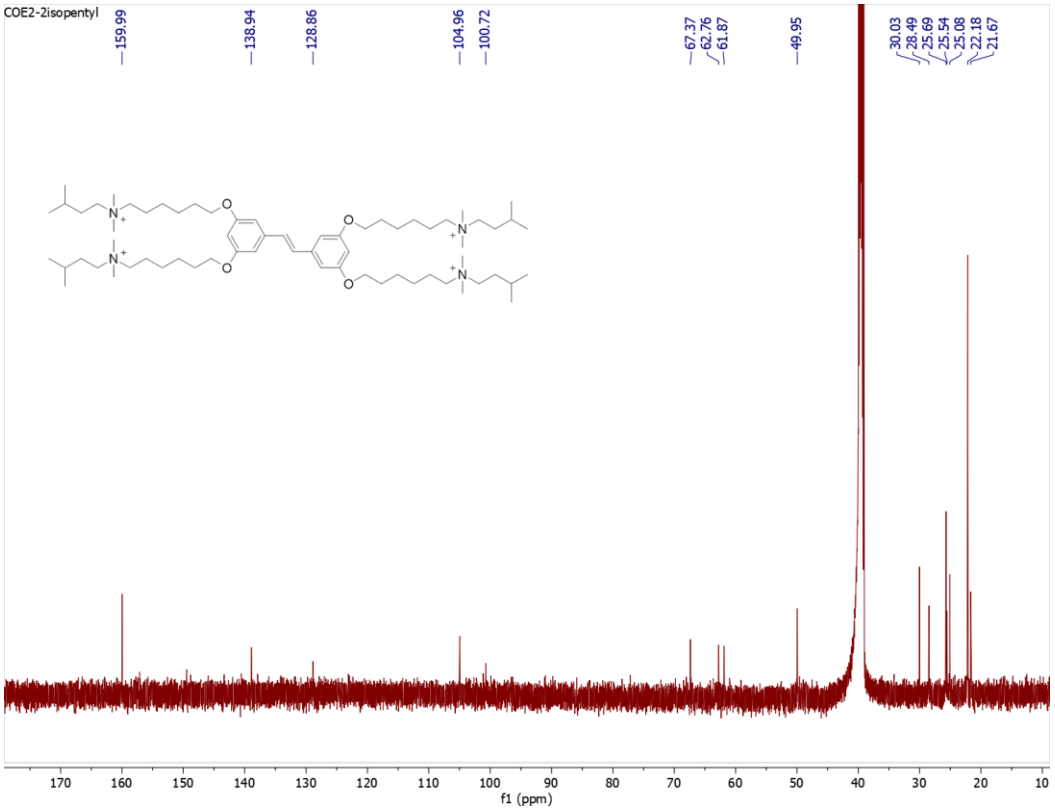
COE2-2isopentyl
f1 (ppm)

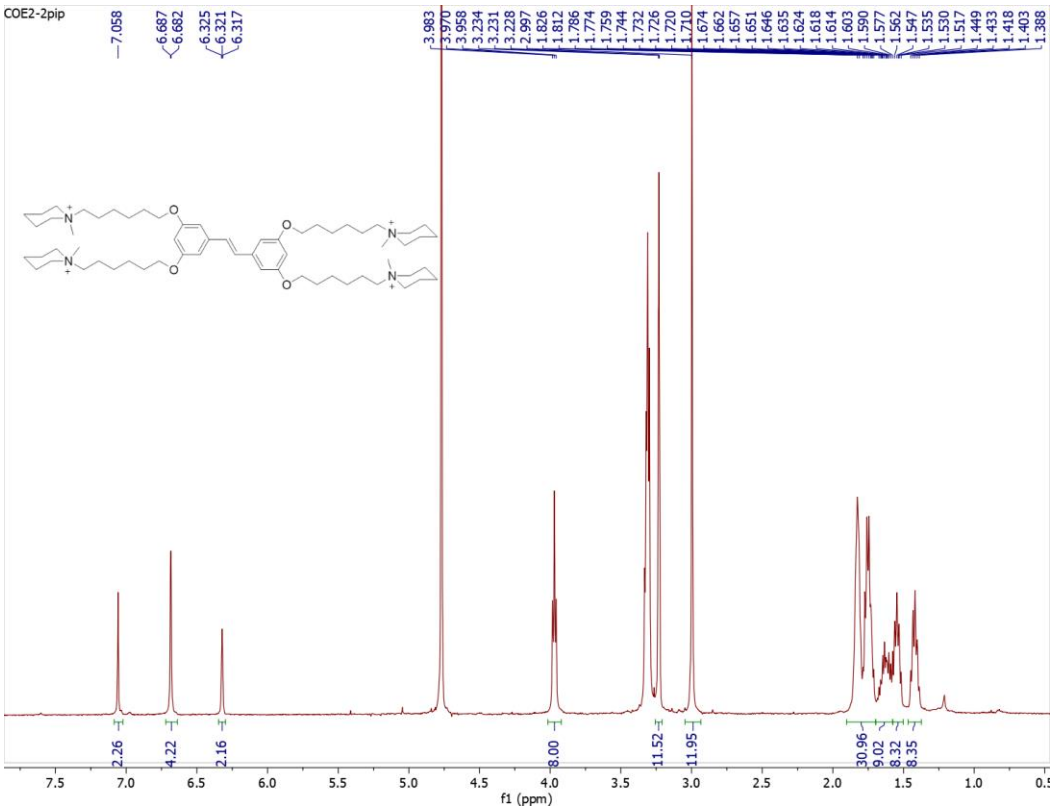
COE2-2pip
7.058
6.687
6.682
6.325
6.321
6.317
3.983
3.970
3.958
3.234
3.231
3.228
2.997
1.826
1.812
1.786
1.774
1.759
1.744
1.732
1.726
1.720
1.710
1.674
1.662
1.657
1.651
1.646
1.635
1.624
1.618
1.614
1.603
1.590
1.577
1.562
1.547
1.535
1.530
1.517
1.449
1.433
1.418
1.403
1.388
2.26
4.22
2.16
8.00
11.52
11.95
30.96
9.02
8.32
8.35
f1 (ppm)

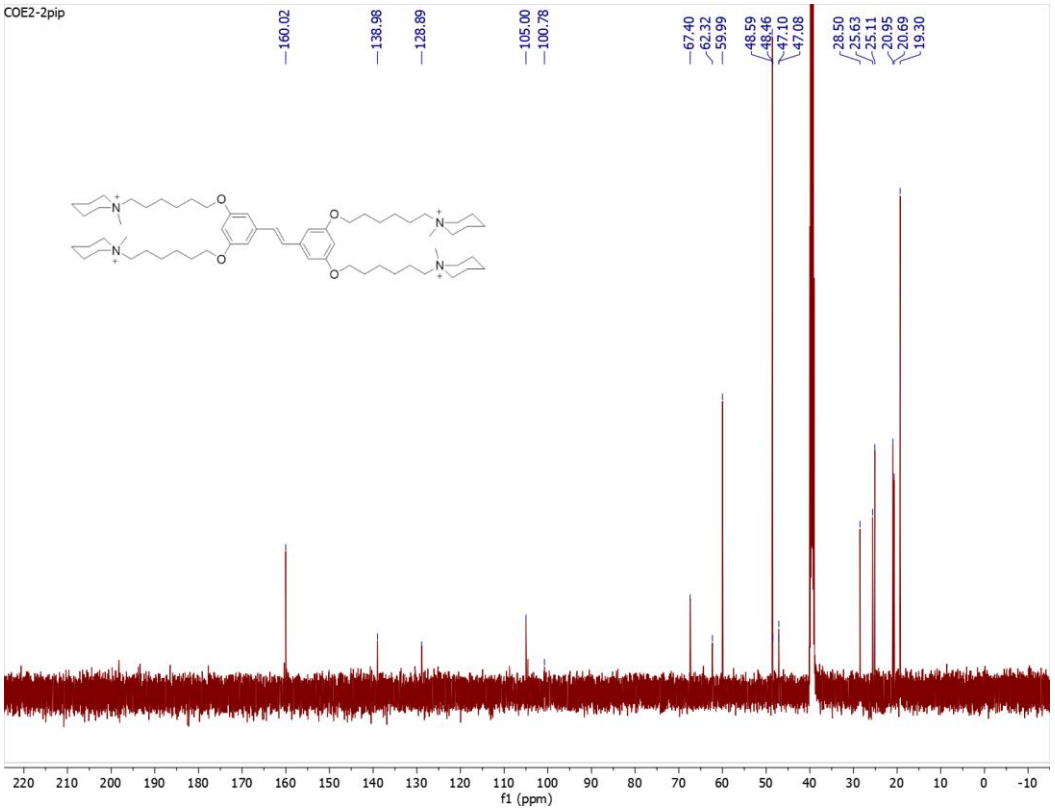
COE2-2pip
160.02
138.98
128.89
105.00
100.78
67.40
62.32
59.99
48.59
48.46
47.10
47.08
28.50
25.63
25.11
20.95
20.69
19.30
f1 (ppm)

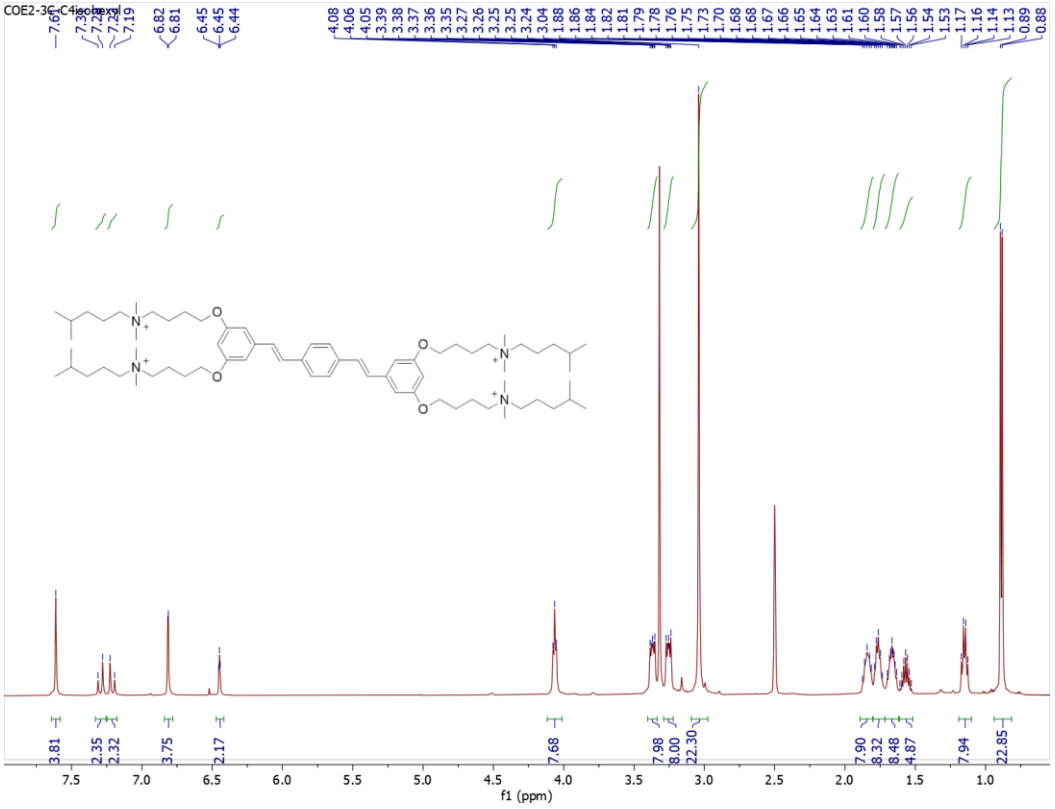
COE2-3C-C4isohexyl
f1 (ppm)

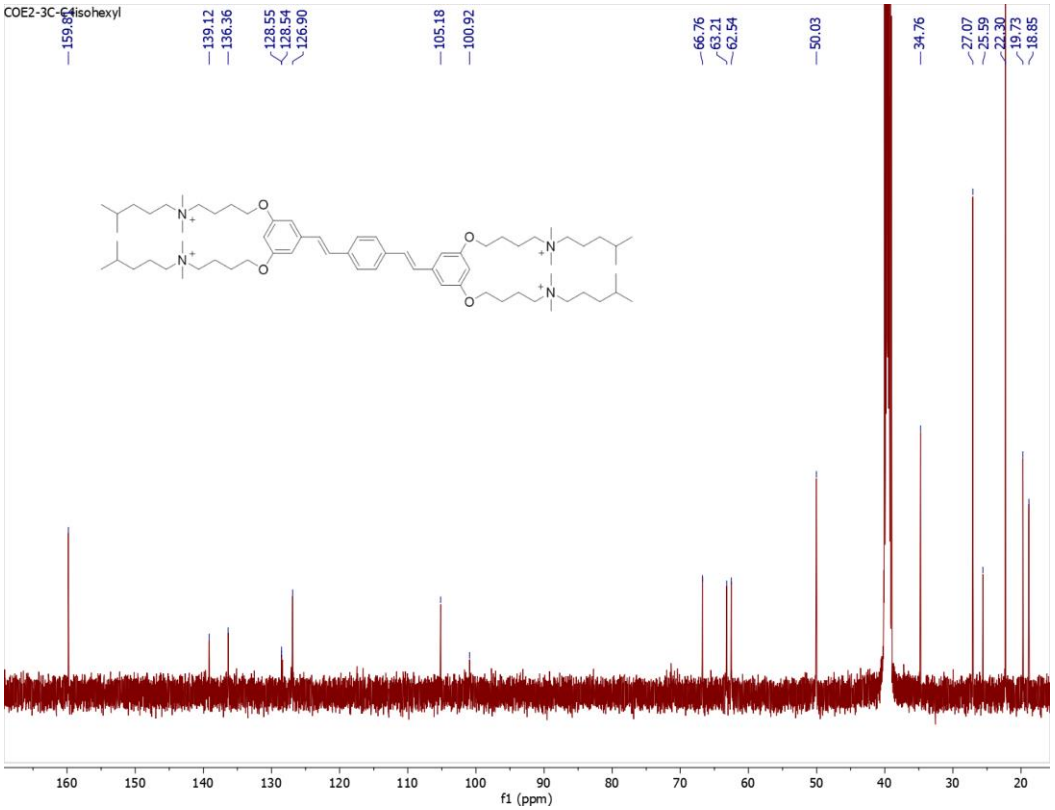
COE2-3C-C4isohexyl
f1 (ppm)

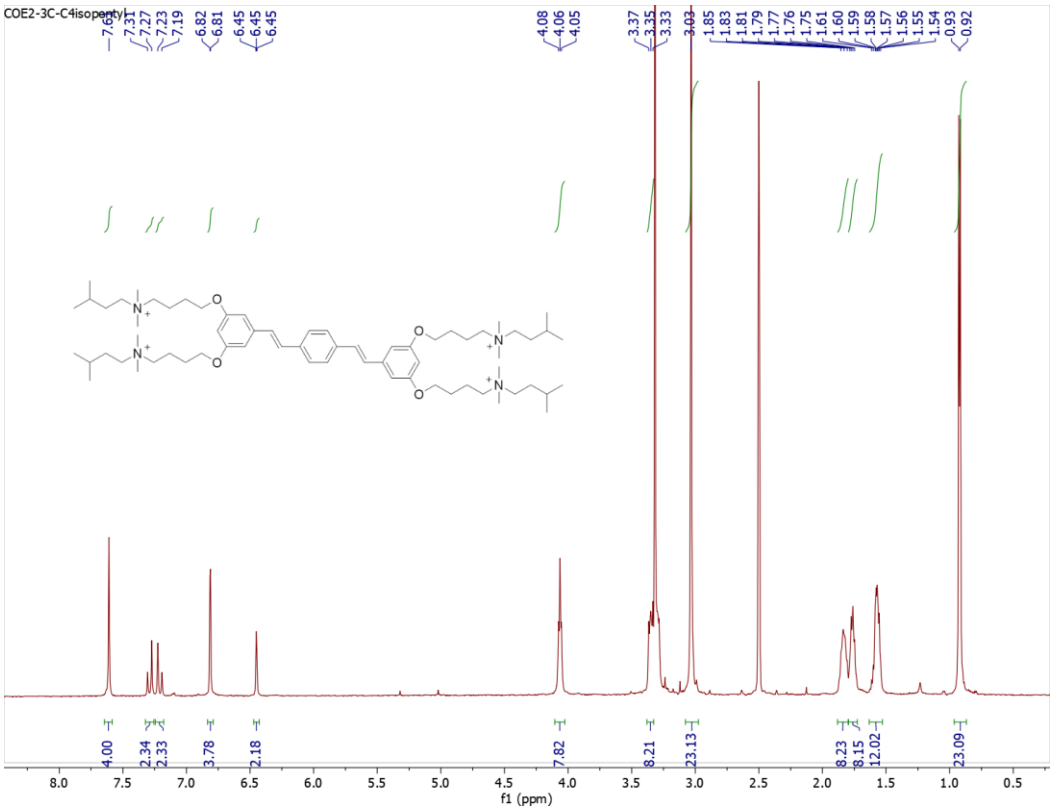
COE2-3C-C4isopentyl
7.61
7.31
7.27
7.23
7.19
6.82
6.81
6.45
6.45
6.45
4.08
4.06
4.05
3.37
3.35
3.33
3.03
1.85
1.83
1.81
1.79
1.77
1.76
1.75
1.61
1.60
1.59
1.58
1.57
1.56
1.55
1.54
0.93
0.92
4.00
2.34
2.33
3.78
2.18
7.82
8.21
23.13
8.23
8.15
12.02
23.09
8.0
7.5
7.0
6.5
6.0
5.5
5.0
4.5
4.0
3.5
3.0
2.5
2.0
1.5
1.0
0.5
f1 (ppm)

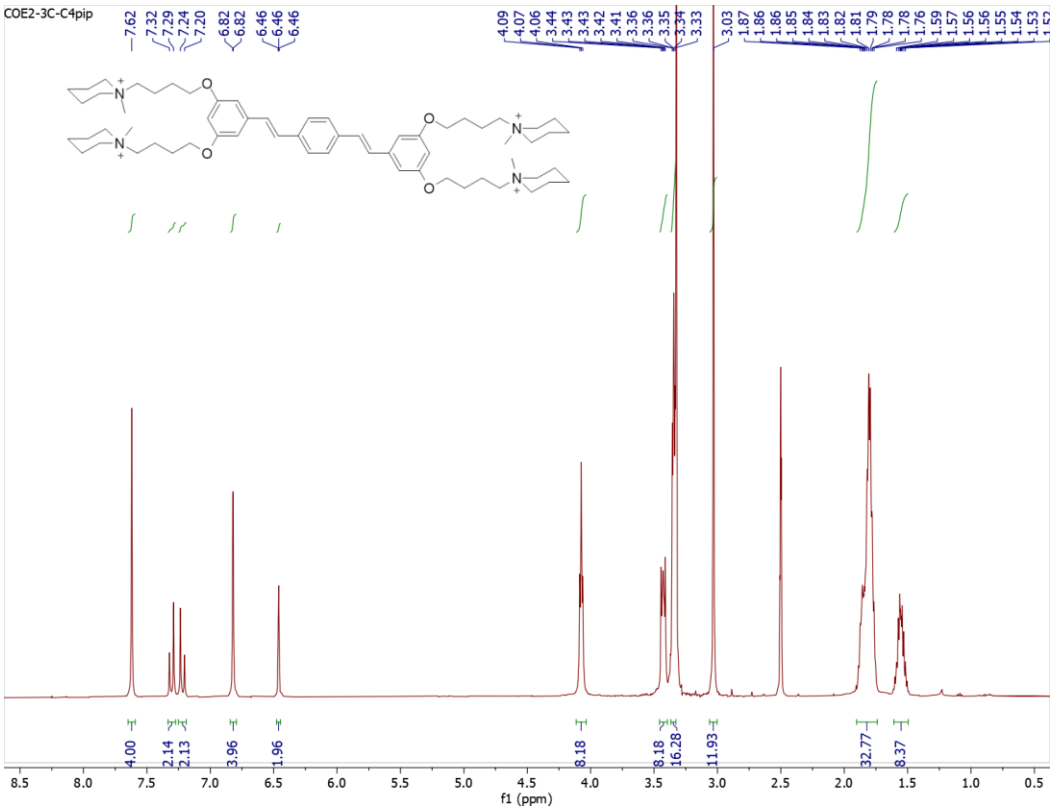
COE2-3C-C4pip
7.62
7.32
7.29
7.24
7.20
6.82
6.82
6.46
6.46
6.46
4.09
4.07
4.06
3.44
3.43
3.43
3.42
3.41
3.36
3.36
3.35
3.34
3.33
3.03
1.87
1.86
1.86
1.85
1.84
1.83
1.82
1.81
1.79
1.78
1.78
1.76
1.59
1.57
1.56
1.56
1.55
1.54
1.53
4.00
2.14
2.13
3.96
1.96
8.18
8.18
16.28
11.93
32.77
8.37
f1 (ppm)

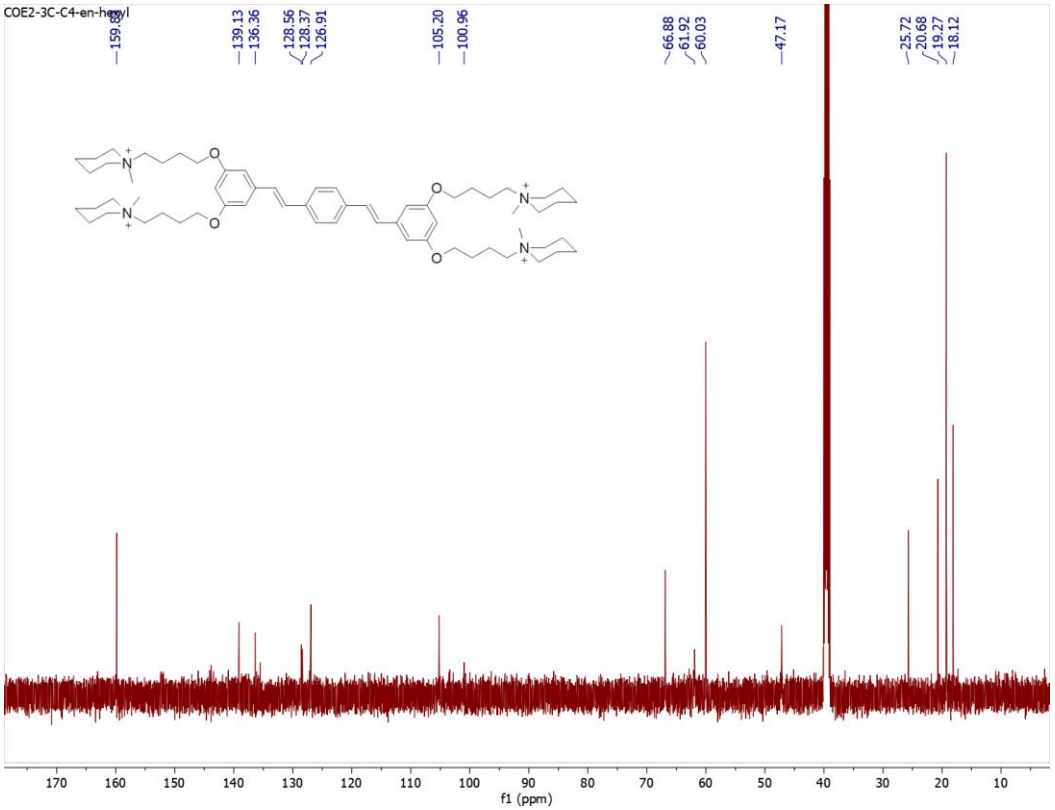
COE2-3C-C4-en-hexyl
159.80
139.13
136.36
128.56
128.37
126.91
105.20
100.96
66.88
61.92
60.03
47.17
25.72
20.68
19.27
18.12
f1 (ppm)